If you have discovered material in AURA which is unlawful e.g. breaches copyright, (either yours or that of a third party) or any other law, including but not limited to those relating to patent, trademark, confidentiality, data protection, obscenity, defamation, libel, then please read our Takedown Policy and contact the service immediately

Numerical Modelling of Dispersion Managed Soliton Transmission

Donald Scott Govan

Doctor of Philosophy

Aston University

March 1999

This copy of the thesis has been supplied on condition that anyone who consults it is understood to recognise that its copyright rests with its author and that no quotation from the thesis and no information derived from it may be published without proper acknowledgement.

Aston University

Numerical Modelling of Dispersion Managed Soliton Transmission

Donald Govan

Doctor of Philosophy

March 1999

This thesis presents the results of numerical modelling of the propagation of dispersion managed solitons. The theory of optical pulse propagation in single mode optical fibre is introduced specifically looking at the use of optical solitons for fibre communications. The numerical technique used to solve the nonlinear Schrödinger equation is also introduced. The recent developments in the use of dispersion managed solitons are reviewed before the numerical results are presented

The work in this thesis covers two main areas; (i) the use of a saturable absorber to control the propagation of dispersion managed solitons and (ii) the upgrade of the installed standard fibre network to higher data rates through the use of solitons and dispersion management.

Saturable absorbers can be used to suppress the build up of noise and dispersive radiation in soliton transmission lines. The use of saturable absorbers in conjunction with dispersion management has been investigated both as a single pulse and for the transmission of a 10Gbit/s data pattern. It is found that this system supports a new regime of stable soliton pulses with significantly increased powers.

The upgrade of the installed standard fibre network to higher date rates through the use of fibre amplifiers and dispersion management is of increasing interest. In this thesis the propagation of data at both 10Gbit/s and 40Gbit/s is studied. Propagation over transoceanic distances is shown to be possible for 10Gbit/s transmission and for more than 2000km at 40Gbit/s. The contribution of dispersion managed solitons in the future of optical communications is discussed in the thesis conclusions.

Additional key words and phrases

Nonlinear optics, optic fibres, optical solitons, optical networks, dispersion management, saturable absorbers.

Acknowledgements

There are several people who have provided valuable assistance during the course of my PhD. I would firstly like to thank my supervisor Professor Nick Doran for his help and support throughout my time at Aston. Nick Smith provided a good deal of guidance during my first year and also wrote the GNLS code used in generating the numerical results presented in this thesis. I would also like to thank all the other past and present members of the photonics research group for their help and friendship.

The experimental results referred to in this thesis, particularly in chapters 4, 5 and 6 were carried out by Paul Harper, Steve Alleston, Ian Penketh and Finlay Knox. I would like to thank Paul Harper for supplying the experimental parameters and many useful discussions. Finally my thanks go to Wladek Forysiak for reading this thesis.

for Mum, Dad, Julie and Mark

Contents

List of Figures

Chapter 1

Introduction

The demand placed on communication systems around the world is constantly increasing. Most of the data from phones, faxes and computers is transmitted on single mode optical fibre. The available bandwidth and low loss of optical fibres make them far more attractive than the alternatives (such as coaxial cable) for cost effective high capacity data transmission. The data rate required for a telephone conversation is 64kbit/s [1] therefore a single optical fibre operating at a data rate of 10Gbit/s is able to carry more than one hundred and fifty thousand telephone calls. However, communications systems are now used to transmit television and radio signals as well as computer data through the internet which greatly increases the required capacity.

1.1 Optical fibres

Optical fibre used for long distance data transmission is made from fused silica. The most common type of fibre is step index fibre, a cross section of a step index fibre is shown in figure 1.1. The core of the fibre has a slightly higher refractive index than the cladding. The transmitted light can therefore be contained in the core through total internal reflection. The fibre can be described using two parameters, Δ, the relative core cladding index difference and V the normalised frequency [2]. These two parameters are given by;

$$\Delta = \frac{n_1 - n_2}{n_1} \tag{1.1}$$

$$V = k_o a(n_1^2 - n_2^2)^{\frac{1}{2}} \tag{1.2}$$

where n_1 and n_2 are the refractive indices of the core and cladding respectively, k_o is the wavenumber and a is the core radius. A typical value for Δ is $\sim 3 \times 10^{-3}$.

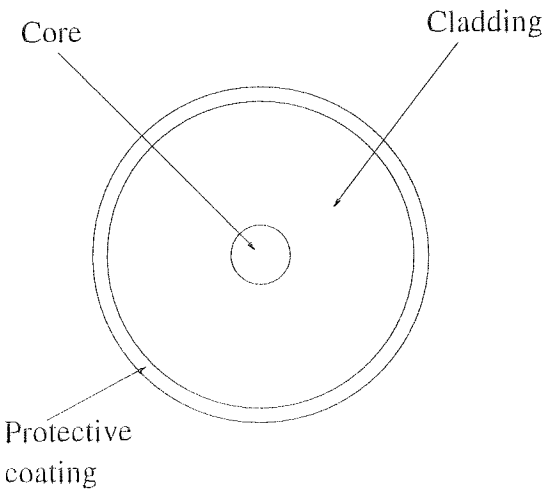

Figure 1.1: Cross section of a step index fibre. The core radius is a, the core has a slightly higher refractive index than the cladding.

Only single mode fibres will be considered in this thesis. For a fibre to operate with a single mode it must be designed such that $V < 2.405$. For operation at $1.55\mu m$ the core radius is $\sim 4\mu m$ and the cladding radius is $\sim 60\mu m$ [2]. The basic characteristics of optical fibre; i.e. loss, chromatic dispersion and nonlinearity will be considered in the next chapter.

1.2 Digital optical data transmission

In this thesis data is taken to be transmitted through an optical fibre as a digital signal. This means that the transmitted signal is a series of 1's and 0's. A 1 is represented by a pulse of light and a 0 is represented by the absence of a pulse. At the detector a decision level is set, if the energy in a bit slot is greater than the decision level then a 1 is registered if the level is less than the decision level it is taken as a 0. In this way the data pattern can be degraded by dispersion, nonlinearity and noise as it propagates along the fibre without causing errors in the received signal. There are two main formats used to transmit optical signals: return-to-zero (RZ) or non-return-to-zero (NRZ). When an NRZ format is used the pulse width is the same length as the bit period and so if there are two consecutive 1's they are formed by a single pulse. NRZ pulses are approximately rectangular in shape. In RZ transmission the pulse width is less than the bit spacing and

the signal level always returns to zero between two consecutive 1's. Although NRZ pulses use the available bandwidth more efficiently and are used in many current systems greater transmission distances are possible using RZ pulses [3, 4]. NRZ pulses are not compatible with all optical processing which is likely to be used in future high capacity systems.

The volume of data transmitted in a single optical fibre can be increased using time division multiplexing (TDM) and wavelength division multiplexing (WDM). In time division multiplexing two or more data signals are added together by interleaving the pulses in the data patterns [5]. In WDM systems high capacities can be achieved by transmitting data at several different wavelengths [6, 7, 8, 9].

1.3 Thesis overview

A review of the theory of optical fibre transmission in single mode optical fibre is presented in chapter 2 of this thesis. This is required to understand the effects which limit the transmission of data in optical fibres. This chapter also introduces the idea of soliton pulses for optical communications and contains a description of the numerical techniques used to carry out the simulations presented in the rest of the thesis. Chapter 3 introduces the more recent development of dispersion management for soliton transmission and gives a brief explanation for the formation of dispersion managed soliton. This chapter also includes a review of the properties of dispersion managed solitons and lists some experimental results for propagation experiments using dispersion managed solitons.

The work presented in this thesis can be split into two groups. Firstly a weak saturable absorber is used as a control element in a dispersion managed transmission line, these results are discussed in chapters 4 and 5. In chapter 4 single pulse transmission for a system with dispersion management and a weak saturable absorber is discussed. This system is found to support stable pulse propagation for a wide range of pulse energies. In chapter 5 the effects of loss, third order dispersion and noise are included to study the propagation of a 10Gbit/s data pattern in the system using dispersion management and a weak saturable absorber. Error free distances of more than 200Mm are found to be possible.

Secondly the problems of upgrading the installed standard fibre to 10Gbit/s and 40Gbit/s are discussed in chapters 6 and 7 respectively. In chapter 6 the effects of altering the dispersion map used to transmit a 10Gbit/s data pattern over transoceanic distances are investigated. In chapter 7 a novel, symmetric dispersion map is used to propagate

data at 40Gbit/s over more than 2000km of standard fibre. In the final chapter the results presented in the thesis are summarised and the future of dispersion managed solitons for optical fibre communications is discussed.

Chapter 2

Solitons and Optical Fibres

2.1 Introduction

In order to make a quantitative study of the propagation of pulses in optical fibre it is necessary to derive equations which accurately describe this process. The nonlinear Schrödinger equation (NLSE) describes the propagation of nonlinear pulses in single mode optical fibres. This chapter will first give the outline of a derivation of the NLSE which will not be rigourous but will include the important points. The main properties of the optical fibre such as dispersion, self-phase modulation and loss will then be considered before the concept of solitons is introduced. The problems involved with soliton transmission are then considered along with the solutions that have been used. The split-step Fourier method of solving the NLSE will also be described.

2.2 Derivation of the NLSE

In order to derive the NLSE the starting point is the wave propagation equation [10];

$$\nabla^2 \mathbf{E} - \frac{1}{c^2}\frac{\partial^2 \mathbf{E}}{\partial t^2} = \mu_o \frac{\partial^2 \mathbf{P}_L}{\partial t^2} + \mu_o \frac{\partial^2 \mathbf{P}_{NL}}{\partial t^2} \tag{2.1}$$

where c is the velocity of light, μ_o is the vacuum permeability, $\mathbf{E}$ is the electric field $\mathbf{E}(\mathbf{r},t)$ and $\mathbf{P}_L$ and $\mathbf{P}_{NL}$ are the linear and nonlinear induced polarisations which are related to the electric field through the dielectric tensors $\chi^{(1)}$ and $\chi^{(3)}$ respectively.

The electric field is given as;

$$\mathbf{E}(\mathbf{r},t) = \frac{1}{2}\hat{x}\left[E(\mathbf{r},t)exp(-i\omega_o t) + c.c.\right] \tag{2.2}$$

where $E(\mathbf{r},t)$ is the slowly varying part of the electric field, $\hat{x}$ is the polarisation vector of the light and c.c. stands for complex conjugate. Similar equations for the slowly varying parts of the linear and nonlinear polarisation can be found.

It is necessary to make some approximations to proceed in the derivation of the NLSE, firstly the nonlinear polarisation is treated as a perturbation to the linear polarisation. This is a good approximation since optical fibres are only weakly nonlinear, the nonlinear refractive index ($n_2 = 2.5 \times 10^{-16} cm^2/W$ [11]) is small when compared to the refractive index of silica (n=1.45). Secondly it is assumed that the light is linearly polarised and its state of polarisation does not change with propagation this means that a scalar approach can be used rather than a vector one [12]. The effects of birefringence will be considered later in sections 2.3.5, 2.3.6 and 2.6.3. The quasi-monochromatic approximation in which the bandwidth of the field, $\Delta\omega$, is assumed to be much less than the carrier frequency ω_o is also made, this is a good approximation for pulses with widths greater than 0.1ps [13]. Finally the nonlinearity is assumed to be instantaneous, which again is a good approximation as long as very short pulses are not being considered [14].

The Fourier transform of the electric field is defined as:

$$\hat{E}(\mathbf{r},\omega-\omega_o) = \int_{-\infty}^{\infty} E(\mathbf{r},t) exp\left[i(\omega-\omega_o)t\right] dt \tag{2.3}$$

which satisfies the equation

$$\nabla^2 \hat{E} + \epsilon(\omega) k_o^2 \hat{E} = 0 \tag{2.4}$$

where $k_o = \omega/c$ and $\epsilon(\omega) = 1 + \chi^{(1)} + \epsilon_{NL}$ is the dielectric constant with the nonlinear part of the dielectric constant given by $\epsilon_{NL} = \frac{3}{4}\chi^{(3)}|E(\mathbf{r},t)|^2$

The dielectric constant can be used to define the refractive index $\hat{n}(\omega)$

$$\hat{n}(\omega) = n(\omega) + n_2|E|^2 \tag{2.5}$$

where $n_2 = \frac{3}{8n} Re(\chi^{(3)})$ is assumed to not change with frequency.

It is now convenient to use a separation of variables to assume a solution of the form;

$$\hat{E}(\mathbf{r},\omega-\omega_o) = F(x,y)\hat{A}(z,\omega-\omega_o) exp(i\beta_o z) \tag{2.6}$$

where $\hat{A}(z,\omega-\omega_o)$ is a slowly varying function of z, β_o is the wave number and $F(x,y)$ is the

modal distribution of the fundamental mode in a single mode optical fibre. Substituting 2.6 into equation 2.4 gives an equation in $\hat{A}(z,\omega)$ and one in $F(x,y)$.

$$\frac{\partial^2 F}{\partial x^2} + \frac{\partial^2 F}{\partial y^2} + \left[\epsilon(\omega)k_o^2 - \beta^2\right] F = 0 \tag{2.7}$$

$$2i\beta_o \frac{\partial A}{\partial z} + \left(\beta^2 - \beta_o^2\right) A = 0 \tag{2.8}$$

The second derivative $\frac{\partial^2 A}{\partial z^2}$ in equation 2.8 is ignored since A is assumed to be slowly varying, this is known as the slowly varying envelope approximation. Re-arranging equation 2.8 and then using an approximation for $\beta^2 - \beta_o^2$ gives;

$$\frac{\partial A}{\partial z} = \frac{i}{2\beta_o}\left(\beta^2 - \beta_o^2\right) A \tag{2.9}$$

$$\frac{\partial A}{\partial z} = i\left[\beta(\omega) + \Delta\beta - \beta_o\right] A \tag{2.10}$$

$\Delta\beta$ can be found from the modal distribution F(x,y) and Δn the perturbation in the refractive index due to nonlinearity and loss [15]. Δn is given by;

$$\Delta n = n_2|E|^2 + \frac{i\alpha}{2k_o} \tag{2.11}$$

β can be expanded in a Taylor series;

$$\beta = \beta_o + (\omega - \omega_o)\beta_1 + \frac{1}{2}(\omega - \omega_o)^2\beta_2 + \frac{1}{6}(\omega - \omega_o)^3\beta_3 + \ldots \tag{2.12}$$

$$\beta_n = \left[\frac{\partial^n \beta}{\partial \omega^n}\right] \omega = \omega_o \tag{2.13}$$

Substituting for β and $\Delta\beta$ and taking the inverse Fourier transform, noting that $\omega - \omega_o$ is replaced by the operator $i\frac{\partial}{\partial t}$ gives;

$$\frac{\partial A}{\partial z} + \beta_1 \frac{\partial A}{\partial t} + \frac{i}{2}\beta_2 \frac{\partial^2 A}{\partial t^2} + \frac{\alpha}{2} = i\gamma|A|^2 A \tag{2.14}$$

where the nonlinear coefficient is given by;

$$\gamma = \frac{n_2\omega_o}{cA_{eff}} \tag{2.15}$$

Substituting for $\Delta\beta$ adds the effects of loss and nonlinearity explicitly into the equation.

A_{eff} is the effective area which is found from the modal distribution [16].

It is useful to change to a frame of reference moving with the pulse.

$$T = t - \beta_1 Z = t - \frac{Z}{v_g} \tag{2.16}$$

where v_g is the group velocity of the pulse.

$$i\frac{\partial A}{\partial z} = -\frac{i}{2}\alpha A + \frac{1}{2}\beta_2 \frac{\partial^2 A}{\partial t^2} - \gamma |A|^2 A \tag{2.17}$$

This equation is known as the generalised nonlinear Schrödinger equation (GNLSE) and gives a very good description of the propagation of pulses through single-mode optical fibre. The first term on the right hand side describes the effect of loss, the middle term deals with dispersion and the final term is the Kerr nonlinearity. This equation can be expanded to include higher order dispersion simply by including more terms from the Taylor expansion of β. The higher order dispersion becomes more important when the pulse's frequency is near to the dispersion zero (i.e the point where β_2=0.0) and in wavelength division multiplexed (WDM) systems.

In order to understand the different propagation regimes that the GNLSE describes it is useful to introduce two length scales [17]. These length scales give a measure of the distance over which the dispersion and nonlinearity have a significant effect on the pulse. The first length scale is the dispersion length (L_D), this length indicates the length over which a Gaussian pulse width is increased by a factor of $\sqrt{2}$ due to dispersion and is given by:

$$L_D = \frac{T_o^2}{|\beta_2|} \tag{2.18}$$

T_o is the 1/e pulse width and is related to the more commonly used full width at half maximum (FWHM) by $T_{FWHM} = BT_o$. B=1.665 for a Gaussian pulse and 1.763 for a sech pulse.

The other important length scale is the nonlinear length (L_{NL}) which is length over which the bandwidth doubles and is given by;

$$L_{NL} = \frac{1}{\gamma P_o} \tag{2.19}$$

where P_o is the pulse's peak power.

If these lengths are of a similar size to the length over which the pulses are propagated then the effect that they relate to becomes important. This lead to 4 different regimes which can be described. The first regime is when $L \ll L_D, L_{NL}$ in this regime neither dispersive effects or nonlinear effects are important. It relates to low power pulses with a large pulse width transmitted over short distances and is of little interest for long distance communications. The other regimes are considered in the following sections. Firstly the case where dispersion dominates ($L \geq L_D, L \ll L_{NL}$), then the case where nonlinearity dominates ($L \geq L_{NL}, L \ll L_D$) and finally the case where both are important ($L \geq L_D, L_{NL}$). The last regime is of particular interest as it describes the conditions where it is possible for solitons to exist and will be considered in section 2.4.2.

2.3 Optical fibre properties

2.3.1 Introduction

In this section some of the properties of optical fibres and their effects on a propagating pulse are considered. It is useful to look at these properties in isolation before their combined effects are examined. The first property of interest is group velocity dispersion (GVD). Next self-phase modulation (SPM) caused by the nonlinear Kerr effect will be discussed. Then the main loss mechanisms of optical fibre will be considered. Next is a section on birefringence which will show that real single mode fibres actually support two modes, one for each polarisation. The final section examines cross-phase modulation which is also a result of the nonlinear Kerr effect.

2.3.2 Group velocity dispersion

Firstly the regime where group velocity dispersion (GVD) is dominant is examined [18]. As stated earlier this regime occurs when $L \geq L_D, L \ll L_{NL}$. The GVD causes the different frequencies that make up the optical pulse to propagate with slightly different velocities. In the normal dispersion region ($\beta_2 > 0$) longer wavelengths travel more quickly whereas in the anomalous region ($\beta_2 < 0$) shorter wavelengths travel more quickly. Since the different frequency components of the pulse are travelling at different velocities the pulse width increases.

In order to look at this mathematically we can use a simplified version of the GNLSE [19]. Firstly since nonlinear effects are not important we can set $\gamma = 0$. The pulse can

then be transformed to remove loss and give the normalised pulse envelope $U(Z,T)$, which is given by;

$$A(Z,T) = \sqrt{P_o} exp\left(-\frac{\alpha Z}{2}\right) U(Z,T) \tag{2.20}$$

This then leaves a simplified equation to describe this regime;

$$i\frac{\partial U}{\partial Z} = \frac{1}{2}\beta_2 \frac{\partial^2 U}{\partial T^2} \tag{2.21}$$

The normalised equation can be solved using the Fourier method. $\hat{U}(Z,\omega)$ is the Fourier transform of $U(Z,T)$ and is defined by;

$$U(Z,T) = \frac{1}{2\pi}\int_{-\infty}^{\infty} \hat{U}(Z,\omega) exp(i\omega T) dT \tag{2.22}$$

which satisfies the ordinary differential equation

$$i\frac{d\hat{U}}{dZ} = -\frac{1}{2}\beta_2 \omega^2 \hat{U} \tag{2.23}$$

This equation can be integrated to give;

$$\hat{U}(Z,\omega) = \hat{U}(0,\omega) exp\left(\frac{i}{2}\beta_2 \omega^2 Z\right) \tag{2.24}$$

$\hat{U}(0,\omega)$ is the Fourier transform of the field at Z=0, i.e.

$$\hat{U}(0,\omega) = \int_{-\infty}^{\infty} U(0,T) exp(i\omega T) dT \tag{2.25}$$

Equation 2.24 shows that the spectrum of the pulses is unchanged as it propagates through the fibre. The phase of the different spectral components does change and this leads to changes in pulse width and pulse shape.

A general solution to this equation is found by substituting equation 2.24 into equation 2.22.

$$U(Z,T) = \frac{1}{2\pi}\int_{-\infty}^{\infty} \hat{U}(0,\omega) exp\ i\left(\frac{1}{2}\beta_2 \omega^2 Z - \omega T\right) dT \tag{2.26}$$

The effects of dispersion on a Gaussian pulse are important in the study of dispersion managed solitons and so that case will be considered here. Taking the input pulse $U(0,T)$

as;

$$U(0,T) = exp\left(-\frac{T^2}{2T_o^2}\right) \tag{2.27}$$

after propagating over a distance Z in fibre with GVD of β_2, the pulse is given by;

$$U(Z,T) = \left(\frac{T_o^2}{T_o^2 - i\beta_2 Z}\right)^{1/2} exp\left(-\frac{T^2}{2\left(T_o^2 - i\beta_2 Z\right)}\right) \tag{2.28}$$

Equation 2.28 shows that the Gaussian pulse retains its shape during propagation however the pulse width increases with Z. The pulse width is given by;

$$T_1 = T_o\sqrt{1 + \left(\frac{Z}{L_D}\right)^2} \tag{2.29}$$

Since the increase in pulse width is inversely proportional to L_D shorter pulses are broadened more quickly than broader ones. This is due to shorter pulses having a wider spectrum and since the different spectral components travel with different velocities there is a wider range of velocities. The amount of broadening also increases if fibre with a greater dispersion is used although the sign of the dispersion does not affect the amount of pulse broadening for this input pulse. Dispersive pulse broadening can be seen in the simulation results given in figure 2.1. This figure shows a Gaussian pulse with a FWHM of 20ps and a peak power of 0.01W broadening over 40km of fibre with dispersion of $-10.0ps^2/km$.

In addition to broadening the pulse the dispersion also induces a chirp on it. A pulse is said to be chirped when the instantaneous frequency changes across the pulse. The difference in the instantaneous frequency is given by the time derivative of the phase, $-\frac{\partial\varphi}{\partial T}$. For the Gaussian pulse which was considered earlier the phase can be found from the imaginary part of equation 2.28;

$$\phi(Z,T) = -\frac{sgn(\beta_2)(Z/L_D)T^2}{1 + (Z/L_D)^2 T_o^2} + tan^{-1}\left(\frac{Z}{L_D}\right) \tag{2.30}$$

The difference in the instantaneous frequency ($\delta\omega$) is therefore given by;

$$\delta\omega = -\frac{\partial\phi}{\partial T} = 2\frac{sgn(\beta_2)(Z/L_D)T}{1 + (Z/L_D)^2 T_o^2} \tag{2.31}$$

This equation shows that the frequency change across the pulse is linear. It also shows

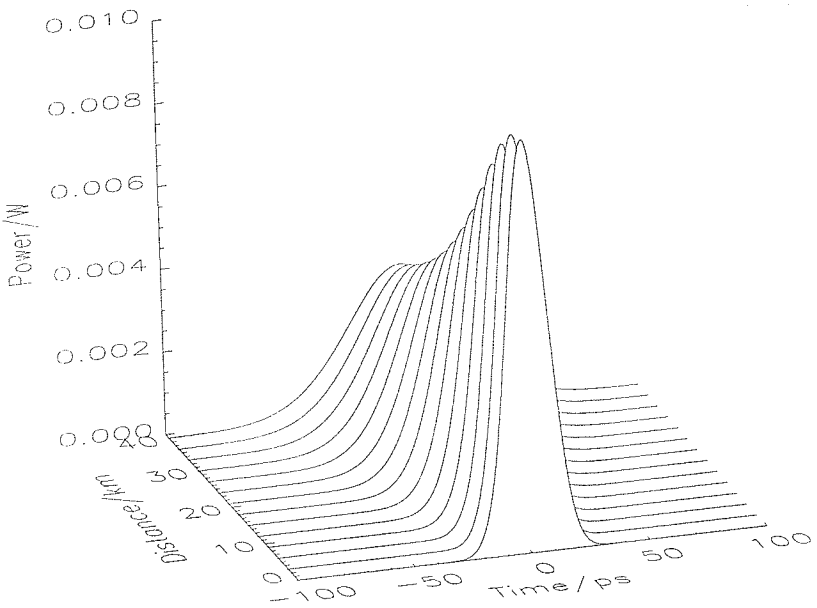

Figure 2.1: A 20ps Gaussian pulse broadening to 58ps over 40km of fibre with dispersion of $-10.0ps^2/km$. The initial pulse is unchirped and has a peak power of 0.01W.

that although the size of the chirp is not affected by the sign of β_2, it affects the sign of the chirp. This means that for normal dispersion fibre the wavelength decreases from the leading edge to the trailing edge; for anomalous dispersion the opposite is true. The input and final instantaneous frequency from the dispersion broadened Gaussian pulse are shown in figure 2.2.

So far only the case where the input pulse is an unchirped Gaussian has been considered. The other pulse shape that is of particular interest here is the hyperbolic secant (sech) as this is the shape of a soliton. Sech pulses behave in the same way as a Gaussian in a purely dispersive system with the pulse retaining its shape but broadening and becoming chirped as can be seen in figures 2.3 and 2.4. Figure 2.3 shows an input sech pulse with a FWHM of 20.0ps and peak power of 0.01W propagating through 40km of fibre with dispersion of $-10.0ps^2/km$, figure 2.4 shows the initial and final instantaneous frequency variation across the pulse. Other pulse shapes such as super Gaussians, which have steeper edges, broaden more rapidly and undergo distortions in their pulse shape.

The final case that must be considered is when the input pulse already has a linear chirp. If the chirp on the pulse is the same sign as the dispersion induced chirp then the pulse broadens as before although at a greater rate than an unchirped pulse with the same pulse width. If the chirp and the dispersion have the opposite sign then the pulse

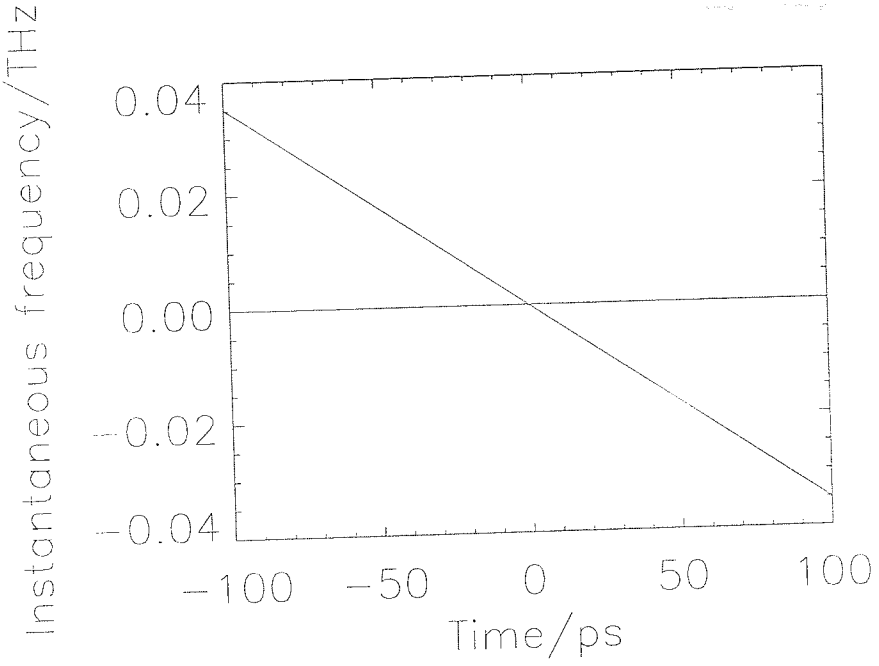

Figure 2.2: The effect of dispersion on the instantaneous frequency of a Gaussian pulse. The horizontal line is for the unchirped input pulse which has a FWHM of 20.0ps and a peak power of 0.01W. The chirped pulse has propagated through 40.0km of fibre with dispersion of $-10.0ps^2/km$.

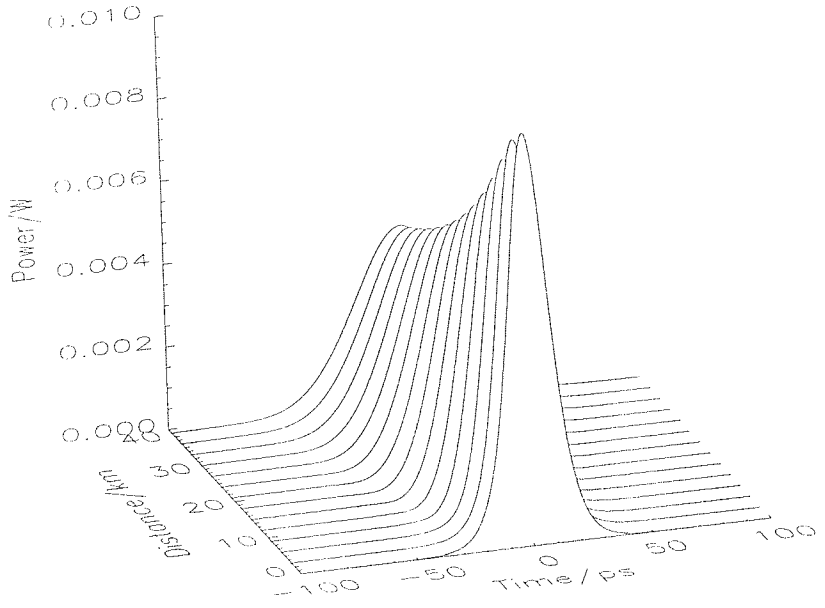

Figure 2.3: A 20ps sech pulse with peak power of 0.01W broadening over 40km of fibre. with dispersion of $10.0ps^2/km$.

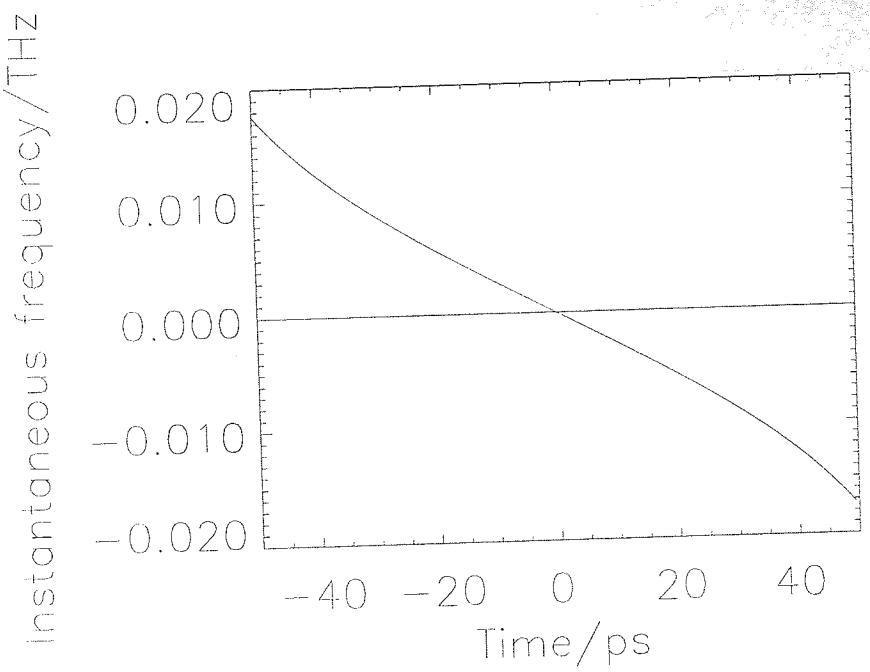

Figure 2.4: The effect of dispersion on the instantaneous frequency of a sech pulse the horizontal line is for the unchirped input pulse which has a FWHM of 20.0ps and peak power of 0.01W. The chirped pulse has propagated through 40.0km of fibre with dispersion of $-10.0ps^2/km$.

first compresses and then expands. When the chirp on the initial pulse and the dispersion induced chirp have opposite signs the frequencies at the leading edge of the pulse are propagating with a lower group velocity than the frequencies on the trailing edge of the pulse. This causes the pulse width and the chirp on the pulse to decrease until it reaches the point where it is unchirped. The pulse then gains a chirp of the opposite sign to its input chirp and the pulse broaden in the way described previously.

Only the lower order terms have been considered here. If higher order terms had been included from the Taylor expansion of β in equation 2.12 then pulse evolution would be more complicated [20]. These higher order terms become important when working close to λ_o (the wavelength where $\beta_2 = 0$) and when using wavelength division multiplexing (WDM), the higher order terms tend to lead to pulse assymetry and the generation of oscillations on the tails of the pulses. The effect of third order dispersion on an input Gaussian pulse (FWHM=20.0ps, peak power=0.01W) is shown in figure 2.5. In this simulation the GVD was set to zero, and the 3rd order dispersion was taken to be $1.0ps^3/km$. This is a value far higher than is found in optical fibre and is used here in order to increase the effect for illustration purposes. Third order dispersion in single mode optical fibre is generally $\sim 0.1ps^3/km$.

The dispersion is also expressed as the group delay dispersion, D, which is in the units

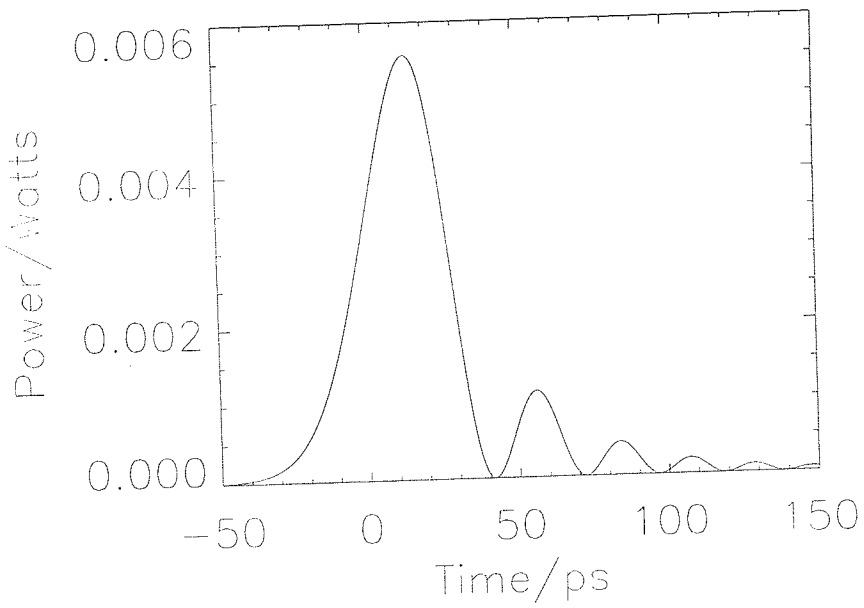

Figure 2.5: The effect of third order dispersion which causes the pulse to develop oscillations on the trailing edge. The input pulse was a Gaussian with peak power of 0.01W and FWHM of 20.0ps. This output is taken after the pulse has propagated over 10000km of fibre with zero GVD and third order dispersion of $1.0ps^3/km$

ps/(nm km) rather than β_2 which is in the units ps^2/km. The two parameters are related through [21];

$$D = -\frac{2\pi c}{\lambda^2}\beta_2 \tag{2.32}$$

It is important to note that the sign of these two parameters is different. β_2 is positive for normal dispersion and negative for anomalous dispersion whereas D is positive for anomalous dispersion and negative for normal dispersion. Both parameters will be used in this thesis.

2.3.3 Self-phase modulation

The next regime that will be considered is where the Kerr nonlinearity dominates, i.e. $L \geq L_{NL}, L \ll L_D$ [22]. This is the case when broad pulses with high peak powers are being considered, or if the wavelength of the pulses is close to λ_o. The effects of

nonlinearity can be investigated by setting $\beta_2 = 0$ in equation 2.17 which gives;

$$\frac{dU}{dZ} = \frac{i}{L_{NL}} exp(-\alpha Z)|U|^2 U \tag{2.33}$$

where α represents the fibre loss which is important when considering the Kerr nonlinearity since as the pulse is attenuated the size of the nonlinear refractive index is also reduced. $L_{NL} = 1/\gamma P_o$ is the nonlinear length. Equation 2.33 can be integrated to give;

$$U(Z,T) = U(0,T) exp(i\phi_{NL}(Z,T)) \tag{2.34}$$

where $U(0,T)$ is the pulse at $Z = 0.0$ and ϕ_{NL} is the nonlinear phase shift and is given by;

$$\phi_{NL}(Z,T) = |U(0,T)|^2 \frac{Z_{eff}}{L_{NL}} \tag{2.35}$$

$$\text{where } Z_{eff} = \frac{1}{\alpha}\left(1 - exp\left(\alpha Z\right)\right) \tag{2.36}$$

Z_{eff} is the effective length scale of the nonlinearity in a lossy system. This length scale is shorter than Z and gives the distance over which the same phase shift would occur in a loss-less system. Equation 2.33 shows that the effect of the nonlinear Kerr effect is to give the pulse an intensity dependent phase shift. This causes a chirp across the pulse.

Self-phase modulation also gives the pulse a frequency chirp which can be seen in the instantaneous frequency across the pulse as given by the time derivative of the phase;

$$\delta\omega(T) = -\frac{\partial \phi_{NL}}{\partial T} = -\frac{\partial}{\partial T}\left(|U\left(0,T|\right)|^2\right)\frac{Z_{eff}}{L_{NL}} \tag{2.37}$$

If the Gaussian input given in equation 2.27 is used in this equation the frequency difference is given by;

$$\delta\omega(T) = \frac{Z_{eff}}{L_{NL}}\frac{2T}{T_o^2} exp\left(-\frac{T^2}{2T_o^2}\right) \tag{2.38}$$

This equation shows that the frequency chirp increases with propagation distance, as new frequencies are created at the leading and trailing edges of the pulse. The frequency decreases towards the leading edge of the pulse and increases towards the trailing edge. In this case, unlike that of pure GVD, the frequencies at the edge of the pulse are not part of the initial pulses spectrum and have been created by the nonlinearity. This can be

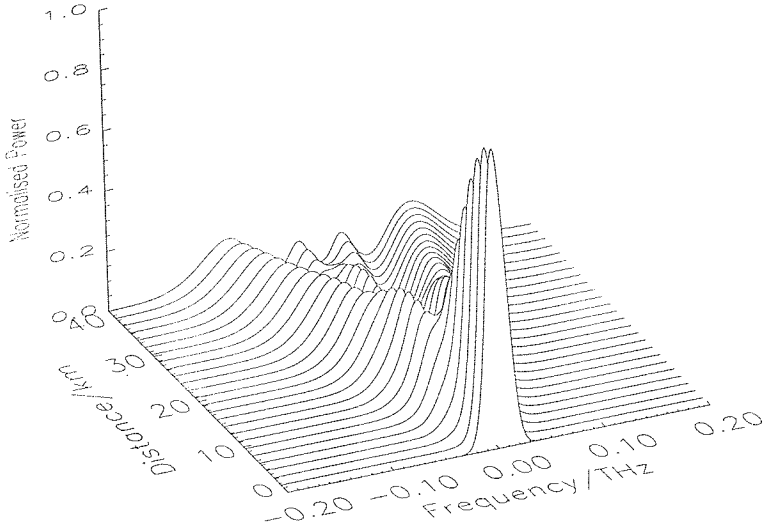

Figure 2.6: The spectrum of a 20ps Gaussian pulse with peak power of 0.1W as it undergoes self-phase modulation in 40km of fibre in the absence of dispersion..

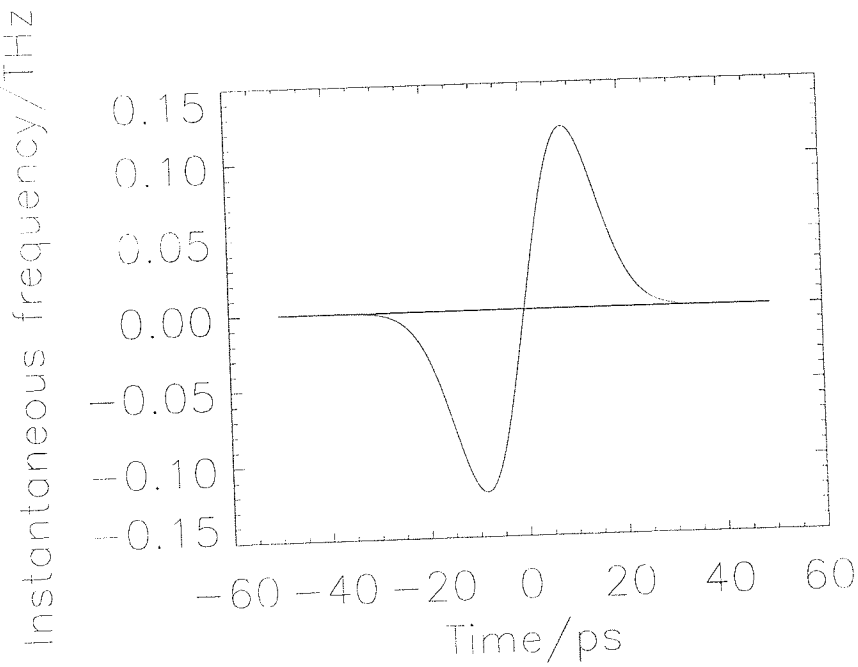

Figure 2.7: The instantaneous frequency across a 20ps Gaussian pulse with a peak power of 0.1W. The horizontal line is the input pulse and the other line shows the pulse after propagating over 40km of fibre with no dispersion and demonstrates the chirp induced by SPM.

seen in figure 2.6 which shows the spectrum of a 20ps Gaussian pulse with a peak power of 0.1W as it propagates through 40km of fibre with no dispersion or loss. It is clear that the frequency broadens substantially during propagation. The reason for the peaks in the spectrum can be seen from figure 2.7 which shows the instantaneous frequency across this pulse at the end of its propagation. This shows that there are two points on the pulse that have the same instantaneous frequency, these two points can be considered as two waves with the same frequency but different phases. These two waves interfere either constructively or destructively depending on their relative phase and lead to the oscillations in the spectrum of the pulse.

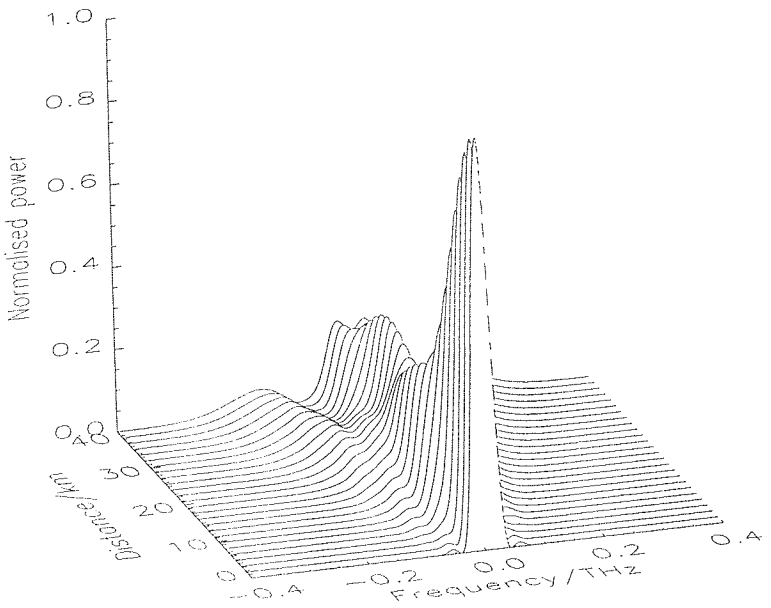

Figure 2.8: The spectrum of a 20ps super-Gaussian pulse with a peak power of 0.1W as it undergoes self-phase modulation. It can be seen that, unlike the Gaussian pulse, here most of the energy remains within the central region

The size of the frequency chirp depends on how steep the leading and trailing edges of the pulses are. Pulses such as a super-Gaussian which have steep leading and trailing edges and relatively little change in the pulses intensity over the central region have a larger frequency chirp as can be seen in figure 2.8 however most of the energy stays in the central part of the spectrum which is shown in figure 2.9. The parameters for this simulation were the same as those for the Gaussian pulse, the only difference was the pulse shape. This means that it is useful to use square pulses if it is necessary to minimise the effects of SPM.

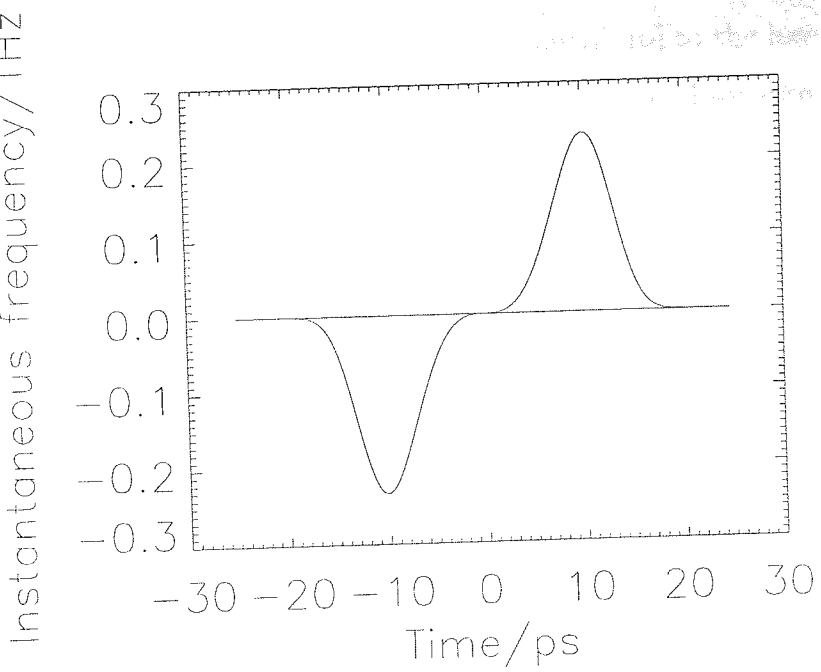

Figure 2.9: The instantaneous spectrum of a 10ps super-Gaussian pulse with a peak power of 0.1W after it has propagated over a 40km of fibre. The SPM induced chirp can clearly be seen although there is no chirp over the central part of the pulse.

2.3.4 Fibre loss

One of the main reasons for the success of optical fibres in long distance communications is their low loss[23]. The fibre loss, α is given by;

$$\alpha = -\frac{1}{L} ln \frac{P_{out}}{P_{in}} \tag{2.39}$$

Where L is the length of the fibre and P_{out} and P_{in} are the output and input powers respectively. The fibre loss is more commonly quoted in units of dB/km in this case the loss, α_{dB}, is given by;

$$\alpha_{dB} = -\frac{10}{L} log \frac{P_{out}}{P_{in}} \tag{2.40}$$

α and α_{dB} are related by;

$$\alpha_{dB} = 10 \alpha log_{10} e \tag{2.41}$$

The loss of an optical fibre is typically 0.2dB/km. The loss profile of silica can be seen in figure 2.10. The three main mechanisms that contribute to the loss are marked on this diagram, they are Rayleigh scattering, infra red electronic absorption and absorption by the OH^- impurity. The first two are intrinsic i.e a fundamental property of the material while the last one is extrinsic as it is the result of an impurity [24].

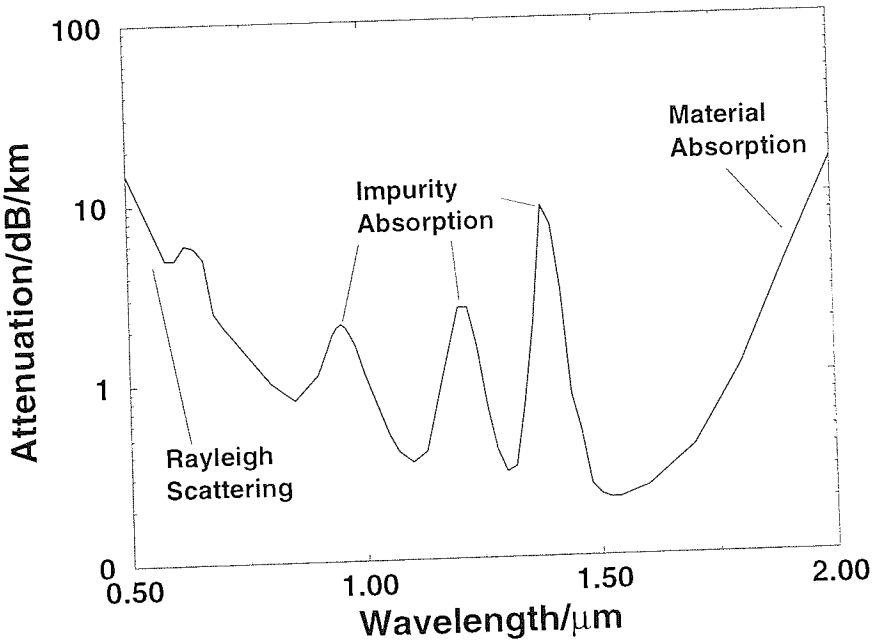

Figure 2.10: The loss profile for silica fibre.

Rayleigh scattering is caused by random fluctuations in the density of the fibre either through variations in the chemical composition of the silica or through the random orientation of the molecular units that make up the silica. The strength of Rayleigh scattering varies as λ^{-4} and so it is strongest at short wavelengths. The other intrinsic loss is caused by electronic absorption due to a lattice absorption band, this is marked on the diagram as material absorption. This absorption peaks at $9\mu m$ but it is a very broad band and so extends down to about $1.6\mu m$. The final major loss mechanism is due to the absorption of the OH^- ion. This absorption occurs at $2.7\mu m$ but there are also peaks at $1.4\mu m$, $0.95\mu m$ and $0.725\mu m$ due to resonances.

This loss profile leaves 3 windows available for optical transmission. The first window occurs at 850nm where the loss is $\sim 10dB$, this window was originally used as there were readily available sources and detectors which operated at this wavelength. The second window occurs at $1.3\mu m$ in this window not only is the loss low but it is also

the wavelength of zero dispersion for standard or step index fibre. This has led to large amounts of standard fibre being installed in the ground. The final window has the lowest loss of $\sim 0.2dB$ and occurs at $1.55\mu m$ this window has become increasingly popular due to the invention of Erbium doped fibre amplifiers [25, 26], and dispersion shifted fibre. With the use of dispersion management it is also possible to use this window in standard fibre (see chapters 6 and 7).

2.3.5 Birefringence

One of the assumptions that was made during the derivation of the GNLSE in section 2.2 was that the field could be treated as a scalar. In real fibres the field has to be treated as a vector. This is because the fibre is birefringent, that is the two polarisations have different refractive indices [27, 28, 29]. This case can be described by two coupled nonlinear Schrödinger equations as given by [30];

$$-i\frac{\partial E_x}{\partial z} = i\frac{\beta_{1x}}{2}\frac{\partial E_x}{\partial t} + \frac{1}{2}\beta_{2x}\frac{\partial^2 E_x}{\partial t^2} + \gamma_{NL}\left(|E_x|^2 + \frac{2}{3}|E_y|^2\right)E_x \tag{2.42}$$

$$-i\frac{\partial E_y}{\partial z} = -i\frac{\beta_{1y}}{2}\frac{\partial E_y}{\partial t} + \frac{1}{2}\beta_{2y}\frac{\partial^2 E_y}{\partial t^2} + \gamma_{NL}\left(|E_y|^2 + \frac{2}{3}|E_x|^2\right)E_y \tag{2.43}$$

An ideal optical fibre, with a perfectly circular core is not birefringent, however in reality all fibres are at least slightly birefringent. This is caused by the ellipticity of the core which means there are two axes with slightly different propagation constants. The ellipticity of the core varies widely along the length of the fibre on a length scale 10-100m and is very susceptible to changing conditions. The birefringence causes the two polarisations to go in and out of phase as the light propagates and so the polarisation state rotates as the light travels down the fibre. The polarisation follows an elliptical path, although if it is launched along one of the axes there is no rotation.

The quickly varying birefringence can scramble the polarisation of non-soliton pulses leaving them with unpredictable polarisation states after they have propagated over short distances [27, 29]. If it is necessary to maintain the polarisation state of an optical signal polarisation maintaining fibre can be used. This fibre is designed to have large birefringence by increasing the ellipticity of the core. This means that fluctuations in the shape are only small perturbations to the designed shape and do not significantly change the birefringence [31]. The special case of solitons in birefringent fibre will be considered in section 2.6.3.

2.3.6 Cross phase modulation and nonlinear polarisation rotation

Cross phase modulation (XPM) is said to occur when the phase of one wave is altered by the intensity of a second wave. This can occur between waves of the same or different frequencies and polarisations. Cross phase modulation is a result of the nonlinear refractive index which was discussed in relation to SPM in section 2.3.3. For waves of the same polarisation the effect of an optical signal on the phase of a copropagating wave is twice the effect on its own. This is not the case for waves of different polarisations which will be looked at in more detail later in this section. The effects of XPM on solitons will be discussed in the section on soliton interactions (section 2.6.6).

As mentioned in the previous section, the birefringence of optical fibres can affect the polarisation state of an optical signal, however the polarisation is also affected by the intensity of the light in each of the polarisation axes which leads to both XPM and SPM. These two effects add a nonlinear birefringence which causes higher intensities to undergo greater polarisation rotation than lower intensities. Although the Kerr effect causes both SPM and XPM the two effects have different magnitudes. The effect of one polarisation's intensity on the phase of the orthogonal polarisation is 2/3 the size of the effect on its own. The two coupled nonlinear Schrödinger equations that describe this process are given below.

$$-i\frac{\partial E_x}{\partial z} = i\frac{\beta_{1x}}{2}\frac{\partial E_x}{\partial t} + \frac{1}{2}\beta_{2x}\frac{\partial^2 E_x}{\partial t^2} + \gamma_{NL}\left(|E_x|^2 + \frac{2}{3}|E_y|^2\right)E_x \qquad (2.44)$$

$$-i\frac{\partial E_y}{\partial z} = -i\frac{\beta_{1y}}{2}\frac{\partial E_y}{\partial t} + \frac{1}{2}\beta_{2y}\frac{\partial^2 E_y}{\partial t^2} + \gamma_{NL}\left(|E_y|^2 + \frac{2}{3}|E_x|^2\right)E_y \qquad (2.45)$$

Nonlinear polarisation rotation (NPR) can be used as a form of saturable absorber by placing a polariser at the end of the length of fibre at an angle so that higher intensities, which have rotated, are transmitted whereas low intensities are attenuated. Such a system tends to produce soliton pulses since solitons rotate as a whole and so the low intensity wings are not attenuated more than the peak. The response of an NPR saturable absorber can be found as below [32, 33, 34, 35, 36]:

Assume the input field $\mathbf{E_o}$ is linearly polarised with an angle of θ, the two input fields will then be given by;

$$E_x = |\mathbf{E_o}|cos\theta \tag{2.46}$$

$$E_y = |\mathbf{E_o}|sin\theta \tag{2.47}$$

After propagating through fibre of length z with refractive indices n_x and n_y on the axes and a nonlinear refractive index of n_2 the fields will be:

$$E_x = |\mathbf{E_o}|cos\theta e^{i\phi_x} \tag{2.48}$$

$$E_y = |\mathbf{E_o}|sin\theta e^{i\phi_y} \tag{2.49}$$

where

$$\phi_x = \frac{2\pi z}{\lambda}\left(n_x + n_2\left(|E_x|^2 + \frac{2}{3}|E_y|^2\right)\right) \tag{2.50}$$

$$\phi_y = \frac{2\pi z}{\lambda}\left(n_y + n_2\left(|E_y|^2 + \frac{2}{3}|E_x|^2\right)\right) \tag{2.51}$$

If the field then passes through a polariser at angle θ_1 such that $\theta_1 = \theta + \frac{\pi}{2}$ then the total field after the polariser is given by;

$$E = |\mathbf{E_o}|sin\theta cos\theta e^{i\phi_y} - |\mathbf{E_o}|sin\theta cos\theta e^{i\phi_x} \tag{2.52}$$

linearly polarised at an angle of θ_1. Note that for $\theta_1 = \theta + \frac{\pi}{2}$, $cos\theta_1 = -sin\theta$ and $sin\theta_1 = cos\theta$.

Translating this field back to the x and y axes gives;

$$E_x = |\mathbf{E_o}|\left(sin^2\theta cos\theta e^{i\phi_x} - sin^2\theta cos\theta e^{i\phi_y}\right) \tag{2.53}$$

$$E_y = |\mathbf{E_o}|\left(sin\theta cos^2\theta e^{i\phi_y} - sin\theta cos^2\theta e^{i\phi_x}\right) \tag{2.54}$$

The output power of the polariser is proportional to the sum of these two fields squared.

$$P \propto |E_x|^2 + |E_y|^2 \tag{2.55}$$

$$= |\mathbf{E_o}|^2 \Big[cos^2\theta sin^4\theta \left(e^{i\phi_x} - e^{i\phi_y}\right)\left(e^{-i\phi_x} - e^{-i\phi_y}\right) + sin^2\theta cos^4\theta \left(e^{i\phi_y} - e^{i\phi_x}\right)\left(e^{-i\phi_y} - e^{-i\phi_x}\right)\Big] \quad (2.56)$$

$$= |\mathbf{E_o}|^2 \Big[cos^2\theta sin^4\theta \left(2 - e^{i(\phi_y-\phi_x)} - e^{-i(\phi_y-\phi_x)}\right) + sin^2\theta cos^4\theta \underbrace{\left(2 - e^{i(\phi_y-\phi_x)} - e^{-i(\phi_y-\phi_x)}\right)}_{= 4sin^2\frac{\Delta\phi}{2}}\Big] \quad (2.57)$$

Where $\Delta\phi = \phi_y - \phi_x = \frac{2\pi z}{\lambda}(n_y - n_x + \frac{n_2}{3}(|E_y|^2 - |E_x|^2))$

$$= |\mathbf{E_o}|^2 4sin^2\frac{\Delta\phi}{2}\left(cos^2\theta sin^4\theta + sin^2\theta cos^4\theta\right) \quad (2.58)$$

$$= |\mathbf{E_o}|^2 4sin^2\frac{\Delta\phi}{2}\left(cos^2\theta sin^2\theta\left(sin^2\theta + cos^2\theta\right)\right) \quad (2.59)$$

$$= |\mathbf{E_o}|^2 sin^2\frac{\Delta\phi}{2} sin^2 2\theta \quad (2.60)$$

In terms of power this gives:

$$P_{out} = P_{in} sin^2\frac{\Delta\phi}{2} sin^2 2\theta \quad (2.61)$$

This formula shows that if the light is launched along one of the fibres axes, i.e $\theta = \frac{n\pi}{2}$, then there is no output from the polariser as there is only one field and so XPM cannot take place. If the light is input at $\theta = \frac{\pi}{2}$ then 100% switching should be possible however in this case the two fields are equal and so there is no rotation. This is effectively because the switching power is infinite for this input angle. An example switching curve is given in figure 2.11.

2.4 Solitons

2.4.1 Introduction

The existence of spatial optical solitons which are not considered in this thesis was first suggested by Zakharov and Shabat in 1972 [37], the use of temporal solitons for optical fibre communications was first suggested by Hasegawa and Tapert in 1973 [38]. It then took several years before suitable sources and low loss fibres were available to carry out experiments. The first experimental observation of solitons in optical fibres was carried out by Mollenauer et al in 1980 [39].

Optical solitons exist when there is a balance between nonlinear effects and dispersive

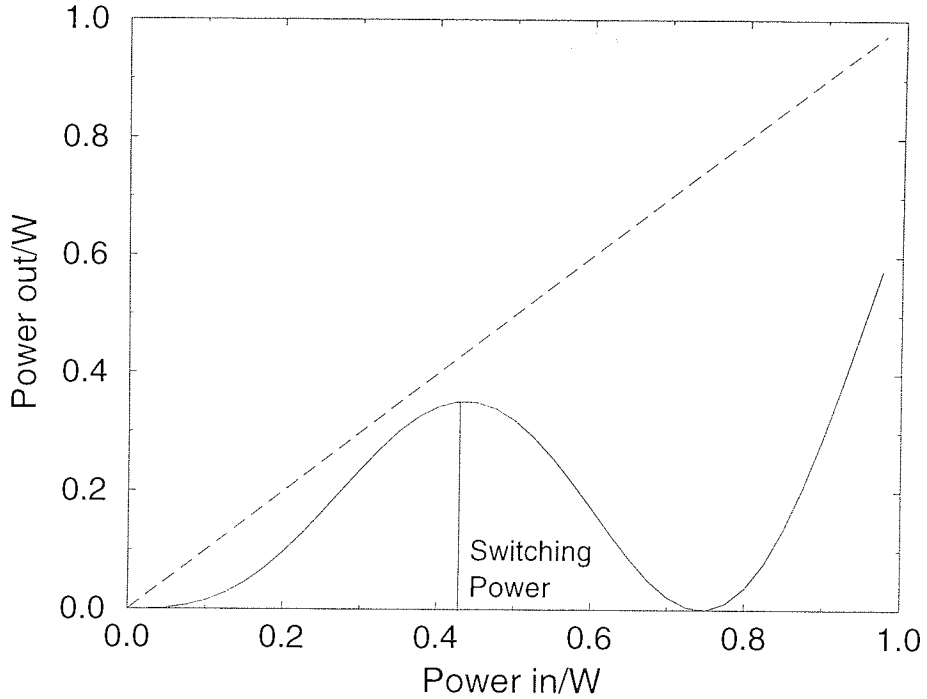

Figure 2.11: Switching curve for an NPR saturable absorber. The launch angle was 0.6rad with the polariser at 2.17rad.

effects. In terms of the length scales discussed in section 2.2 this is the regime where $L \geq L_D$ and $L \geq L_{NL}$. The dispersion must also be of the correct sign if solitons are to be created. In normal dispersion fibre stable continuous wave (CW) propagation is possible but pulses are unstable and broaden more quickly than they would due to dispersion alone because the induced chirps from these two effect are of the same sign. High frequencies are created on the trailing edge of the pulse and low frequencies are created on the leading edge of the pulse. High frequencies have a lower velocity in normal dispersion fibre so the nonlinearity and dispersion combine to cause a large amount of pulse spreading.

In anomalous dispersion CW is no longer stable due to an effect called modulation instability [40]. This means that any deviation from a perfect CW signal leads to pulses being formed. Optical pulses called solitons can exist without broadening when there is anomalous dispersion.

2.4.2 Soliton solution of the nonlinear Schrödinger equation

In order to examine solitons it is necessary to look at the nonlinear Schrödinger equation [41]. For simplicity the lossless case will be considered. The effects of loss on optical solitons will be examined in section 2.6.2.

$$i\frac{\partial A}{\partial Z} = \frac{1}{2}\beta_2\frac{\partial^2 A}{\partial T^2} - \gamma|A|^2 A \tag{2.62}$$

This equation can now be normalised with the sign of β_2 taken as -1 since only the anomalous regime will be considered. For the normalisation we take [42];

$$u = N\frac{A}{\sqrt{P_o}}, z = \frac{Z}{L_D}, \tau = \frac{T}{\tau_o}, \tag{2.63}$$

where P_o is the peak power of the pulse, L_D is the dispersion length. τ_o is the input pulse width and N is defined as;

$$N^2 = \frac{L_D}{L_{NL}} = \frac{\gamma P_o \tau_o^2}{|\beta_2|} \tag{2.64}$$

This gives;

$$i\frac{\partial u}{\partial z} + \frac{1}{2}\frac{\partial^2 u}{\partial \tau^2} + |u|^2 u = 0 \tag{2.65}$$

If the equation is being used to describe propagation in normal dispersion fibre the second term becomes negative.

The NLSE can be solved using the inverse scattering method which was devised by Gardener et al [43] and was originally used to solve the NLSE by Zakharov and Shabat [37]. This method will not be discussed here however the result is given below.

$$u(z,\tau) = 2\sigma sech\left(2\sigma\tau\right) exp\left(2i\sigma^2 z\right) \tag{2.66}$$

The eigenvalue σ gives the soliton amplitude and is also related to the pulse width and phase. Normalising such that $2\sigma = 1$ gives the normal form of the fundamental soliton.

$$u(z,\tau) = sech(\tau)exp(iz/2) \tag{2.67}$$

Therefore if a hyperbolic secant pulse with width and peak power such that N=1, i.e.

$$P_o = \frac{|\beta_2|}{\gamma\tau_o^2}, \tag{2.68}$$

is launched into a lossless optical fibre with no higher order dispersion and only Kerr

nonlinearity it will propagate undistorted for an infinite length without altering its shape, peak power or width. An example of a first order soliton can be seen in figure 2.12. The pulse width and peak power of a first order soliton are linked so a pulse with a higher peak power must have a shorter pulse width to form a first order soliton [44].

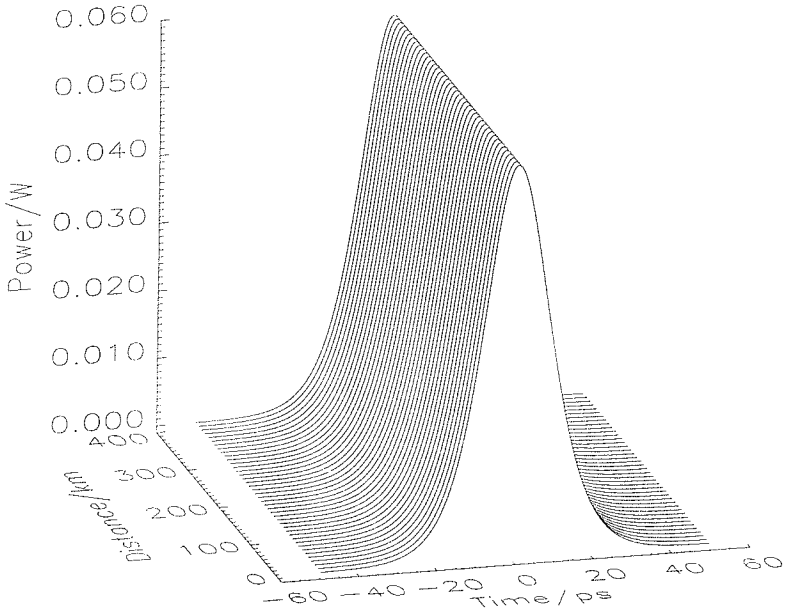

Figure 2.12: A 20.0ps first order soliton in lossless standard fibre (D=16.75ps/(nm km)) propagating over 40 soliton periods

Solitons have a characteristic length scale associated with them. It will be seen later that for higher order solitons this length scale represents the distance over which the soliton returns to its original pulse shape. Although first order solitons do not change shape the soliton period is significant when any perturbations are included in the system [45]. The soliton period is given by;

$$Z_o = \frac{\pi}{2} L_D = \frac{\pi \tau_o^2}{2|\beta_2|} \tag{2.69}$$

Over this length scale the phase of the soliton changes by $\pi/2$ this length is used largely due to its significance with higher order solitons. It is often more appropriate to use the length over which the phase changes by 2π which is 8 times the soliton period.

One of the factors that make solitons useful in practical terms is their stability, i.e. even if the pulse shape is incorrect or if the balance between peak power and pulse width is not precisely met then a soliton will emerge after travelling over a few soliton periods

by shedding excess energy as dispersive radiation. As will be noted in later chapters this effect also means that solitons will return to their original pulse shape if subjected to perturbations. It also means that if two solitons collide they retain their shape after the collision which makes them ideal for wavelength division multiplexing [46].

2.4.3 Higher Order Solitons

Although only first order solitons are used in fibre optic transmission it is interesting to consider higher order solitons [44]. Higher order solitons have an initial pulse shape of the form;

$$u(0,\tau) = Nsech(\tau) \tag{2.70}$$

where the number N gives the order of the soliton. For the same pulse width a higher order soliton has a peak power that is N^2 times that of a first order soliton. Higher order solitons do not retain their initial shape for the entire transmission distance. They undergo a complicated evolution which becomes more complicated as the order of the soliton increases. The soliton returns to its initial pulse shape every soliton period. The reason for this evolution is that the nonlinear length is shorter than the dispersion length and so the pulses become chirped. The chirping causes the pulse to split into two or more smaller pulses which then interact and collapse to form a single pulse again. An example of the evolution of a third order and a fifth order soliton over one soliton period are shown in figures 2.13 and 2.14.

2.5 Numerical solution of the GNLSE

The results presented in this thesis rely on numerical simulations of the GNLSE. These simulations were carried out using a number of routines written in FORTRAN-77. By far the most important of these is the one used to calculate the effects of propagating an optical signal down a fibre. This was carried out using the split-step Fourier method which is the fastest technique for equivalent accuracy [47].

The split-step method works by solving the linear and nonlinear parts of the equation separately over a length δz and it is this splitting of the equation which gives the technique its name. The GNLSE is then considered to have two parts as given below.

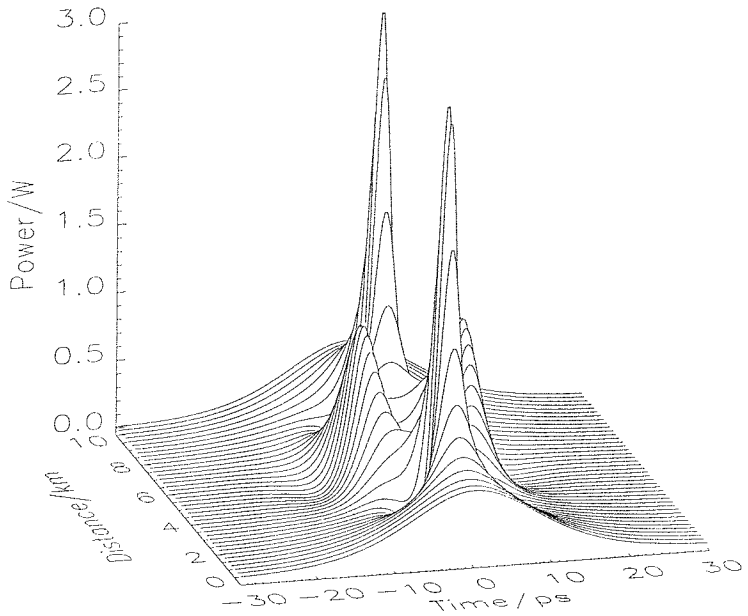

Figure 2.13: A 20.0ps third order soliton in lossless standard fibre (D=16.75ps/(nm km)) evolving over 1 soliton period

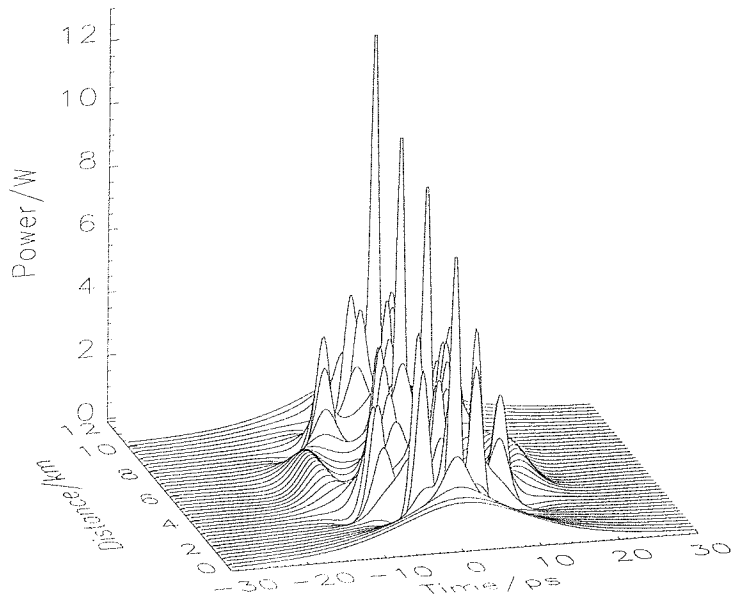

Figure 2.14: A 20.0ps fifth order soliton in lossless standard fibre (D=16.75ps/(nm km)) evolving over 1 soliton period. It should be noted that the pulse returns to its initial shape at the end of the period.

$$i\frac{\partial u}{\partial z} = \hat{L}(u) + \hat{N}(u) \tag{2.71}$$

If only the simplest case is considered, i.e. no loss or higher order dispersion then the two parts of the equation are given by;

$$\hat{L}(u) = \frac{\beta_2}{2}\frac{\partial^2 u}{\partial t^2} \tag{2.72}$$

$$\hat{N}(u) = \gamma_{NL}|u|^2 u \tag{2.73}$$

Further terms such as loss and higher order dispersion can be added to the linear term. Both of these equations can be integrated quite easily. The linear part is integrated by first taking its Fourier transform. This is done because under the Fourier transform $\frac{\partial u}{\partial T} = -i\omega$ once this transformation has been used the linear part of the equation has the solution;

$$u(\omega, z+\delta z) = u(\omega, z) exp\left(i\frac{\beta\delta z\omega^2}{2}\right) \tag{2.74}$$

Once this calculation has been done the inverse Fourier transform is taken.

The nonlinear part of the equation can be integrated to give;

$$u(t, z+\delta z) = u(t, z) exp\left(i\gamma_{NL}\delta z|u|^2\right) \tag{2.75}$$

The main reason for the relative speed of this technique is the efficiency with which computers can calculate Fourier transforms using the fast Fourier Transform (FFT). The majority of calculations in this thesis were carried out using the split-radix FFT rather than the more traditional radix-2 method [48]. This method is faster than the radix-2 method as it maximises the number of trivial multiplications [49, 50, 51, 52].

The accuracy of the split-step Fourier method is improved by carrying out each stage of length δz in the following manner. Firstly a half linear step of length $\delta z/2$ is carried out, followed by a full nonlinear step. Finally another half linear step is done to complete the calculation. This increases the accuracy of the calculation to $(O\delta z^3)$. When several steps are calculated one after the other the consecutive half steps can be combined to make full steps.

A further improvement to the accuracy of this model can be attained through the use of an extrapolation scheme [53]. In order to calculate a length of $6\delta z$ four forward steps of length δz are calculated first. Then one backwards step of length $2\delta z$ is calculated followed by a further four forward steps of length δz. By using this method the errors of size $O\delta z^3$ cancel each other leaving an error of $O\delta z^5$. Although this technique increases the number of calculations it is compensated for as larger step sizes can be used.

The accuracy of the results does not only depend on the integrity of the algorithm. The size of the steps used and the temporal/spectral resolution are also important. In terms of the temporal/spectral resolution it is important to keep the pulse so that it occupies the same proportion of both the spectral and temporal windows. It is also best to keep the grid spacing in these windows as small as possible. The integrity of the results can be checked in several ways. Firstly it is possible to run known results such as an N=2 soliton over one soliton period. It is also best to try decreasing the step size (i.e increasing the accuracy) to ensure that this does not cause any noticeable change in the results. In the cases where the numerical simulations relate to an experiment then the results can be compared to the experimental findings. It is not possible to get an exact match with experimental results since the experimental parameters are not always precisely known and it is not practical or possible to include everything that occurs in an experiment. Indeed the purpose of carrying out numerical simulations is to keep the system as simple as possible to gain greater understanding. For this reason such things as loss or third order dispersion are only included when their effects are of specific interest or thought to have a large contribution to the result.

In the simulations where data is used the calculations are usually carried out using 4 separate simulations with the results combined. Four files with 24 bits are used rather than a single file with 96 bits to increase efficiency and to make sure that resolution of the results is not sacrificed. As the temporal window "wraps round" the pulses at the edge of the temporal window still experience interactions on both sides due to the pulse at the opposite edge of the window.

Other elements such as filters, saturable absorbers, polarisers and amplifiers are also used. The equations used to describe some of these elements are given later in the thesis. The amplifier used simply increases the size of the pulse by the correct amount and adds noise if required. It is sometimes necessary to simulate the amplifier working in saturation in order to stabilise the pulse energy. This is done simply by comparing the pulse energy to the input value and giving a linear decrease of the gain (in dB) as the pulse energy

increases. The amplifier noise is added in the spectral domain with uniform phase and amplitude distribution. The amount of noise is determined by the initial conditions and a standard random number generator is used.

2.6 Solitons in optical communications

2.6.1 Introduction

So far solitons have only been considered in ideal conditions. In real optical fibre and when more than one soliton is considered there are several additional problems. Due to the stability of the soliton they do not tend to break up under perturbations and can recover their shape afterwards.

The first problem to be considered is the effect of loss and gain. This leads to the introduction of the idea of an average or guiding centre soliton. The introduction of gain into the system also leads to noise being added at the amplifier. Noise causes two major problems, the first is a timing jitter known as Gordon-Haus jitter and the second is the signal to noise ratio at the receiver. There are several solutions to these problems including filtering and the use of a saturable absorber.

There can also be undesirable effects caused by soliton interactions. If the solitons are in the same channel then the two pulses can collapse to form a single pulse. If the solitons are in different channels then they pass through each other and retain their original shape however they can be left with a timing jitter. Other effect such as Raman scattering, Brillouin scattering and the effects of electrostriction will also be considered.

2.6.2 Loss and the average soliton

Since solitons are formed when there is a balance between the nonlinear self-phase modulation and group velocity dispersion the effect of loss could be quite considerable [54]. As the pulse is attenuated the peak power drops and so the amount of self-phase modulation is reduced. This clearly means that it is impossible to retain a balance between GVD and SPM throughout the length of the fibre unless the GVD also experiences an exponential decay [55, 56, 57] or there is amplification along the entire length of the fibre [58]. The pulse power can be periodicly restored through the use of Erbium doped fibre amplifiers and it has been shown that as long as the peak power of the pulse averaged over the length of fibre is equal to the first order soliton power then stable propagation is possible. The

idea that it is the average power which is important is called the average [59] or guiding centre soliton model [60, 61].

As the length of the amplifier in these systems is so small compared to the length of attenuating fibre it can be considered to give lumped amplification. In order to examine what happens in lossy fibre the starting point is the GNLSE with loss.

$$i\frac{\partial u}{\partial z} + \frac{1}{2}\frac{\partial^2 u}{\partial \tau^2} + |u|^2 u = -i\gamma u \tag{2.76}$$

where γ is the normalised loss given by;

$$\gamma = \frac{\alpha}{2} L_D \tag{2.77}$$

Equation 2.76 describes the propagation of the pulse through the attenuating fibre. In order to describe the effect of the lumped amplification the field before the amplifier will be taken as u_1 and the field after the amplifier as u_2 these two field are then related by;

$$u_2 = u_1 exp(\gamma z_a) \tag{2.78}$$

where z_a is the distance between amplifiers.

If the transformation $u(z,\tau) = \Lambda(z)R(z,\tau)$ is used in equation 2.76 to account for the loss the equation becomes;

$$i\frac{\partial R}{\partial z} + \frac{1}{2}\frac{\partial^2 R}{\partial \tau^2} + \Lambda^2(z)|R|^2 R = 0 \tag{2.79}$$

where

$$\Lambda(z) = \Lambda(0)e^{-\Gamma(z-mz_a)} \tag{2.80}$$

$\Lambda(z)$ is used in this equation to represent the periodically varying nonlinear constant. The idea behind the average soliton is that if the amplifier period is short compared to the soliton period then it is the average of this value which is important. Therefore for a fundamental soliton the average of $\Lambda^2(z)$ should be set equal to 1.

$$< \Lambda^2(z) >= \frac{1}{z_a}\int_0^{z_a} \Lambda^2(z)dz = 1 \tag{2.81}$$

this gives;

$$\Lambda^2(0) = \frac{2\gamma z_a}{1 - e^{-2\gamma z_a}} \tag{2.82}$$

The input power for an average, N=1 soliton is therefore a factor of $\Lambda^2(0)$ greater than the value found for the lossless case. For the average soliton condition to apply the distance between amplifiers L_a must be given by $L_a \ll 8Z_o$ [59]. In general average soliton transmission is possible if $L_a < 8Z_o/10$.

Figure 2.15 gives a graph of pulse peak power against distance for an average soliton. Figures 2.16 and 2.18 show the propagation of a soliton. Figure 2.16 shows the case where the amplifier distance is much less than the soliton period whereas figure 2.18 shows the case where they are about the same size. In figure 2.16 a pulse of width 20ps is being propagated down fibre with dispersion of 0.5ps/(nm km) and loss of 0.2dB/km. This gives a soliton period of 268.8km which is far longer than the amplifier span length of 50km. The correct pulse power for this loss and amplifier span is N=1.6. It is clear from this figure that there is very little instability in this system. In figure 2.18 the fibre dispersion has been increased to 17ps/(nm km) (standard fibre) which reduces the soliton period to 20km so that this is no longer an average soliton. There are clear amplitude and pulse width fluctuation in this pulse and the pulse is shedding dispersive radiation. The pulses break down because there is resonant coupling between the soliton and the background radiation which is phase matched by the periodic nature of the amplifier train [62, 63, 64]. As energy is lost to the side bands the pulse breaks up [65]. The growth of these sidebands can clearly be seen in figure 2.19 which is a plot of the pulse's spectrum this can be contrasted with figure 2.17 which shows the same plot for the case where the average soliton criteria are fulfilled.

It is, therefore, possible to propagate solitons in a real system where periodic loss and gain have to be taken into account [66]. The correct input power must be used and the amplifier span must be shorter than the soliton period. The idea that the perturbation caused by loss and gain must take place over a shorter distance than the soliton period can be extended to other perturbations such as changes in the fibre dispersion, either through design or fluctuations in the fibre [45].

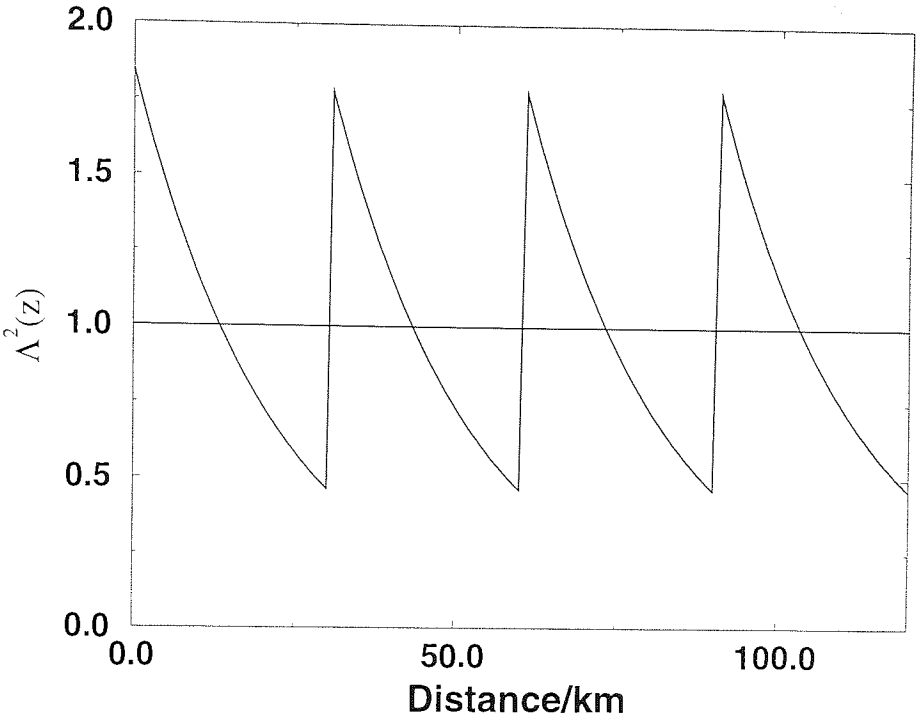

Figure 2.15: $\Lambda^2(z)$ against distance for an average soliton in fibre with loss of 0.2dB/km and a 40km amplifier span.

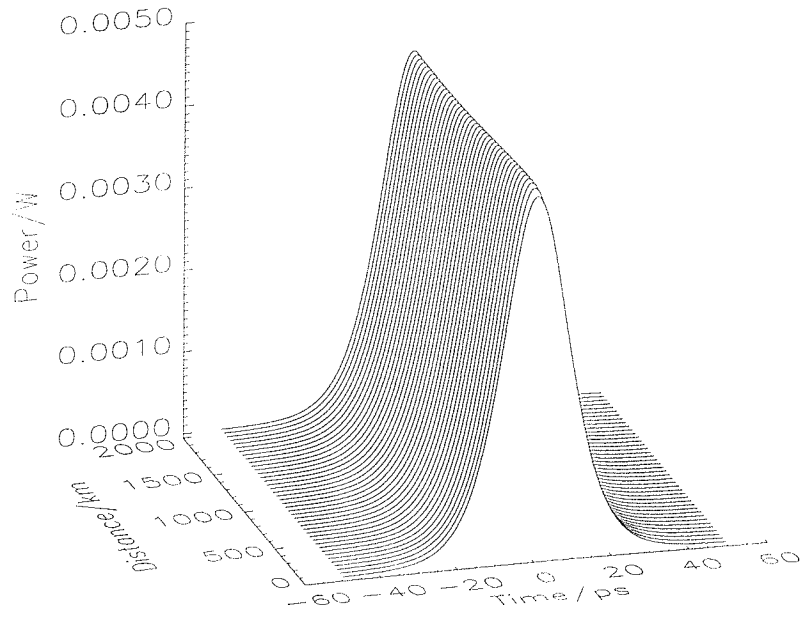

Figure 2.16: A 20ps soliton pulse that fulfils the average soliton criteria.

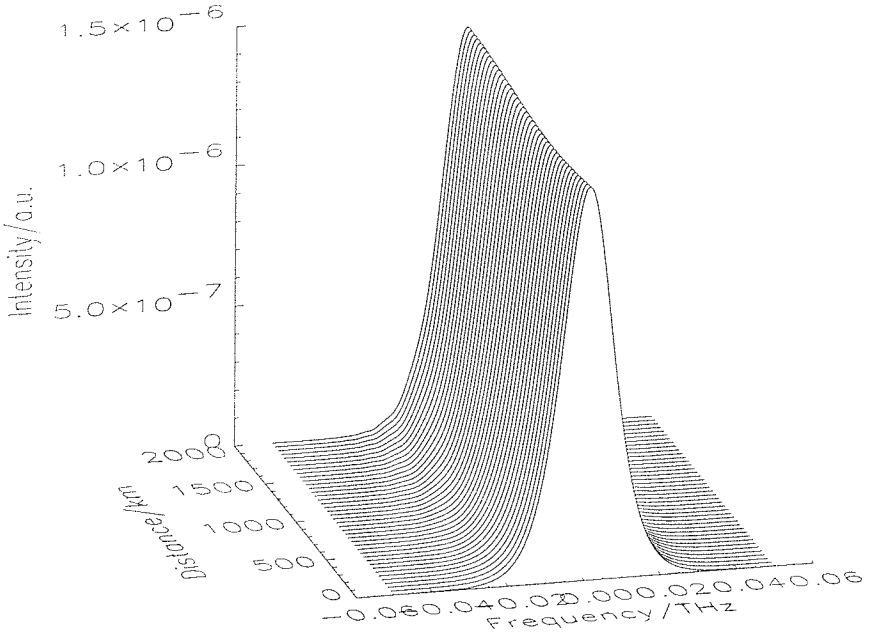

Figure 2.17: Spectrum of the above pulse that fulfils the average soliton criteria. The spectrum does not change substantially during propagation.

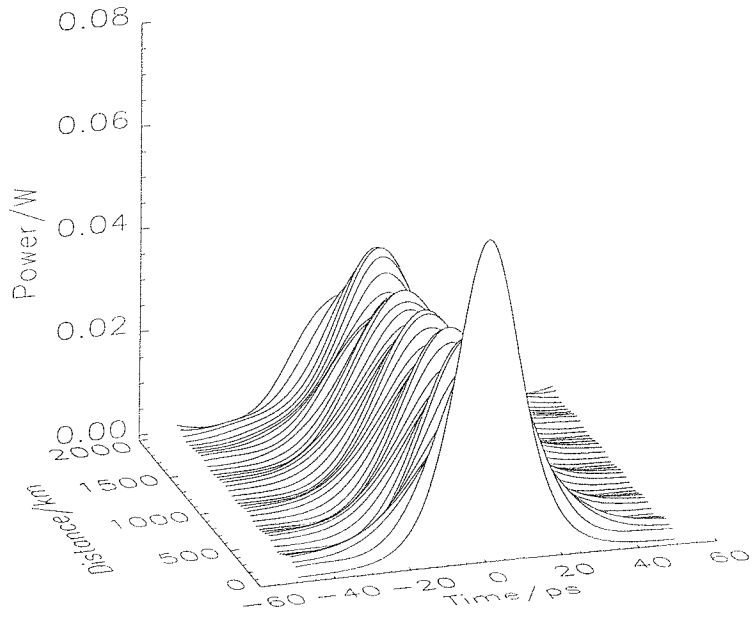

Figure 2.18: A 20ps soliton pulse that does not fulfil the average soliton criteria. Amplitude and width fluctuations can be seen along with the shedding of radiation.

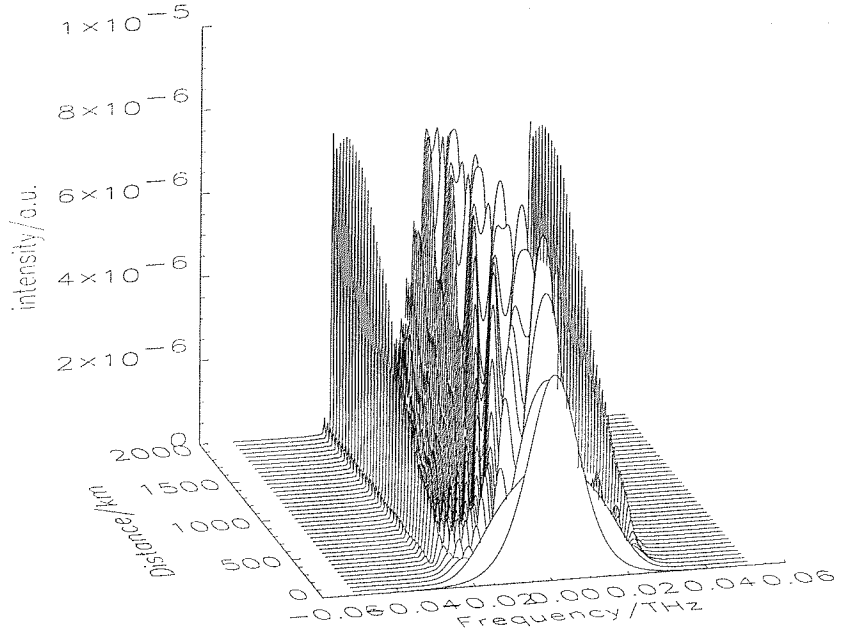

Figure 2.19: Spectrum of the pulse that does not fulfil the average soliton criteria. The growth of spectral sidebands can clearly be seen.

2.6.3 Polarisation effects

The slight birefringence in real optical fibre, as discussed in section 2.35, can result in the two polarisation modes of an optical signal splitting which leads to errors [27, 29]. The state of polarisation varies rapidly along a length of fibre which can lead to an optical signal developing a complicated polarisation state after propagating over a short distance. This is known as polarisation mode dispersion (PMD) and due to its effect it is necessary to test the components of a linear optical transmission line carefully to minimise the amount of PMD [67, 68].

Cross phase modulation due to the nonlinear Kerr effect can limit the effect of PMD in both non-return to zero [69] and soliton systems [12, 70]. The two polarisation modes of the soliton shift each other's frequency by enough to bring the velocities of the two polarisations to the same value. This can only happen if the GVD is large compared to the PMD to give sufficient nonlinearity. The size of the required dispersion is given by;

$$\Delta\beta/h^{1/2} \leq 0.3D^{1/2} \tag{2.83}$$

where $\Delta\beta$ is the differential delay between the two polarisations, D is the dispersion and h is the rate at which light is scattered from the slow axes to the fast axes. Therefore

using soliton pulses gives a benefit when PMD is considered.

The other polarisation effect that is important is that the interactions (see section 2.6.6) are reduced between solitons in orthogonal polarisations [71, 72]. This means that higher data rates can be used if alternate solitons have orthogonal polarisations which gives a relatively simple method of doubling the data rate of a transmission line. This concept is known as polarisation multiplexing and has been successfully used in several experiments [73, 5, 74, 75].

2.6.4 Signal-to-noise ratio.

Once amplifiers have been included in a soliton system other problems must also be considered. Not only do the amplifiers add gain to the system they also introduce noise through spontaneous emission. The noise is then amplified with the signal at the next amplifier and is also added to through more spontaneous emission. This noise is called amplified spontaneous emission (ASE). This means that after several amplifier spans there is a significant noise level which can introduce errors. There are other sources of noise such as shot noise and thermal noise from the detector but these are far less significant when considering long distance propagation with long amplifier spacing and therefore high gain at the amplifiers [76].

The signal-to-noise ratio is used to give the relative sizes of the signal and the noise it is generally given by the mean square current due to the signal over the mean square current of the noise, both at the receiver.

$$SNR = \frac{< i_s^2 >}{< i_n^2 >} \tag{2.84}$$

where i_s and i_n are the detector currents due to the signal and the noise.

If it is assumed that the photodiode is placed immediately after an amplifier then the signal current is given by;

$$< i_s^2 >= \frac{(P_o e)^2}{(h\nu)^2} \tag{2.85}$$

where P_o is the power output from the amplifier, h is Planck's constant, e is the charge on an electron and ν is the frequency of the signal.

Since, for long amplifier spacings (i.e high gain), the noise caused by beating between the signal and the ASE is the most significant aspect in the SNR only it will be considered

here. This noise is particularly damaging as it occurs in the same frequency range as the signal current. The noise from this source at one amplifier is given by;

$$< i_n^2 >= \frac{4e^2 P_o F_o}{(h\nu)^2} \tag{2.86}$$

here F_o is the ASE noise power which is given by;

$$F_o = (G-1)\mu h\nu \Delta\nu \tag{2.87}$$

where G is the gain of the amplifier, μ is the inversion factor for the amplifier ($\mu = 1$ for an ideal amplifier) and $\Delta\nu$ is the bandwidth of the amplifier.

The signal to noise ratio given by equations 2.85 and 2.86 after n amplifiers is:

$$SNR = \frac{(P_o e/(h\nu))^2}{(4ne^2 P_o F_o)/(h\nu)^2} = \frac{P_o}{4nF_o} \tag{2.88}$$

$$SNR = \frac{P_o}{4n(G-1)\mu h\nu \delta\nu} \tag{2.89}$$

Equation 2.89 can be used to see what effect the different parameters have on the SNR. Obviously if the signal power is increased the SNR is increased. In a soliton system where the signal power is fixed by the dispersion and the pulse width the best way to maximise P_o is to take the output straight after the amplifier. The SNR, therefore, puts a limit on how low the dispersion of a soliton transmission line can be. The most interesting parameters to look at are the gain and the number of amplifiers. For a fixed system length these two parameters are closely linked since if you reduce the number of amplifiers it would at first glance appear to increase the SNR however since the distance between amplifiers would be increased there would have to be an increase in the gain and since the change in gain is exponential with distance the overall effect is to reduce the SNR. Reducing the bandwidth can also increase the SNR, however, if the bandwidth is too small then the information in the signal can be lost. The receiver bandwidth cannot be less than half the data rate.

2.6.5 Gordon-Haus Jitter

The ASE produced by the amplifier has a more direct effect on the soliton due to the way the soliton adjusts to perturbations. The soliton parameters tend to adjust in order to retain the balance between dispersion and nonlinearity. This means that the ASE is

absorbed into the soliton and causes small changes in the soliton parameters. The most serious of these changes is the one to the pulse's central frequency which leads to a timing jitter which is known as Gordon-Haus jitter [77, 78].

Gordon-Haus jitter is caused when energy from the ASE is included in the soliton's spectrum. This causes a slight, random change in the pulses spectrum. The change in central frequency is then translated to a change in pulse velocity due to the GVD. This change in velocity results in a change in arrival time at the receiver after propagation. Since each individual pulse is affected by a different noise spectrum and is affected at every amplifier they no longer arrive in equally spaced time slots and this change in arrival time is Gordon-Haus timing jitter. When the size of the timing jitter is significant compared to the time difference between the pulses it can result in errors as pulses arrive in the wrong time slot. In order to find the limit this sets on the total propagation distance it is necessary to find the variance of the timing jitter caused by a number of amplifiers.

If the variance in the frequency from one amplifier is taken to be $< \delta\omega^2 >$ then the variance after N amplifiers is given given by;

$$< \Delta\omega_N^2 >=< \delta\omega_1^2 > + < \delta\omega_2^2 > + < \delta\omega_3^2 > +...+ < \delta\omega_N^2 > \tag{2.90}$$

if all the $< \delta\omega^2 >$ are the same this gives;

$$< \Delta\omega_N^2 >= N < \delta\omega^2 > \tag{2.91}$$

After one amplifier and propagation over one amplifier span L_a with dispersion β_2 the timing jitter is given by;

$$t_1 = L_a\beta_2\delta\omega_1 \tag{2.92}$$

The variance in the timing jitter is therefore given by;

$$< \delta t_1^2 >= L_a^2\beta_2^2 < \delta\omega_1^2 > \tag{2.93}$$

The timing jitter after two amplifiers is then given by;

$$t_2 = L_a\beta_2(2\delta\omega_1 + \delta\omega_2) \tag{2.94}$$

The variance at this point is;

$$< \delta t_2^2 >= L_a^2\beta_2^2(4 < \delta\omega_1^2 > + < \delta\omega_2^2 >) \tag{2.95}$$

The variance in the timing after N amplifiers can be given by;

$$< \Delta t_N^2 >= L_a^2\beta_2^2 \sum_{i=1}^{N} i^2 < \delta\omega^2 >= L_a^2\beta_2^2 \int^N i^2 < \delta\omega^2 > \tag{2.96}$$

$$< \Delta t_N^2 >= L_a^2\beta_2^2 \frac{N^3}{3} < \delta\omega^2 > \tag{2.97}$$

The variance in the frequency is given by;

$$< \delta\omega^2 >= \frac{2\pi n_2 N_{sp} hc(G-1)}{3t_o\beta_2\lambda^2 A_{eff}\Lambda_o^2} \tag{2.98}$$

Where n_2 is the nonlinear refractive index, N_{sp} is the spontaneous emission noise factor of the amplifier, h is Planck's constant, c is the velocity of light, G is the gain of the amplifier and Λ_o^2 is the soliton amplitude found from the average soliton model and defined in equation 2.82.

Therefore the variance after N amplifiers is given by;

$$< \Delta t_N^2 >= \frac{2\pi n_2 N_{sp}|\beta_2| hc(G-1)L^3}{9t_o\lambda^2 A_{eff} L_a \Lambda_o^2} \tag{2.99}$$

where $L = NL_a$ is the total system length. The r.m.s. jitter is found by taking the square root of this equation. This shows that the jitter increases with distance and can therefore cause problems with long distance systems. The r.m.s. jitter is proportional to $L^{3/2}$. The dependence of the jitter on amplifier span length is interesting to consider. At first glance it may appear that increasing L_a would decrease the jitter however as with the signal to noise ratio changing this parameter also affects the gain, G and the average soliton parameter Λ_o^2 which means that increasing the amplifier span in fact increases the jitter. The best way to reduce the jitter is to reduce the dispersion, however due to the

dependence of soliton power on the dispersion there is a limit on how low this parameter can be set. If the dispersion is too low there are also problems with higher order dispersion and polarisation mode dispersion.

In order to give an indication of the limits Gordon-Haus jitter sets on the total possible propagation distance it is first necessary to define the amount of jitter that would give an unacceptably low bit error rate (BER). Assuming Gaussian statistics a BER of 10^{-9} requires [77];

$$< \Delta t_N^2 > \leq \left(\frac{t_w}{6.1}\right)^2 \tag{2.100}$$

where $2t_w$ is the width of the timing window of the detector.

Using this it is now possible to find the maximum propagation distance which is given by:

$$L_{max}^3 = 0.1372 \frac{t_{fwhm} T_w^2 A_{eff} L_a \Lambda_o^2}{n_{sp} n_2 D_2 h (G-1)} \tag{2.101}$$

where $D_2 = -2\pi c \beta_2 / \lambda^2$ has been used to simplify the expression.

So far this equation does not include an explicit indication of the data rate R. R can be included in the equation but it is necessary to make some assumptions about the size of the timing window of the detector compared to the time between pulses and the mark to space ratio of the pulses (i.e. the width of the pulse compared to the time between pulses). In order to do this two new parameters are required $\kappa_s = RT_{fwhm}$ which represents the mark to space ratio and is generally taken to be between 0.1 and 0.2. The other parameter represents the relative size of the timing window $\kappa_w = Rt_w$. We can now get an equation that gives the maximum propagation distance for a given data rate.

$$L_{max} = \frac{0.5158}{R} \left[\frac{\kappa_s \kappa_w^2 A_{eff} L_a \Lambda_o^2}{N_{sp} n_2 D_2 h (G-1)}\right]^{1/3} \tag{2.102}$$

This equation can easily be changed to give the maximum data rate for a given propagation distance. In the section on soliton control (2.7) it will be seen that Gordon-Haus jitter can be limited by proper use of filters, dispersion compensation, phase conjugation and other techniques.

2.6.6 Soliton Interactions

One of the other limits on the length of a soliton based communications line is a result of soliton-soliton interactions. Solitons interact due to cross phase modulation through the nonlinear Kerr effect [79, 80, 81, 82, 83]. Soliton interactions can take place between solitons of the same wavelength and solitons of different wavelengths. The case of solitons in the same wavelength channel will be considered in some detail in this section as all the results in this thesis relate to single channel systems. The processes involved in WDM interaction will be described briefly at the end of the section.

Soliton interactions occur due to nonlinearity acting on the overlapping tails of adjacent solitons. Taking the simplest case of two pulses with equal amplitude and phase the process follows this course. As the tails of the solitons overlap there is constructive interference which leads to the refractive index of the fibre increasing at this point. The higher refractive index causes the leading pulse be shifted to a lower frequency and so slow down. The trailing pulse is shifted to a higher frequency and so speeds up. As this happens it causes the overlap to increase which leads to a greater nonlinear refractive index which increases the rate at which the pulses are attracted to each other. Finally the pulses collapse to form one pulse, however as the pulses are now travelling at different velocities they separate out again with the pulse that was previously trailing now leading. The nonlinear Kerr effect causes the pulses to return to their original frequencies as they separate and eventually to collapse again. The pulses continue to interact in this way periodically.

Soliton interactions have been studied using numerical simulations, inverse scattering and soliton perturbation theory [79, 81, 84]. The latter two methods have led to a better understanding on the effects of using pulses with different amplitudes and phase. Two solitons launched into an optical fibre can be described using;

$$u(0,\tau) = sech\left(\tau - \frac{T_R/2}{\tau_o}\right) + rsechr\left(\tau + \frac{T_R/2}{\tau_o}\right)e^{i\theta} \tag{2.103}$$

where $T_R = 1/R$ is the initial separation which is defined by the data rate R, r is the relative amplitude and θ is the relative phase of the two input pulses.

If the simple case where $r = 1$, $\theta = 0$ and loss, higher order dispersion and nonlinearity are neglected is considered and we take the case where the initial separation is large compared to the pulse width (which would be the case in practice) then the period over

which the solitons collapse and separate is given by;

$$Z_p = Z_o exp\left(\frac{T_R/2}{\tau_o}\right) = Z_o exp\left(\frac{1}{2R\tau_o}\right) \tag{2.104}$$

The point where the pulses collapse occurs at half this distance this means that systems must be less than $Z_p/2$. The soliton collapse length is strongly affected by the mark to space ratio. The collapse length can be increased by either reducing the data rate which leads to the pulses starting off further apart or by reducing the pulse width which means that the intensity of the overlapping tails is reduced. The collapse distance can also be increased by having a longer soliton period. This can be done by reducing the average dispersion although the SNR means that there is a limit to how small this can be made. The soliton period can also be increased by increasing the pulse width however due to the exponential dependence of the collapse length on pulse width any increase in the soliton period by this method would lead to a net decrease in collapse length.

An example of a soliton collapsing under these conditions is given in figure 2.20. In this figure the two 20ps first order solitons are launched separated by a distance of 80ps. The fibre has dispersion of 5ps/(nm km), this means that the pulses collapse after propagating 568km and have a periodic interaction with a period of 1136km.

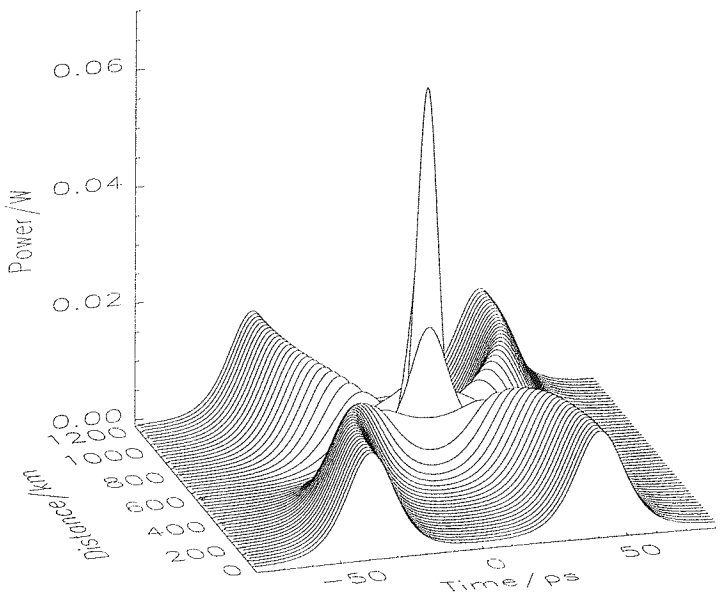

Figure 2.20: Two pulses of equal phase and amplitude as they interact and collapse before passing through each other

In the case where the two solitons are out of phase with each other, i.e $\theta = \pi$, the solitons do not attract each other but repel [84]. This is because instead of the tails of the solitons adding constructively they add destructively causing the refractive index to be lower between the solitons and so the pulses are repelled. This does not give any advantage over the case where the pulses attract each other since the solitons continue to move apart irrespective of how far they are separated and so move out of their time slots which leads to errors. This can be seen in figure 2.21 the parameters used in this simulation are the same as those used previously however here the two solitons have a π phase difference causing them to repel each other. If the solitons have a phase difference of $\theta = \pi/2$ they do not experience any interaction, however this situation is unstable and any perturbation causes the solitons to reach one of the extremes already discussed. It may appear that the interactions would be limited if the pulses were in a data stream with pulses on either side of them this is not true. Since there are spaces for 'zeroes' on the data stream the interactions can still cause large numbers of errors.

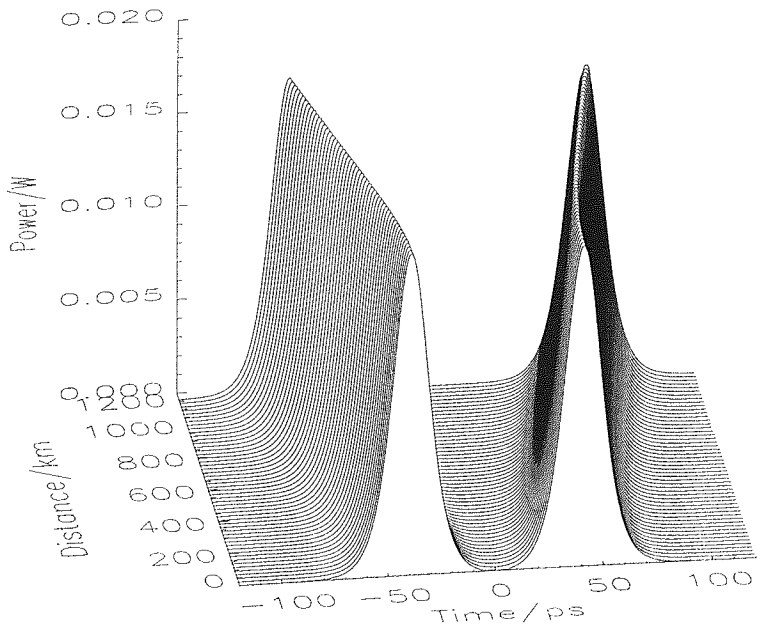

Figure 2.21: Two pulses of opposite phase and equal amplitude as they interact with each other leading to separation.

It is possible to limit the interactions by using solitons with different amplitudes [83, 85]. The difference in the amplitude of the pulses leads to the phase of the two pulses evolving at different rates and so there is only a limited periodic interaction as the pulses alternatively attract and repel each other. This method of reducing interactions is

shown in figure 2.22 and has been used successfully in propagation experiments [85, 86]. Figure 2.22 again uses the same parameters as before, although this time the pulses once again have equal phase and there is a 10% difference between the initial pulse amplitudes.

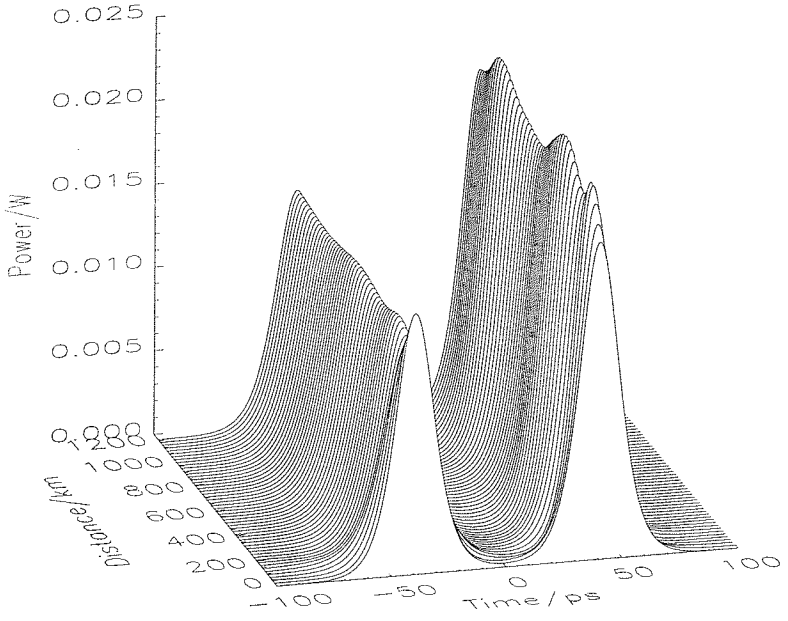

Figure 2.22: Two pulses with equal phase but a 10% difference in amplitude show much reduced interactions.

Soliton interactions between the different channels of a WDM system are also caused by the nonlinear Kerr effect however due to the pulses in different channels having different GVD they do not undergo periodic interactions. In a WDM interaction as the faster pulse moves towards the trailing edge of the slower pulse the tails of the pulses overlap. Then, as in the single channel case the pulses are attracted to each other and so the trailing pulse speeds up and the leading pulse slows down. Once the pulses collapse they separate again as they are still moving with different velocities. As the pulses separate the nonlinearity causes them to return to their original velocity. Since the solitons emerge more or less unaffected by the collision this does not cause any problems however so far this discussion has not included loss. If loss is included then the pulses do not suffer the same nonlinear shift in the second half of the collision as they did in the first and so are left with a net frequency shift by the collision. As the pulses in the different channels suffer many collisions with pulses in both slower and faster channels and since the number of collisions is essentially random as it depends on the data in the other channels the overall effect on the data is to introduce a timing jitter on the pulses.

2.6.7 Electrostriction

Electrostriction is the cause of both a self frequency shift of the solitons and an interaction which can cause timing jitter [87]. Electrostriction causes the soliton to excite acoustic waves, as these waves travel to the cladding and are reflected back towards the core they cause density changes which alter the refractive index. The self frequency shift causes a constant change in the frequency of all the pulses and so does not result in a timing jitter. It causes a larger shift for long pulses and so is not a problem for high bit rate communications. The interaction can cause timing jitter since it depends on the data pattern. The acoustic interactions are long range which means that in high bit rate systems the interactions are not between adjacent pulses. It takes the acoustic wave $\sim 20ns$ to be reflected back into the core in a fibre with a diameter of $125\mu m$. The interaction is proportional to the square of the propagation distance although filtering can reduce this to a linear dependence. It is also proportional to the square of the dispersion and so once again it is advantageous to use low dispersion to reduce this problem.

2.6.8 Higher order nonlinear effects

There are other nonlinear processes which have an effect on solitons propagating in optical fibre. The other effects that will be considered are stimulated Raman scattering, stimulated Brillouin scattering and four wave mixing.

Stimulated Raman scattering can be used to amplify solitons [54] and before being superseded by the Erbium doped fibre amplifier was the main method used to do this. It can also cause problems if very short pulses are used by causing a shift in the pulses wavelength towards longer wavelengths. This process is known as soliton self frequency shift [88, 89].

Raman scattering is best described by considering photons interacting with the medium they are travelling through. What occurs is that the incident photon is scattered by a molecule in the fibre to a lower frequency photon while the molecule goes into a higher vibrational state. The amount of downshift in the lights frequency depends on the material being used, in silica it is 13.2 THz. In general this down shift in frequency happens at a very low rate however when there is a small signal already at the lower frequency the gain at the lower frequency is almost exponential with distance.

Raman Scattering can therefore be used to amplify an optical signal by copropagating a CW signal along with the data at a frequency that is 13.2Thz above the signal frequency

[54]. This technique has been used successfully in soliton transmission schemes however the high pump powers required are not available from semi-conductor lasers and this makes an EDFA cheaper and easier to implement.

Soliton self frequency shift is also caused by Raman scattering but only affects pulses of less than 1ps. This is because these short pulses have a bandwidth which is close to the peak of the Raman gain. The high frequencies in the pulse act as a pump which amplifies the lower frequencies leading to the central frequency of the pulse moving towards longer wavelengths. Since this does not affect the bandwidth of the pulses the shift continues throughout the length of the fibre. The size of these changes in frequency can be very large with shifts in frequency that are the same size as the pulses bandwidth possible after a few hundred km of fibre.

When soliton self frequency shift is combined with ASE noise from amplifiers it can cause a timing jitter which is comparable in size to Gordon-Haus jitter [90]. This jitter comes about due to the ASE causing random changes in the pulse width which changes the size of the self-frequency shift and leads to a timing jitter through the group velocity dispersion. Pulses short enough to cause these effects are not required for single channel data rates of less than 100Gbit/s.

A related effect is stimulated Brillouin scattering [91]. It is also caused by an interaction between the light wave and phonons in the fibre. Whereas Raman scattering is caused by an interaction with optical phonons Brillouin scattering involves interaction with acoustic phonons. This means that although the interaction causes light to be scattered to a lower frequency the Stokes shifted wave is only 10GHz lower in frequency than the signal wavelength. Only pulses with narrow bandwidths are significantly affected by SBS. Pulses with widths of $> 10ns$ are degraded by SBS however these pulse are far too broad to be used in high bit rate communications systems. The powers required to cause SBS are far lower than those required for SRS. This effect does not cause a large shift in the propagating waves frequency however, because the Stokes wave propagates in the opposite direction to the incident wave, SBS causes a loss of the signal by generating a counter propagating Stokes shifted wave. Like SRS it can be used to amplify a signal and due to the narrow bandwidth involves it can be used to selectively amplify a well defined narrow frequency band.

The final nonlinear process to be considered is four wave mixing[92]. Four wave mixing (FWM) is caused by the χ_3 nonlinearity that is also involved in self- and cross- phase modulation. Four wave mixing occurs when two waves of frequency ω_1 and ω_2 interact

through a nonlinear material to produce two new waves at frequencies ω_3 and ω_4 such that;

$$\omega_1 + \omega_2 = \omega_3 + \omega_4 \tag{2.105}$$

Equation 2.105 means that the energy is conserved in the process however it is also important that the momentum is conserved which means that phase matching is also important. The phase matching condition is given by;

$$k_3 + k_4 - k_1 - k_2 = 0 \tag{2.106}$$

This type of four wave mixing can cause problems in wavelength division multiplexed systems where two of the wavelength channels can interact [93]. It is still possible to get FWM in single channel communications through degenerate four wave mixing. The conditions for energy and momentum conservation for this are given by;

$$\omega_1 + \omega_1 = \omega_3 + \omega_4 \tag{2.107}$$

$$k_3 + k_4 - 2k_1 = 0 \tag{2.108}$$

In this case the input frequencies are both at the same frequency and produces two new frequencies one up shifted and the other down shifted. These two are referred to as the Stokes and anti-Stokes bands in an analogy with SRS. This process is only properly phase matched at the dispersion zero where constant dispersion soliton propagation is not possible although it can affect RZ systems which use this frequency. There can be significant gain at the Stokes and anti-Stokes bands even when phase matching is not complete. This means that at low dispersions there can still be significant four wave mixing although this can be limited by filtering.

2.7 Soliton Control

2.7.1 Introduction

In order to combat effects such as Gordon-Haus jitter, soliton interactions and the build up of ASE noise it is necessary to add components such as filters and saturable absorbers into a transmission line. These added components can be regarded as controlling the soliton transmission. The first and most fundamental method of soliton control is the use of bandpass filters. Filters can be used to suppress the build up of ASE outside the passband and can reduce the effects of Gordon Haus jitter. They can also be effective in limiting soliton self frequency shift and soliton interactions. Further suppression of the Gordon-Haus effect can be gained by sliding the frequency of the filters along the transmission line. Other soliton control techniques that will be discussed include the use of saturable absorber, phase and amplitude modulators and phase conjugation.

2.7.2 Filtering

The main beneficial effect of filters in a soliton transmission line is that they substantially reduce the problems caused by Gordon Haus jitter [94, 95, 96, 97]. Filtering can have several other beneficial effects including stabilising the amplitude of the solitons and reducing interactions and well as suppressing the build up of ASE noise and dispersive radiation outside the passband.

As stated in section 2.6.5 the inclusion of noise from the amplifier into a soliton causes random changes in its central frequency which in turn leads to a timing jitter. The effect of the filter is to force the central frequency of the pulse back towards the pass band of the filter. This can also cause a clipping of the wings of the soliton which can be compensated for by having excess gain at the central frequency, the wings can then be restored through self phase modulation.

If the filter is too narrow then the amount of excess gain that has to be used to compensate for the clipping of the spectrum is increased. This leads to greater ASE noise which reduces the signal to noise ratio and so can result in a drop in the error free propagation distance. The effect of filters on Gordon-Haus jitter has been studied and shown to increase the total propagation distance. With filters the variance of the timing jitter is reduced by a factor f [95];

$$< T_o^2(Z) >_{filtered} = < T_o^2(Z) >_{unfiltered} f(4\delta Z) \tag{2.109}$$

where Z is the total propagation distance and δ is the excess gain to overcome the loss of the filter and is given by;

$$\delta = \frac{\pi}{6} \frac{2}{|\beta| z_a \Omega_s z_o} \tag{2.110}$$

where Ω_s is the bandwidth of the filter, z_o is the soliton period and z_a is the amplifier span length. The function f is given by;

$$f(x) = \frac{3}{2} \frac{1}{x^3} [2x - 3 + 4exp(-x) - exp(-2x)] \tag{2.111}$$

It is clear from this that for large x, which relates to large Z that the function f varies as x^{-2} which essentially means that it varies with Z^{-2}. When this dependence is considered in the context of equation 2.108 it means that the dependence of jitter with distance is not longer Z^3 but is now linear with Z. This represents a substantial reduction in the accumulated jitter over a long distance communications system.

Filters can also increase the collapse length of two adjacent solitons [98, 84, 99]. They do this because the pulses get chirped as they pass through the filter. This leads to the tails of adjacent pulses no longer interfering constructively and so there is less self-phase modulation between the pulses. As a result of the reduced self-phase modulation the pulses do not acquire the same changes to their central frequency and so the collision distance is increased. The size of the increase depends on the bandwidth of the filter and the filter profile.

A refinement of the use of filters is to use sliding guiding filters [100, 101, 102]. This involves gradually sliding the central frequency of the filter along the transmission line [103]. This has the advantage over fixed filters that narrower bandwidth filters can be used without encountering the problems of increased ASE noise through the extra excess gain required due to the loss from the filters. This is because although the soliton is able to follow the central frequency of the filters and so do not experience significant extra loss due the the sliding of the filters, the system as a whole is opaque to noise and so it is kept to a minimum [104]. Sliding the frequency of the filter passband can also give further

suppression of soliton interactions [105] Several successful experiments have been carried out using sliding guiding filters in both single channel and WDM systems [106].

The shape of the filters used can also have a beneficial effect both in terms of reducing Gordon-Haus jitter and soliton interactions [107]. Filters with a flat pass band and steeper edges such as higher order Butterworth filters [108, 109] and super Gaussian filters [110] can have narrower pass bands without requiring as much excess gain as Fabry-Perot filters. There is a down side to using higher order Butterworth filters in that the higher the order of the filter the more third order dispersion it introduces into the system. There is therefore a trade off between suppressing interactions and Gordon-Haus jitter and the introduction of third order dispersion.

2.7.3 Amplitude Modulation

Amplitude modulators can also be used to suppress Gordon-Haus jitter. An amplitude modulator is a semiconductor device which is driven by an electrical signal so that its transmission varies with time, the variation in transmission occurs at the data rate of the signal. The amplitude modulator is set so that its peak transmission occurs at the time when the pulse should be present if it has remained in the correct time slot. If the soliton has moved out of its time slot then the pulse is 'pushed' back towards the correct slot. This occurs because the part of the soliton that is at the peak of the transmission experiences less loss than other parts of the pulse. Therefore in much the same way as a filter pushes the pulse back towards the correct frequency an amplitude modulation pushes the pulse back to the correct time. Amplitude modulators do not correct the change in the pulses frequency so the pulses continue to move with different velocities. Like filtering this reduces the dependence of jitter on distance to a linear response rather than a cubic one. Amplitude modulators can also help to suppress interactions since as the pulses interact they move closer together and therefore out of their correct time slots. The amplitude modulator will push them back towards their correct time slot in this case as well which means that the interactions are effectively suppressed.

The main disadvantage of using amplitude modulators is that they are an active component and require a recovered clock signal to drive them. This adds complication and expense to the system. It also means that the system is no longer bit rate transparent as it is required to work at the rate of the modulators. If the pulse has moved too far from its correct position it could be pushed into the incorrect time slot rather than the one from which it originated since this method simply guides the pulses into the nearest time

slot, this problem does not arise as long as the modulators are used frequently enough. Amplitude modulators in conjunction with frequency guiding narrow band filters have been used successfully in experiments [111, 112, 5] and numerical simulations [113] with high data rates over, what are effectively, unlimited distances.

2.7.4 Phase Modulation

The next method of soliton control is to use phase modulators. These can either be used at every amplifier or less frequently. Like amplitude modulators, phase modulators are a form of active control and are therefore more expensive and complicated to implement than passive techniques. Phase modulators can suppress any form of timing change, whether it is caused by Gordon-Haus jitter or interactions [114].

Phase modulators work by giving the pulse a chirp if it moves out of its correct time slot. Since solitons naturally have constant phase across the entire pulse the change in the instantaneous frequency is averaged across the entire pulse to give a change in the central frequency. This frequency change can be set to over compensate for the original frequency change that caused the pulse to move from its correct time slot and so allow it to walk back towards the centre of the time slot. In this way phase modulators do not simply correct the frequency or the position changes but correct both. Unlike amplitude modulators and filters they do not significantly increase the loss of the system and so do not require excess gain and the extra ASE associated with it.

Although it is possible to use phase modulators at every amplifier this is not necessary. They can be used less frequently and simply set to give a larger frequency chirp to compensate for the larger timing and frequency changes. As with the amplitude modulator the phase modulators must be placed frequently enough so that the nearest time slot is the one to which the pulse belongs, otherwise the effect of the modulator will be to accelerate the accumulation of errors rather than to suppress them.

Phase modulation can be implemented either through the use of a bulk modulator or through cross phase modulation with a stream of clock pulses that are copropagated with the data stream in a short section of fibre or in a section of a different nonlinear material such as a semiconductor [115]. As with all active methods of control phase modulators add extra cost and complication to the system. They also remove the bit rate transparency that a system without active control would have.

2.7.5 Saturable Absorbers

So far all the control methods discussed have been aimed at removing timing jitter and suppressing interactions. Most of them have not decreased the ASE to improve the signal-to-noise ratio and if anything, due to the excess gain required to counteract the extra losses involved in these components, these techniques would increase the ASE and so degrade the signal-to-noise ratio. Saturable absorbers do not suppress the timing jitter, however they can be used to suppress the ASE and dispersive radiation, counteract soliton interactions [116, 117, 118] and to help suppress the problems that arise when the average soliton criteria given in section 2.6.2 are not met.

Saturable absorbers are optical components that absorb low intensities while transmitting high intensities. They can be fibre or semiconductor based. In fibre saturable absorption can be attained by using the Kerr nonlinearity either through nonlinear polarisation rotation [119] as described in section 2.3.6 or through the use of a nonlinear optical loop mirror [120, 121]. Both of these techniques have the disadvantage that they require long lengths of fibre and polarisation control. It is also possible to use semiconductor, multiple quantum well saturable absorbers [122, 116, 123, 124].

The concept behind using saturable absorbers to suppress ASE and dispersive radiation is quite simple. The pulse has high power and so does not experience much loss at the saturable absorber whereas the noise and dispersive radiation which are low power experience more loss and so are attenuated. When this happens it obviously improves the SNR as the noise level is greatly reduced. When saturable absorbers are being used to suppress the build up of ASE and dispersive radiation it is often not necessary to use the saturable absorber at every amplifier which means that the cost of adding saturable absorbers is reduced.

There are substantial added benefits from the saturable absorbers ability to suppress the build up of CW radiation as it is often the instability of the soliton when interacting with dispersive radiation and the degradation of the SNR from the addition of the CW radiation which leads to pulses breaking up [119, 125]. This means that with the addition of saturable absorbers it is possible to use stronger filtering without problems that arise when a large amount of excess gain is required to compensate for the clipping of the trailing edges of the spectrum leading to a build up of CW radiation at the peak of the filter transmission [126, 127]. The saturable absorber can remove the radiation and so stronger filtering leading to reduced Gordon-Haus jitter can be used.

The other area where saturable absorbers can be useful is when very short pulses

are being propagated. Since short pulses have a short soliton period it becomes difficult to fulfil the average soliton criteria which leads to the pulses breaking up as spectral sidebands are formed. A saturable absorber can effectively suppress the build up of the dispersive radiation and so extend the propagation distance possible [128].

Saturable absorbers can also increase the collision distance for adjacent solitons [129, 130]. The reason for the collision distance increasing is that the saturable absorber induces a chirp on the pulse. This leads to the pulses having a rapidly changing phase and so the pulses can neither attract or repel on a long term basis. As the pulses go in and out of phase they attract and repel each other leading to a slight oscillation in their position but no long term change in position or collapse. The use of saturable absorbers with dispersion management will be discussed in some detail in chapters 3 and 4 of this thesis.

2.7.6 Optical Phase Conjugation.

Other methods that have been used to control solitons include optical phase conjugation (OPC) or spectral inversion. When an optical signal undergoes optical phase conjugation it is transformed into its complex conjugate. This can be carried out through four wave mixing in either a piece of fibre or in a semiconductor laser amplifier. When an optical phase conjugator is placed at some point in an optical fibre transmission line the effect is to reverse the accumulated chirp up to that point in the transmission line. If the next section of fibre is the same as the fibre which induced the original chirp then the chirp will be 'undone' in the second section.

For linear pulses, OPC can be used at the midpoint of the transmission line to reverse the effects of self-phase modulation and group velocity dispersion [131, 132, 133, 134]. OPC does not reduce the effects of third order dispersion and cannot take account of self-phase modulation efficiently unless distributed amplification is used or the amplification period is much shorter than the distance over which the OPC occurs.

When OPC is used with solitons it can be either be placed at the midpoint of the transmission line or they can be placed at every amplifier [135]. When they are placed at the midpoint of the transmission line soliton interactions can be effectively suppressed or even undone [136]. This is because the solitons interact by inducing a chirp on the adjacent soliton which results in the attractive force. When the chirp is reversed so is the direction of the force and the solitons start to repel. This is only possible if the average soliton criteria are met. OPC can also be used to reduce the effects of Gordon-Haus jitter by a factor of about 2 [137] and can reverse the effects of soliton self frequency shift [138].

It is also possible to use OPC at every amplifier [135]. In this case the solitons are operating in a completely different regime. Since the conjugation is taking place on a length scale much shorter than the soliton period NLSE solitons are not formed since the GVD [131] and SPM [139] are both compensated for through the effects of OPC. It is still possible to form solitons through the balance of third order dispersion and nonlinear dispersion both of which cannot be compensated for. When the terms for third order dispersion and nonlinear dispersion are used the describe the propagation of pulses in optical fibre the resultant equation is of the form of a modified Korteweg-de Vries equation. This is a well known soliton supporting equation. Since the field is being conjugated at every amplifier soliton interactions are effectively suppressed and the effects of noise resulting in Gordon-Haus jitter are also much reduced leading to the RMS jitter increasing linearly with distance rather like the case where guiding filters are used.

2.8 Summary

The nonlinear Schrödinger equation describes the propagation of pulses in single mode optical fibre including the effects of dispersion and nonlinearity. If there is a correct balance between these two effects it is possible to propagate pulses called solitons that do not change their spectral or temporal shape during propagation. When loss and gain are added to the system it is still possible to propagate these pulses through the use of the average soliton. Solitons are stable under other perturbations such as the addition of noise however the addition of noise does induce Gordon-Haus timing jitter. The solitons can also interact with adjacent pulses. These problems can be controlled through the use of techniques such as filtering, phase and amplitude modulators, optical phase modulators and saturable absorbers.

Chapter 3

Dispersion Management

3.1 Introduction

Over recent years the potential of constructing a transmission line using sections of fibre with different dispersions has been realised [140]. This technique is known as dispersion management. The simplest and most successful dispersion maps involve alternating lengths of normal and anomalous dispersion fibre to give high local dispersion but low average dispersion. Maps of this sort have been found to support stable nonlinear pulses known as dispersion managed solitons [141]. This chapter will give a review of dispersion managed solitons.

Dispersion managed systems have high local dispersion and low average dispersion which gives many advantages. One expected advantage of low dispersion is that the Gordon-Haus timing jitter is reduced. Equation 2.99 shows how the timing jitter depends on the size of the dispersion. The low average dispersion also means that the soliton period (given by equation 2.68) is increased which means that the amplifier span length can be increased as a result of the constraints set by the average soliton model (see section 2.6.2). The high local dispersion means that the four wave mixing is inefficient as it is phase matched at zero dispersion. There are also less expected advantages that result from using dispersion management, for example dispersion managed solitons demonstrate enhanced pulse energies when compared to average solitons in optical fibre with constant dispersion [141, 142, 143, 144, 145]. This means that it is possible to use lower average dispersions and so gain further advantage from the reduced Gordon-Haus jitter [146, 147, 148, 149, 150] without degrading the signal-to-noise ratio. A further advantage of using dispersion managed solitons is that it makes it possible to operate at the zero dispersion and even to operate with a normal average dispersion [151, 152, 145, 153, 154].

This chapter will give a review of the work that has been done previously on dispersion managed solitons. This will include an examination of the effect of dispersion maps on the properties of solitons such as the pulse energy and pulse shape as well as the effect of dispersion management on such things as Gordon-Haus jitter and soliton interactions. There will also be a review of some of the experimental and numerical results that have been published for high bit rate transmission systems that use dispersion management.

3.2 Background

Dispersion management in the context of this thesis will be taken to mean a transmission line made up of alternating steps of normal and anomalous dispersion fibre. The average dispersion of the transmission line is set to be significantly less, in magnitude, than the dispersion of the constituent fibres. An example of a dispersion map is given in figure 3.1, although in this map the two sections of fibre are the same length this does not have to be the case, maps proposed for the upgrade of the standard fibre network consist of long sections of standard fibre (with anomalous dispersion) and short lengths of dispersion compensating fibre (which has large normal dispersion) [155, 156] as will be seen in chapters 6 and 7. The dispersion map can also consist on mainly normal dispersion fibre with only a short length of anomalous dispersion fibre [157] such as the dispersion map used in chapters 4 and 5.

Transmission lines made up of different dispersion fibres have been used for some time. The first dispersion maps were used in an attempt to have a dispersion profile that followed the exponential loss of the fibre. This technique involves minimising the difference between a true exponential dispersion decreasing fibre [158] (which have also been used [55, 56]) and a dispersion profile that decreases in steps and so can be more easily constructed. All the fibres used in these systems have anomalous dispersion so are not what are considered dispersion managed systems in the context of this thesis. A second precursor to dispersion management is using a section of dispersion compensating fibre at the end of the transmission line to remove some of the accumulated timing jitter from the pulses [159]. The idea behind this is that the dispersion of the line is unaffected and so a lower average dispersion could be used without having an effect on the signal-to-noise ratio [159]. In this case the decrease in dispersion at the end of the transmission line is gained at the expense of an increased pulse width which limits the amount of compensating fibre that can be used.

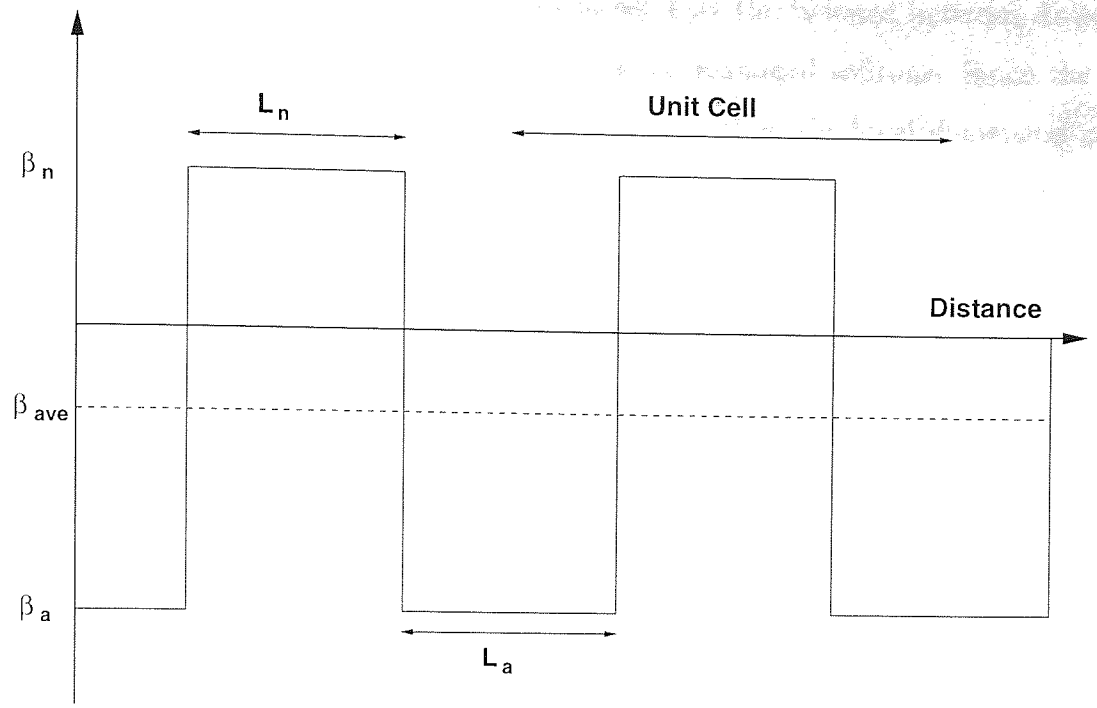

Figure 3.1: A dispersion map with equal lengths of normal and anomalous dispersion fibre. β_a and L_a are the dispersion and length of the anomalous dispersion fibre respectively, β_n and L_n are the same quantities for the normal dispersion fibre.

Dispersion managed solitons were discovered when a transmission line made up of alternating lengths of anomalous and normal dispersion was used. The lengths of each section of fibre are generally 100km or less so the length of the dispersion map in total is of the same order as an amplifier span. One of the major areas where dispersion management is found to be useful is for the upgrade of the standard fibre network. Standard fibre was originally intended for use at a wavelength of $1.3\mu m$ and has low dispersion at this wavelength. The invention of the Erbium doped fibre amplifier has made it more attractive to work around $1.55\mu m$ so it is now necessary to operate these fibres at this wavelength where standard fibre has dispersion of between 16 and 20ps/(nm km). Dispersion management can be used with this fibre to reduce the average dispersion which makes working at higher data rates possible without the use of regenerators [155, 156]. Standard fibre propagation will be discussed in more detail in chapters 6 and 7.

3.3 Dispersion Managed solitons

This section will give an explanation for the formation of solitons in a transmission line with dispersion management. Before examining the pulse shapes and energies found for dispersion managed soliton it is interesting to look at what happens to the pulse width

and bandwidth through one dispersion map to see how the balance between dispersion and nonlinearity is attained in the case of dispersion managed solitons. Since the average dispersion of the transmission line is much smaller than the local dispersion at any point the powers being used are low relative to the local dispersion and so the dispersion dominates, however the nonlinearity of self-phase modulation still has an important role to play in the formation of dispersion managed solitons [160].

When an unchirped pulse is launched into a length of anomalous dispersion fibre with a power less than that required to form a soliton the high dispersion causes the pulse width to increase as the pulse becomes chirped, this can be seen in figures 3.2, 3.3 and 3.4 which show the pulse shape, FWHM and chirp of a pulse in a length of anomalous dispersion fibre, the fibre was taken to have no loss and no higher order dispersion. These figures are of a 20ps Gaussian pulse with a pulse energy of 0.014pJ in 100km of anomalous dispersion fibre with dispersion of $-3.0ps^2/km$ this is well below the pulse energy for a first order soliton which would be 0.2pJ. Figure 3.5 shows the bandwidth of the same pulse as it propagates over the length of fibre. The bandwidth of the pulse decreases as it propagates through the fibre, this is caused by the nonlinearity. The reason for the decrease in the pulses bandwidth is that the nonlinearity is acting on a chirped pulse.

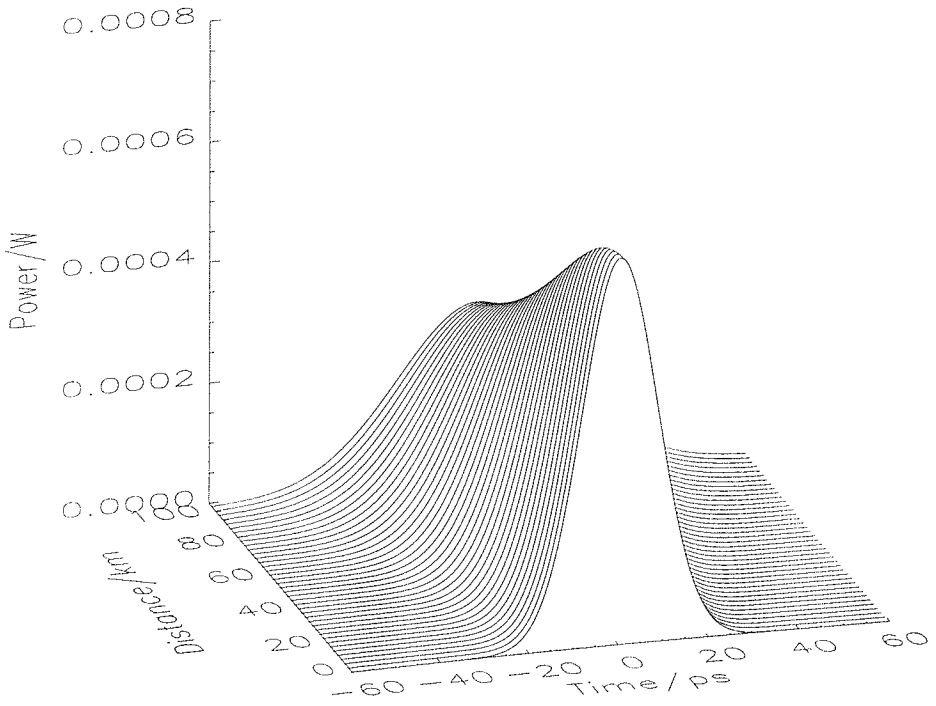

Figure 3.2: The pulse shape evolution of a Gaussian pulse is 100km of anomalous dispersion fibre.

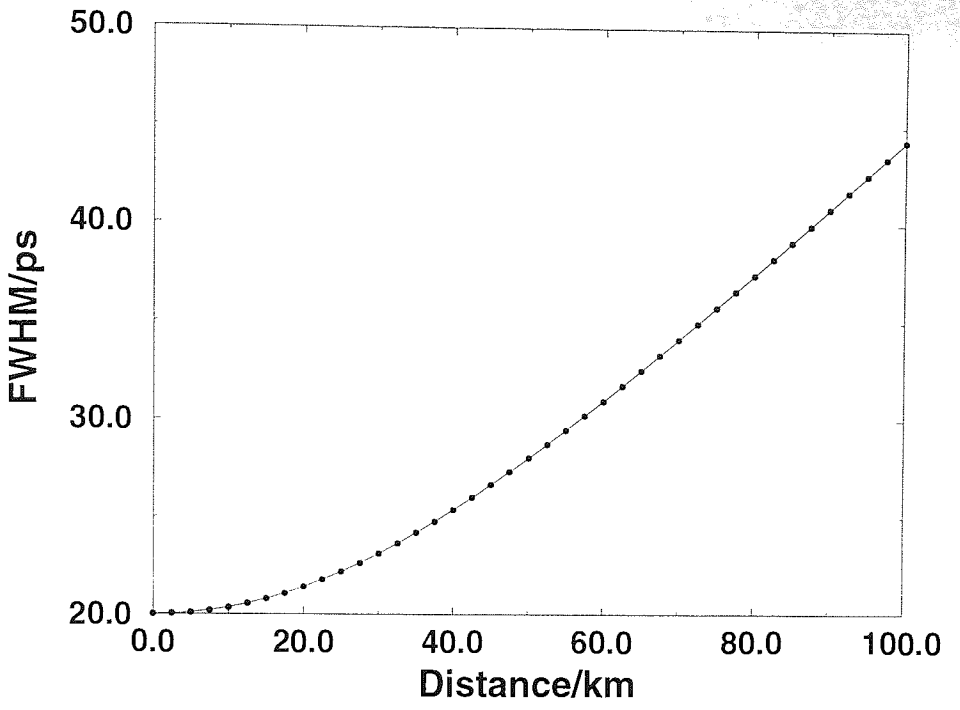

Figure 3.3: The pulse width increasing as the Gaussian pulse propagates through 100km of anomalous dispersion fibre.

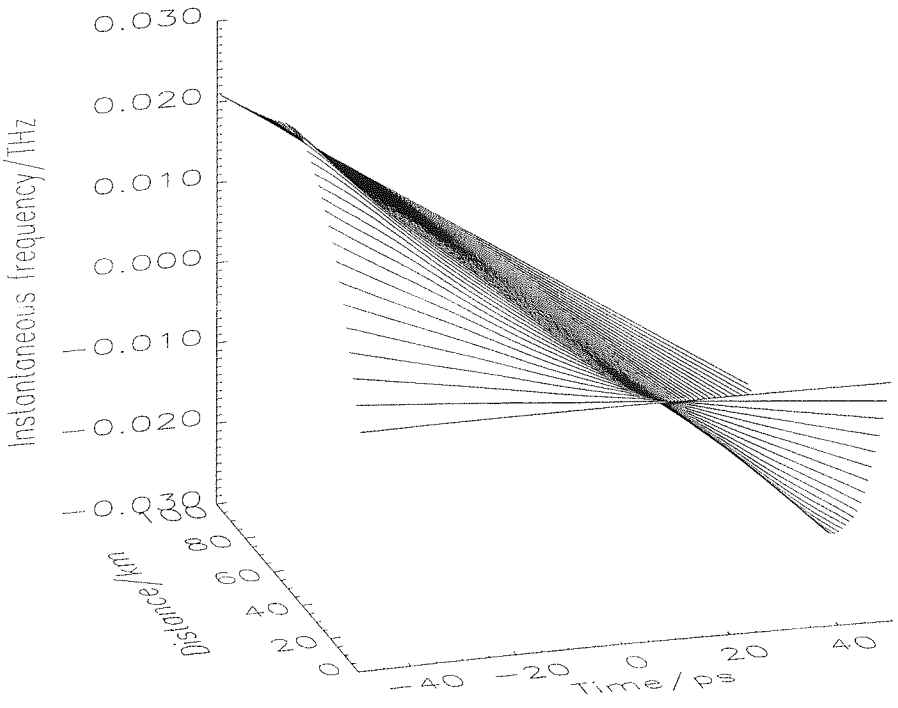

Figure 3.4: The instantaneous frequency across the Gaussian pulse as it propagates through 100km of anomalous dispersion fibre. The pulse can be clearly seen to accumulate a chirp as it propagates.

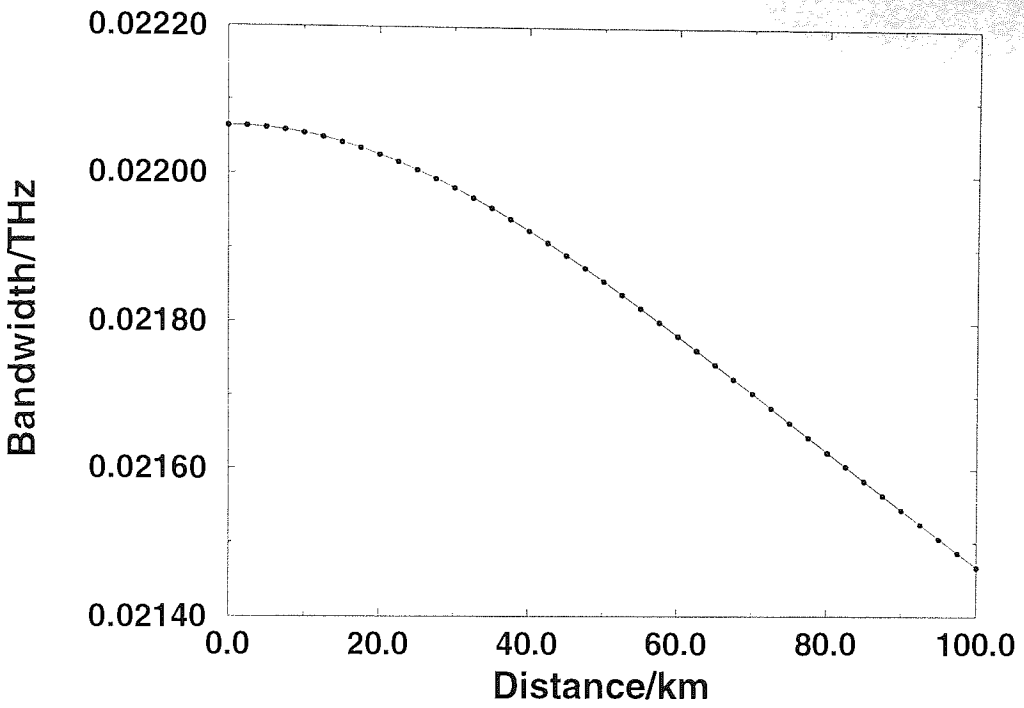

Figure 3.5: The bandwidth of the Gaussian pulse decreasing as it propagates through 100km of anomalous dispersion fibre.

The reduction in the bandwidth can be thought of like this. Since the dispersion dominates the pulse quickly becomes chirped in such a way that the leading edge is up shifted in frequency and the trailing edge is down shifted. The effect of the nonlinearity is to reduce the frequency of the front of the pulse and to increase the frequency of the trailing edge of the pulse. This means that the extremes of the spectrum are destroyed creating frequencies closer to the centre of the pulses bandwidth resulting in a decrease in the bandwidth.

Figure 3.6 shows the same unchirped Gaussian pulse as it is input into a length of normal dispersion fibre. The parameters for this simulation are the same as those for the anomalous dispersion simulation however here the dispersion of the fibre is $3.0ps^2/km$ Once again the effect of the dispersion on this pulse is to increase the pulse width as can be seen in figure 3.7. The bandwidth of the pulse in the normal dispersion fibre (given in figure 3.9) increases, this is because in the normal fibre the chirp induced on a transform limited input pulse is of the opposite sense to that found in the anomalous dispersion fibre, this can be seen in the plot of the instantaneous frequency given in figure 3.8. This means that the pulse has lower frequencies in its leading edge and higher frequencies on its trailing edge. Since the effect of the nonlinearity is still to reduce the frequencies on

the leading edge and increase the frequencies on the trailing edge the overall effect of the normal dispersion fibre is to increase the bandwidth of a chirp free input pulse.

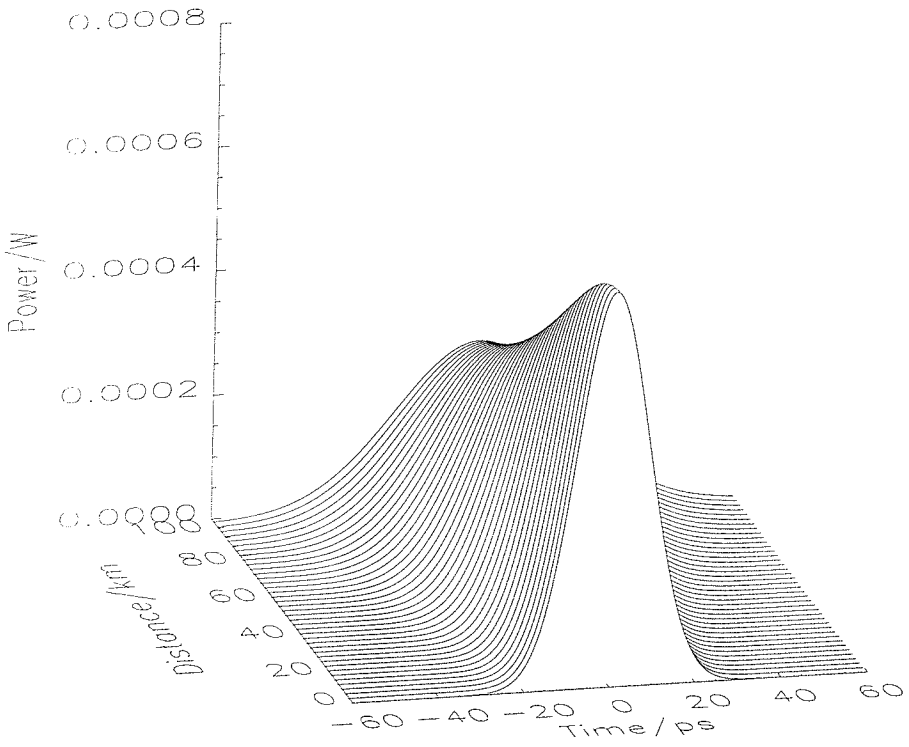

Figure 3.6: The pulse shape evolution of a Gaussian pulse is 100km of normal dispersion fibre.

It is also interesting to look at the evolution of the pulse parameters as they vary throughout one section of the dispersion map [161, 162]. One section of the dispersion map is taken to consist of a half length of anomalous dispersion fibre followed by a full step of normal dispersion fibre and finally another half step of anomalous dispersion fibre. The half steps are used because the input pulse is transform limited and in loss-less dispersion managed systems the stable pulses are unchirped at the midpoints. For this simulation the dispersion map consists of 100km of anomalous dispersion fibre with dispersion of $-3.0ps^2/km$ and 100km of normal dispersion fibre with dispersion of $2.8ps^2/km$ this gives an average dispersion of $-0.1ps^2/km$, both fibres are taken to have no loss or higher order dispersion. The input pulse was a 20.0ps Gaussian pulse with a peak power of 0.65mW this map and input are chosen because the stable pulse shape for this map is almost exactly Gaussian.. Figure 3.10 shows the pulse as it propagates through this dispersion map. reference should also be made to the pulse width in figure 3.11 and figures 3.13 and 3.12 which show the bandwidth and the instantaneous frequency respectively.

The pulse width increases as the pulse propagates through the first section of anoma-

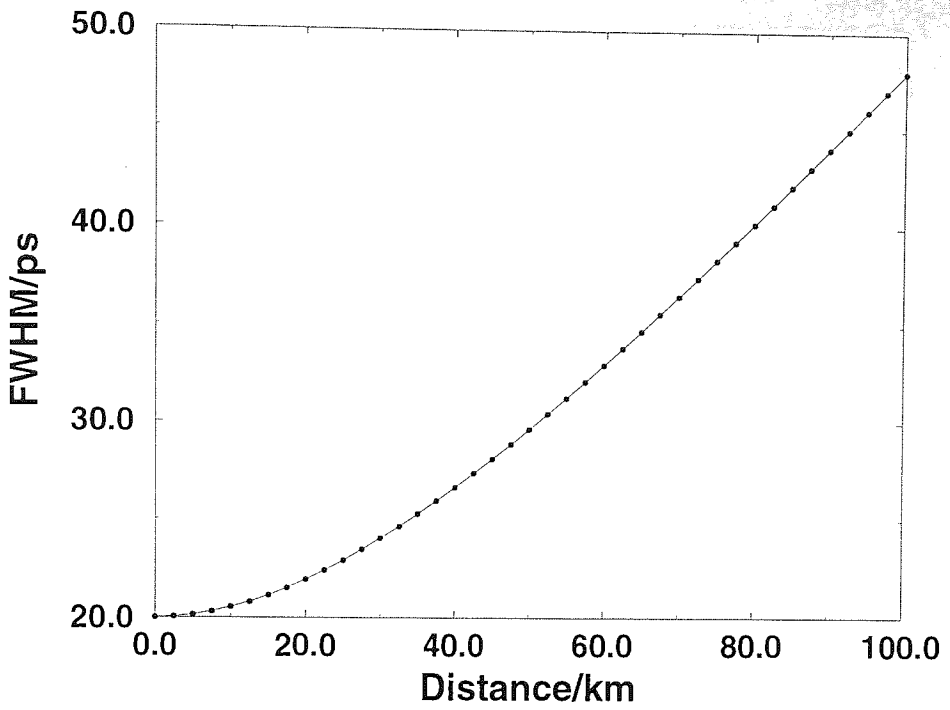

Figure 3.7: The pulse width increasing as the Gaussian pulse propagates through 100km of normal dispersion fibre.

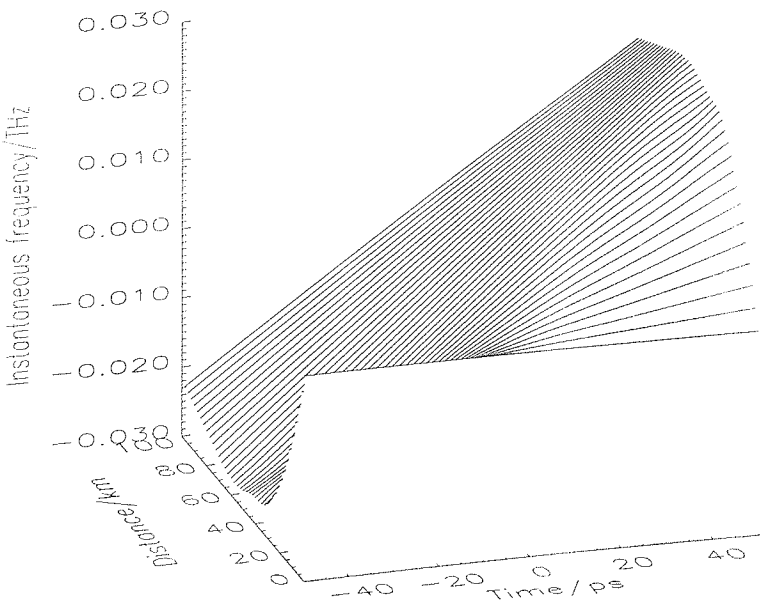

Figure 3.8: The instantaneous frequency across the Gaussian pulse as it propagates through 100km of normal dispersion fibre. The direction of the chirp is opposite to that seen for the pulse in anomalous dispersion fibre.

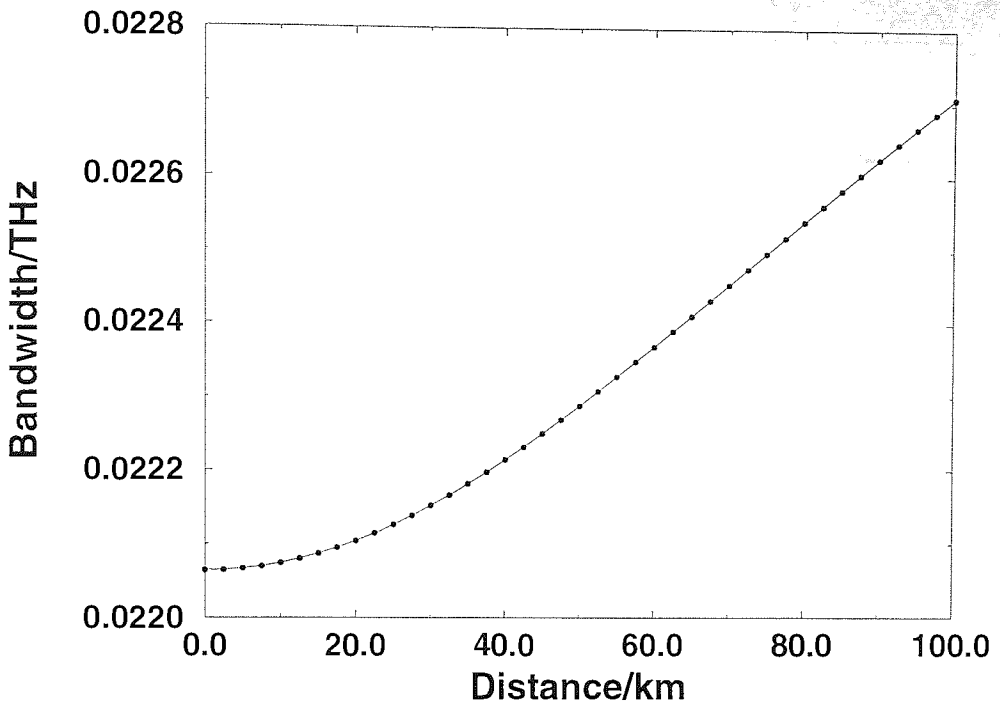

Figure 3.9: The bandwidth of the Gaussian pulse increasing as it propagates through 100km of normal dispersion fibre.

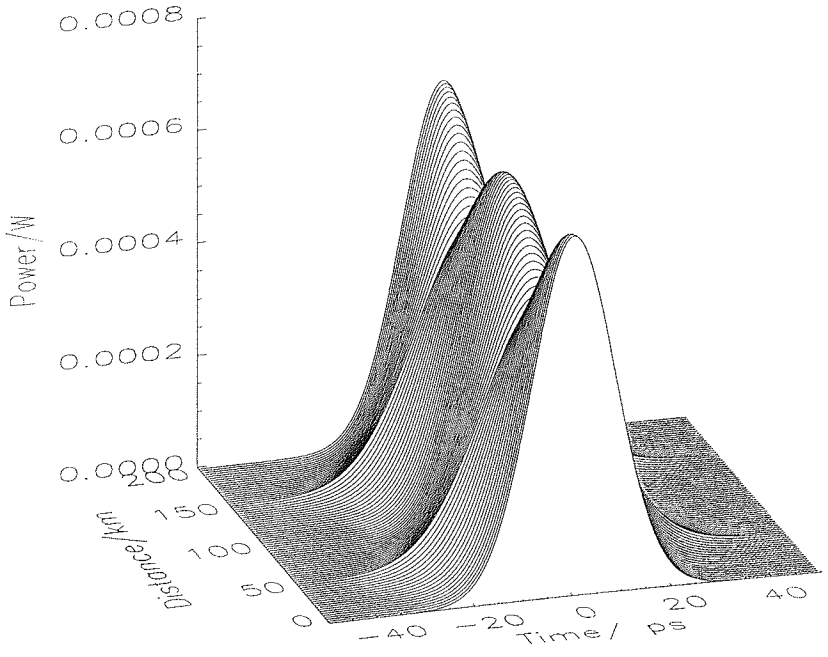

Figure 3.10: A dispersion managed soliton propagating through one unit cell of the dispersion map. This pulse is a 20.0ps Gaussian with a peak power of 0.64mW

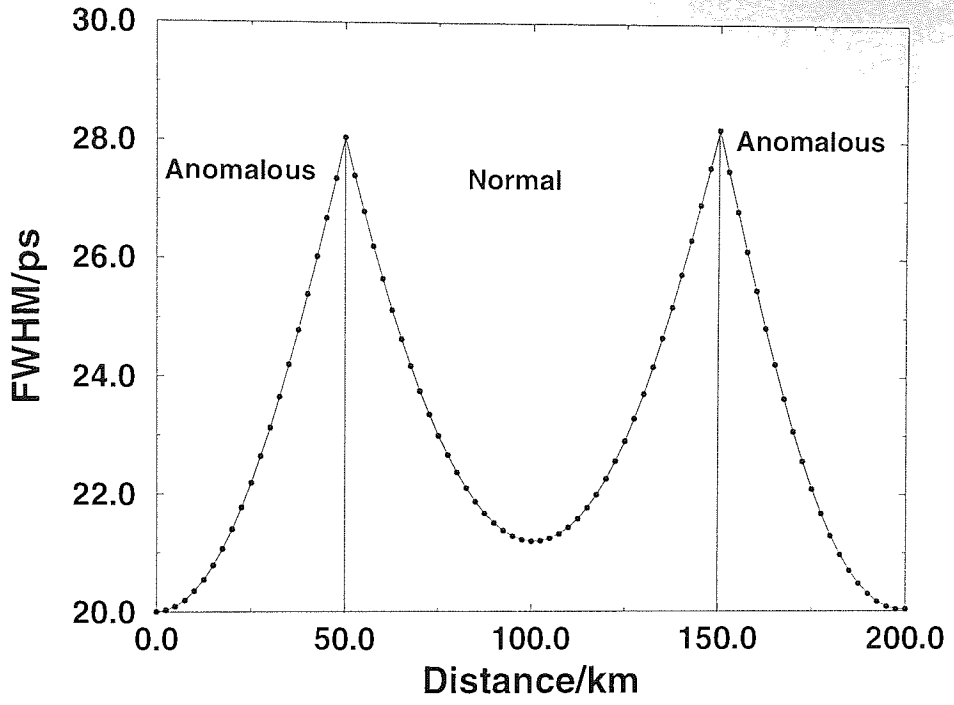

Figure 3.11: The pulse width evolution of a dispersion managed soliton through one unit cell.

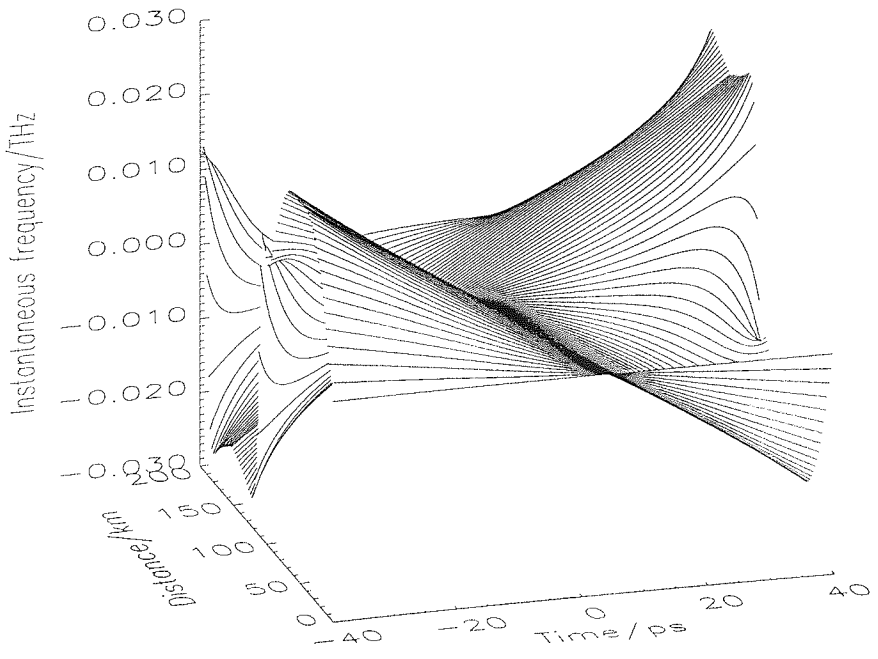

Figure 3.12: The instantaneous frequency of a dispersion managed soliton through one unit cell. This gives an indication of the manner in which the chirp of the pulse evolves through the dispersion map.

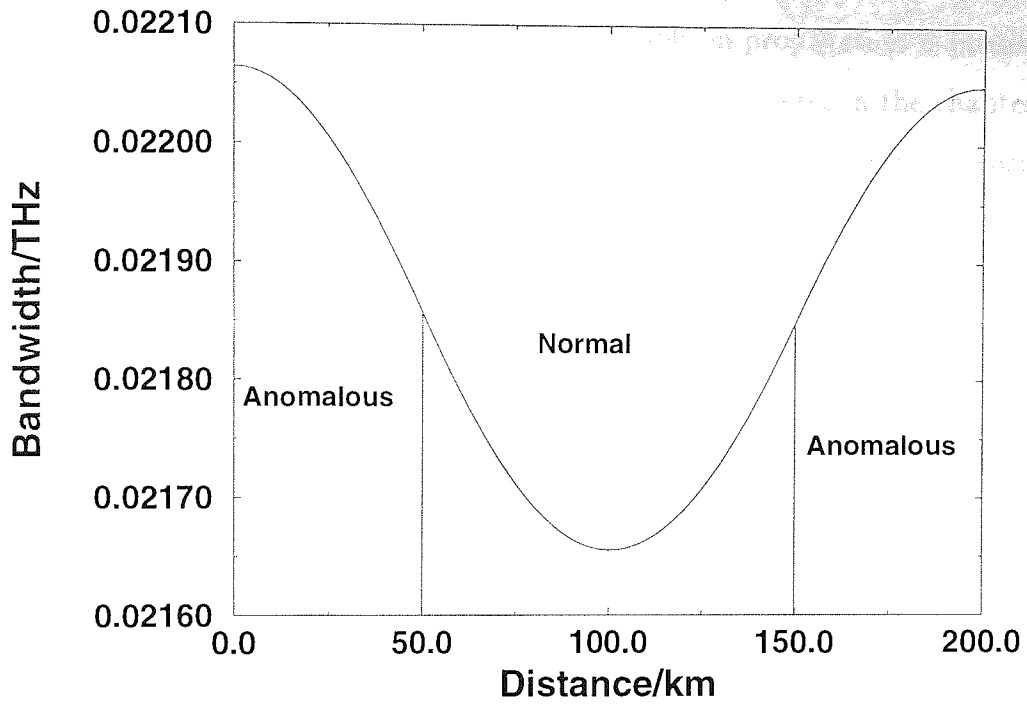

Figure 3.13: The bandwidth of a dispersion managed soliton as it changes during propagation through one unit cell.

lous dispersion fibre because it becomes chirped, during this same section of fibre the bandwidth decreases. Then when the pulse enters the normal dispersion fibre the pulse width decreases as the pulse becomes less chirped. Since it is the sign of the chirp that defines whether the bandwidth increases or decreases the bandwidth continues to decrease during the first half of the normal dispersion fibre. At the midpoint of this fibre the pulse width reaches a minimum as it is unchirped at this point. After the midpoint the pulse once again becomes chirped and so the pulse width increases. As the chirp is now in the opposite sense the bandwidth also increases during the second half of the normal dispersion fibre. When the pulse propagates through the final half step of anomalous dispersion fibre the pulse width is once again reduced as the pulse becomes less chirped and reaches a minimum at the end of this section of fibre. Throughout this section of fibre the chirp is also being reduced but is still in the same sense as before and so the bandwidth continues to increase and reaches a peak at the end of this fibre.

It is interesting to note that the minimum pulse width is less in the anomalous dispersion fibre than it is in the normal dispersion fibre. This is because the bandwidth is greater in the anomalous dispersion fibre and so a transform limited pulse can have a shorter temporal width. This also means that the anomalous dispersion fibre has a

greater dispersive effect on the pulse since the amount of pulse spreading is increased when the bandwidth is increased. This leads to the idea of an effective dispersion which is the deciding factor when considering whether soliton propagation is possible or not. The idea of effective dispersion will be discussed more fully later in the chapter [152].

For the balance between the nonlinearity and the dispersion to be correct it is necessary to have the correct pulse shape and energy, as is the case with traditional solitons [163]. When dispersion management is used the shape and energy required depend on the dispersion map as well as the pulse width and the average dispersion [141, 162, 151, 164]. The dispersion map can be described using the average dispersion, β_{ave}, the dispersion difference $\Delta\beta$ and the normalised average dispersion given by $D = -\beta_{ave}/\Delta\beta$ $(= D_{ave}/\Delta D)$. The final parameter used to describe the dispersion map is the dispersion map strength S. this is given by [143];

$$S = \frac{l\Delta\beta}{T^2} \tag{3.1}$$

where l is the length of the sections of fibre, and T is the full width half maximum pulse width. This definition of the map strength can only be used for maps with equal lengths of normal and anomalous dispersion fibre. A more general definition is;

$$S = \frac{l_n\beta_n - l_a\beta_a}{T^2} \tag{3.2}$$

where l_n and β_n are the length and dispersion of the normal fibre, l_a and β_a are the length and dispersion of the anomalous dispersion fibre and T is the full width at half maximum pulse width. The map strength is used to give an indication of the amount of pulse spreading the pulses undergo in the dispersion map. A high map strength which is caused by either high dispersion fibre or short pulses means that the dispersion length of the pulse is short compared to the length of fibre. Map strengths up to 12 have been used to give stable propagation [143, 165].

The stable pulses in dispersion managed systems have different pulse shapes from those in constant dispersion systems. The pulse shapes vary from being very close to sech shaped for weak dispersion maps to Gaussian pulse and on to pulses with shapes closer to a sinc function [142, 164]. There is no one set shape for a dispersion managed soliton, the pulses correct shape can be found numerically using an averaging technique first used

in reference [143]. If the pulse shape or width of a dispersion managed soliton are not exactly correct they do not evolve into the correct pulse but oscillate around the correct solution [166]. The pulse energy is dependent on the strength of the dispersion map as well as the average dispersion.

The original work to find the stable pulse energies was presented in reference [141] in this paper the stable enhanced power dispersion managed solitons were found by letting the pulses evolve over a long propagation distance and removing the dispersive radiation to help the pulse evolve. It was noticed that the energy enhancement of these pulses had a quadratic relationship with what is now known as the dispersion map strength. An empirical relationship for the energy enhancement is given by;

$$E_{sol} = E_o \left[1 + 0.7 \left(\frac{(\beta_1 - \beta_{ave})\, l_1 - (\beta_2 - \beta_{ave})\, l_2}{T^2} \right)^2 \right] \tag{3.3}$$

$$E_{sol} = E_o \left(1 + 0.7 S^2 \right) \tag{3.4}$$

where β_1 and β_2 are the dispersions of the two fibres, l_1 and l_2 are the length of the two fibres, β_{ave} is the average dispersion, T is the FWHM pulse width, S is the dispersion map strength and E_{sol} and E_o are the energies of the dispersion managed soliton and the equivalent first order soliton respectively. In the same paper it was first realised that the pulse shape also varies with dispersion map strength.

The development of the averaging technique to find the exact periodic solutions to dispersion managed systems has allowed further investigation of the energy enhancement and the possibilities opened up by using stronger dispersion maps. It has been found that for systems with $S > 4$ the energy enhancement does not just depend on the strength of the dispersion map but also depends on the normalised average dispersion. A semi-empirical formula for the energy of a soliton for map strengths $S > 4$ is given by [143];

$$E_{sol} \simeq \frac{a}{SD} \left(S - b\sqrt{(S-b)^2 + cSD} \right) \tag{3.5}$$

where a=0.2, b=3.7, c=180, S is the map strength and D is the normalised average dispersion.

The concept of energy enhancement breaks down when solitons that exist in the average zero dispersion or in the normal dispersion regime since traditional solitons do not exist in these regions there is no energy to compare the value for dispersion managed solitons. It is for this reason that the idea of an effective dispersion rather than an average

dispersion is useful.

As stated earlier the effect of the anomalous dispersion on the soliton is greater than the effect of the normal dispersion fibre because the bandwidth of the pulse is greater in the anomalous dispersion fibre. This means that the dispersion induced chirp on the pulse can be anomalous even if the average dispersion is zero or normal. This chirp is caused by the effective dispersion and it is balanced by the nonlinearity to give stable propagation of dispersion managed solitons when the average dispersion is zero or anomalous. The effective dispersion has been found using the variational method and is given by [152];

$$\beta_{eff} = \frac{<\beta\Omega^2>}{<\Omega^2>} \tag{3.6}$$

where β_{eff} is the effective dispersion, β is the dispersion, and Ω is the bandwidth. Both the dispersion and the bandwidth vary with propagation distance.

The dispersion map has to be stronger than S=3.9 for propagation at zero dispersion or in the normal average dispersion. This value has been found through numerical simulations but similar values can be obtained through analytical methods [145].

The opportunity to work with zero or normal average dispersion is of particular interest in WDM systems. Gordon-Haus jitter means that it is advantageous to work as close to zero dispersion wavelength (λ_o) as possible. In WDM systems the third order dispersion means that the wavelength channels that are further away from λ_o experience greater dispersion and so suffer more from timing jitter. If it is possible to use wavelengths on both sides of the dispersion zero then the outer wavelengths can be closer to the dispersion zero and so experience less dispersion. It is also possible to use dispersion compensating fibre that compensates for both second order and third order dispersion which flattens the dispersion of the fibre [8, 9].

3.3.1 Properties of Dispersion Managed Solitons

It is interesting to look at the effect of loss, noise and polarisation mode dispersion on dispersion managed solitons as well as looking at interactions between dispersion managed solitons. These effects are well known for systems with constant dispersion and were discussed in the previous chapter.

In constant dispersion systems the effect of loss is to cause a reduction in the nonlinearity as the pulse power decreases. To counteract this the average soliton is used as

was seen in section 2.6.2. In dispersion managed soliton systems there is some evidence to suggest that the effect of loss is to reduce the enhanced power required to create the soliton [167]. This paper suggests that the size of the power enhancement is reduced as the loss is increased. It is clear, however, that an enhanced power is required to propagate dispersion managed soliton in the presence of loss [167, 142]. The usual average soliton constraints (as given in section 2.6.2) still apply i.e the amplifier span must be significantly less that the soliton period. The inclusion of loss also moves the points in the dispersion map where unchirped pulses exist from the midpoint of the fibres to a point closer to the boundary going from the normal dispersion fibre to the anomalous dispersion fibre. This is because the effects of the nonlinearity are less as the peak power of the pulses is reduced. From reference [168] the position of the unchirped pulses and therefore the correct position to launch an unchirped pulse is given by the zeroes of the following equations.

$$F(z_o) = F(0) + D_1 z_o + R_1 a_o^2 \frac{1 - exp(-2\Gamma_1 z_o)}{2\Gamma_1} \tag{3.7}$$

for $z_o \leq z_1$

$$F(z_o) = F(z_1) + D_2(z_o - z_1) + R_2 a_o^2 exp(-2\Gamma_1 z_1) \frac{1 - exp[-2\Gamma_2(z_o - z_1)]}{2\Gamma_2} \tag{3.8}$$

for $z_o > z_1$

where

$$F(0) = \frac{z_a}{2} - \frac{R_1 a_o^2}{2\Gamma_1} - \frac{D_2}{2\Gamma_2} + \frac{a_o^2}{2z_a}\left[D_2 z_2 \left(\frac{R_2}{\Gamma_2} - \frac{R_1}{\Gamma_1}\right) exp(-2\Gamma_1 z_1) + R_1 \left(\frac{1 - exp(-2\Gamma_1 z_1)}{2\Gamma_1}\right)\left(\frac{D_2}{\Gamma_2} - \frac{D_1}{\Gamma_1}\right)\right] \tag{3.9}$$

D_1 and D_2 are the dispersions of the two fibres, a_o^2 is the power enhancement factor for the soliton in the dispersion map, Γ_1 and Γ_2 are the losses of the two fibres, R_1 and R_2 give a measure of the nonlinearity of the fibre. z_1 is the length of the first section of fibre, z_2 is the length of the second section of fibre.

The introduction of loss and gain into the system means that the effects of amplifier noise must also be considered. As with constant dispersion solitons, dispersion managed solitons are affected by noise in two major ways. The first is a degradation in the signal-

to-noise ratio and the second is Gordon-Haus timing jitter caused by the shifting of the pulses spectrum by the inclusion of noise photons, these two effects were discussed in relation to average solitons in sections 2.6.4 and 2.6.5 respectively. The performance of dispersion managed solitons is better than conventional solitons when noise is included as a result of the enhanced power required to form the pulse.

In reference [144] the signal-to-noise ratio for a dispersion managed soliton after propagating over a distance Z was found to be;

$$SNR = \frac{E_o Z_a}{n_{sp}(G-1)h\nu Z} \tag{3.10}$$

Where E_o is the energy of the pulse at the output of the amplifier, Z_a is the length of the amplifier span, n_{sp} is the spontaneous emission factor of the amplifier, G is the gain, h is Planck's constant and ν is the frequency. The SNR is increased when compared to the value of an average soliton because the value of E_o is greater for a given average dispersion. Essentially the signal level is higher and so the SNR is greater.

The effect of using dispersion managed solitons on the level of Gordon-Haus jitter is more complicated [149, 167, 148]. This is because the Gordon-Haus jitter does not just depend on the pulse energy although the enhanced energy does reduce its effect. The size of the jitter is also affected by the bandwidth of the pulse at the amplifier. The pulse's spectrum is only affected by noise photons within the spectral width of the pulse. Figure 3.13 showed that the pulses spectral width changes during the dispersion map therefore the size of the Gordon-Haus jitter is affected. This can also be thought of as the jitter depending on the pulse width and the chirp. From reference [144] the timing jitter after n amplifiers is given by;

$$< \delta t^2 >= \frac{2n_{sp}(G-1)h\nu}{E_o}\left(\sum_{p=1}^{n}\Omega_p^2\beta_p^2 + \frac{\pi^2}{12}ZZ_a\tau_c^2\right) \tag{3.11}$$

where E_o is the energy of the pulse at the output of the amplifier, Z_a is the length of the amplifier span, n_{sp} is the spontaneous emission factor of the amplifier, G is the gain, h is Planck's constant, ν is the frequency, Ω_p^2 is the quadratic bandwidth, β_p is the cumulative dispersion after the pth amplifier, Z is the total system length, Z_a is the amplifier span length and τ_c is the minimum pulse width.

From this equation it is clear that the enhanced pulse energy reduces the value of the jitter. The equation also shows that it is best to avoid amplifying the pulse where it has

the greatest bandwidth. This means that the worst place to amplify the pulse is at the unchirped point in the anomalous dispersion fibre.

Polarisation mode dispersion is becoming increasingly important as shorter pulses are used in an effort to propagate data at higher rates. It is, therefore, important to understand how dispersion managed solitons respond to PMD. In constant dispersion systems solitons are resistant to PMD as was discussed in section 2.6.3. Since the resistance is due to a nonlinear process, i.e. cross-phase modulation between the two polarisations, it might be possible that the enhanced powers of dispersion managed solitons could mean that they are more resistant. It has been found that dispersion managed solitons perform in much the same way as traditional soliton under the influence in PMD with limited improvement for weaker maps. The main cause of the instability of dispersion managed solitons under PMD is through interactions with dispersive radiation [169]. With further optimisation of the launch position, pulse shape and amplifier position it should be possible to limit the amount of dispersive radiation and so improve the performance of dispersion managed solitons in fibre with PMD [170].

Single channel interactions are another important property of solitons and are affected by the use of dispersion management [171, 172, 173, 174, 175]. Interaction for constant dispersion solitons occur due to constructive interference between the tails of adjacent solitons leading to a refractive index change. There are three ways in which this process is altered by the use of dispersion management. Firstly the solitons are no longer sech shaped, this has an effect because the intensity of a Gaussian pulse for example drops off more quickly than the sech pulse, this means that the tails have a smaller effect on the refractive index of the fibre and so the interaction forces are decreased.

The interaction forces are also changed because the pulse breathes as it propagates through the dispersion map. This means that the pulse width increases and decreases during propagation and so the overlap of the tails also varies along the fibre. This would tend to increase the the interaction forces. The final property of dispersion managed solitons that affects the size of the interactions is that the tails of the pulses are chirped. This means that the tails do not necessarily constructively interfere and so the fact that the pulse breaths does not necessarily increase the interactions. All of these effects mean that the soliton interactions are now more complicated as the collapse distance depends on the strength of the dispersion map as well as the pulse width and it will be seen later that when loss and gain are considered the collapse length is strongly affected by amplifier position. Since lower dispersion can be used with dispersion managed solitons,

interactions are increasingly being found to limit the total propagation distance [174].

In the lossless case interactions are suppressed for weak maps and the collapse length is increased. As the map strength is increased and so the breathing of the pulses becomes greater the collapse length is decreased and is eventually shorter than the collapse length for a non-dispersion managed soliton.

When loss is included in the consideration of dispersion managed soliton interactions the collapse length is found to depend critically on the amplifier position. Experimental evidence suggests that the collapse length can be more than doubled by correct positioning of the amplifier [155]. These results have been backed up by analytical and numerical studies. The experimental results have suggested that the best place to situate the amplifier is immediately following the the normal dispersion fibre. The analytical results suggested that the collapse length could be further increased by placing the amplifier in the normal dispersion fibre [176].

Techniques that have previously been used to improve the performance of soliton systems have been found to offer equivalent improvement for dispersion managed solitons. These include the use of filters [161] and sliding guiding filters [177, 178], amplitude modulators and, as will be seen in chapters 4 and 5 saturable absorbers. Dispersion management has also been shown to offer substantial improvements in wavelength division multiplexed systems by reducing the collision induced timing jitter [179, 180, 181].

3.4 Conclusions

The use of dispersion managed solitons has been found to offer many advantages over solitons in conventional transmission lines with constant dispersion fibre. Dispersion managed solitons exist when the transmission line is constructed from alternating sections of normal and anomalous dispersion fibres. Dispersion dominates the evolution of these pulses however self-phase modulation plays an important role in their formation. The pulse width and bandwidth of dispersion managed solitons oscillate as they propagate along the optical fibre, however periodically they return to their original values.

Dispersion managed solitons are not sech shaped, they tend to have a shape closer to Gaussian and they also have enhanced power compared to conventional solitons. The strength of the dispersion map is an important parameter in describing the dispersion map and the soliton pulses. It gives a measure of the amount of dispersive broadening the pulses undergo in the dispersion map. For weaker maps the energy enhancement

depends quadratically on the dispersion map strength although it saturates for stronger maps. Dispersion management also means that it is possible to propagate solitons in a transmission line with average zero or normal dispersion as long as the dispersion map is stronger than S=4.

The enhanced power of dispersion managed solitons means that they are able to perform better than conventional solitons in terms of both signal-to-noise ratio and Gordon-Haus jitter. The effect of Gordon-Haus jitter also depends on the position on the dispersion map where the pulse is amplified as the bandwidth of the pulse at the amplifier is important. The collapse length of adjacent solitons can be longer in a dispersion managed system as long as the map is weak. The collapse length has also been shown to depend strongly on the position of the amplifier in the dispersion map.

The use of dispersion management has led to many impressive experimental results over recent years. Using standard fibre it has been possible to propagate single channels at 10Gbit/s over transoceanic distance [4, 182, 183]. It has also been possible to use several channels at 10Gbit/s over standard fibre [184]. Standard fibre can also be used to propagate single channel at 20Gbit/s [185] over 2000km and 40Gbit/s [186, 156, 187] over distances greater than 1000km. It is also possible to use WDM with higher data rates in each channel with total data rates of up to 450Gbit/s possible over 1200km [188, 7].

When the choice of fibre is not constrained to standard fibre it is possible to improve the performance of dispersion managed systems. Data has been propagated at 20Gbit/s in single channels over distances well in excess of transoceanic distance [189, 4, 146] and over shorter distance for several channels [9]. It is now becoming possible to use dispersion managed solitons to transmit data at 40Gbit/s over transoceanic distance [190, 5]. There have also been some field trials of dispersion managed solitons at both 10Gbit/s [191] and 40Gbit/s [192, 193, 194] which show that dispersion managed solitons can be used successfully outside the laboratory.

Chapter 4

Dispersion management and saturable absorption.

4.1 Introduction

This chapter will take the experimental parameters from reference [195] and carry out numerical simulations to identify the individual roles of dispersion management and saturable absorption in order to understand the mechanism for the observed stable pulse evolution. The results show that a combination of dispersion management and periodic saturable absorption allows stable pulses to propagate with a wide range of energies (from 0.165 to 1.30pJ) with the same input pulse width of 6.0ps. The pulses with the highest energies have far more energy than would be expected from dispersion management alone. The stable, high energy pulses can only be propagated when both dispersion management and a saturable absorber are used.

Effects such as Gordon-Haus jitter [77] and soliton interactions [80, 82] mean that it is often beneficial to work close to the dispersion zero. However, as noted in section 2.6.4, since the power of a soliton depends on the fibre dispersion, there is a limit on how near to the dispersion zero soliton propagation is viable due to the signal-to-noise ratio (SNR). In chapter 3 it was shown that dispersion management allows solitons with enhanced energy to propagate [141]. This means that lower average dispersions can be used without an unacceptably low SNR. The use of saturable absorber has also been shown to improve soliton propagation by suppressing the build up of amplified spontaneous emission noise (ASE) and dispersive waves [128, 116, 196, 197] (see section 2.7.5). It has been shown experimentally that if dispersion management is used in conjunction with a weak saturable absorber the stable pulses have a further increase in energy [195]. In fact

stable pulses have been found that have the same energy as an N=10 average soliton for the same average dispersion. These solitons were also found to be extremely stable and were able to maintain their shape and peak power for more than half an hour, this gives a propagation distance of 360000Mm. The saturable absorption in this experiment came about through nonlinear polarisation rotation (NPR) utilising the polarisation dependent loss of the filter. The use of NPR to form a saturable absorber was discussed in section 2.3.6. The dispersion map and saturable absorber used in these simulations are based on those used in the experiment.

To identify the key effects, initially a point saturable absorber is used in place of NPR. The response of the saturable absorber is designed to be similar to that of NPR. In order to examine the effect of the two different aspects of this system (i.e. saturable absorption and dispersion management) they are looked at separately to begin with and then the combined system is examined. When the saturable absorber is used without dispersion management it is possible to produce shortened pulses in a similar way to mode locked lasers. The dispersion map alone supports pulses with enhanced energies as found with other dispersion maps. The combined system supports pulses with a wide range of pulse energies, these pulses have energies that are higher than those found for systems with dispersion management alone. Finally a 2D model is created to properly model the NPR of the original experiment which confirms the results of the simpler model. Throughout the simulations the fibres are taken to be lossless and to have no higher order dispersion, in order to help identify the key effects by keeping the model as simple as possible.

4.2 1D Model

4.2.1 Saturable Absorber

A system with constant dispersion and a point saturable absorber is examined in order to identify the effect of the saturable absorber on its own. A schematic of this model is shown in figure 4.1. The model consists of 26.3km of fibre with dispersion of 0.1ps/nm/km, the saturable absorber, an amplifier and a 3nm Gaussian filter. The fibre was taken to have no higher order dispersion and no loss, so the amplifier was used purely to recover the loss from the saturable absorber and the filter and did not add any noise to the signal.

The equation used to describe saturable absorption through NPR was derived in sec-

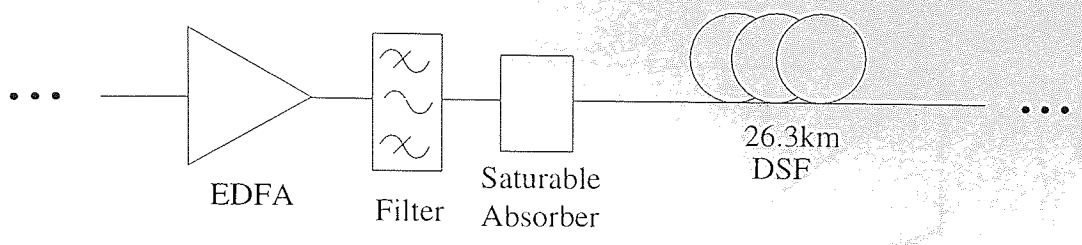

Figure 4.1: Schematic for the system with constant dispersion and the saturable absorber

tion 2.3.6 and is given by [33, 34, 35];

$$P_{out} = P_{in} sin^2 \frac{\Delta\phi}{2} sin^2 2\theta \tag{4.1}$$

where P_{out} and P_{in} are the output and input powers respectively, $\Delta\phi$ is the accumulated nonlinear phase shift between the two polarisations and θ is the polarisation angle of the input.

For the purposes of the simplified 1D model the saturable absorber is modelled using the equation:

$$P_{out} = P_{in} \left[1 - A cos^2 \left(\frac{P_{in}\pi}{2P_{noabs}} \right) \right] \tag{4.2}$$

Where P_{noabs} is the switching power of the saturable absorber and is set to 0.1W for the following simulations. The strength of the absorber is defined by A, this is set to be equivalent to a maximum absorption of 1.5dB. A switching curve for this weak saturable absorber is given in figure 4.2

When this saturable absorber is added to the system the gain of the amplifier can not be kept at a constant value because as the pulses change peak power, width and shape they suffer different loss as they pass through the saturable absorber and filter. In order to stabilise the pulse energy, the energy is calculated at the start of the simulation and the correct gain to restore the energy to this value is used, this is similar to using an amplifier in saturation which is the case in many practical systems.

With the amplifier gain controlled in this way it is possible to propagate solitons for more than 50 soliton periods but only for a small range of pulse energies. Pulses with a full width half maximum (FWHM) of 6.0ps and a variety of different energies are used. Stable propagation can be observed in two different regions, the first of these is for pulses with energy between 2.64×10^{-2} and 5.94×10^{-2}pJ (launched soliton order N=1.0 to N=1.5). These pulses have peak powers that are low on the switching curve of the

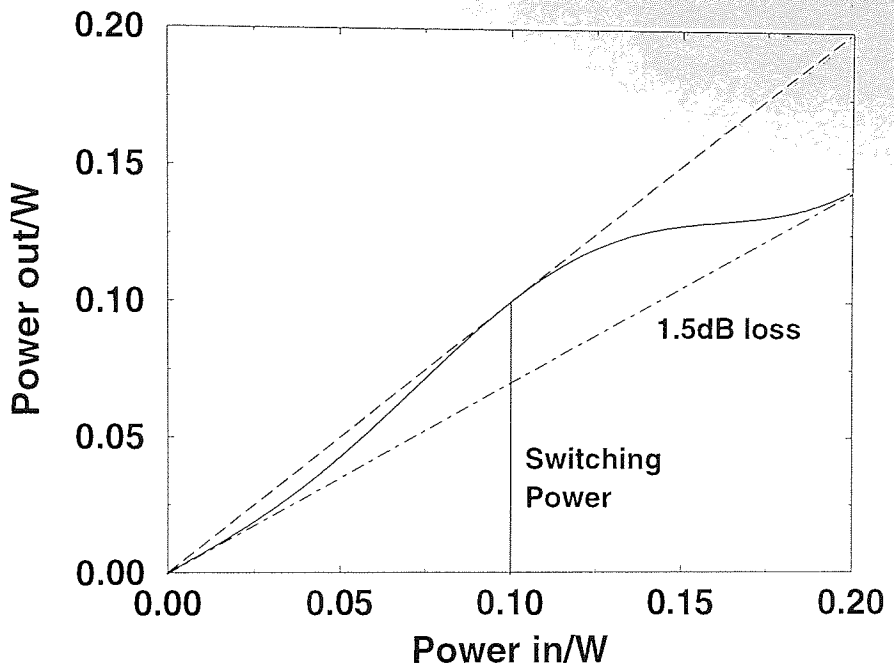

Figure 4.2: Switching curve for the 1D saturable absorber used in these simulations. The solid curve shows the output power as a function of input power; the dashed line shows the output without the saturable absorber and the dotted-dashed line shows the output for a constant 1.5dB loss. The switching power for this saturable absorber is 0.1W.

saturable absorber and so as they pass through the saturable absorber and the amplifier they undergo lumped loss followed by lumped gain. An example of one of the low power pulses is given in figure 4.3, this pulse has energy of $E = 4.12 \times 10^{-2} pJ$, the evolution of the pulse width is given in figure 4.4 and the spectral evolution is given in figure 4.5. These plots show the pulse immediately following the saturable absorber. The pulses amplitude shows some fluctuations after an initial drop but does not show much variation over 10000km. The pulse width drops from the input of 6.0ps to oscillate around 5.6ps. There is a more obvious long term evolution in the spectrum which develops some fine structure.

The second area of stable propagation is for pulses with energies between 0.134 and 0.300 pJ (launched soliton orders N=2.25 to N=2.75). In this region the system produces shortened pulses in much the same way as a mode-locked laser using NPR [119, 198, 199, 200]. An example of one of these pulses is given in figure 4.6. This pulse has an input pulse width of 6.0ps and a pulse energy of 0.165 pJ, the pulse width quickly reduces to 1.5ps. It is clear from figure 4.7 that once the pulse width is compressed it remains steady at its new value. The only plot that shows any long term evolution is the spectrum given in figure 4.8. The spectrum broadens quickly as the pulse width is reduced and the

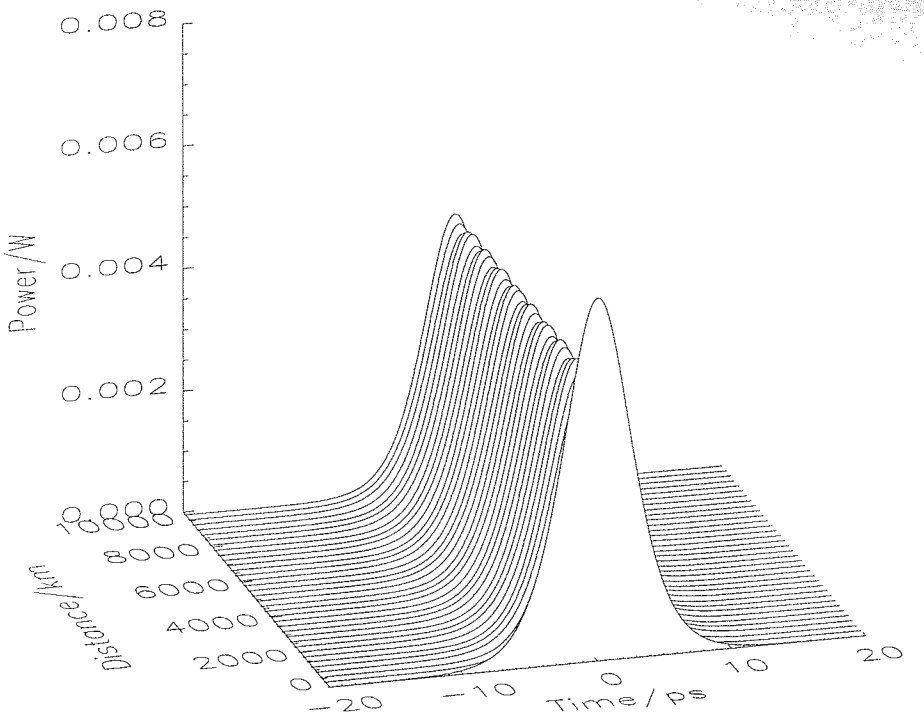

Figure 4.3: The pulse shape evolution of a pulse with energy of $E = 4.12 \times 10^{-2} pJ$, the peak power of this pulse is well below the switching power of the saturable absorber which is 0.1W.

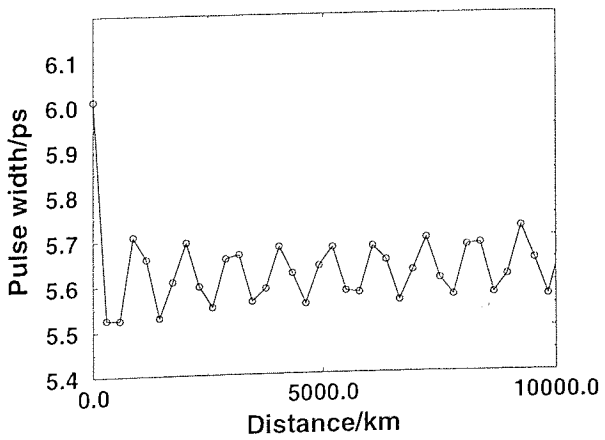

Figure 4.4: The evolution of the pulse width of a low energy pulse ($E = 4.12 \times 10^{-2} pJ$) in a system with constant dispersion and a saturable absorber.

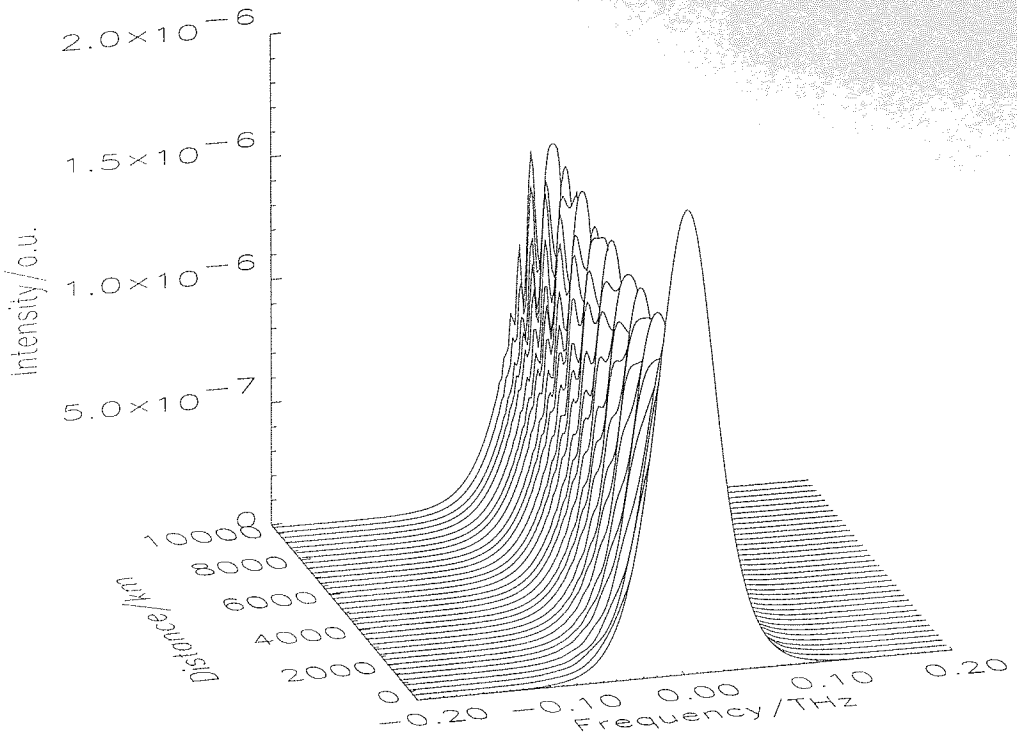

Figure 4.5: The spectral evolution of a pulse with energy of $E = 4.12 \times 10^{-2} pJ$, the spectrum can be seen to develop some fine structure as the pulse propagates.

peak power increases, however the spectrum is not smooth although the fluctuations are reduced as the pulse propagates. These pulses have peak powers that are close to the switching power of the saturable absorber. The pulse with energy of 0.3pJ has a peak power of 0.1W.

In between the two stable regions there is a region of pulse energies where the pulses break up. The peak powers of these pulses are not high enough for mode locking to take place however they are high enough for there to be a significant difference in the loss experienced by the peak and the tails leading to instability. The pulse shape and spectrum of one of these pulses are shown in figure 4.9 and 4.10 respectively. This pulse has an input energy of 0.08pJ, the pulse initially undergoes pulse width shortening and the pulse peak power increases however after this initial evolution the pulse width increases and the peak power decreases. The spectrum undergoes a complicated evolution but shows no signs of reaching a stable state.

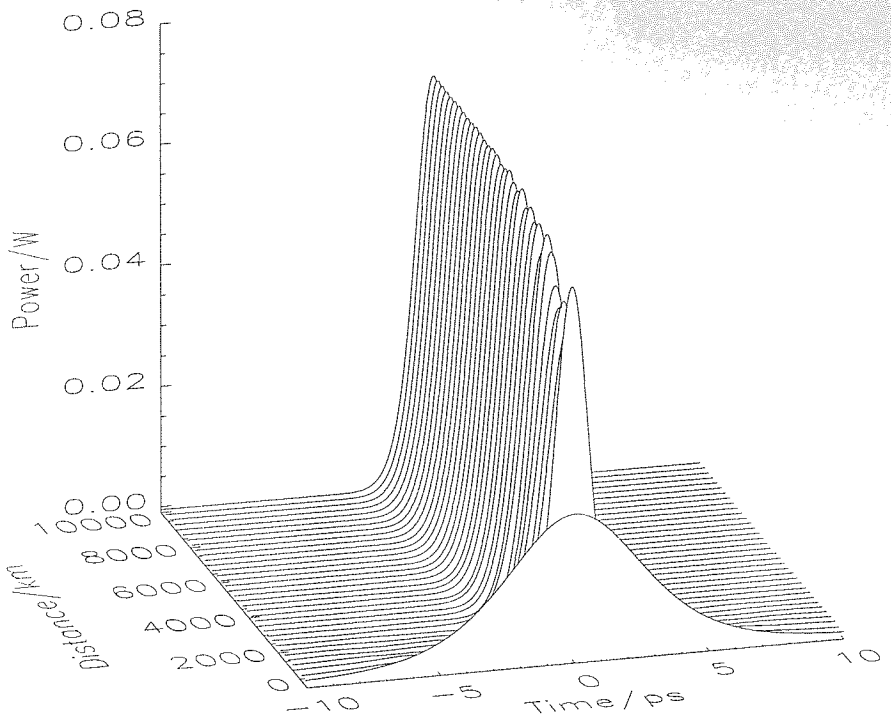

Figure 4.6: A pulse with an input pulse width of 6.0ps and a pulse energy of 0.165pJ showing the pulse shortening when the saturable absorber is used in a system with constant dispersion.

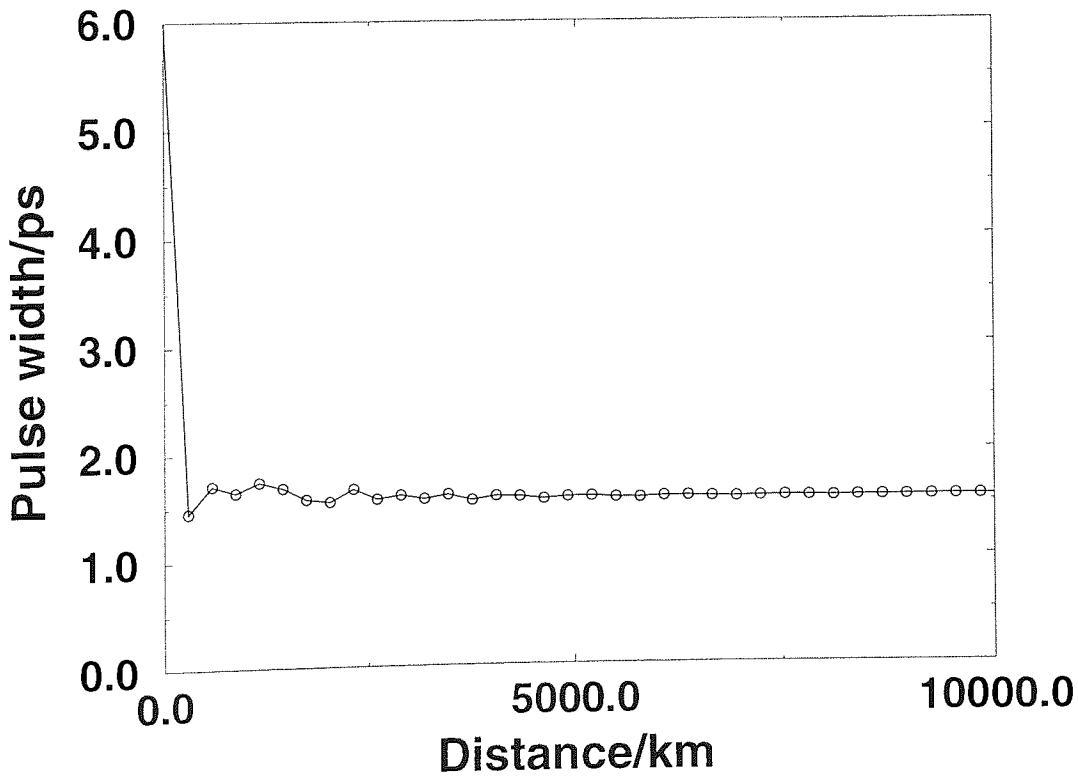

Figure 4.7: The evolution of the pulse width for a 0.165pJ pulse which undergoes compression similar to mode locking, the pulse width is reduced to 1.5ps.

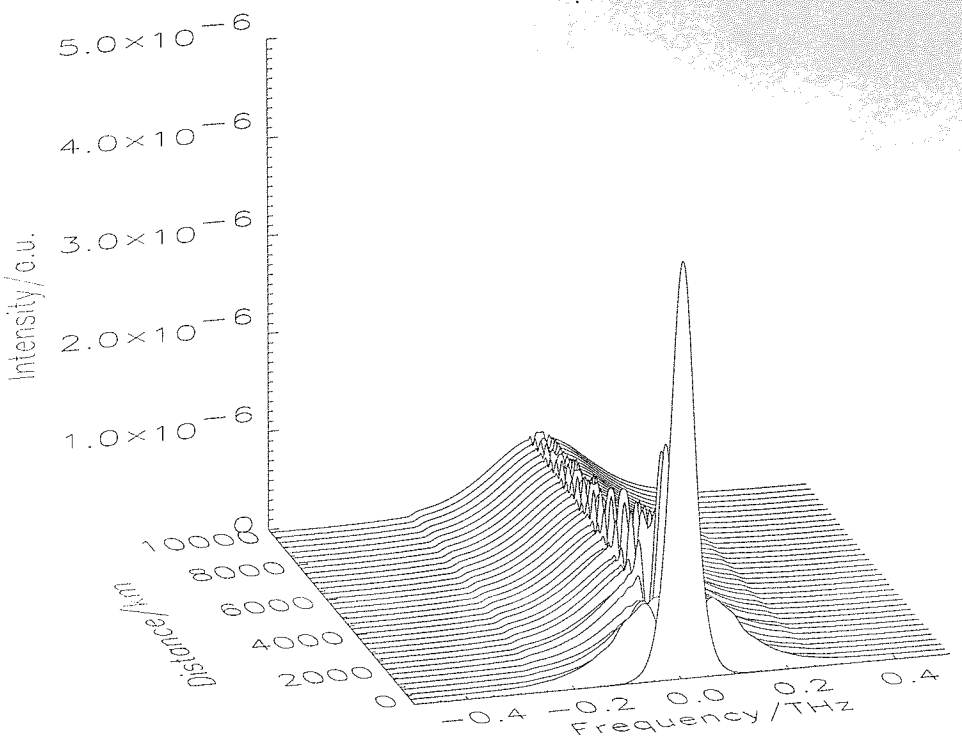

Figure 4.8: The spectral evolution of a pulse with energy of 0.165pJ.

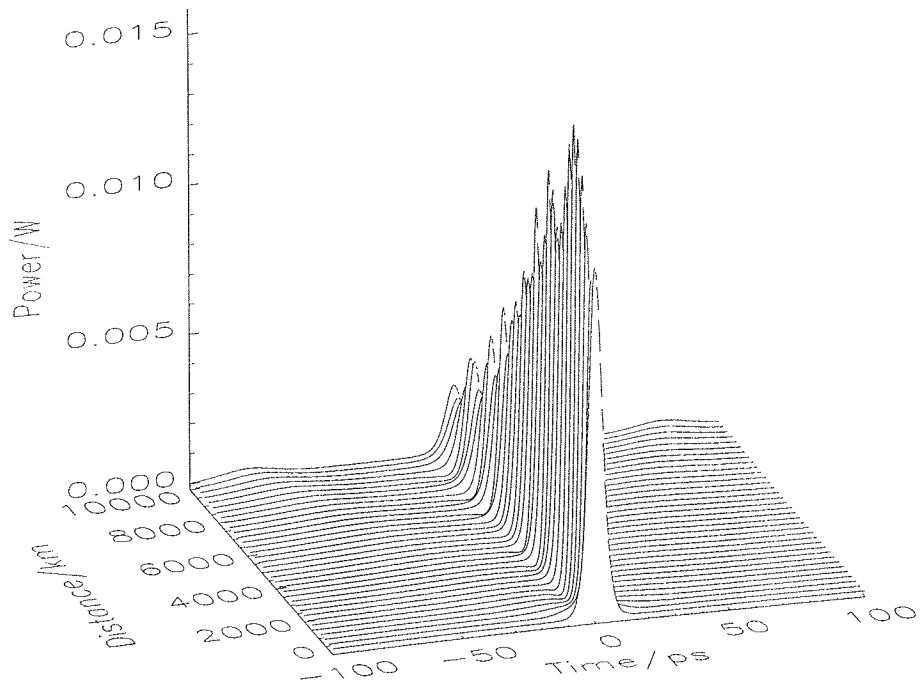

Figure 4.9: A 0.08pJ pulse that breaks up in the system with constant dispersion and a saturable absorber.

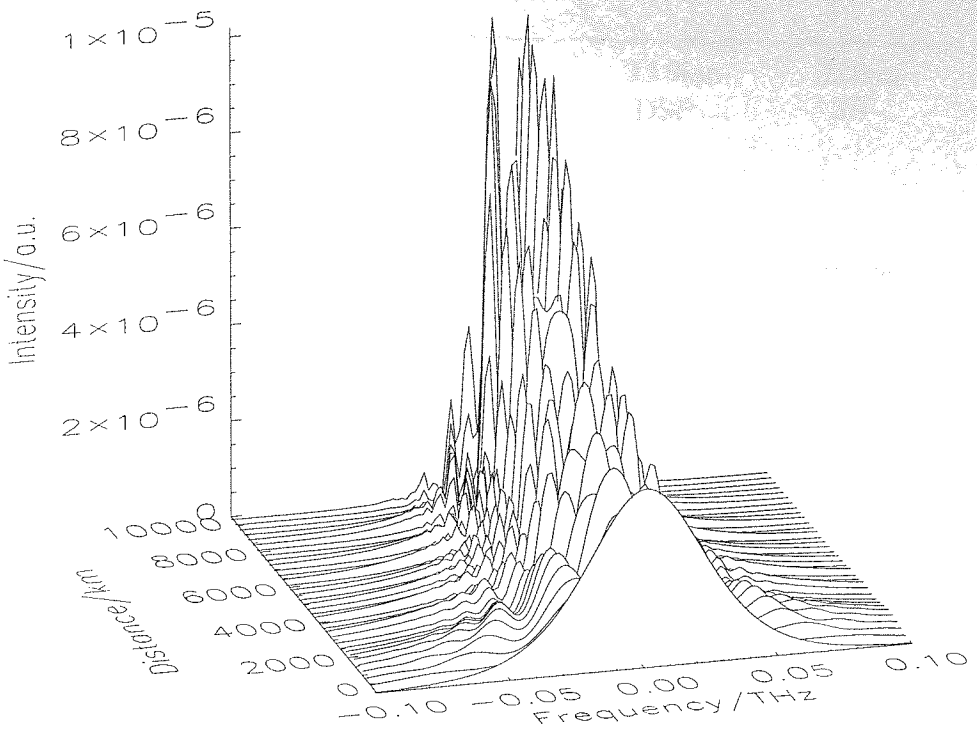

Figure 4.10: Spectral evolution of the 0.08pJ pulse.

4.2.2 Dispersion Map

Simulations carried out using the dispersion map alone are now considered so that the effect of the dispersion management can be isolated. The system used here is shown in figure 4.11. The dispersion map consists of 23.9km of dispersion shifted fibre with dispersion of -1.49ps/nm/km and 2.4km of standard fibre with dispersion of 16.0ps/nm/km this gives an average dispersion of 0.1ps/nm/km. This dispersion map is chosen to be the same as that used in reference [195] The fibre is taken to have no loss and no higher order dispersion. This dispersion map differs to many others in that it consists of mainly normal dispersion fibre which is not soliton supporting with only a short length of fibre with anomalous dispersion[157]. The pulses are launched into a half step of standard fibre (1.2km) in order to minimise the amount of dispersive radiation that is produced.

Pulses with widths of 6.0ps are again used with a variety of different pulse energies. The strength of this dispersion map with a 6.0ps pulse is 2.46. According to the simple formula given in equation 3.4 this gives a stable pulse energy for a first order soliton of 0.138pJ. As with first order solitons in a system with constant dispersion it is not necessary to input exactly the correct pulse width or energy since some pulse evolution takes place. It is therefore possible to get propagation for a small range of input pulse

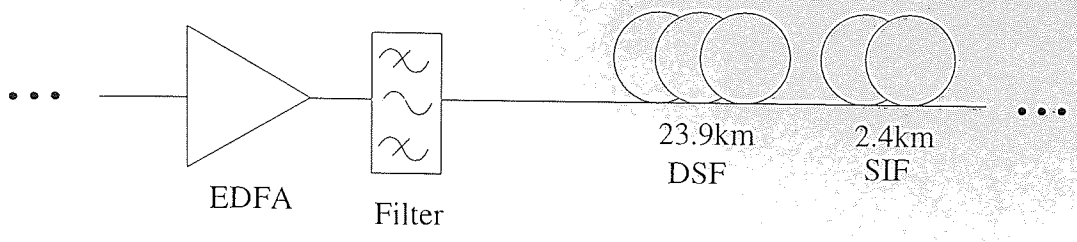

Figure 4.11: Schematic of the system used to test the dispersion map on its own.

energies. Pulses with energies between 0.03 to 0.2pJ are able to propagate over more than 10000km. These simulations show that this system is able to support solitons with slightly enhanced energy without the saturable absorber. The stable pulses are found to have the higher time-bandwidth product associated with dispersion managed systems. The time-bandwidth products for these pulses is ~ 0.4 which is closer to a Gaussian pulse than the input sech pulse

As an example of the pulses that propagate in this dispersion map figures 4.12 and 4.13 show a pulse with an input pulse width of 6.0ps and a pulse energy of 0.138pJ at the midpoints of the anomalous and normal dispersion fibres respectively. It is clear that

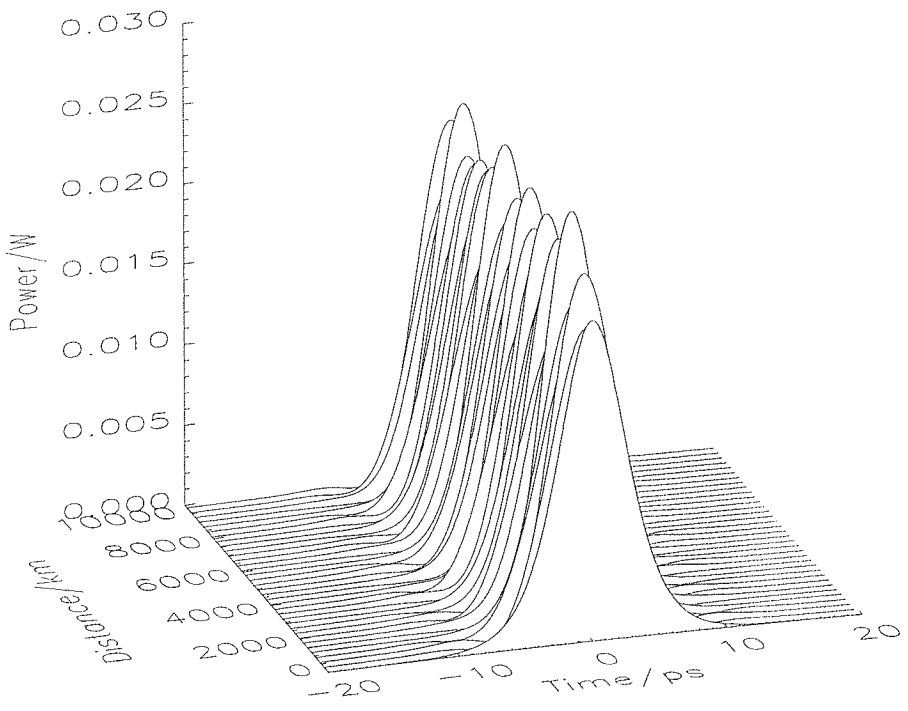

Figure 4.12: A 6.0ps, 0.138pJ sech pulse at the midpoint of the anomalous dispersion fibre. This simulation is for dispersion management alone.

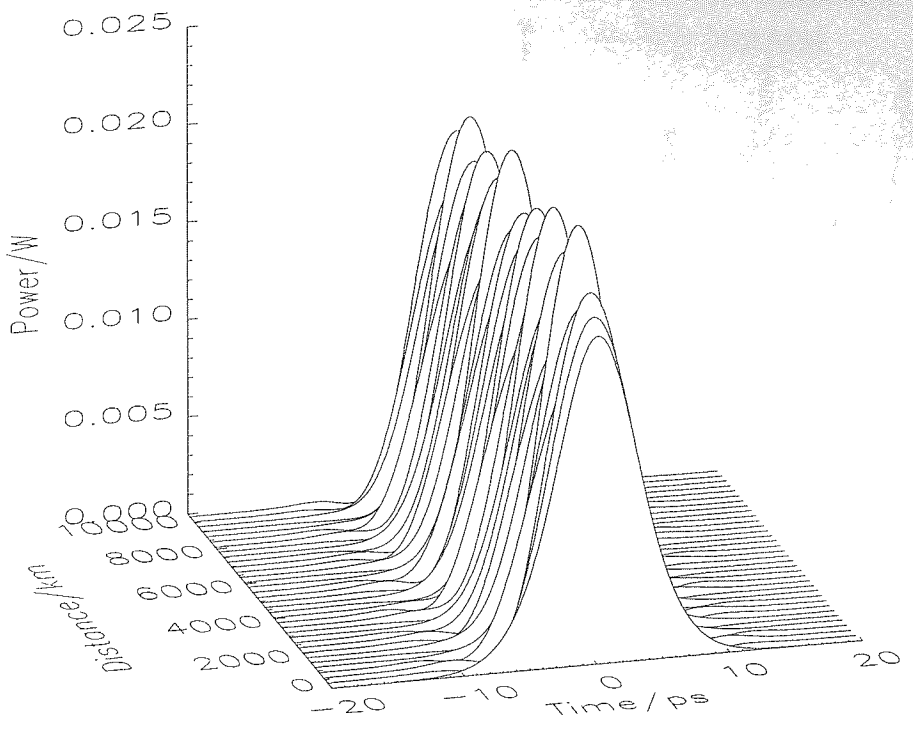

Figure 4.13: A 6.0ps, 0.138pJ sech pulse at the midpoint of the normal dispersion fibre. This simulation only used dispersion management

there are significant fluctuations in the pulse width and peak power of this pulse. This can also be clearly seen in figure 4.14 which shows the pulse width evolution at the midpoints of the two fibres. The reason for these fluctuations is that the input pulse does not have the correct shape and so undergoes an evolution. This behaviour is typical of a dispersion managed soliton when the input pulse is not the correct shape for the dispersion map, the pulse does not evolve into the correct pulse shape [166]. It is also possible to see the effect of using the incorrect pulse shape by looking at the spectrum. The spectra at the two midpoints are given in figures 4.15 (anomalous) and 4.16 (normal). These figures show that the spectrum is no longer smooth after propagating through the dispersion map and now has a lot of detailed features. The features resemble the sidebands generated when the average soliton criteria are not met [65, 62] and can be seen most clearly in figure 4.19. The frequency of these sidebands can be calculated for the average soliton case using [62];

$$\delta\nu_n = \frac{1}{2\pi\tau}\sqrt{1 + 8n\frac{z_o}{z_a}} \tag{4.3}$$

where $\delta\nu_n$ is the frequency of the nth sideband relative to the central frequency of the pulse, τ is the full width half maximum pulse width, z_o is the soliton period and z_a is the

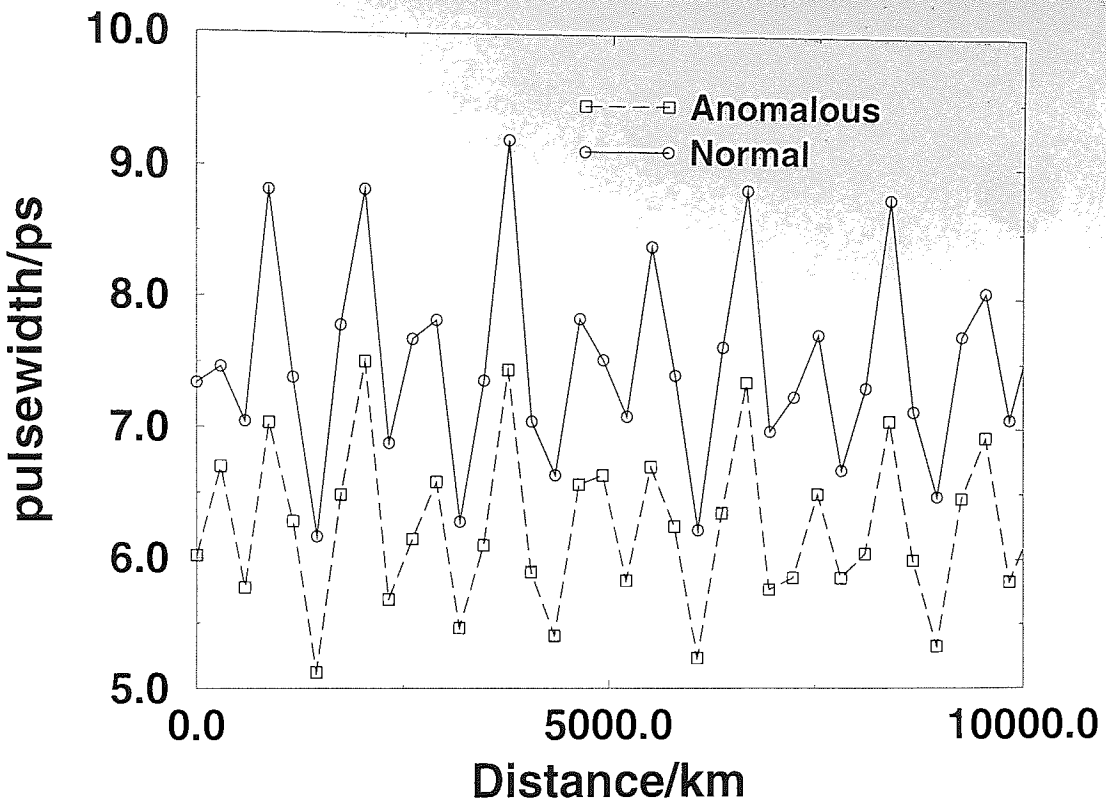

Figure 4.14: The evolution of the pulse width for the 0.138pJ pulse in the dispersion map. The pulse width undergoes a similar evolution in both fibres.

amplifier span length. Taking the pulse width as 5.5ps with dispersion of 0.1ps/(nm km) and an amplifier span length of 26.4km the frequency of the first sideband is 0.18THz for the average dispersion. In figure 4.19 the first sideband is at 0.015THz this value is an order of magnitude smaller than expected however it is of the correct order when the soliton period of the pulse in the anomalous dispersion fibre is used. Sideband generation has not been studied for dispersion managed systems.

It is also interesting to look at the way these parameters change over one pass through the dispersion map. The pulse evolution, pulse width and spectrum for one trip through the dispersion map are given in figures 4.17, 4.18 and 4.19 respectively. Although there is quite a significant change in the pulse width and peak power over the course of one dispersion map there is not a significant change in the spectrum due to the low power and so low nonlinearity.

It is therefore possible to propagate pulses over long distances using the dispersion map alone. However the pulses undergo long term changes in pulse shape, width and spectrum as they propagate if the incorrect initial pulse shape is used.

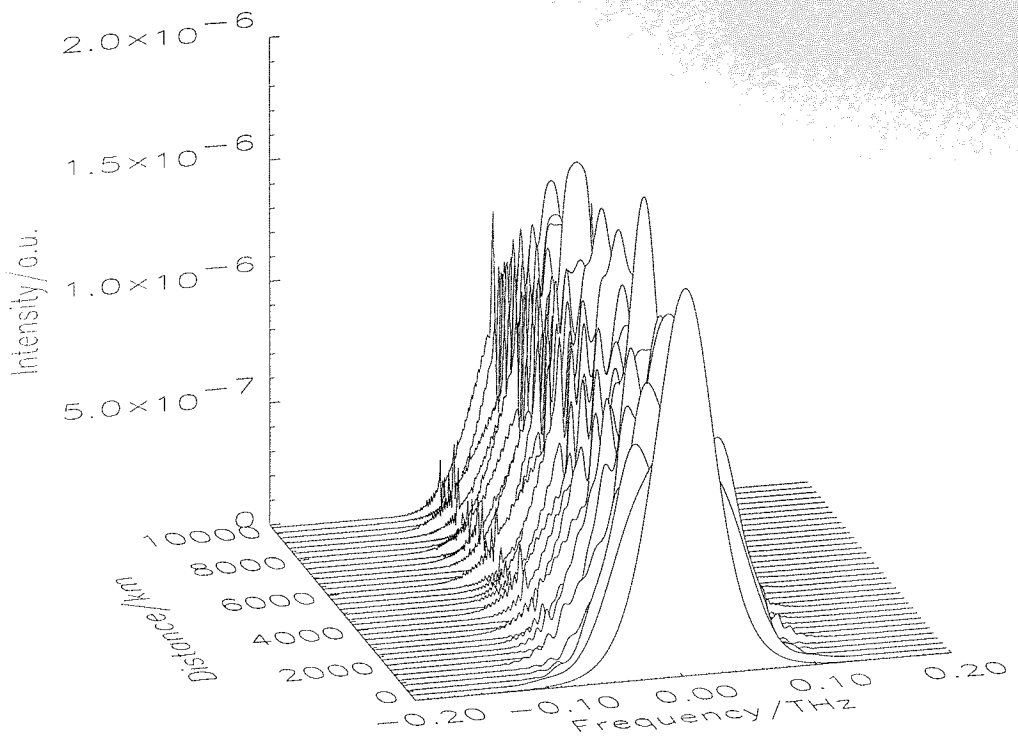

Figure 4.15: Spectrum of a 6.0ps, 0.138pJ sech pulse at the midpoint of the anomalous dispersion fibre. This simulation only used dispersion management

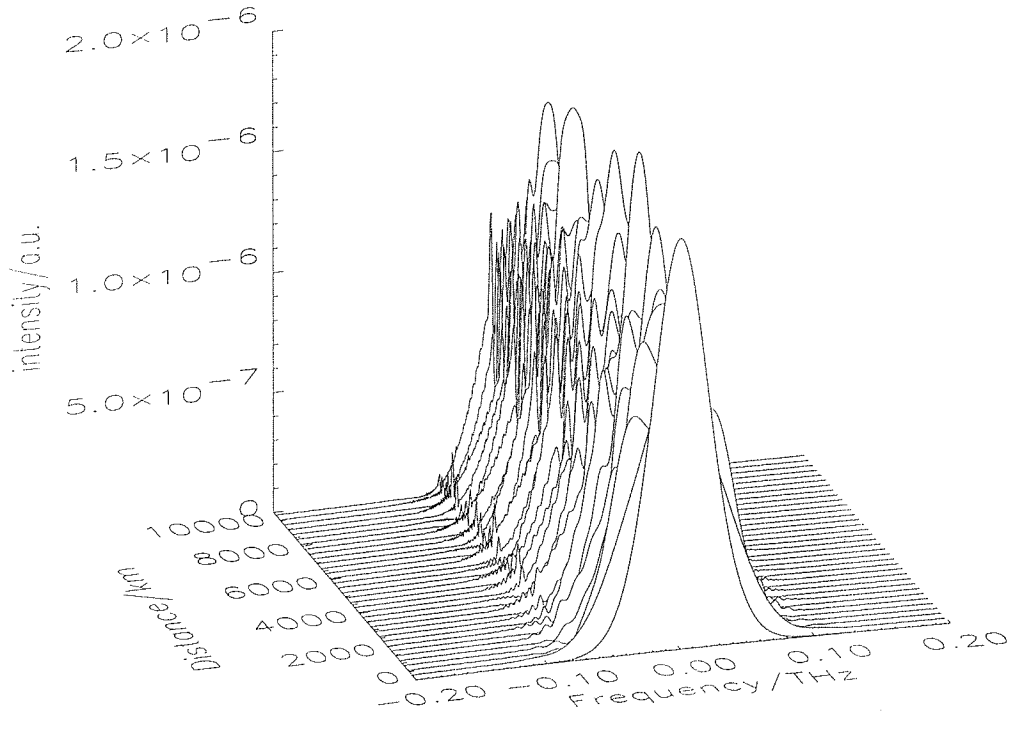

Figure 4.16: Spectrum of a 6.0ps, 0.138pJ sech pulse at the midpoint of the normal dispersion fibre. This simulation only used dispersion management

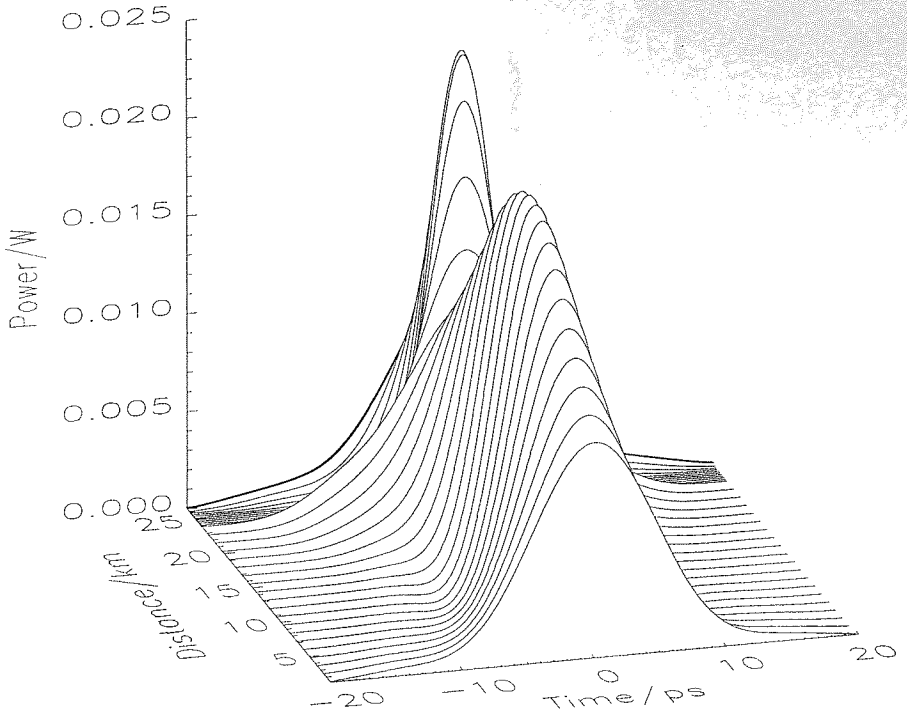

Figure 4.17: A 6.0ps, 0.138pJ sech pulse as it propagates through the dispersion map.

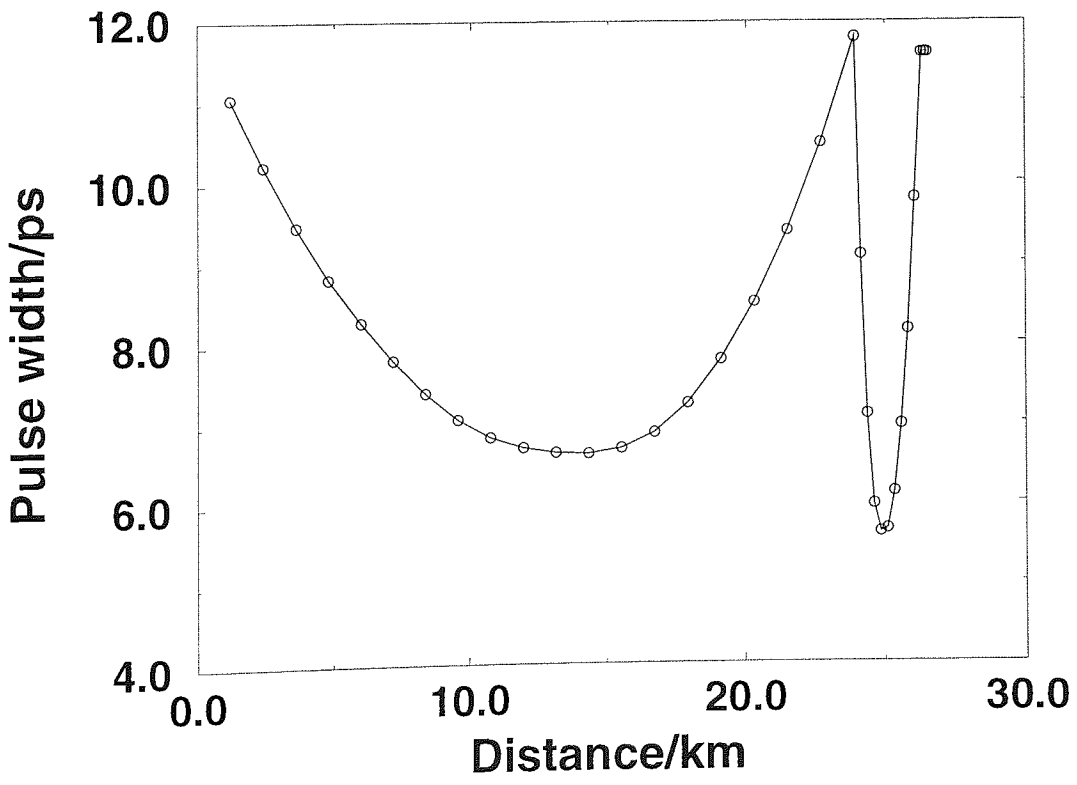

Figure 4.18: The evolution of the pulse width for the 0.138pJ pulse during one pass through the dispersion map.

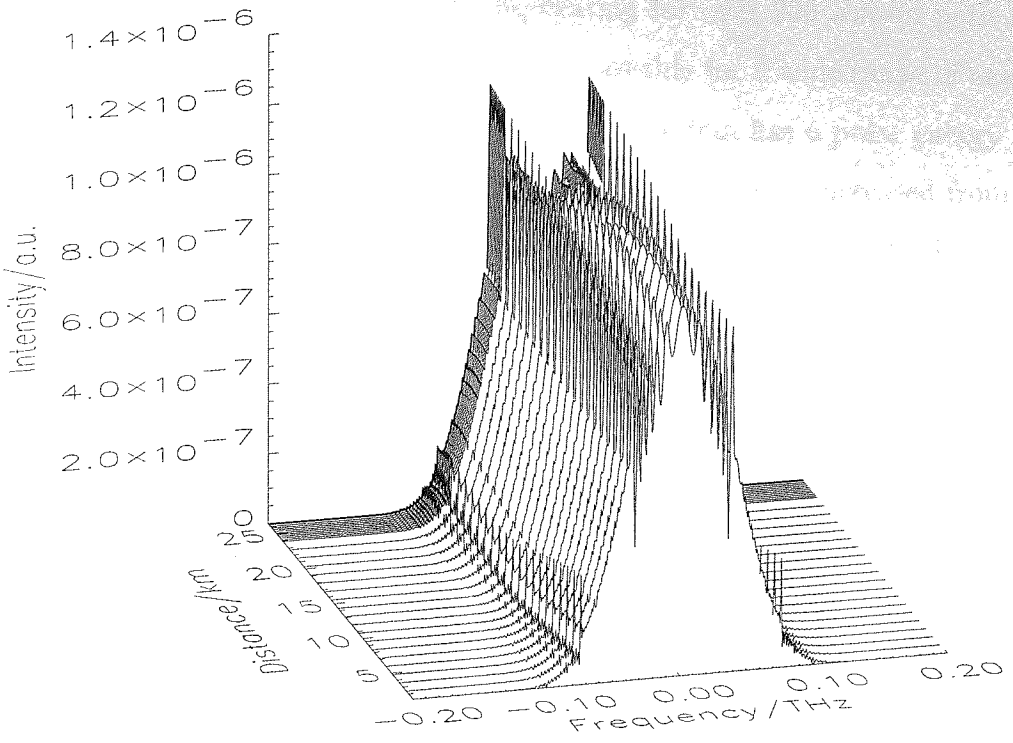

Figure 4.19: Spectrum of a 6.0ps, 0.138pJ as it goes through one dispersion map.

4.2.3 Combined System

The system with both dispersion management and a saturable absorber is now considered. A schematic of this system is given in figure 4.20, the dispersion map and saturable absorber are the same as those described in the previous two sections. All the fibres used are again taken to have no loss and no higher order dispersion, the amplifier has controlled gain and is used to compensate for the loss from the saturable absorber and the filter. Soliton pulses with a FWHM of 6.0ps and a variety of pulse energies are again launched into a half step of standard fibre. Each simulation is run until the full-width at half maximum, time-bandwidth product and peak power of the pulse have reached a constant value.

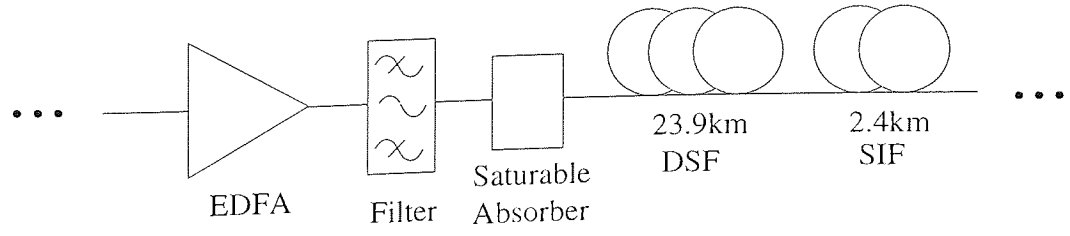

Figure 4.20: Schematic of the combined system.

Low energy pulses that propagated in the system with constant dispersion do not reach a stable pulse shape even after propagating for over 200 soliton periods. As the pulse energy is increased stable propagation is possible for a wide range of energies. The lowest energy pulse to reach a steady state in this system has a pulse energy of 0.165pJ (the launched soliton was of order N=2.5). As the energy was increased from this value a range of stable pulses can be found with energies from 0.165 to 1.30pJ (launch orders from N=2.5 to 7.0).

It is interesting to look at a range of these pulses from those at the lower end of the energy scale to those with higher energy. The first pulse has an energy of 0.165pJ. The evolution of the pulse shape is given in figure 4.21, all the plots of this pulse are taken from the midpoint of the anomalous dispersion fibre. The pulse undergoes some initial changes in its shape, peak power and width. If this pulse is compared with the one from the dispersion map alone it is clear that the saturable absorber adds to the stability of the system and assists the pulse in reaching the correct pulse shape. However from the plot of the spectrum of this pulse (figure 4.22) it can be seen that it is still undergoing some evolution even after 10000km and the spectrum of this pulse has the same sidebands that were seen in the previous section. The plot of the pulse in dBm, given in figure 4.23, shows that the pulse sheds some dispersive radiation, although it is kept at a low level by the saturable absorber.

As with the pulses in the dispersion map alone the lower power pulses in the combined system show a large change in pulse width and peak power through one dispersion map due to the breathing of the pulses, but there is not much change in the spectrum over one map. This can be seen in figures 4.24 and 4.25 which show the evolution of the pulse and its spectrum respectively over one dispersion map.

A pulse from the middle of the stable region is now examined. This pulse has an input energy of 0.422pJ, the plots for this pulse are taken at the midpoint of the normal dispersion fibre. As with the lower power pulse, this one (shown in figure 4.26) quickly evolves into the 'correct' pulse shape for this dispersion map and rapidly reaches the stage where there are no longer any obvious changes in pulse width or peak power. This is contrary to what is seen from purely dispersion managed solitons which do not successfully evolve into the correct pulse shape [166]. In contrast to the lower power pulse the spectrum of this pulse (figure 4.27) also reaches a steady state and does not have the sidebands that were seen previously. It is also interesting to note in figure 4.28 that the saturable absorber is now able to remove the dispersive radiation more efficiently as the pulse power

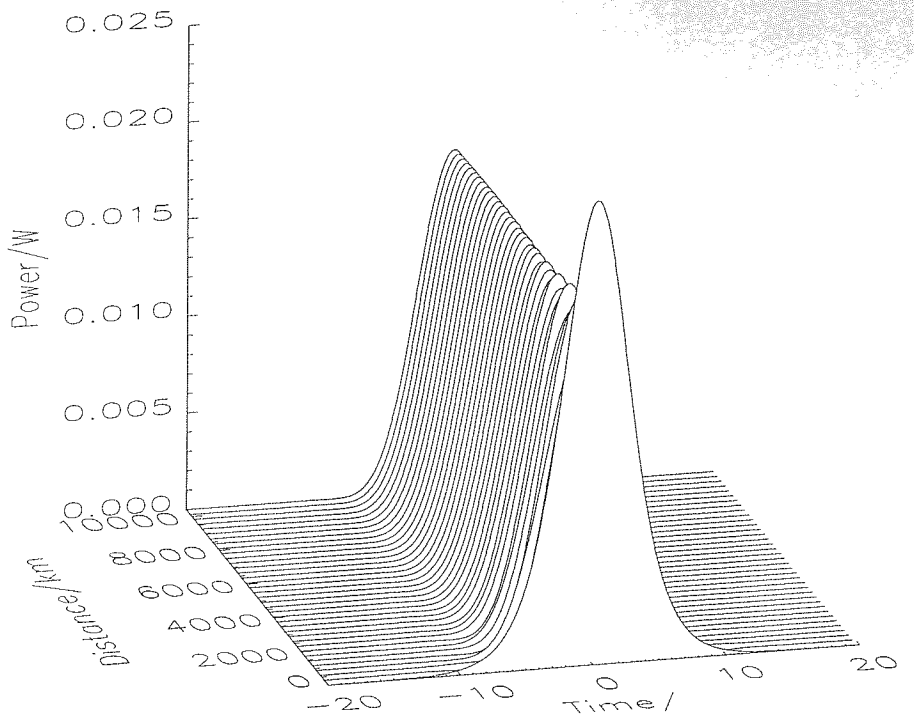

Figure 4.21: A 0.165pJ pulse taken at the midpoint of the anomalous dispersion fibre.

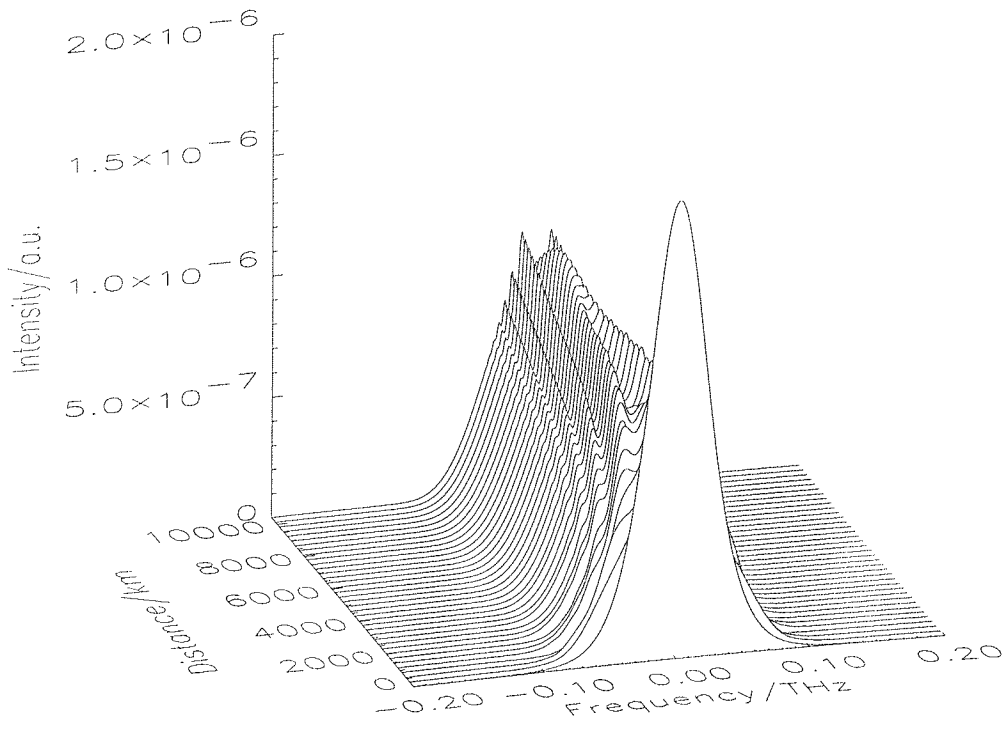

Figure 4.22: The spectrum of the 0.165pJ pulse taken at the midpoint of the anomalous dispersion fibre.

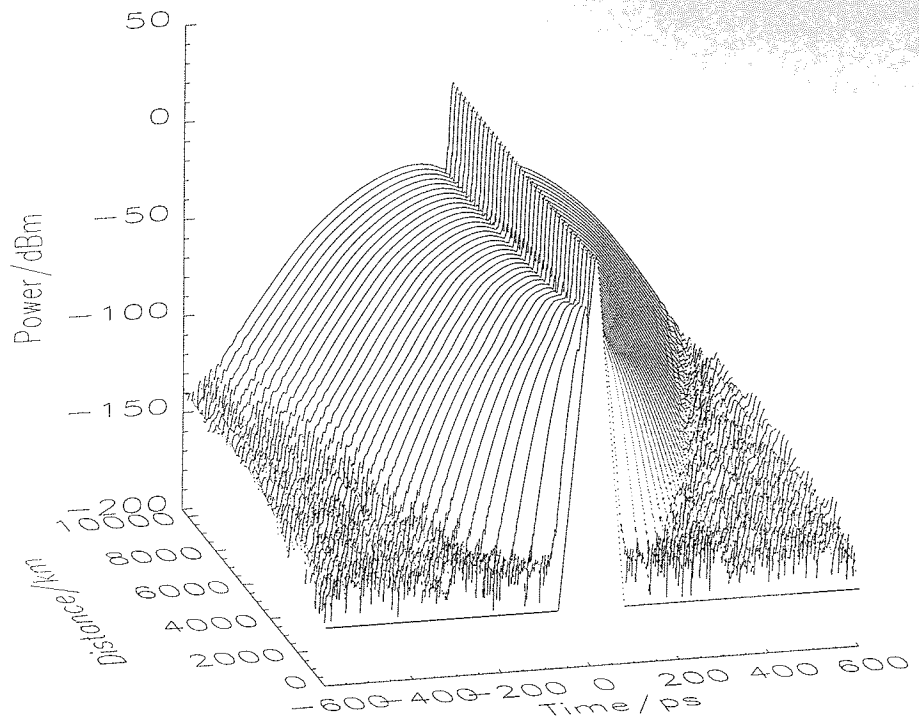

Figure 4.23: The 0.165pJ pulse shown in dBm at the midpoint of the anomalous dispersion fibre.

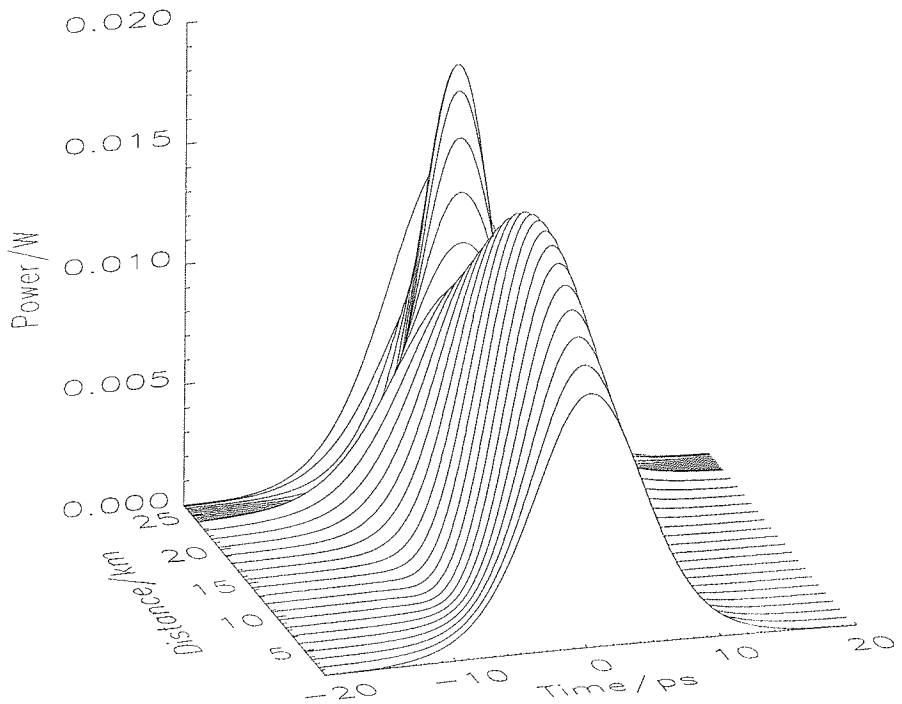

Figure 4.24: A 0.165pJ pulse as it breathes through one dispersion map

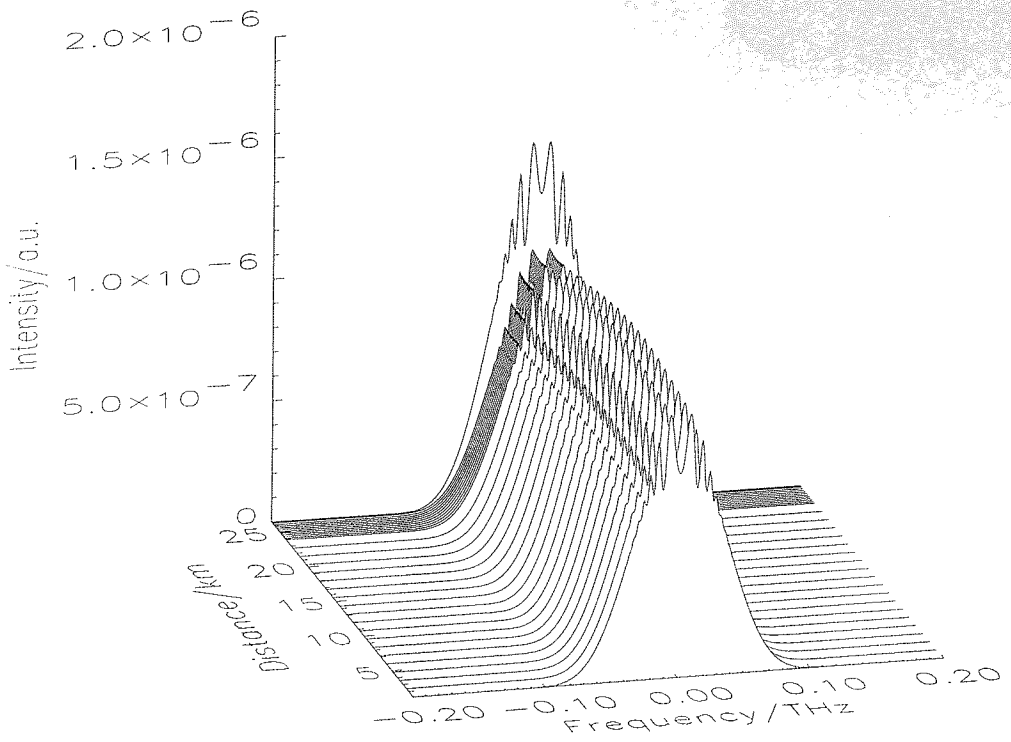

Figure 4.25: The spectrum of the 0.165pJ pulse as it passes through the dispersion map once.

is now further up the switching curve and so there is a greater contrast between the loss experienced by the pulse and the loss experienced by the radiation.

There are further differences between the lower power pulse and the 0.422pJ pulse when the pulse evolution through one dispersion map is examined. Figure 4.29 shows the pulse as it propagates through one dispersion map and as seen in the earlier results this pulse undergoes breathing as it passes through the dispersion map. This pulse breathes more than the previous one as it has a greater bandwidth. This can be seen in figure 4.30 which also shows that with the higher powers, leading to more nonlinearity, there are now larger changes in the pulses spectrum over one amplifier span.

A pulse at the top end of the range of energies is now used. This pulse has an input energy of 1.3pJ and so has a peak power which is again higher on the switching curve of the saturable absorber. As with the previous two, this pulse rapidly reaches the stage where its peak power, shape and width reach a steady state as can be seen in figure 4.31 which is again taken from the midpoint of the normal dispersion fibre. The large contrast in powers between the peak of the pulse and the dispersive radiation means that the dispersive radiation in this case is almost completely suppressed as can be seen in the dBm plot in figure 4.33. The spectrum of this pulse like the last one also rapidly reaches

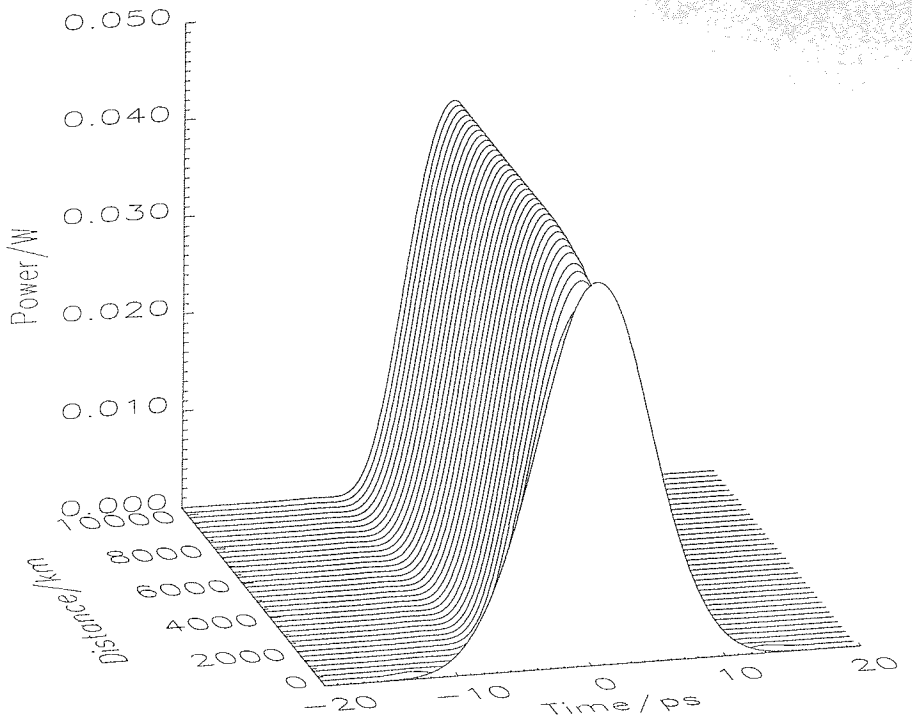

Figure 4.26: A 0.422pJ pulse taken at the midpoint of the normal dispersion fibre.

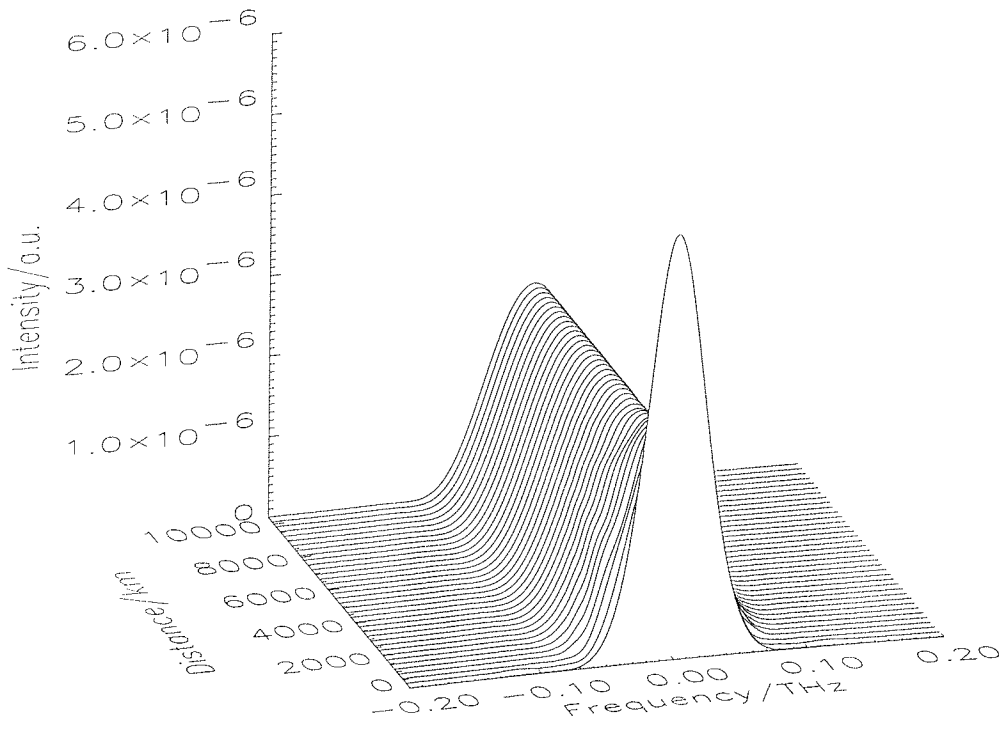

Figure 4.27: The spectrum of the 0.422pJ pulse taken at the midpoint of the normal dispersion fibre.

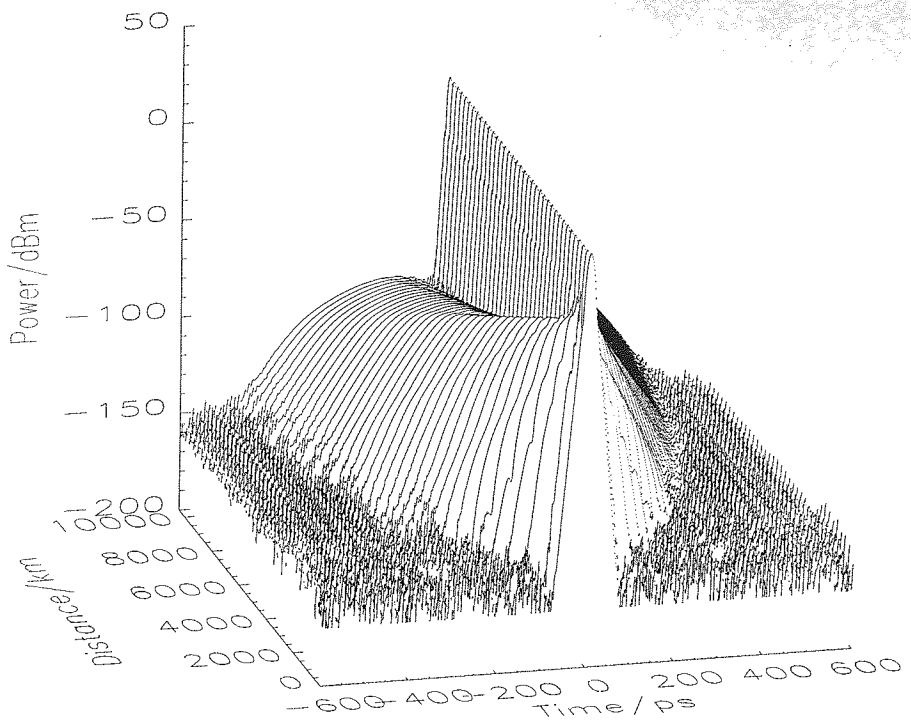

Figure 4.28: The 0.422pJ pulse shown in dBm at the midpoint of the normal dispersion fibre.

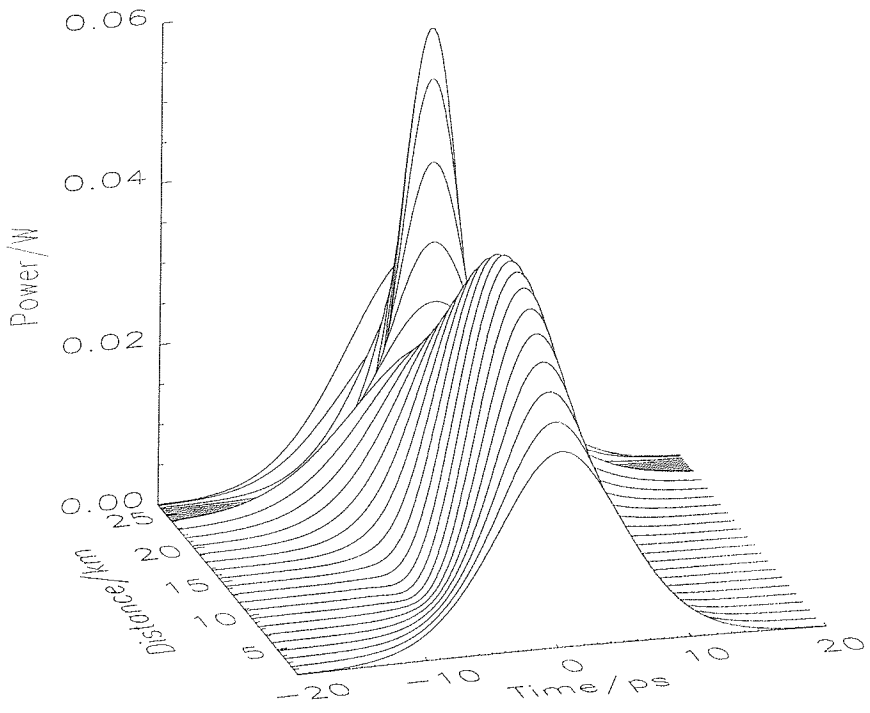

Figure 4.29: A 0.422pJ pulse as it breaths during propagation through one dispersion map

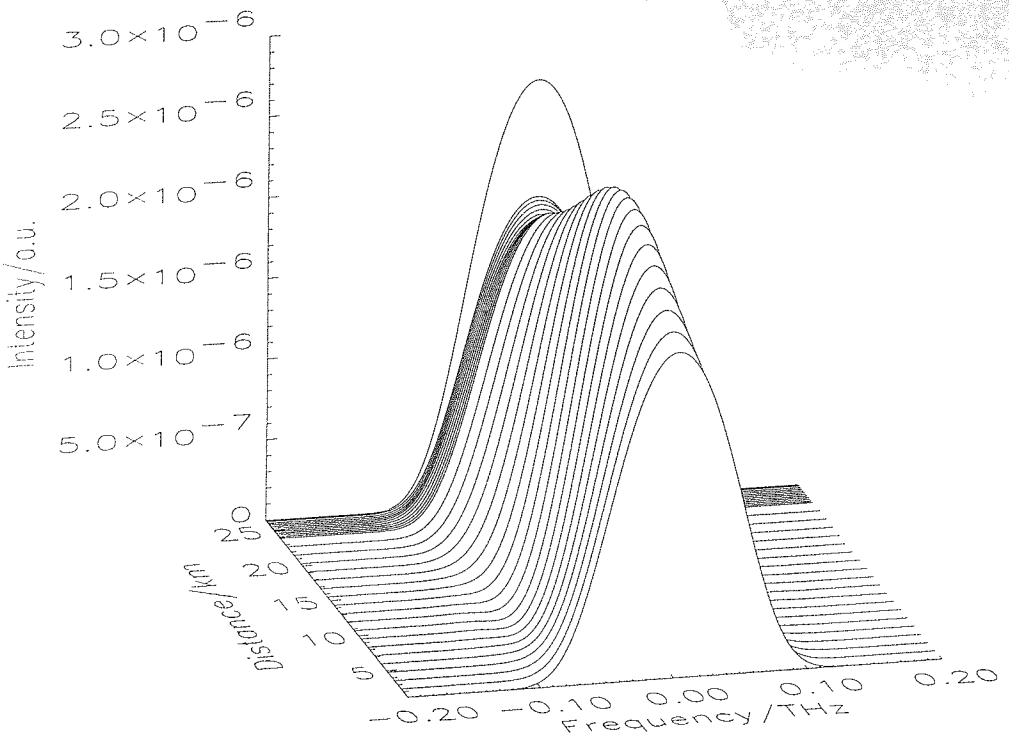

Figure 4.30: The spectrum of the 0.422pJ pulse as it passes through the dispersion map once. The spectrum of this pulse undergoes an obvious evolution over the course of the dispersion map.

the stage where it has reached a stable state, this can be seen in 4.32.

The higher powers lead to greater nonlinearity and so there are further differences in the evolution of this pulse over one amplifier span. Looking at the pulse shape first in figure 4.34 there is more pulse broadening once again due to the wider bandwidth. As a result of the greater nonlinearity there is more change in the spectrum over the dispersion map as can be seen in figure 4.35. This means that the spectrum is much broader in the anomalous dispersion fibre than it is in the normal dispersion fibre leading to a greater difference between the peak powers and pulse widths of the pulse at the midpoints of the two fibres as the pulse energy gets bigger. This will be more clearly demonstrated later in the chapter.

When the pulse energy is further increased to 1.687pJ stable single pulse propagation is no longer possible, but the pulses do not completely break up. Instead, as can be seen from the temporal and spectral plots in figures 4.36 and 4.37 respectively, these pulse appear to be undergoing a periodic evolution. The pulses cannot maintain their shape as the peak power of the pulse is now much greater than the switching power of the saturable absorber and thus the centre of the pulse experiences greater loss than the rest

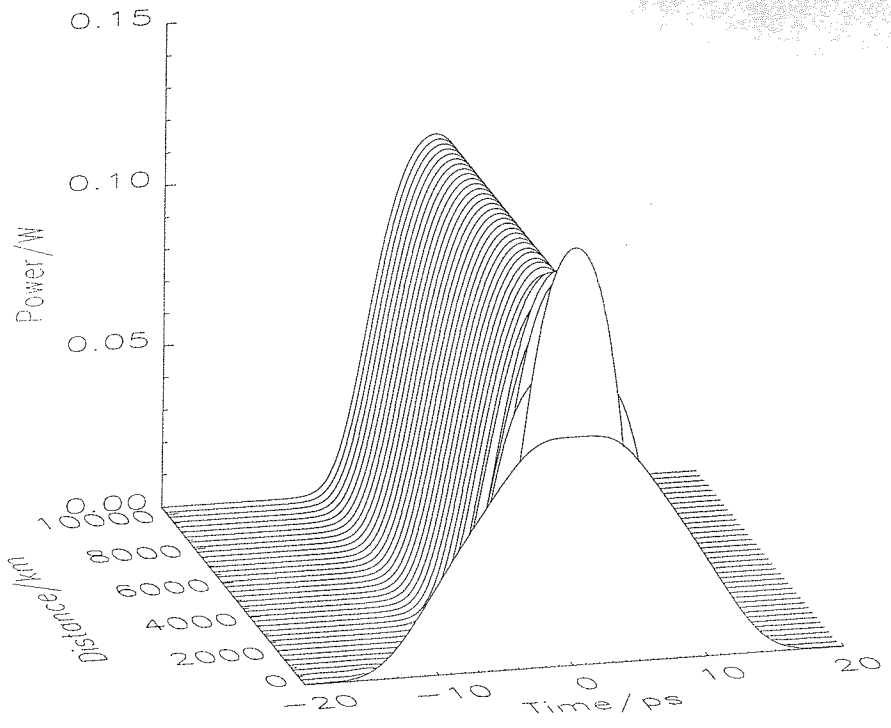

Figure 4.31: A 1.30pJ pulse taken at the midpoint of the normal dispersion fibre.

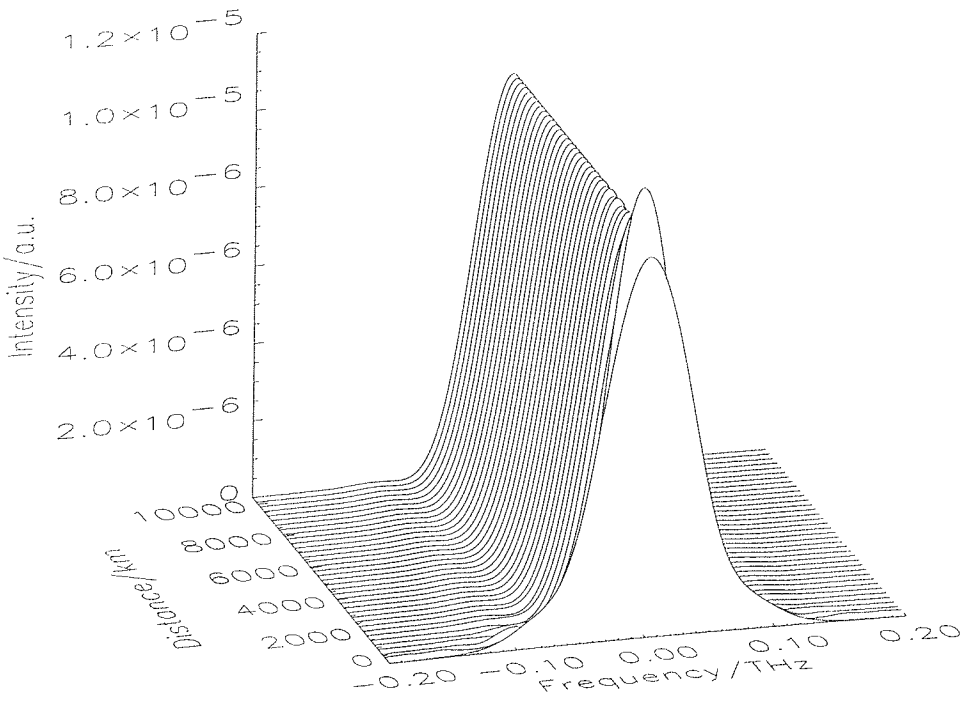

Figure 4.32: The spectrum of the 1.30pJ pulse taken at the midpoint of the normal dispersion fibre.

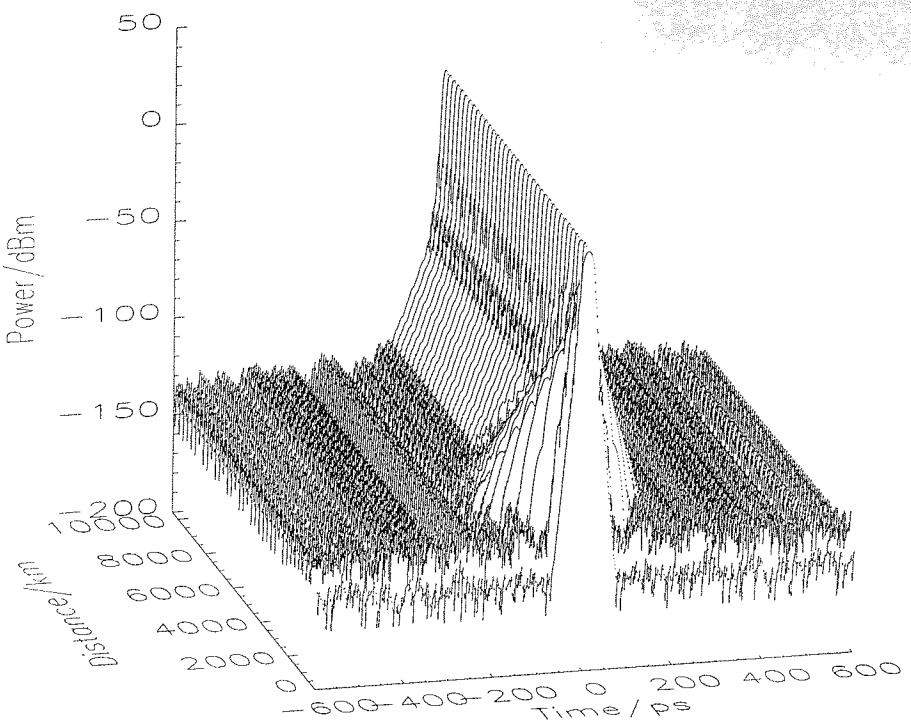

Figure 4.33: The 1.3pJ pulse shown in dBm at the midpoint of the normal dispersion fibre.

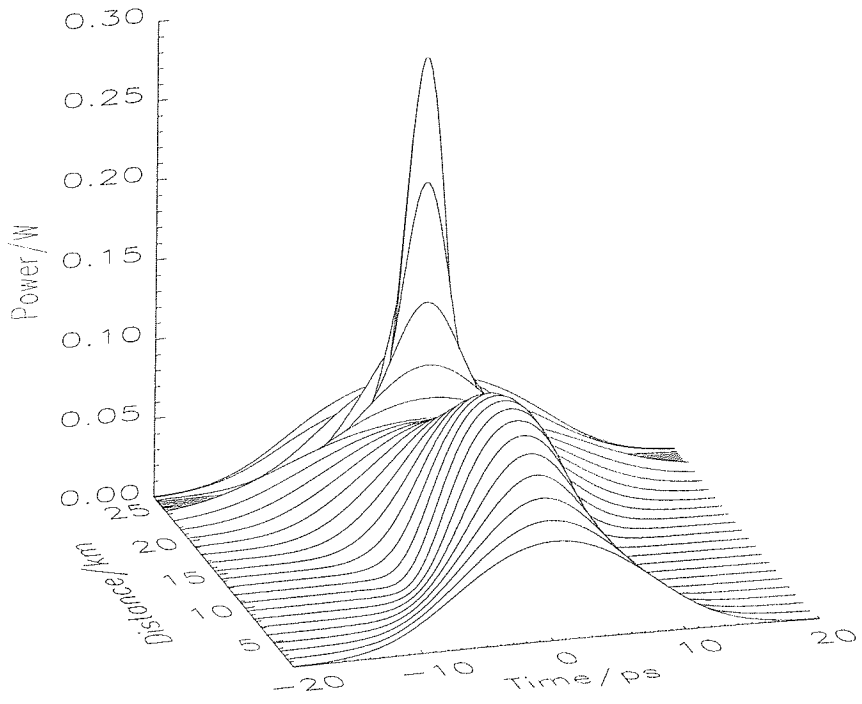

Figure 4.34: A 1.7pJ pulse as it breaths during propagation through one dispersion map the higher nonlinearity leads to greater breathing and a large difference in the pulse widths and peak powers at the midpoint of the two fibres.

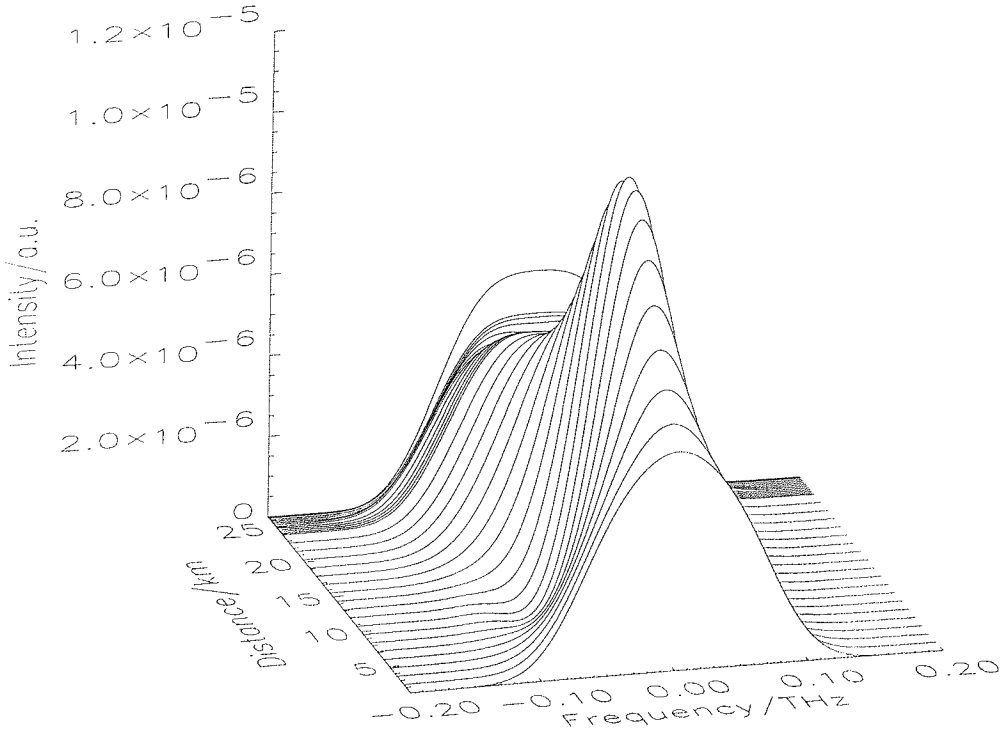

Figure 4.35: The spectrum of the 1.3pJ pulse as it passes through the dispersion map once. The spectrum of this pulse undergoes greater evolution over the course of the dispersion map than the lower energy pulses.

of the pulse causing it to develop two peaks which are symmetrical about the centre.

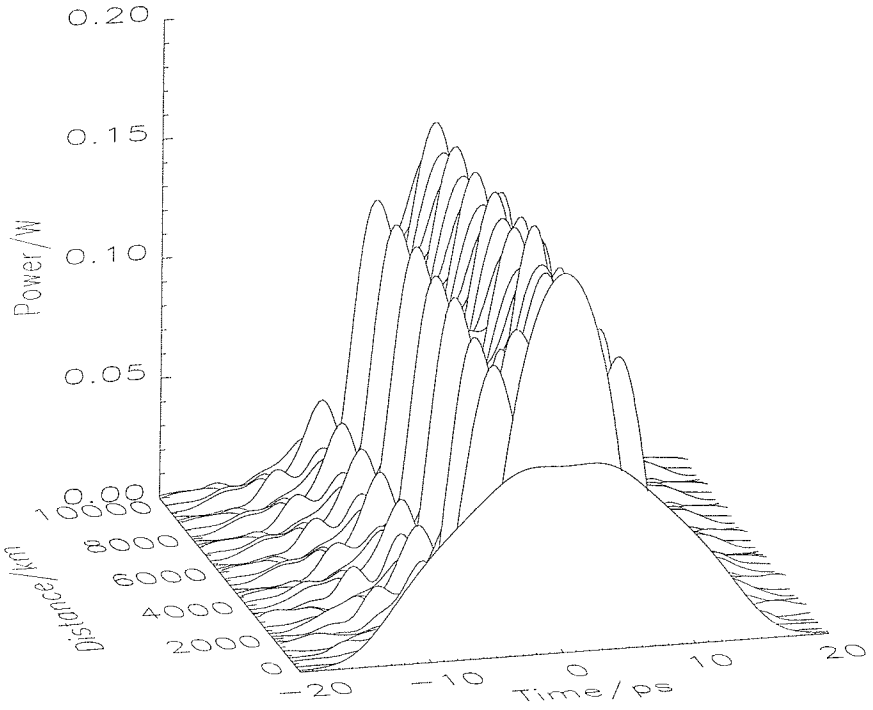

Figure 4.36: A 1.68pJ pulse at the midpoint of the normal dispersion fibre. This pulse has a more complicated evolution than the lower power pulses.

It is interesting to look in more detail at the pulse width and the bandwidth of the stable pulses as they travel through one dispersion map. The pulse width is shown in figure 4.38. Starting at the midpoint of the normal dispersion fibre the pulse width increases as it becomes more chirped. As it travels through the anomalous dispersion fibre the pulse width reduces to a deep minimum and then increases. As the pulse passes through the amplifier, filter and saturable absorber there is a reduction in pulse width as the low intensity wings are attenuated. Finally the pulse width is further reduced as it passes through the normal dispersion fibre.

The bandwidth also increases during the first half step of DSF as can be seen in figure 4.39. The bandwidth continues to increase in the first half of the anomalous fibre and then decreases during the second half. As the pulse passes through the amplifier, filter and saturable absorber the bandwidth is further reduced. This is partially due to the filter and partially due to the saturable absorber which causes a reduction in the bandwidth because the pulse is chirped and therefore the low intensity wings, which are absorbed, contain the extremes of the pulses spectrum. The pulse then passes into the normal dispersion fibre and the bandwidth continues to decrease.

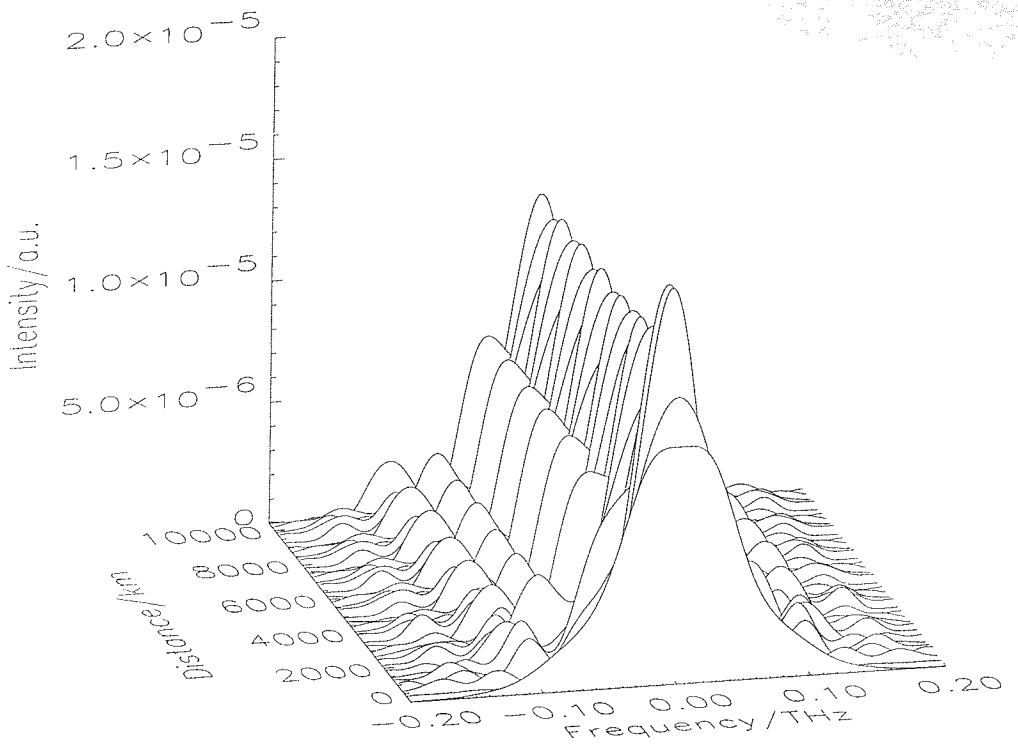

Figure 4.37: The spectrum of the 1.68pJ pulse as it propagates over 10000km, this output is taken from the centre of the normal dispersion fibre.

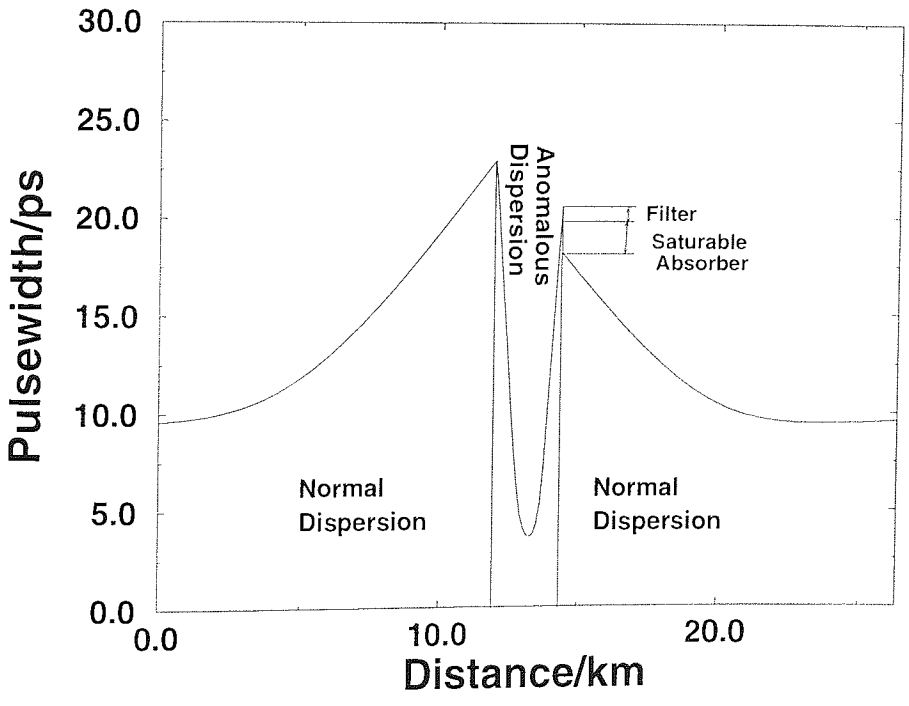

Figure 4.38: The evolution of the pulse width as it passes through one amplifier span.

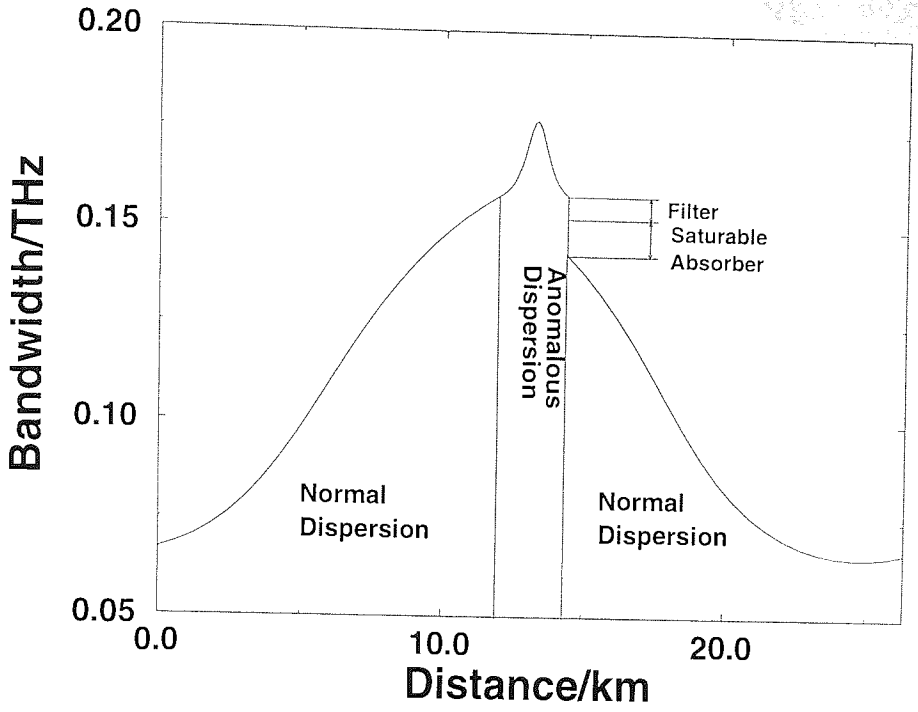

Figure 4.39: The evolution of the bandwidth of the pulse as it passes through one amplifier span.

The steady state pulse width was recorded at the midpoints of each of the two fibres. The midpoints of the fibres were chosen because these are the points where the pulses are unchirped and so their widths are at a minimum. A graph of how the pulse width at these two points changes with energy is given in figure 4.40, the data for a first order soliton in a constant dispersion system is included for comparison. The pulse width from the midpoint of the DSF appears to reach a minimum for pulses with an energy of $\sim 0.23pJ$, after this point the pulse width increases with energy. This is contrary to what is expected for a soliton system. In general the pulse width is expected to decrease with increasing energy as can be seen from the curve representing the first order soliton energy for a constant dispersion system. The pulse width in the standard fibre does decrease with pulse energy. However the change in pulse width with energy is very slight when compared to the constant dispersion soliton. This also shows how much higher the energy of these pulses is when compared to the constant dispersion soliton. It can also be seen that as the nonlinearity is increased with increasing pulse energy there is a greater difference between the pulse width at the two midpoints. This is because, as noted above, the increased self-phase modulation leads to large bandwidth changes during propagation. When the bandwidth is larger then the chirp free pulse width can be less.

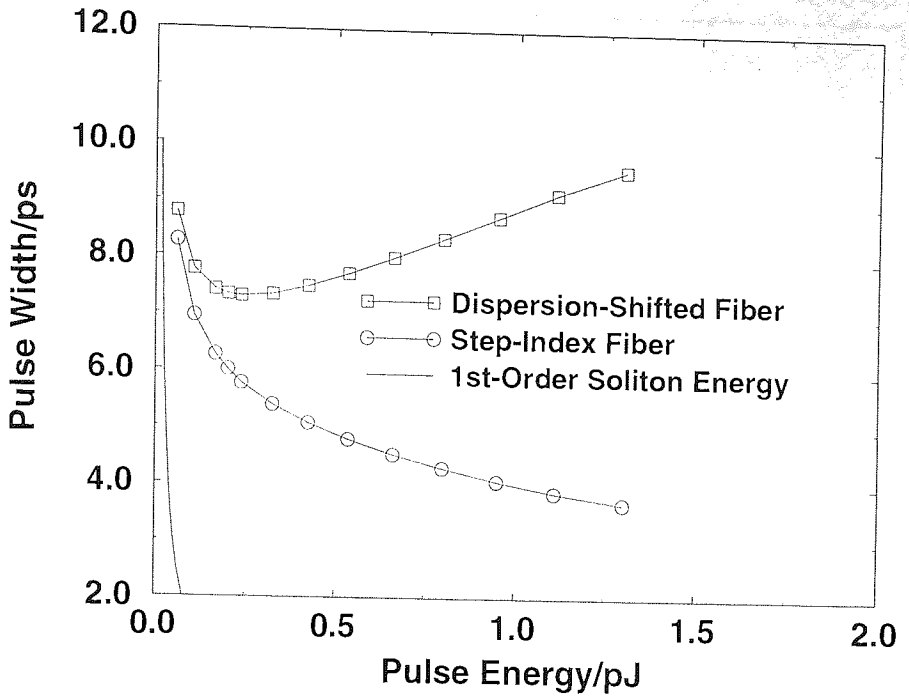

Figure 4.40: Pulse width against energy at the midpoints of the two fibres, first order soliton energy is included for comparison

The TBW product for this system is similar in both fibres as can be seen in figure 4.41. Initially the TBW product rises quickly with increasing energy but the rate of increase slows at higher energies. The value is always higher than the value for an unchirped sech pulse (0.32). The values plotted on the graph are all taken from the midpoints of the fibre where the pulses are unchirped.

4.3 2D Model

In order to more completely model the NPR a 2D model was created. The 2D model involves solving two coupled nonlinear Schorödinger equations as given in equations 2.42 and 2.43. This model is a more accurate representation of the experiment as the saturable absorption now takes place due to NPR in the fibre and a polarisation discriminator after the amplifier. A $\lambda/2$ wave plate also has to be added to the model to reset the polarisation at the start of each span.

It will be recalled from section 2.3.6 that the output from the polariser in this system is given by [33, 34, 35];

$$P_{out} = P_{in} sin^2 \frac{\Delta\phi}{2} sin^2 2\theta \tag{4.4}$$

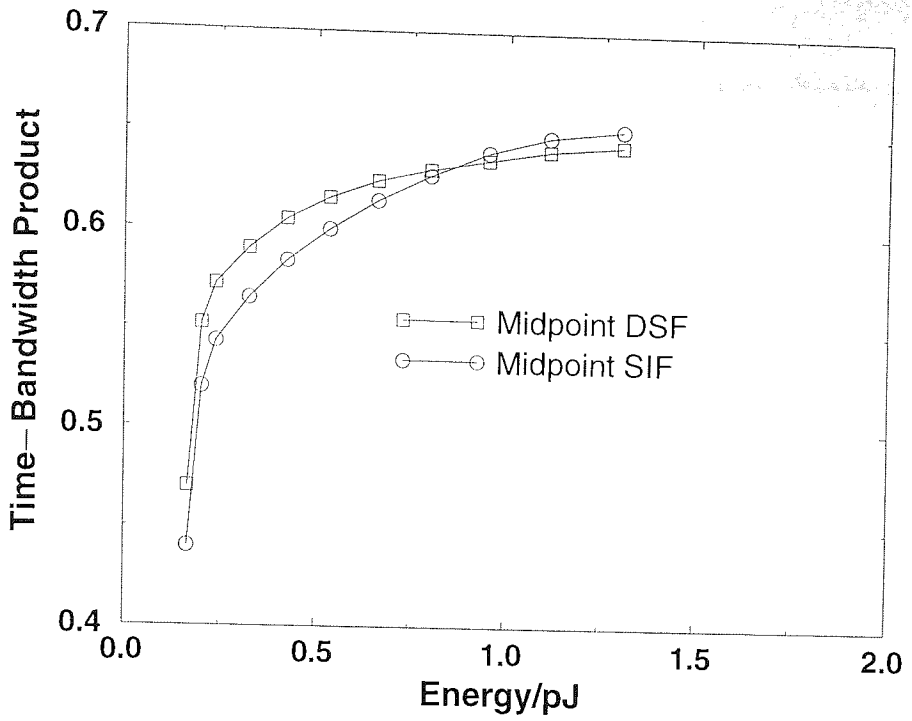

Figure 4.41: Time bandwidth product against pulse energy at the midpoints of the two fibres.

where θ is the launch angle and $\Delta\phi = (2\pi z/\lambda)(n_y - n_x + (n_2/3)(|E_y|^2 - |E_x|^2))$ is the nonlinear phase shift.

For these simulations a launch polarisation angle of 0.6 rad is used with the polariser at an orthogonal polarisation (i.e 2.17rad). When a polarisation dependent loss of 1.5dB is used it is found that the pulses are unstable. A stronger polariser results in stable propagation. Thus in the following a polariser that is 100% transmitting in one polarisation and 0% in the orthogonal polarisation is used. Further experiments have shown that the polarisation dependent loss of the filter used in the experiment [195] may be substantially higher than the 1.5dB used above and that the polarisation dependent loss varied with wavelength.

The switching curve for this nonlinear polarisation rotation saturable absorber shown in figure 4.42. Although it appears that the switching power for this system is far higher than the one used in the 1D model the difference in the way the two systems are modelled means that the comparison is not that straightforward. The saturable absorber in the 1D model was at the position in the loop where the pulse's peak power was lowest and so a low switching power could be used. Since the NPR takes place throughout the fibre where the pulses peak power is higher the switching power of the saturable absorber must also be higher. However there is a difference in the switching powers of the two systems since it is difficult to compare them effectively due to the variations in peak power caused

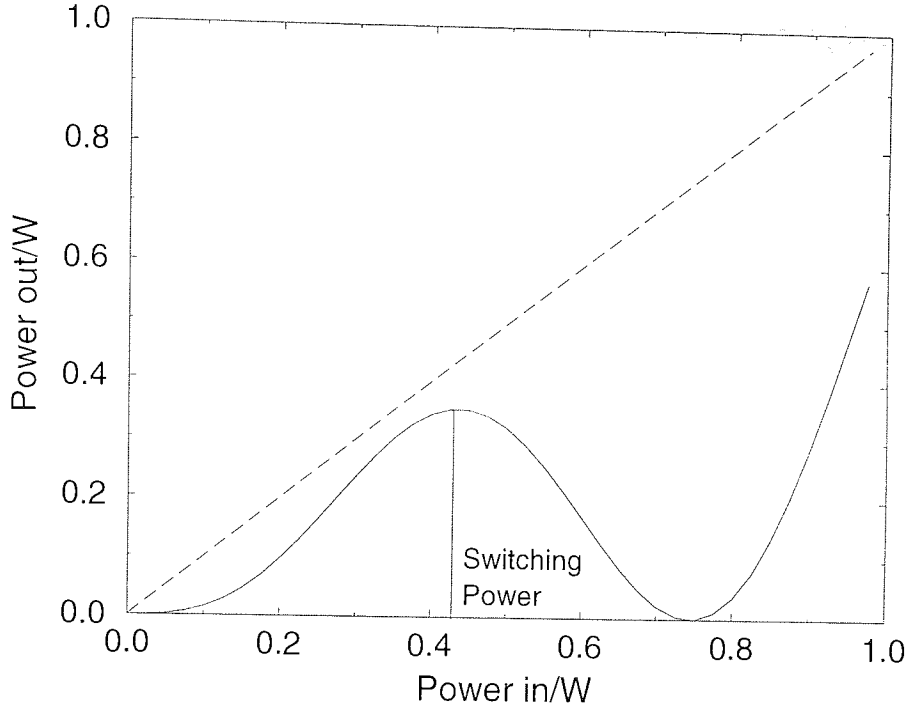

Figure 4.42: Switching curve for an NPR saturable absorber. The launch angle was 0.6rad with the polariser at 2.17rad.

by the dispersion map.

The simulations are carried out as before with a variety of input pulse energies. Each simulation is run until the peak power, FWHM and TBW have settled to a constant value. The dispersion map and the 6.0ps pulse width are unchanged from the 1D simulations.

The evolution of these pulses is very similar to that found for the 1D case. Figure 4.43 shows a launched 1.39pJ (order N=6.5) as it settles to a steady state, the two pictures represent the two polarisation states that make up the soliton. The pulse undergoes some initial changes in its shape before it reaches a stable pulse shape. As in the 1D case the stable pulse is no longer sech shaped and has a far higher TBW. Figure 4.44 shows the same pulse plotted on a log scale the strong polariser used here ensured that the dispersive radiation is almost entirely suppressed. The spectrum of this pulse is shown in figure 4.45. As with the pulse shape, the spectrum quickly settles to a steady shape and width which is retained during propagation. Figure 4.46 shows the same pulse as it undergoes pulse breathing through one dispersion map.

Stable pulses exist for a wide range of pulse energies as can be seen in figure 4.47. This graph is similar to figure 4.40 for the 1D simulations. The pulse width reaches a minimum in the DSF for a pulse energy of 0.2pJ and a pulse width of 7.08ps. The pulse width then increases with pulse energy. In the SIF the pulse width decreases with increasing energy.

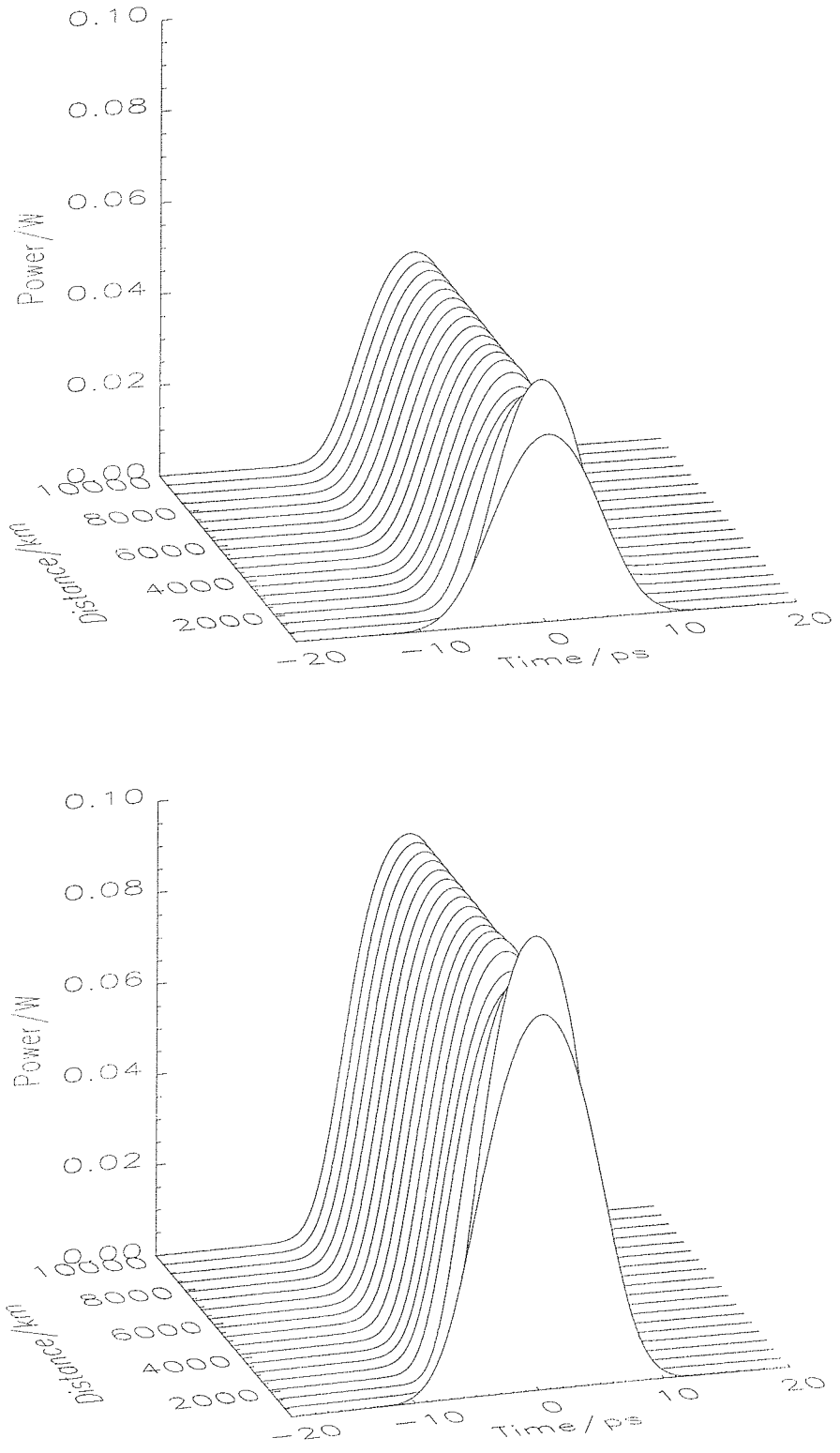

Figure 4.43: The two polarisations of the 2D model as it settles to a steady state. This pulse has an energy of 1.39pJ.

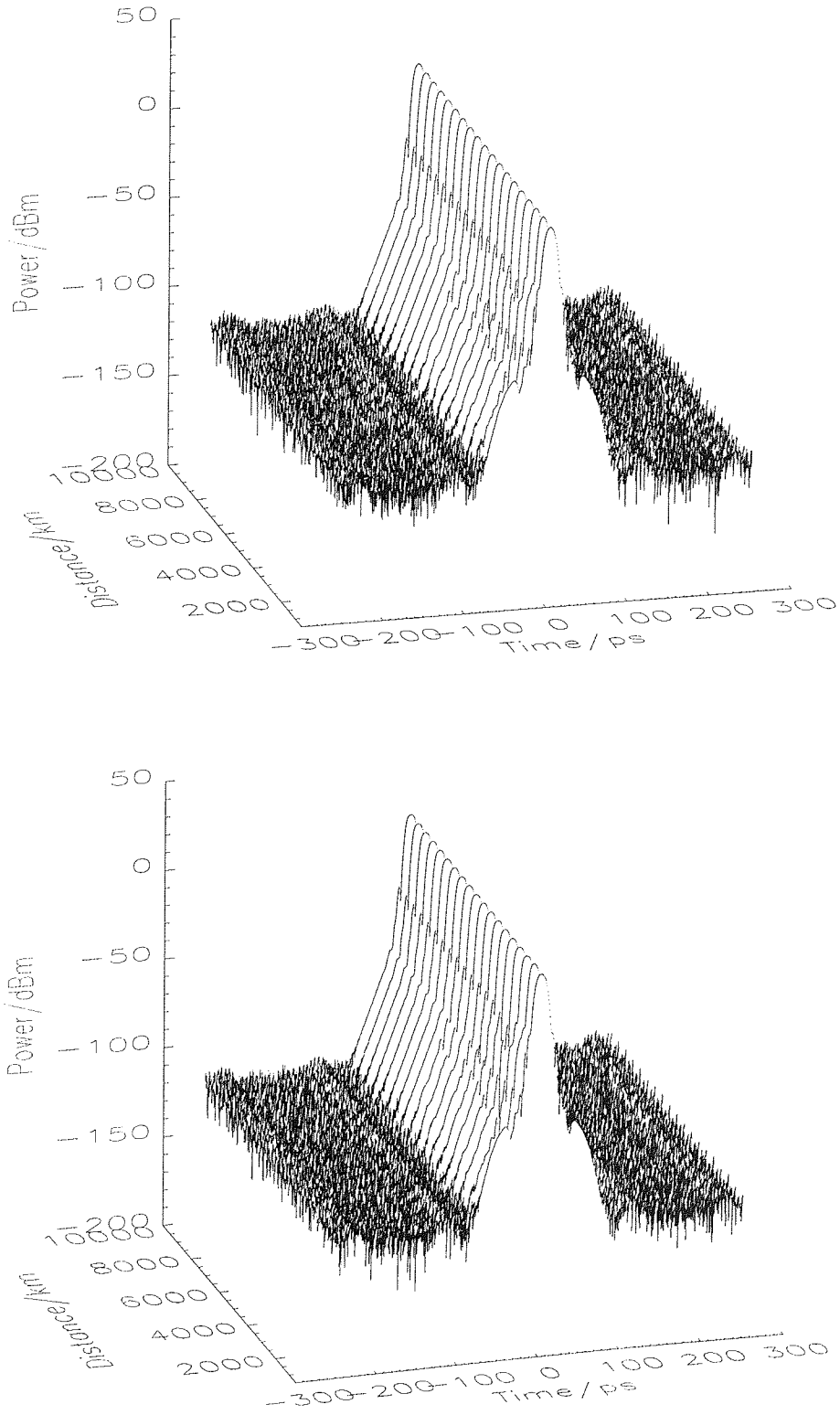

Figure 4.44: dB plot of the 1.39pJ pulse which shows the suppression of the dispersive radiation.

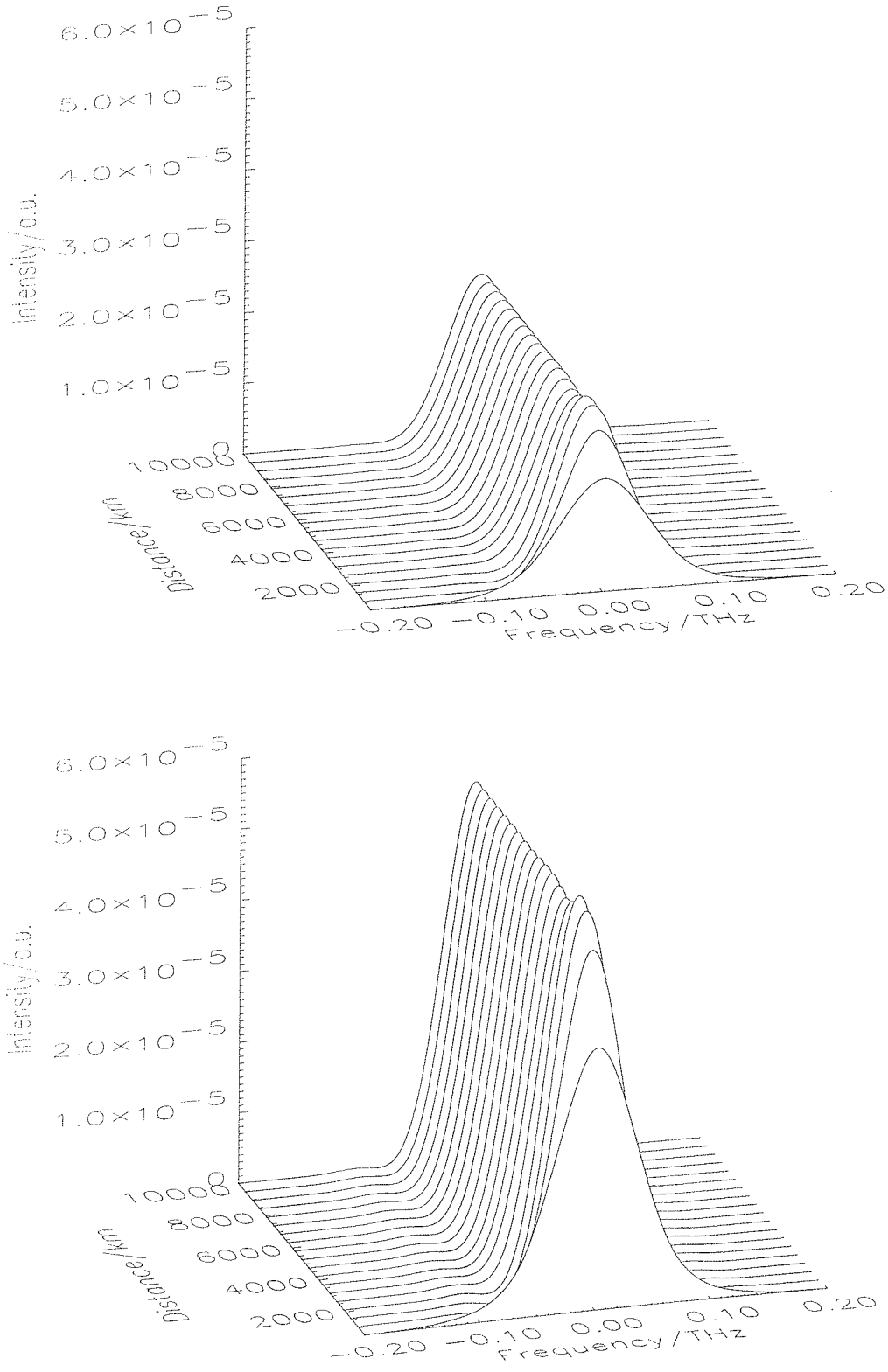

Figure 4.45: Spectrum of the 1.39pJ pulse in the 2D system, the two pictures show the spectrum on the two polarisation axes.

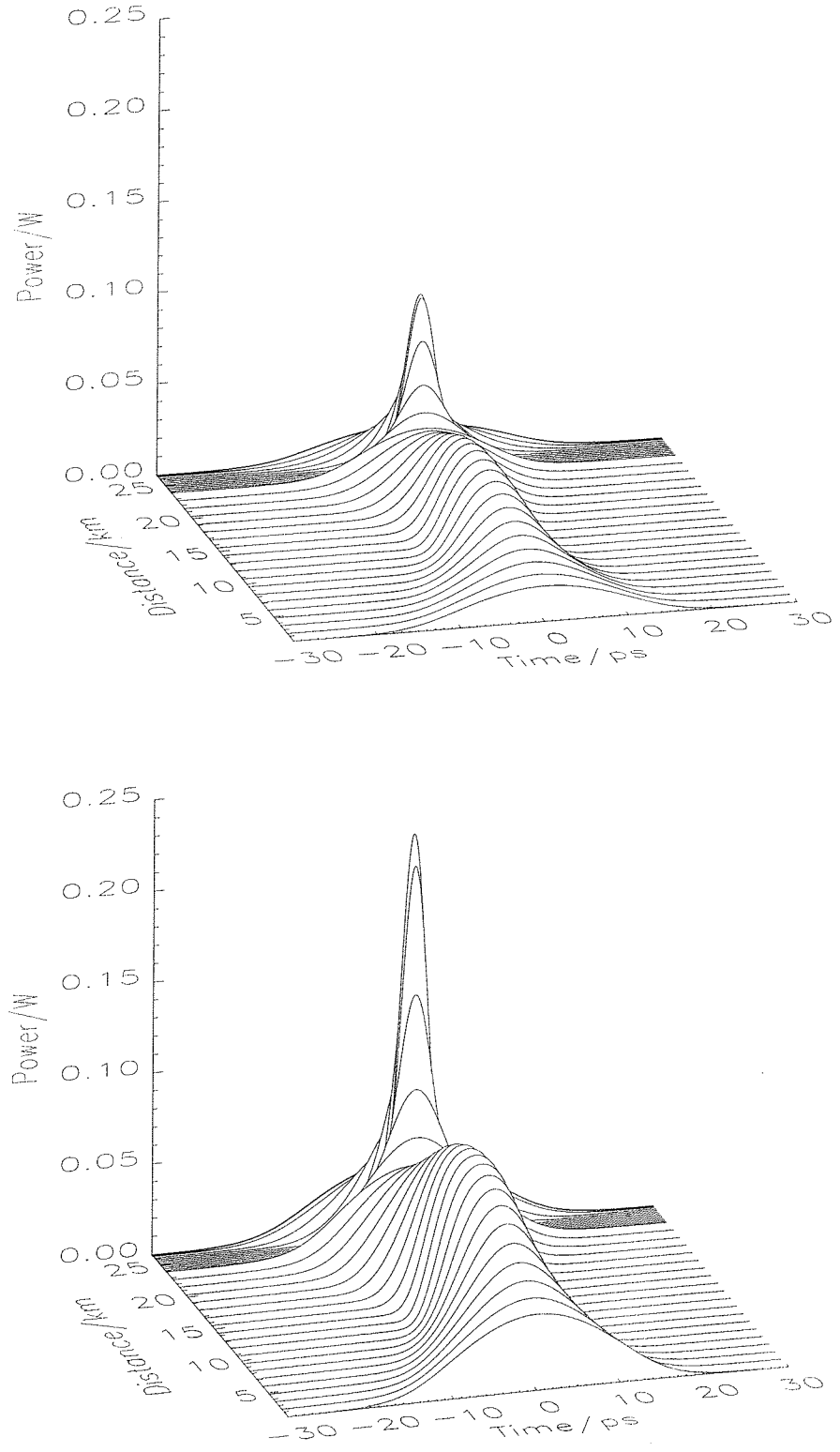

Figure 4.46: The 1.39pJ pulse as it propagates through one amplifier span.

This model supports stable pulses with higher pulse energies than those in the 1D model. This difference can probably be accounted for by the different strength and switching power of the saturable absorber.

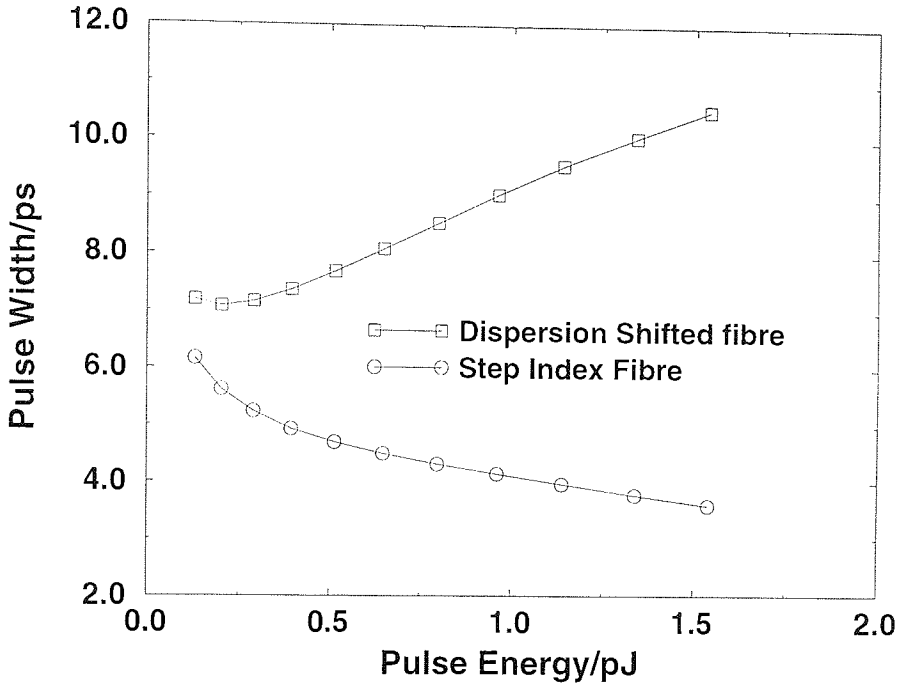

Figure 4.47: Pulse width against energy at the midpoints of the two fibres for the 2D model.

The values of the TBW for this model are given in figure 4.48. The value is always greater than that for an unchirped sech pulse, however unlike the 1D case here the TBW reaches a peak in both fibres. In the DSF the peak is 0.636 for a pulse energy of 1.14pJ. In the SIF the peak is 0.614 for a pulse energy of 1.34pJ. These values were again taken from the midpoints of the two fibres where the pulses were unchirped and clearly show that the stable pulses are not the sech shape that is launched.

4.4 Conclusions

In this chapter the numerical results from a system using both dispersion management and saturable absorption were presented. Initially the two effects were treated separately and the combined effect was investigated using both a 1D model, with a point saturable absorber, and a 2D model that used nonlinear polarisation rotation and a polariser to give the saturable absorption effect.

The system with just a saturable absorber produced shortened pulses in much the same way as a mode locked fibre laser. The pulses had peak powers of around the same

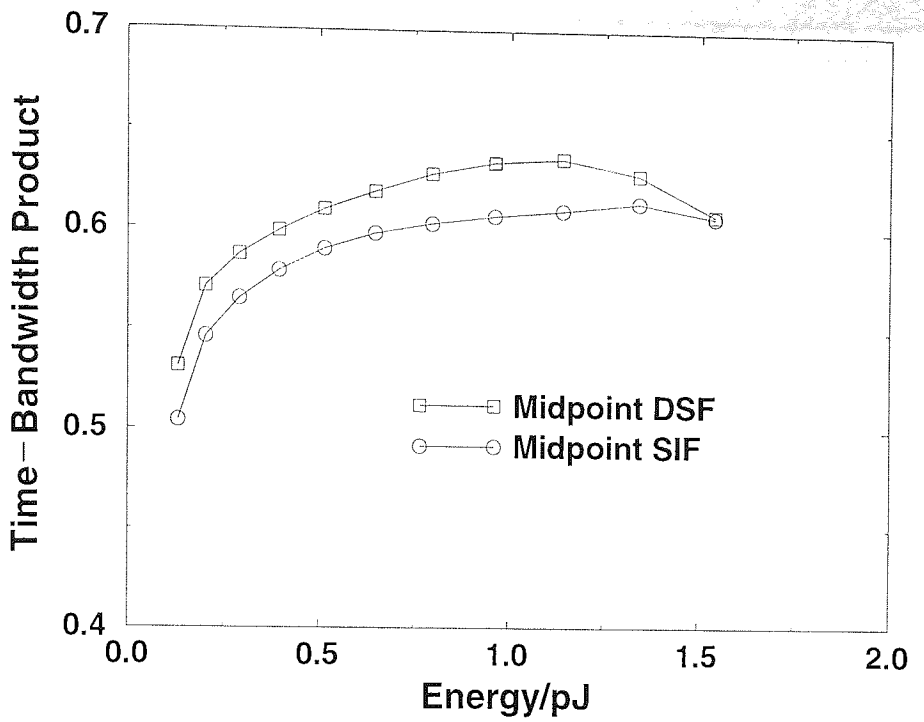

Figure 4.48: Time-bandwidth product against energy at the midpoints of the two fibres for the 2D model.

value as the switching power of the saturable absorber the shortened pulses were still approximately sech shaped. When the dispersion map was used on its own the system produced the expected dispersion managed solitons with slightly enhanced powers and a time-bandwidth product slightly greater than that of a sech pulse.

It was found that systems which employed both dispersion management and a saturable absorber were able to support stable pulses over a wide range of pulse energies and that the energy of these pulses is far greater than the energy of an equivalent average soliton or dispersion managed soliton. Figure 4.49 shows the stable regions for all of the various models employed. Throughout the launched pulses were 6.0ps sech shaped pulses. Figure 4.49 clearly shows that the systems with both dispersion management and a saturable absorber are able to support stable pulses over a far wider range of energies than was possible using either dispersion management or a saturable absorber alone.

Since NPR is intrinsically polarisation sensitive it requires polarisation control which means that systems using this form of saturable absorber would be complicated to implement. A more practical system could use a quantum well saturable absorber as these are potentially polarisation insensitive [116]. However they tend to have high switching powers and long recovery time which could make them unsuitable for use at high data rates.

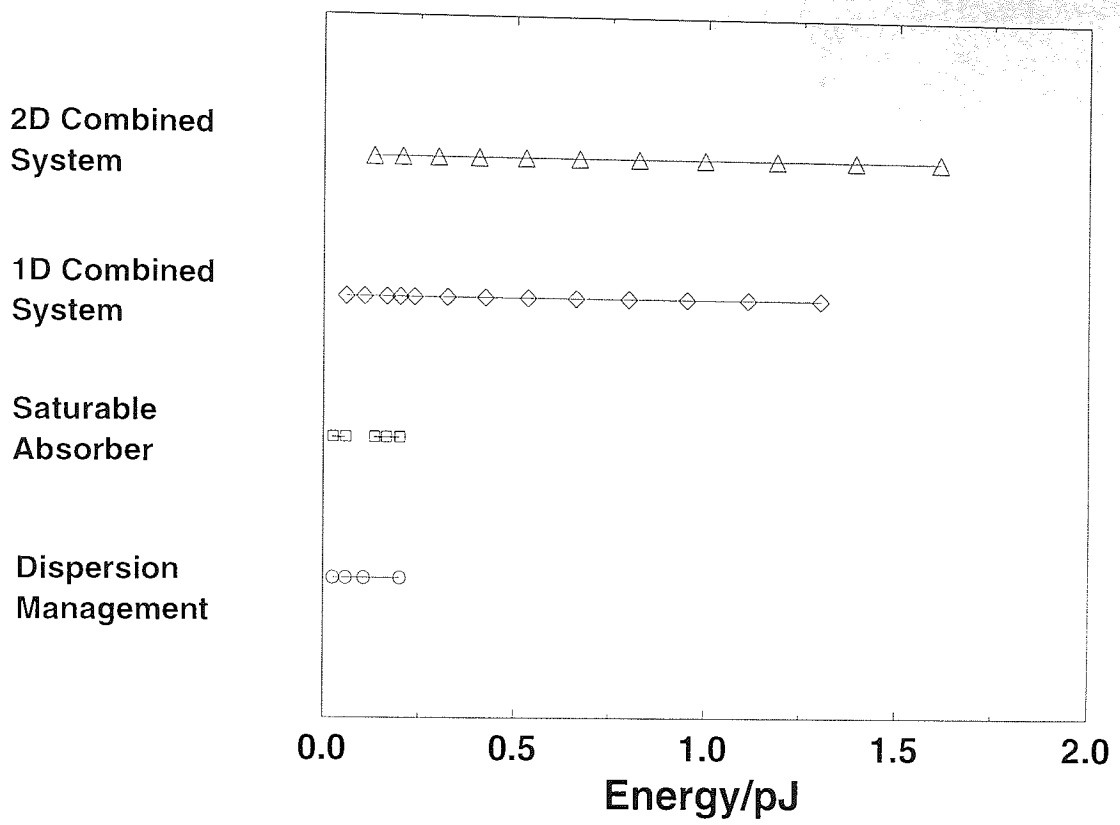

Figure 4.49: The energies for which stable propagation was possible for the various systems investigated.

This chapter considered only single pulses and fibres with no loss or higher order dispersion. In the next chapter we shall consider a system on the above model for 10Gbit/s transmission which shows that it is possible to transmit data over extremely large distances without significant degradation of the signal-to-noise ratio or timing jitter [201].

Chapter 5

10Gbit/s transmission using dispersion management and periodic saturable absorption.

5.1 Introduction

In the previous chapter the benefits of using dispersion management with a periodic saturable absorber were discussed. In this chapter this idea is extended from the idealised, lossless, single pulse case to a more practical system which transmits data over large distances. It is found that using dispersion management with a periodic saturable absorber it is possible to transmit data at 10Gbit/s over hundreds of thousands of km [201]. In terms of optical communications this is effectively an unlimited distance since the maximum required distance are $\sim 10000km$.

The main limits on propagating solitons over extremely long distances are the accumulated effects of Gordon-Haus jitter [77], the build up of noise from the amplifier leading to degradation of the signal-to-noise ratio (SNR) [76] and single channel soliton interactions [80, 82]. Using filters it is possible to suppress Gordon-Haus jitter and soliton interactions but filters do not suppress the build up of noise in the signal bandwidth. If strong filtering is used to limit the timing jitter the amount of ASE at the centre of the filter passband is increased leading to greater degradation of the SNR. Strong filtering also causes growth of linear waves at the peak of the filters transmission which lead to instability of the pulse [119].

Saturable absorbers remove the low power noise and dispersive waves which both improves the SNR and allows greater filtering of the pulse [129, 117]. The SNR is improved

because the low intensity noise is attenuated while the pulse which is higher up the switching curve experiences less attenuation [121]. The pulse stability is improved because the dispersive radiation is also low intensity and so the growth of CW at the centre of the filter bandwidth is suppressed which means that stronger filtering can be used without degrading the pulse stability. There are also the added benefits from using a saturable absorber with dispersion management as discussed in chapter 4. These are that the pulses have enhanced energy and so the SNR is further improved by having a high signal power at low dispersions where the Gordon-Haus jitter is reduced. Also because the saturable absorber is acting on a chirped pulse it works as an extra filter since the wings of the pulse which are low intensity and therefore suffer a significant amount of loss, contain the extremes of the spectrum. This extra filtering also helps to reduce the Gordon-Haus jitter and means that high powers are required so that the pulses spectrum can be restored through self-phase modulation.

In this chapter the effects of using a slightly stronger saturable absorber as well as including the effect of loss and third order dispersion will be identified for the case of a single pulse. Then the system will be used with a 10Gbit/s data pattern.

5.2 Single Pulse Transmission

It is interesting to look at the effects of loss and gain on a single pulse before looking at the transmission of a data pattern through the dispersion managed/saturable absorber system. In this section a single pulse from the 10Gbit/s data pattern will be used in a dispersion map with loss and gain and its long term evolution along with the bandwidth and pulse width changes over one amplifier span will be examined.

One amplifier span of the system used in these simulations is given in figure 5.1 the parameters used are chosen to be the same as those in reference [201] to allow comparison of the results. The dispersion map consists of 23.6km of dispersion shifted fibre (DSF) with dispersion of -1.11ps/(nm km) and loss of 0.252dB/km and 1.7km of step index fibre (SIF) with dispersion of 16.5ps/(nm km) and loss of 0.294dB/km. The filter has a Gaussian profile and a pass band of 2.5nm. The amplifier is working in saturation and has a noise figure of 4.5dB. The saturable absorber is the point saturable absorber used in the previous chapter however the power dependent loss has been increased to 3dB to make it a closer match to the experimental system and the switching power is 0.06W.

The response of the saturable absorber is defined by;

$$P_{out} = P_{in}\left[1 - Acos^2\left(\frac{P_{in}\pi}{2P_{noabs}}\right)\right] \tag{5.1}$$

where A defines the maximum loss of the absorber and P_{noabs} is the switching power. A graph of the response of this saturable absorber with loss of 3dB and a switching power of 0.06W is given in figure 5.2.

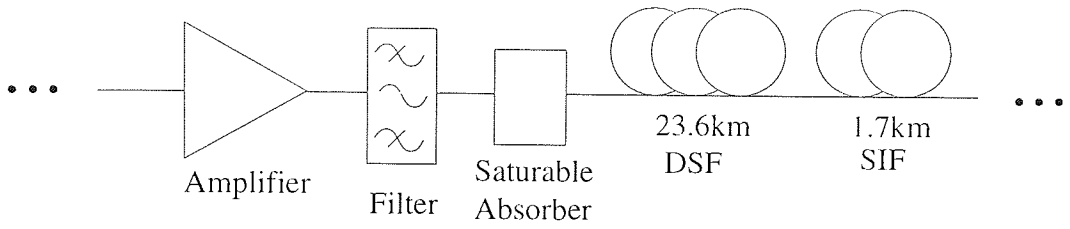

Figure 5.1: Schematic for the system used in these simulations. The SIF has dispersion of 16.5ps/(nm km). the DSF has dispersion of -1.11ps/(nm km) giving an average dispersion of 0.07ps/(nm km). The amplifier has a noise figure of 4.5dB, the filter has a passband of 3.0nm, the saturable absorber has 3dB of power dependent loss and a switching power of 0.06W.

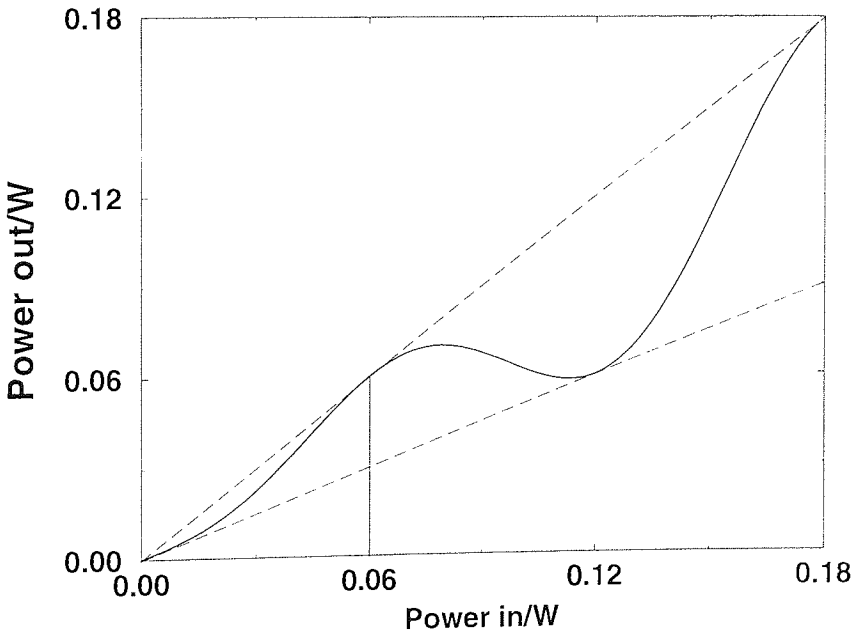

Figure 5.2: The response of the saturable absorber. The loss is 3dB, the upper dashed line represents 100% transmission and the lower dashed line represent 3dB loss. The switching power is 0.06W.

There are several differences between the system modelled here and the one used in the previous chapter. The fibres have been changed to include loss and third order dispersion,

the loss of the saturable absorber has been increased to 3dB with the switching power reduced to 0.06W and the amplifier does not now restore the pulse energy to its initial value but works in saturation by reducing the gain as the pulse power increases which allows the natural stability of the system to control the energy as can be seen in figure 5.3. Finally the input pulse width is increased to 20.0ps and the pulse is input without an initial step of prechirping fibre. All these changes were made to more realistically model the experimental system [201].

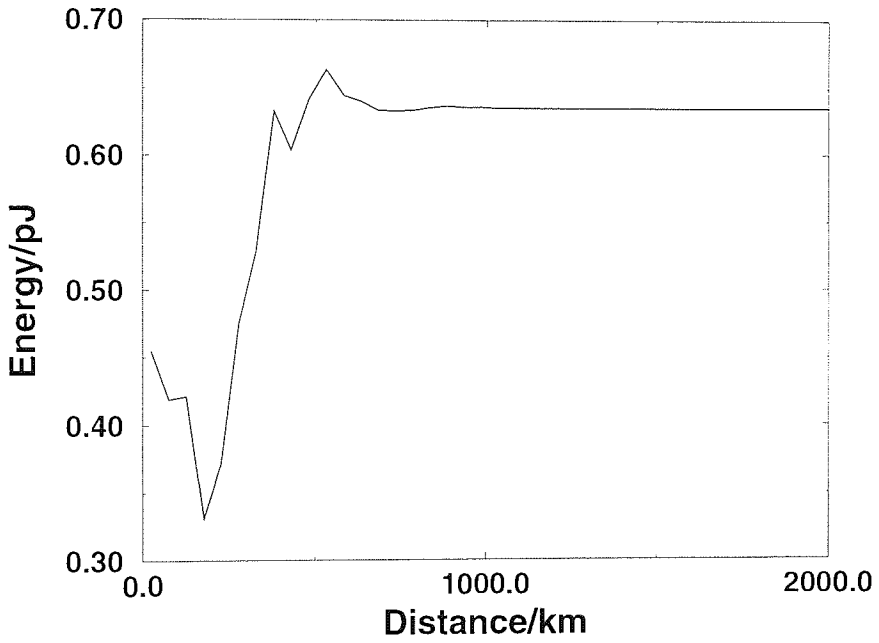

Figure 5.3: The energy of the pulse reaching its steady value of 0.63pJ. This gives an average power of 3.15mW at 10Gbit/s

A single sech pulse with a peak power of 0.02W and a pulse width of 20.0ps is launched into this system. This pulse is shown in figure 5.4, the output is taken after the pulse has passed through the saturable absorber. After passing through the saturable absorber the pulse has two peaks, this is a result of the peak power of the pulse being greater than the switching power of the saturable absorber and does not affect the use of these pulses for data transmission as the filtering of the receiver means that the pulse shape is not significant. The pulse evolve into its final pulse shape in less than 500km. The final pulse has a narrower width and greater peak power than the input. The spectrum, given in figure 5.5, also evolves quickly into its final state, although in this case self-phase modulation, due to the higher peak power, causes a broadening of the spectrum and an equivalent reduction in peak power.

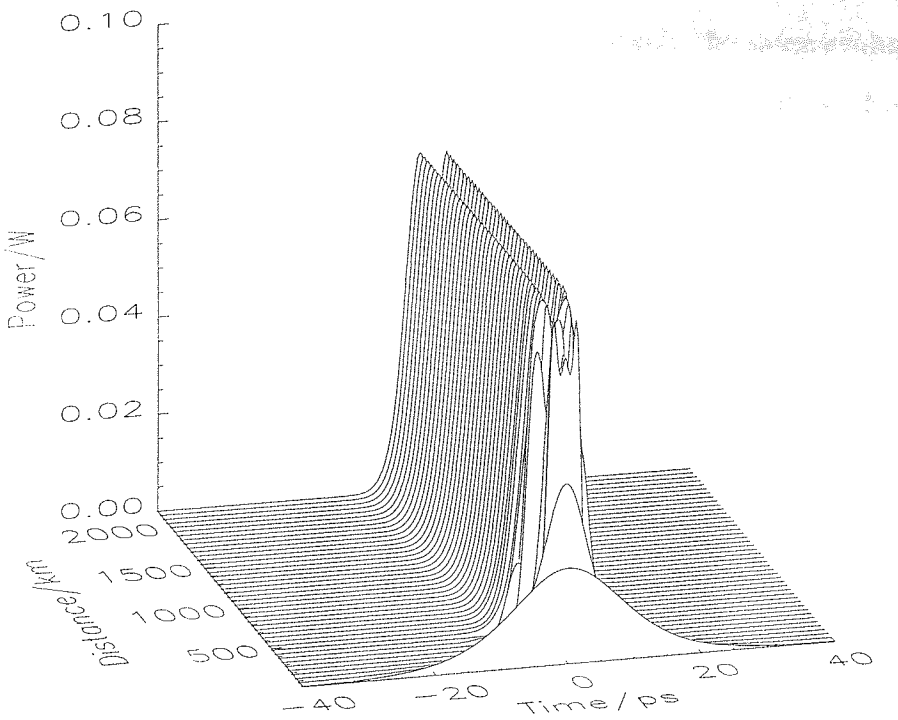

Figure 5.4: The evolution of a single pulse, the input pulse was a 20ps sech with a peak power of 0.02W.

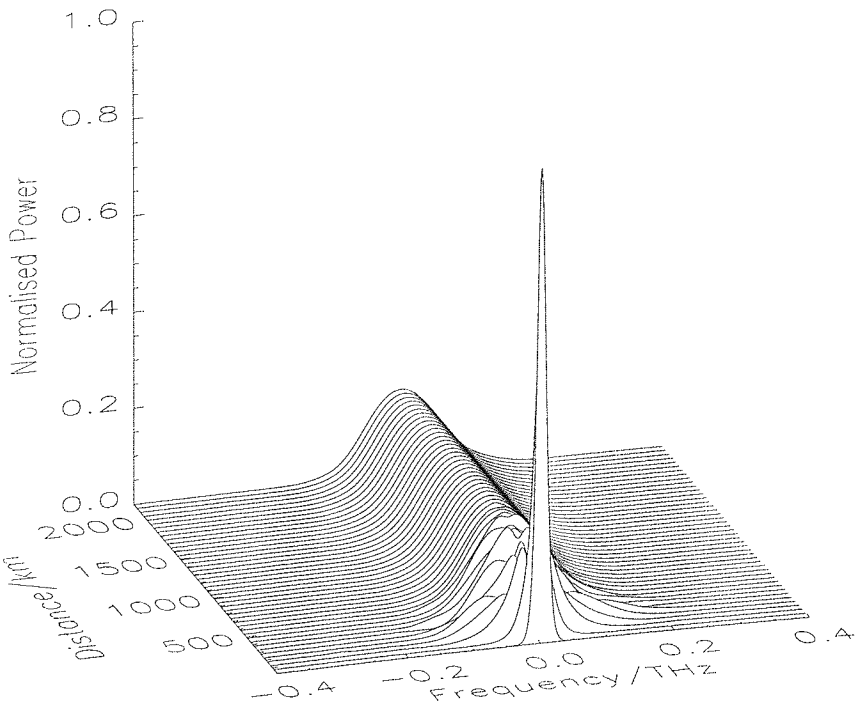

Figure 5.5: The spectral evolution of a single pulse, the input pulse was a 20ps sech with a peak power of 0.02W.

The evolution of the pulse through one dispersion map is shown in figure 5.6. This plot shows that the pulse undergoes the same breathing evolution as in the lossless case. The spectrum of the pulse, shown in figure 5.7, also has largely the same evolution as the lossless case. Differences between the lossy and lossless systems can be most clearly seen in the plots of pulse width and bandwidth in figures 5.8 and 5.9 respectively. The loss breaks the symmetry of the system to move the minima of the pulse width and the minimum and maximum of the bandwidth. The minima of the pulsewidth are now earlier in the normal dispersion fibre and later in the anomalous dispersion fibre, this is because the nonlinear effect are reduced in the later part of the dispersion map the same nonlinear phase shift requires a greater distance. Experimental results taken from [201] are also plotted on this graph and show very close agreement with the numerical data. The spectrum also shows some differences from the lossless case, there is now very little change in the spectrum over the anomalous dispersion fibre. The minimum and maximum values of the bandwidth are now no longer at the midpoints of the sections of fibre and are in fact closer to the amplifier which is located at the end of the anomalous dispersion fibre. This is again due to less self-phase-modulation occuring as the power is reduced [168]. The minimum pulse width is 3.5ps, using this value in equation 3.2 gives a map strength of 5.3.

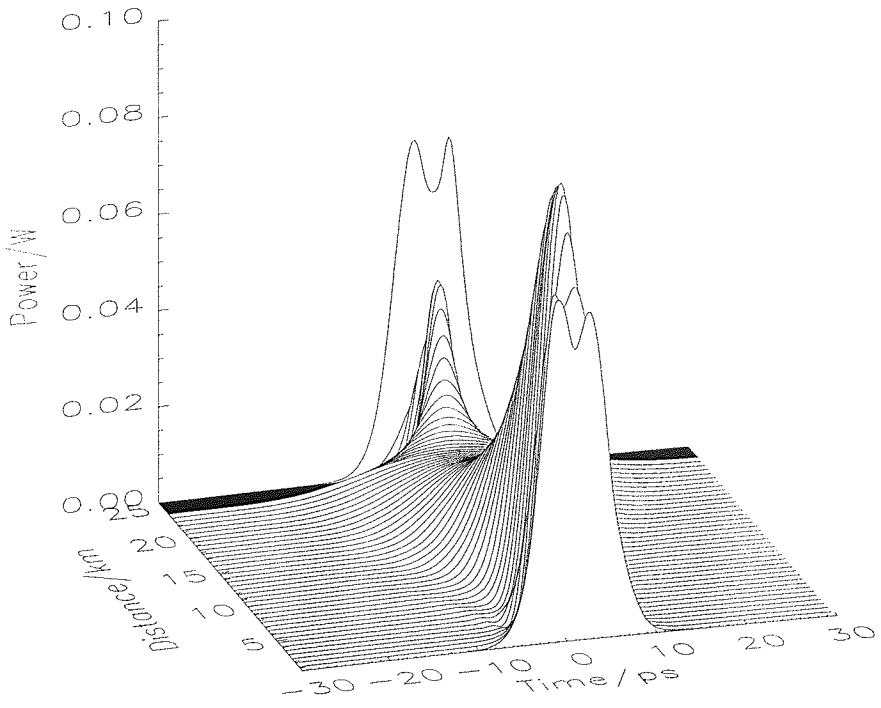

Figure 5.6: The evolution of a single pulse, the input pulse was a 20ps sech with a peak power of 0.02W.

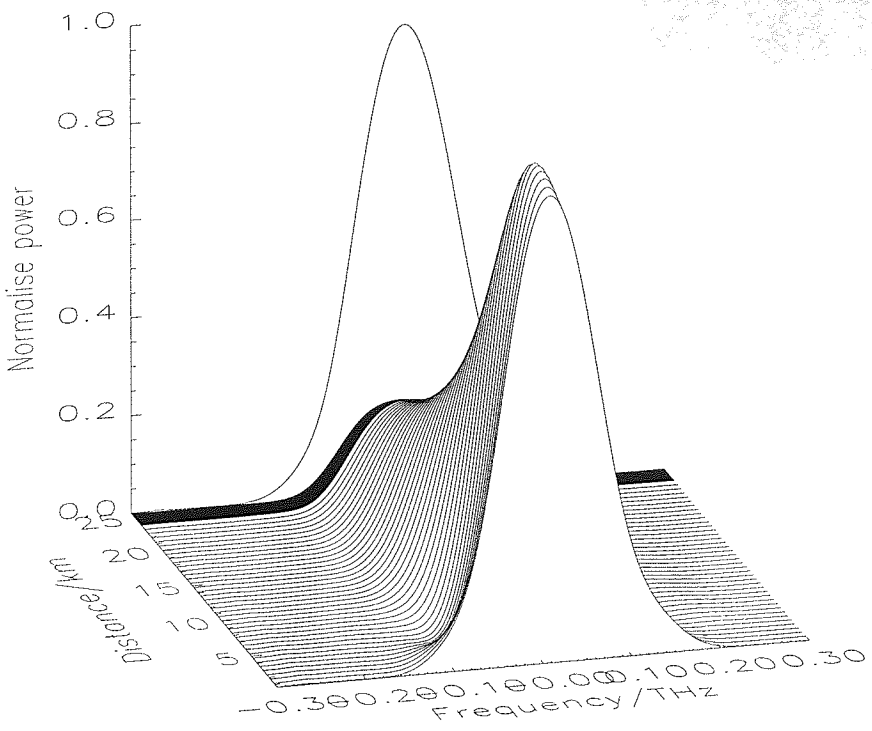

Figure 5.7: The spectral evolution of a single pulse, the input pulse was a 20ps sech with a peak power of 0.02W.

The inclusion of loss and 3rd order dispersion does cause some changes in the evolution of the pulse in a system with dispersion management and a saturable absorber. However stable pulse propagation is still possible.

5.3 10Gbit/s Transmission

The previous section showed that it is still possible to propagate single solitons in this system when loss, gain and higher order dispersion are taken into consideration. For these pulses to be used in a real system they must also be able to propagate over long distances without suffering from interactions. The other factor that must be considered is the effect of adding noise to the system at each amplifier. The amplifier is now taken to have a noise figure of 4.5dB. The input Gaussian pulses have peak power of 0.02W and pulse width of 20.0ps, they are placed 100ps apart to give a data rate of 10Gbit/s.

The performance of this system will be measured using Q-values. Q-values are defined by the equation;

$$Q = \frac{\mu_1 - \mu_0}{\sigma_1 + \sigma_0} \tag{5.2}$$

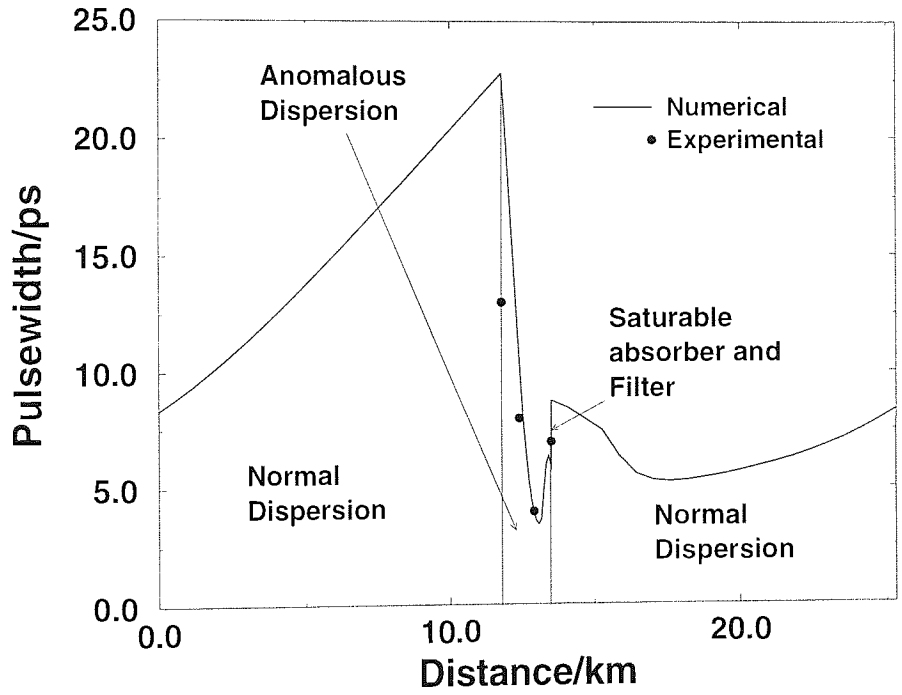

Figure 5.8: The variation of the pulsewidth through one dispersion map period. The solid line are the numerical results and the circular points are experimental results. The pulsewidth evolution is complicated by the changes in pulse shape, in particular the two peaks caused by the saturable absorber causes irregularities in the pulsewidth evolution.

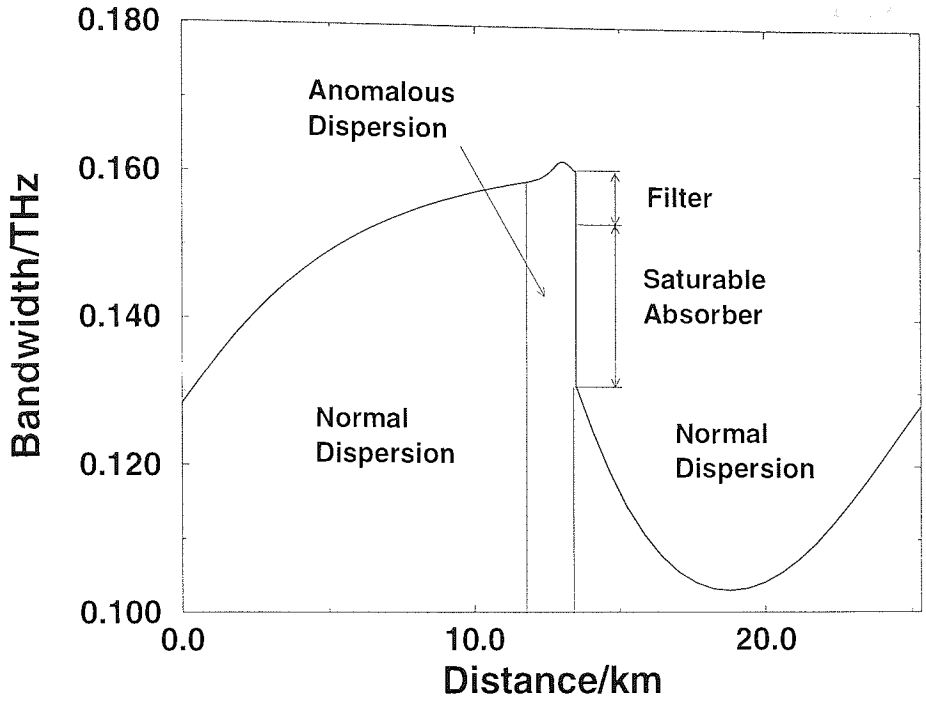

Figure 5.9: The variation of the bandwidth through one dispersion map, the loss due to the filter and saturable absorber are marked on the graph.

where μ_1 and μ_0 are the mean level of the 1 and 0 and σ_1 and σ_0 are the standard deviations of the 1 and 0. The standard deviations are calculated using;

$$\sigma_1 = \sqrt{\frac{\sum_{i=1}^{n} (P_i - \mu_1)^2}{(n-1)}} \tag{5.3}$$

where n is the number of 1's in the data pattern, P_i is the peak power of pulse i and μ_1 mean level of the 1's.

If the levels of the one and zero are assumed to have a Gaussian variation then the bit error rate (BER) for the system can be found using the formula

$$BER = \frac{1}{2\pi} \frac{exp(-Q^2/2)}{Q} \tag{5.4}$$

Using this equation a BER of 10^{-9} is equivalent to a Q-value of 6. The simulations were carried out using a random bit pattern of 96 bits. These were contained in 4 files of 24 bits and the results were combined to form eye-diagrams and to calculate the Q-values.

5.3.1 Results

The simulations were run using the same parameters as the single pulse in section 5.2. The amplifier used in the simulations has a noise figure of 4.5dB. The pulse were propagated for more than 200000km with very high Q-values throughout the propagation distance. A graph of Q-value against propagation distance is given in figure 5.10. There is an initial drop in the Q-value at the start of the simulation, the Q-values then show a decrease with propagation distance, although the variations in the Q-value due to noise are larger than the decrease which makes it hard to distinguish.

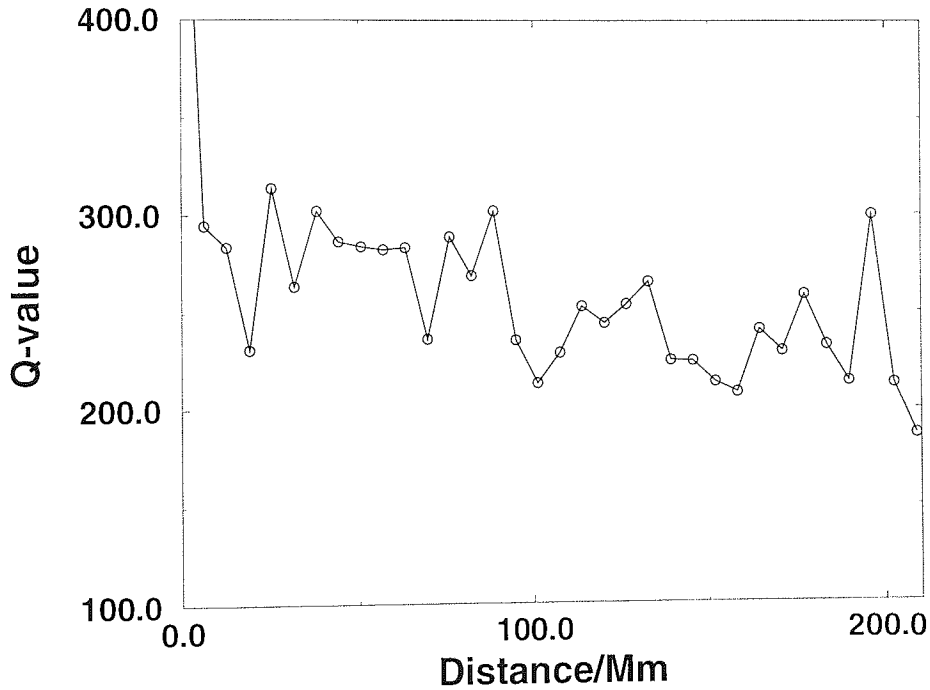

Figure 5.10: The variation of the Q-value with distance.

One of the reasons for the high Q-values throughout the long propagation distance is that the noise level is suppressed by the saturable absorber. Figure 5.11 shows a section of the bit pattern on a dB scale taken after 6Mm and the same section of the bit pattern after 200Mm. The noise level has remained $\sim 35dB$ below the signal level, this demonstrates the effectiveness of the weak saturable absorber in suppressing the noise level. The low noise level can also be seen in figure 5.12 which shows an eye-diagram from 208Mm. The simulated detector used to produce this eye-diagram has an electrical filter with a bandwidth of 0.2THz which accounts for the pulse being a different shape to those from the single pulse simulations. The eye at 208Mm is very open, there is only a small amount

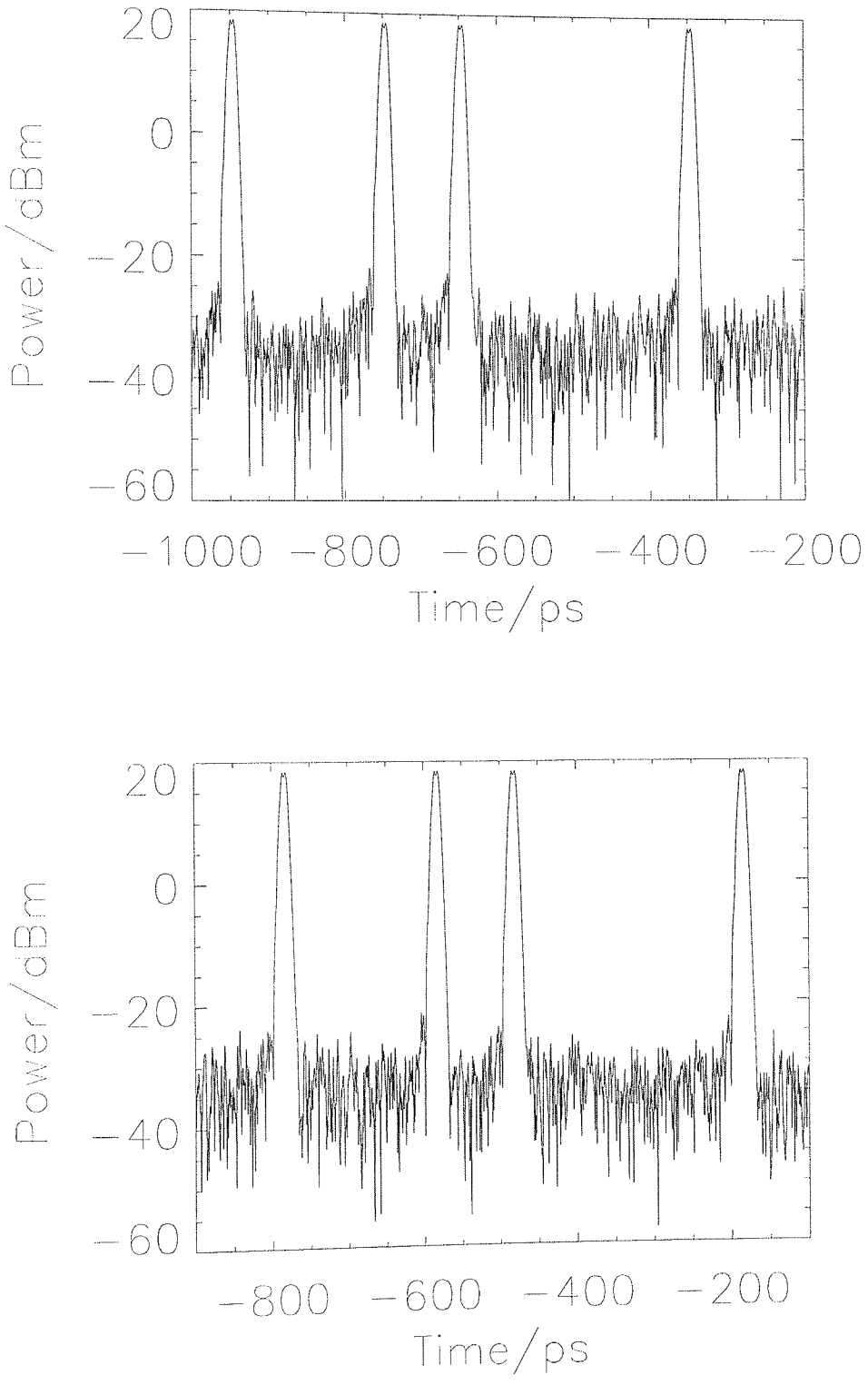

Figure 5.11: The upper plot is taken after 6000km and the lower plot is taken after 208000km. Both plots show the same section of the bit pattern and it is clear that there is only a small increase in the noise level during the propagation. The noise is suppressed by the saturable absorber. The pulse have moved in the timing window due to the effects of third order dispersion.

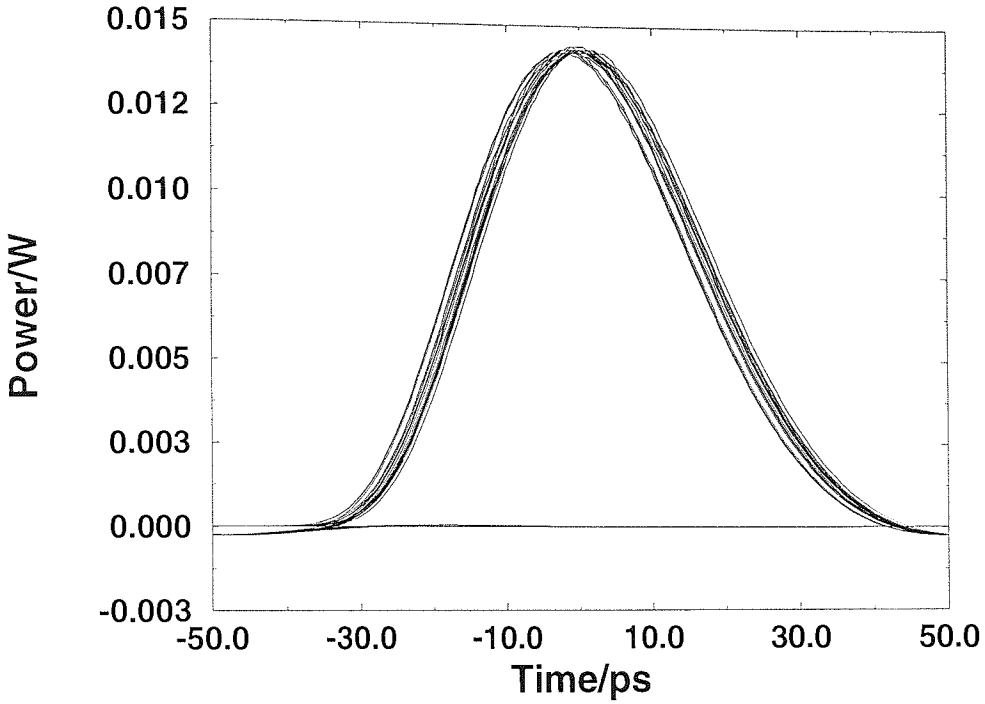

Figure 5.12: An eye-diagram taken after the data has propagated over 208Mm. The data has a small amount of timing jitter but there is very little evidence of noise.

of timing jitter and the signal-to-noise ratio is high. The reduced timing jitter is also due to the saturable absorber. Without any filtering the timing jitter can be calculated using [77, 78];

$$T_{rms} = \sqrt{\frac{2\pi n_2 N_{sp}|\beta_2|hc(G-1)L^3}{9t_o\lambda^2 A_{eff}L_a\Lambda_o^2}} \tag{5.5}$$

where $L = NL_a$ is the total system length, n_2 is the nonlinear refractive index, N_{sp} is the spontaneous emission noise factor of the amplifier, h is Planck's constant, c is the velocity of light, G is the gain of the amplifier and Λ_o^2 is the soliton amplitude.

Using the parameters for this system and taking the pulse width to be 3.5ps which is the minimum pulse width in the system, the RMS jitter after 200Mm is $> 1000ps$. With a pulse spacing of 100ps this level of jitter obviously means that any information would be lost after this propagation distance.

It is clear from figure 5.9 that not only does the filter reduce the bandwidth of the pulses but since the pulse is chirped when it passes through the saturable absorber there is also a filtering effect. This means that these pulses are being strongly filtered which is

known to reduce Gordon-Haus jitter. Usually the strength of filtering is limited by the growth of dispersive radiation at the peak of the passband of the filter, however here the dispersive radiation is removed by the saturable absorber.

The effects of this filtering can be included in the calculation of the timing jitter using equation 2.111 [95]. The strength of the filtering is inferred from the amount of excess gain required to restore the pulse energy. The wider bandwidth of the pulses used in these simulations is accounted for in the calculation by using a pulse width calculated from the bandwidth of the pulse at the saturable absorber assuming a sech shaped pulse. Since the bandwidth of the pulses is 0.160THz the pulse width is taken as 2.1ps. In this way the jitter after 200Mm is found to be $9.4 \times 10^{-2} ps$. This is obviously smaller than the jitter in the eye-diagram which is $\sim 1ps$. The likely reason for the discrepancy between the calculated jitter and the jitter from the simulations is that the derivation of the formula used to calculate the timing jitter for a filtered system [95] assumes that the filter does not have a large effect on the pulses bandwidth and so is able to be treated as a perturbation. Figure 5.9 shows that the filtering effect in this case is very strong and so the perturbation approximation is not valid. The other possible reason for increased timing jitter is that soliton interactions contribute to the jitter. Figure 5.13 is an eye-diagram for a simulation run without noise to isolate any jitter caused by soliton interaction. There is no significant jitter in this eye-diagram which implies the the jitter in the previous eye-diagram is purely a result of noise.

It is clear that not only does the saturable absorber have the expected benefit of reducing the growth of noise and dispersive radiation but, due to the dispersion management it also has a filtering effect which reduces the Gordon-Haus jitter.

5.4 Conclusions

Using a saturable absorber combined with dispersion management it is possible to propagate pulses at a data rate of 10Gbit/s over more that 200Mm. As expected the saturable absorber suppresses the build up of noise and dispersive radiation as well as stabilising the pulse energy. A less expected benefit of using the saturable absorber is that it helps to suppress Gordon-Haus jitter. This is due to the dispersion management and the positioning of the saturable absorber which means that the saturable absorber acts on chirped pulses. Since the pulses are chirped the low intensity wings of the pulse contain the extremes of the pulses spectrum. These wings are attenuated leading to a strong filtering

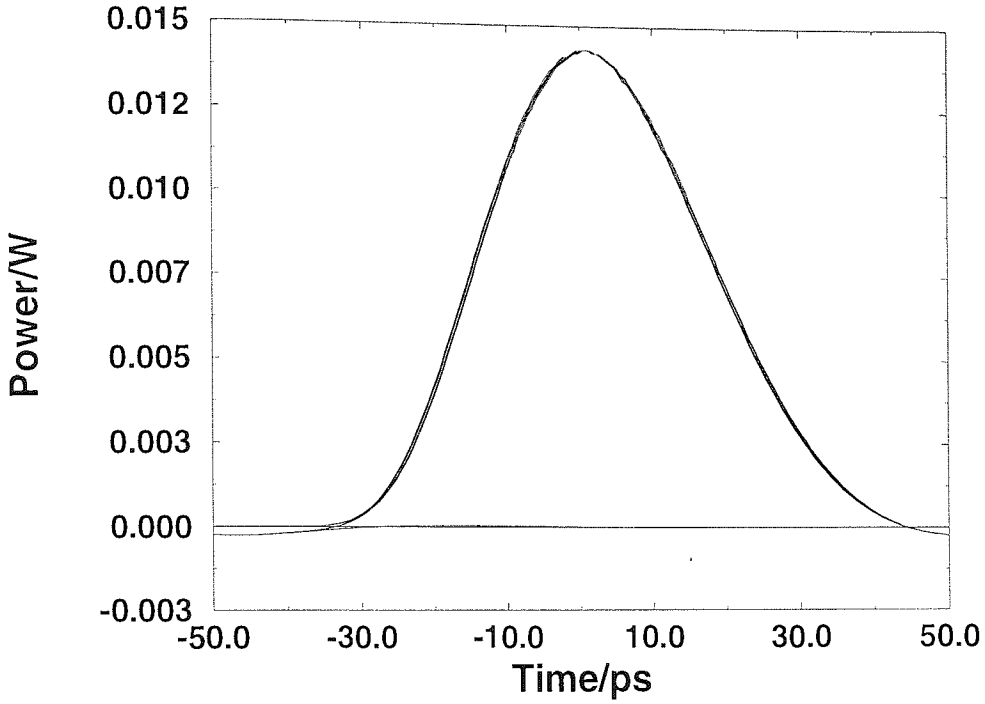

Figure 5.13: An eye-diagram taken after the data has propagated over 208Mm. This simulation was run without noise and shows very little timing jitter.

effect. The spectrum of the pulse is reduced by $\sim 25\%$ as it passes through the saturable absorber and the filter.

Strong filtering would normally lead to growth of dispersive radiation at the centre of the filter pass band, however saturable absorbers have been used in the past to control the growth of dispersive radiation and it is controlled in that way here. It is clear that the use of saturable absorbers is compatible with dispersion management and even brings added benefits in the control of Gordon-Haus Jitter.

Chapter 6

10Gbit/s standard fibre transmission

6.1 Introduction

This chapter examines the transmission of dispersion managed solitons over standard fibre at 10Gbit/s making a direct comparison between modelling and recent experimental results [202]. For the given dispersion map that was used in the experimental investigation of this problem, the effects of changing the length of the initial step of prechirping fibre and the position of the output are identified. Oscillations in the pulse width/peak power lead to oscillations in the Q-values which can be suppressed by altering the position and order of the fibres even in a very restricted manner. These results confirm those of recirculating loop experiments carried out by Harper et al [202]. These simulations are a good opportunity to compare the results of numerical simulations to experimental results.

The majority of fibre currently installed is standard fibre which has low dispersion in the second communications window of $1.3\mu m$. This communications window was used at the time the fibre was laid as there were readily available semiconductor sources and detectors which worked at this wavelength and due to the low dispersion of the fibre. The dispersion of this fibre in the third transmission window ($1.5\mu m$) is between 16.0 and 20.0 ps/(nm km).

Current systems employ 3R repeaters that restore, re-time and reshape the signal. These repeaters rely on electronics to carry out this task and so the speed of the transmission line is dictated by the speed of the electronics. This also means that the transmission line is not bit rate transparent, therefore in order to upgrade a transmission line to a higher bit rate or to use wavelength division multiplexing it is necessary to replace the electronics. The major advantage of using repeaters is that the signal is restored to its original state periodically. This means that any degradation that the pulses suffer during

propagation will not accumulate along the entire transmission line and so the accumulated effects of nonlinearity, dispersion and noise do not need to be considered.

The need to work at 10Gbit/s or higher means that the use of electronics to restore the signal is not cost effective. The alternative is to use all optical amplification. The first suggested method for amplifying an optical signal was to use the Raman effect as discussed in section 2.6.9. [54]. Erbium doped fibre amplifiers (EDFA) are now used in most soliton propagation experiments and optically amplified transmission lines. An EDFA is formed by a length of fibre (a few meters long) which is lightly doped with the rare earth element Erbium which is pumped at either 980nm or 1480nm, the signal is then amplified by stimulated emission. The gain peak is for a transition at 1535nm and with proper design and the correct dopants in the fibre it is possible to have a gain bandwidth of 30nm [203, 204].

The use of fibre amplifiers rather than repeaters means that the long term effects of nonlinearity and dispersion have to be considered. It also means that the signal must propagate at $1.5\mu m$ where the dispersion of standard fibre is high. As seen in chapter 2 high dispersion increases the power required to create a soliton, increases Gordon-Haus jitter and reduces the soliton period which causes problems with the average soliton model and reduces the collapse length for adjacent solitons.

Dispersion management can be used to reduce the average dispersion of the fibre links and can offer the possibility of large increases in propagation distance [205, 206, 155, 184, 207, 7, 208, 209, 188, 210, 182, 202]. Dispersion management can be used to upgrade the current standard fibre network as the compensating fibre can be installed along with amplifiers at the sites of repeaters in the current network and so the upgrade would not involve the laying of large amounts of fibre.

6.2 10Gbit/s propagation

The high dispersion of standard fibre in the $1.5\mu m$ window means that it is not possible to propagate solitons at 10Gbit/s without dispersion management or some other form of soliton control. The high dispersion leads to three major problems, the first of these is that the soliton period is short compared to the amplifier span leading to problems with the average soliton [59, 61]. Using equation 2.68 a 20ps soliton in standard fibre ($D = 16.75ps/(nmkm)$) has a soliton period of 10.0km. To fulfil the average soliton criteria given in section 2.6.2 would require an amplifier span of less than 8km which is

far shorter than the spans of $\sim 50km$ that are generally used. Figure 6.1 shows an average soliton propagating over 50 amplifiers. The input pulse had a soliton order of N=1.47 calculated using equation 2.82 for a 36km amplifier span with loss of 0.22dB/km and a pulse width of 20ps. It is clear that this pulse does not maintain its pulse shape as it sheds dispersive radiation. When these pulses are used in a data pattern the information

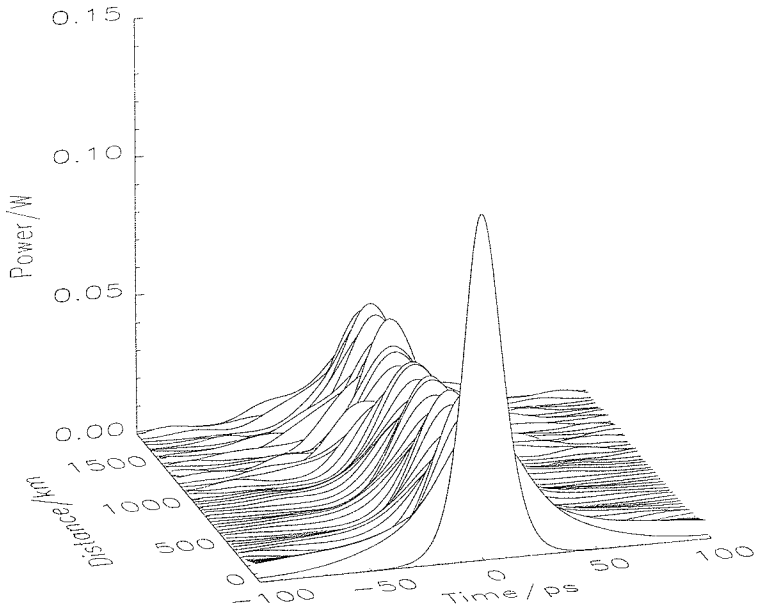

Figure 6.1: A 20ps first order average soliton in standard fibre with a 36km amplifier span. This pulse not fulfil the average soliton criteria as the distance between amplifiers is more than 3 times the soliton period.

is lost after two amplifier spans. The pulse spreading and the dispersive radiation that the pulses shed lead to greater soliton interactions and the pulses becoming indistinct. This can be seen in figure 6.2 which shows a section of a bit pattern at the start of the system and after 72km which is 2 amplifier spans.

There are also problems because the high dispersion leads to the pulse accumulating large amounts of timing jitter through the Gordon-Haus effect. Using a 20ps pulse in standard fibre with loss of 0.22dB/km, an amplifier span of 36km and taking the amplifier to have a noise figure of 4.5dB equation 2.102 gives the maximum error free distance to be less than 1500km [77, 78]. The final difficulty with using average solitons is that the average power required is higher than the powers generally used with an EDFA. The pulse in figure 2.15 has an input energy of 2.8pJ which gives an average power at the output of the amplifier of 14mW.

The Gordon-Haus limit could be extended using one of the control techniques discussed

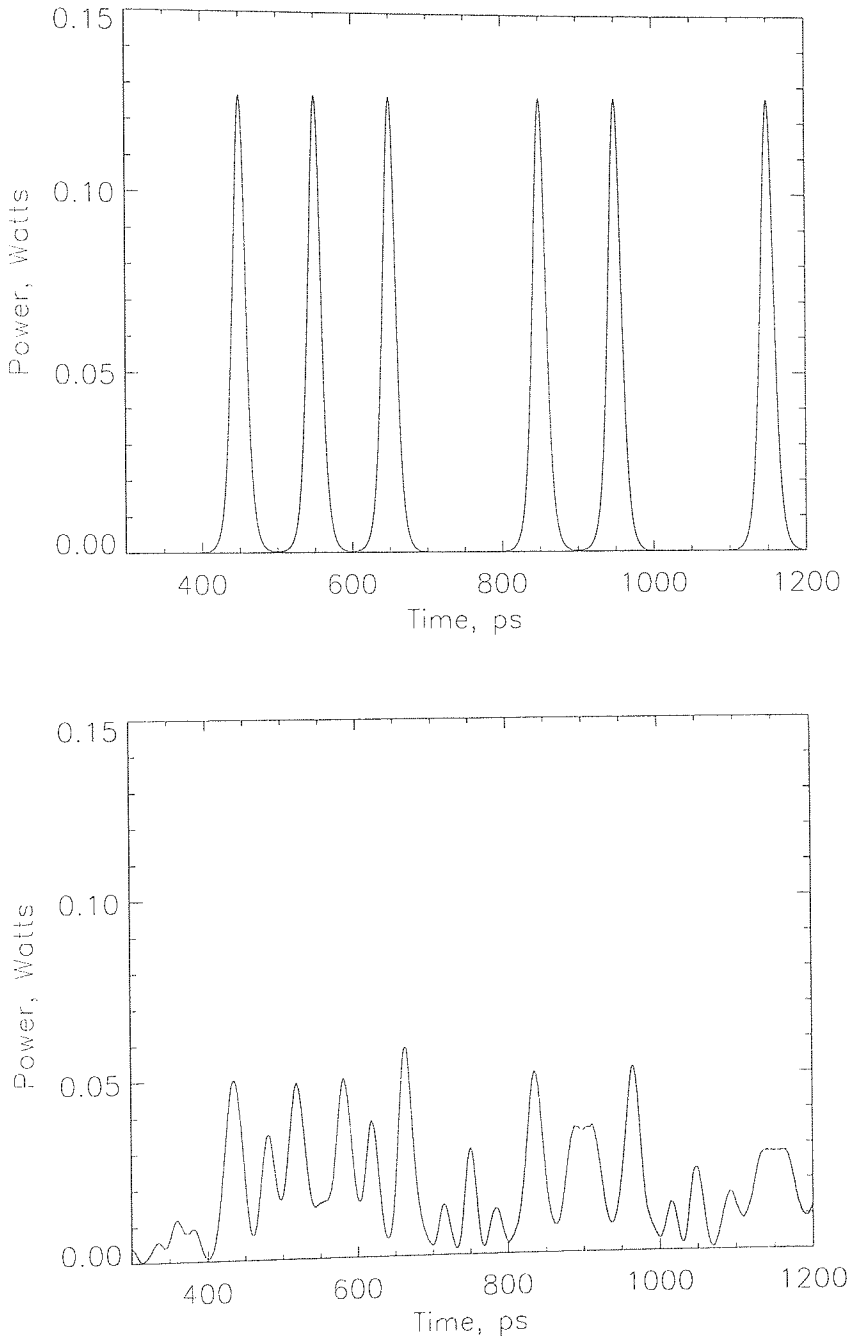

Figure 6.2: The top figure shows a section of a bit pattern at the start of the simulation. The lower picture shows the same bit pattern after it has propagated over 72km, the amplifier span length is 36km.

in chapter 2 however the problems associated with the average soliton and average powers would be more difficult to deal with. Linear pulse propagation is also limited due to the high dispersion which would lead to the pulse width increasing and so the pulses would interfere with each other. The dispersion length of a 20ps pulse in standard fibre is $\sim 6.5km$ using equation 2.18.

6.3 Modelled System

The three modelled systems taken from the experiment detailed in [202] are shown in figure 6.3. The dispersion map consists of 31.6km of standard fibre which is split into two sections, one section is 25km long and the other section is 6.6km long. There is also 6.8km of compensating fibre. The dispersion of the standard fibre is taken to be 16.75ps/(nm km) with third order dispersion of $0.07ps/(nm^2km)$ and loss of 0.22dB/km. The compensating fibre has dispersion of -76.76ps/(nm km), third order dispersion of $0.07ps/(nm^2km)$ and loss of 0.62dB/km, this loss includes the losses incurred due to splicing the different types of fibre together. This gives an average dispersion of 0.19ps/(nm km). The nonlinearity is the same in all the fibres and and effective area of $50\mu m^2$ is used throughout. The amplifier restores the power lost through the fibre loss and the loss due to the 3nm filter, the amplifier is taken to have a noise figure of 4.5dB.

The input pulses used are all 20.0ps sech pulses with powers dependent on the position in the dispersion map where the pulse are input. In the experiment of reference [202] the optimum input energy was found to be 5.4 times the average soliton power. This is slightly less than would be expected for a map of this strength. Using equation 3.2 the map strength used here is 3.1 from equation 3.4 this would give an expected energy enhancement of 7.9. This confirms earlier results which suggested that the power enhancement was reduced when loss is included although it should be noted that the power is still significantly enhanced.

Using this level of power enhancement in map A the input pulses are N=3.9 (soliton number is related to the average dispersion), in map B and C the correct input is found by reducing the input power so that the power at the output of the amplifier remains the same for all three systems. This gives an input pulse of N=2.034 for map B and in map C an input of N=3.3. The strength of the map means that this map is well within the range where propagation of long term stable pulses should be expected, it is not strong enough to allow propagation at the dispersion zero nor into the region of average normal

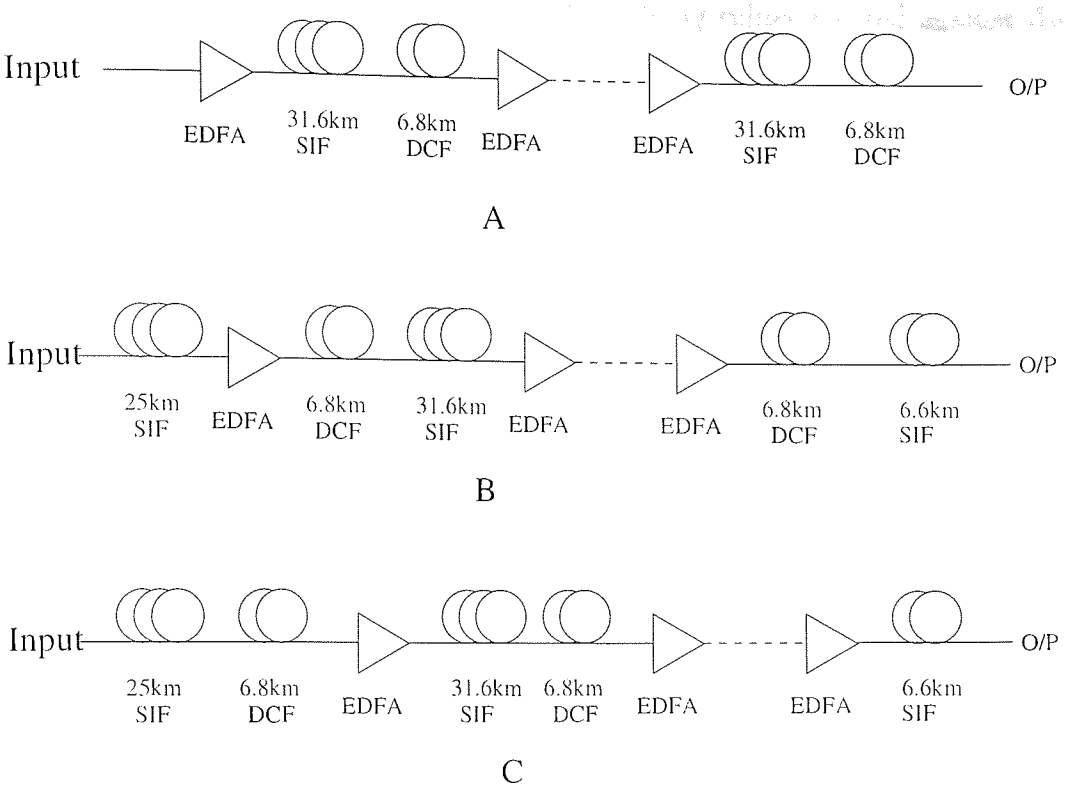

Figure 6.3: Schematic of the three systems

dispersion.

As the purpose of these simulations is to examine the suppression of the oscillations in Q-values and pulse width and to compare the results with those found experimentally each simulation was run for distances of about 10000km rather than until the Q-value dropped below 6. It would be inaccurate to compare the total propagation distances possible from the simulations to those found experimentally as the input pulses used here are perfect sech shaped pulses which can never be produced experimentally. The input Q-value from the simulations are $\sim$ 70 whereas the maximum input Q-value from the experimental results were 12.0. The Q-values are calculated as in the previous chapter using;

$$Q = \frac{\mu_1 - \mu_0}{\sigma_1 + \sigma_0} \tag{6.1}$$

where μ_1 and μ_0 are the mean level of the 1 and 0 and σ_1 and σ_0 are the standard deviations of the 1 and 0.

The first set of simulations are carried out using system map A. A random bit stream containing 96 bits generated by the computer is used. The input pulses are sech pulses with a width of 20.0ps and a pulse energy of 0.23pJ giving an average power of 1.15mW in

accordance with the powers used experimentally. The Q-values plotted against distance are given in figure 6.4 for this system.

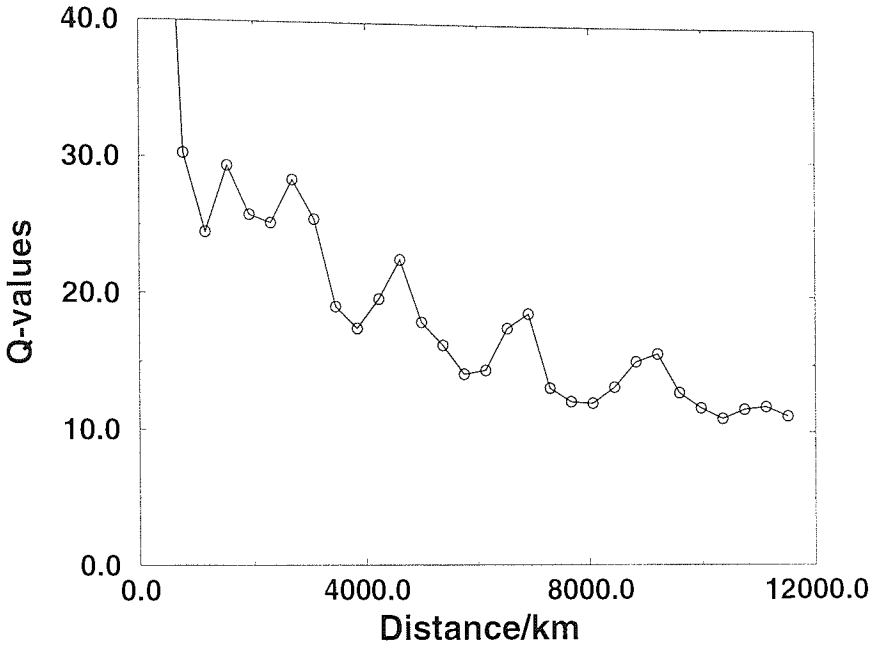

Figure 6.4: Q-value against distance for system A. It is clear that there are substantial oscillations in the Q-values.

The oscillations in the Q-value can be clearly seen in figure 6.4. These oscillations occur as the pulses are not being launched at the optimum place in the dispersion map. The period of the oscillations is approximately 2000km so the evolution of these pulses is long compared to the dispersion map. The oscillations can also be seen in the plots of the pulse shape which is shown in figure 6.5. They can be more clearly examined in the graphs of the pulsewidth evolution (figure 6.6) and the time-bandwidth product (figure 6.7).

The minima in the pulse width relate to pulses with high peak powers and approximately coincide with the high Q-values. The maximum Qs also relate to the minima in the time-bandwidth product. The reason for these fluctuations in the pulse parameters (chirp and width) is that the pulse shape is not matched with the dispersion map and more specifically the chirp free pulses are not being input at the optimum point in the dispersion map. The pulse undergoes a long term evolution as the pulse sheds dispersive radiation and the peak power, pulse width, shape and chirp all change. In the lossless case the correct launch point is at the midpoint of one of the pieces of fibre. When loss is included this point moves as detailed in section 3.3.1, however the start of the standard

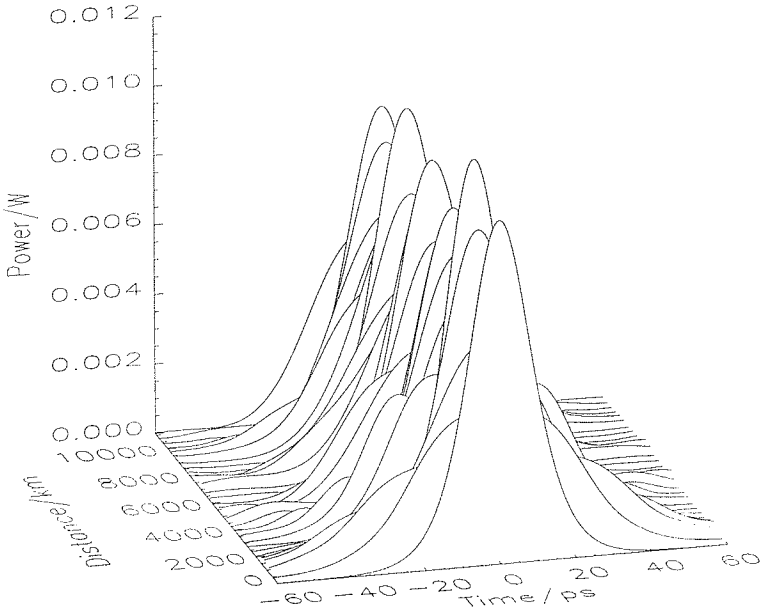

Figure 6.5: The pulse width evolution from system A, the instability of the pulse and the shedding of dispersive radiation can be clearly seen.

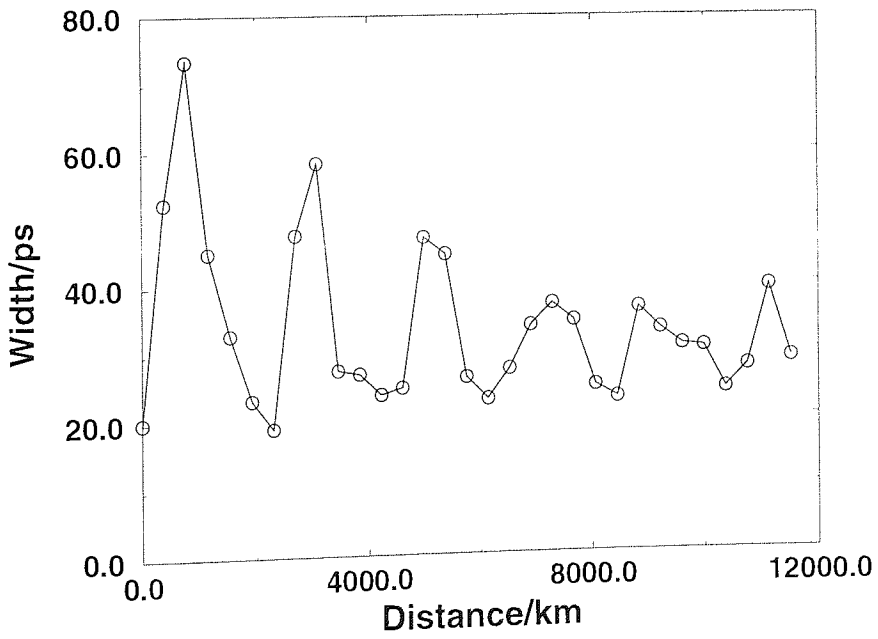

Figure 6.6: The pulse width against distance for map A. The fluctuations in this are similar those in the Q-value.

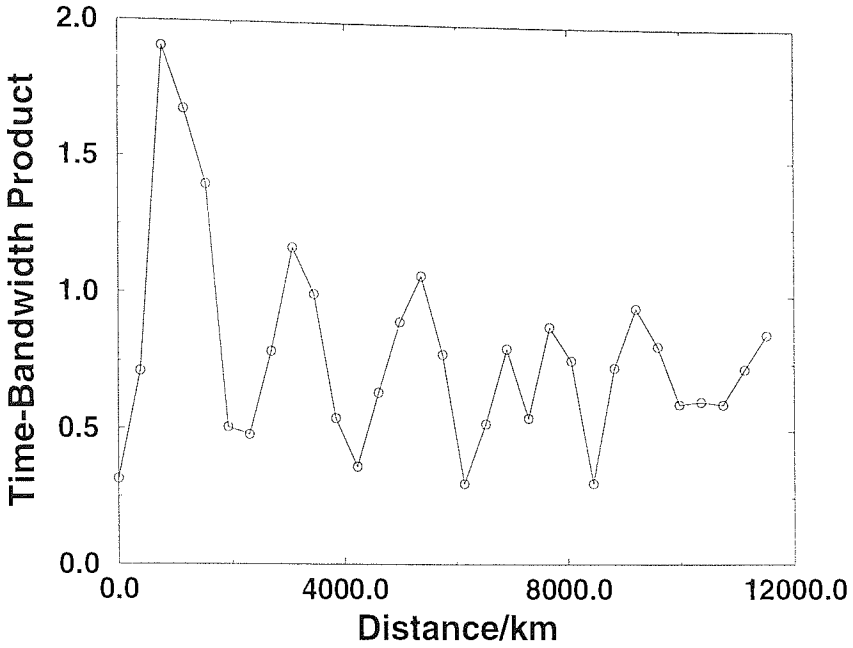

Figure 6.7: The time-bandwidth product against distance for map A, there are clear fluctuations in the value during propagation.

fibre is where the pulses would be expected to be most chirped and so this is the worse point to launch unchirped pulses.

If the chirp of the pulse is examined by looking at the instantaneous frequency given in figure 6.8 then it is clear that although the pulse is initially chirp free at the output point in the map it soon accumulates a complicated chirp. The points where the pulse width and Q are highest coincide with the points where this chirp is at a minimum. These oscillations are typical of dispersion managed solitons that are not launched in the optimum position [166].

The reason the incorrect launch point leads to this instability of the pulses can be seen by looking at the pulse width and bandwidth over two periods of the dispersion map. The pulse width, shown in figure 6.9 varies a lot during the course of each dispersion map due to the high local dispersion but at the end of the dispersion map it has returned to be close to its original value. By contrast the bandwidth of the pulse is reduced throughout the dispersion map. This can be seen in figure 6.10. The reason for this continuous reduction in the bandwidth is that the chirp on the pulse is always of the same sign and so the bandwidth cannot be restored as would happen in the area of the dispersion map where the pulse is chirped in the opposite sense. This is obviously an unstable situation since the bandwidth cannot continue to decrease for the entire system. The reduction can also

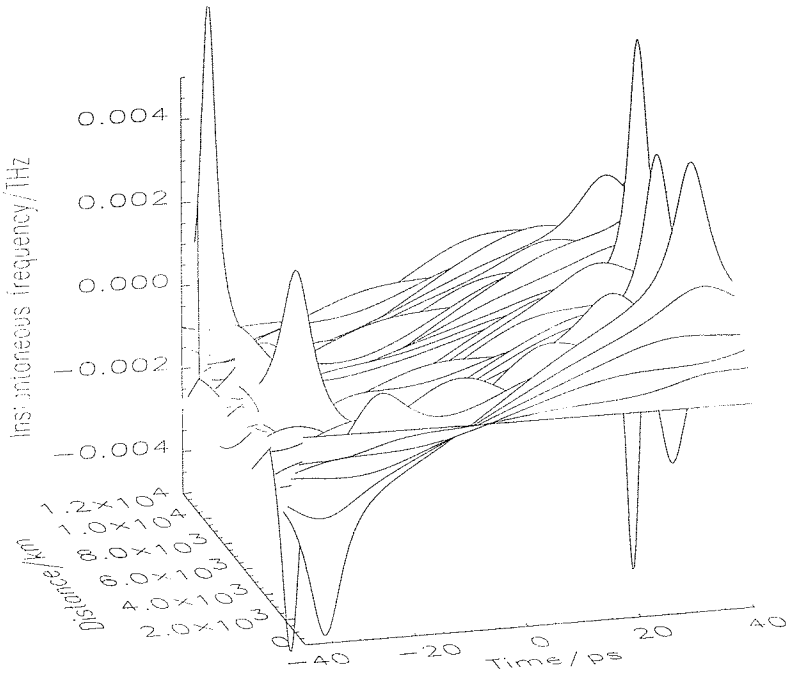

Figure 6.8: Instantaneous frequency for map A this shows how the chirp evolves during propagation. The point where the instantaneous frequency is flattest corresponds to the points where the pulse has the minimum amount of chirp.

lead to long term changes in the pulse width since the minimum pulsewidth is defined by the bandwidth of the pulse.

In order to minimise the pulse width fluctuation and to stabilise the bandwidth of the pulses the dispersion map was altered to give system B in figure 6.3. In this case an initial step of pre-chirping fibre 25km long is place before the first amplifier. This more closely matches the point in the standard fibre where the unchirped pulses would be expected and so leads to a reduction in the pulse shape changes. The compensating fibre has been moved to immediately follow the amplifier and is then followed by the standard fibre. In order to account for the new launch position the launch soliton order is reduced to N=2.03, (pulse energy=0.062pJ), this gives the same average power over one amplifier span as map A. The Q-values are given in figure 6.11.

The fluctuations in Q for this system are considerably less that those for system A. The chirp-free pulses are now being input at a point closer to the natural chirp free point of the dispersion map. The period for the fluctuations in Q with this initial step of fibre is $\sim 2500km$. It interesting to note that although the oscillations in Q-value have been suppressed this has not led to any significant improvement in the Q-values. It is clear from the plot of the pulse given in figure 6.12 that although there are still significant fluctuations in the pulse width these are now more regular and less dispersive radiation

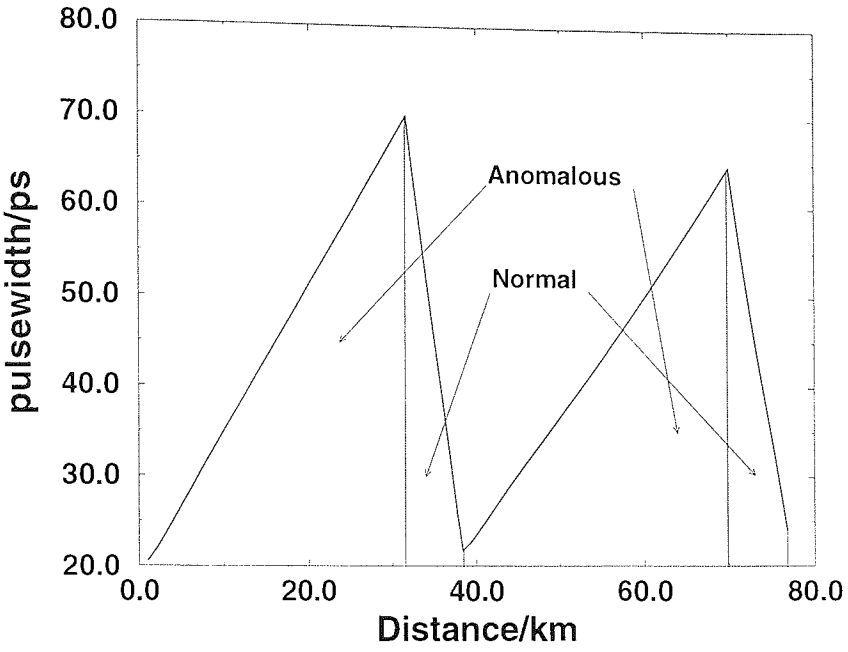

Figure 6.9: Pulsewidth evolution through two periods of dispersion map A. The pulsewidth varies a lot due to the high dispersion of the fibre.

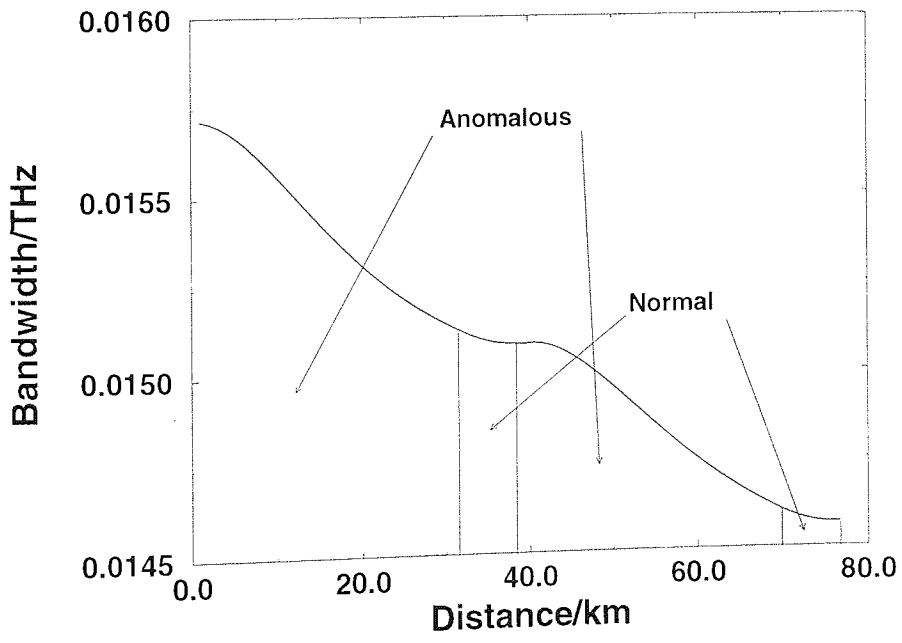

Figure 6.10: The bandwidth evolution through two dispersion maps. The bandwidth is continuously decreasing as the launch position means the pulse only experiences chirp of one sign.

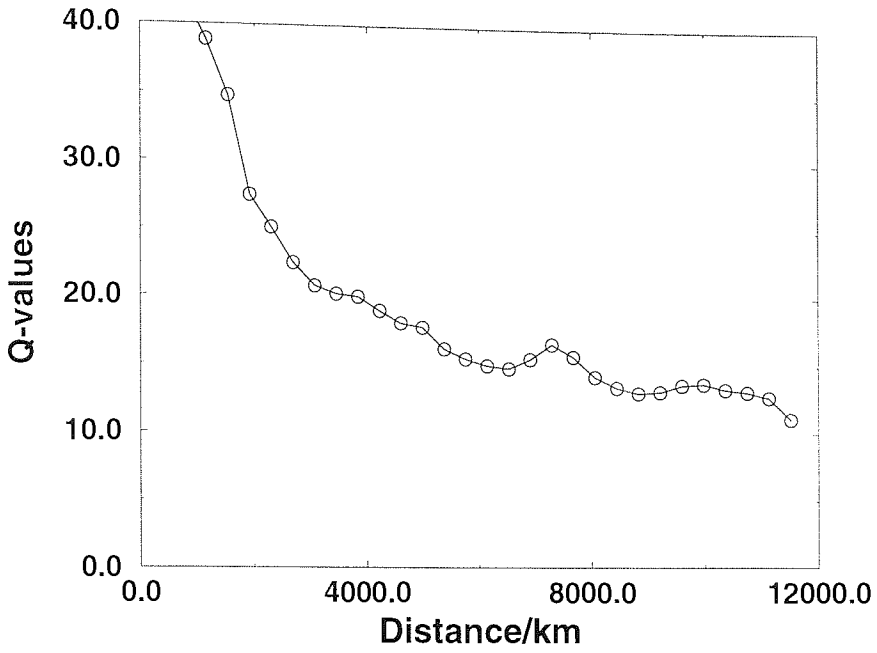

Figure 6.11: Q-value against distance for system B. The oscillations are significantly smaller than those from map A.

is being shed. Oscillations are again clearly seen in the plots of pulse width (figure 6.13) and time-bandwidth product (figure 6.14) which also show that the oscillations are far more regular in this case.

There are still quite large oscillations in the width and time-bandwidth product of the pulse and once again these oscillations are reflected in the chirp of the pulses, on this occasion the evolution of the chirp is less complicated as can be seen is figure 6.15.

The pulse width evolution over two dispersion map periods is given in figure 6.16. The pulsewidth again changes substantially during the dispersion map but on the scale of one amplifier span there is not much change. The amplifiers are situated at the border from the anomalous to the normal dispersion fibre. Figure 6.17 shows the bandwidth variation for this system over two dispersion map periods. The bandwidth is again lower at the end of the simulation than it is at the beginning, however the reduction is less than half that seen in the previous system. In this case the chirp does change sign and so the bandwidth increases for part of each amplifier span.

It is known that placing the compensating fibre immediately following the amplifier, as it is in map B, can increase the amount of dispersive radiation shed by the pulses [170]. The effect of this dispersive radiation can be to cause instability in the pulse leading to the fluctuations in pulse width, and time-bandwidth product and through them to fluctuations

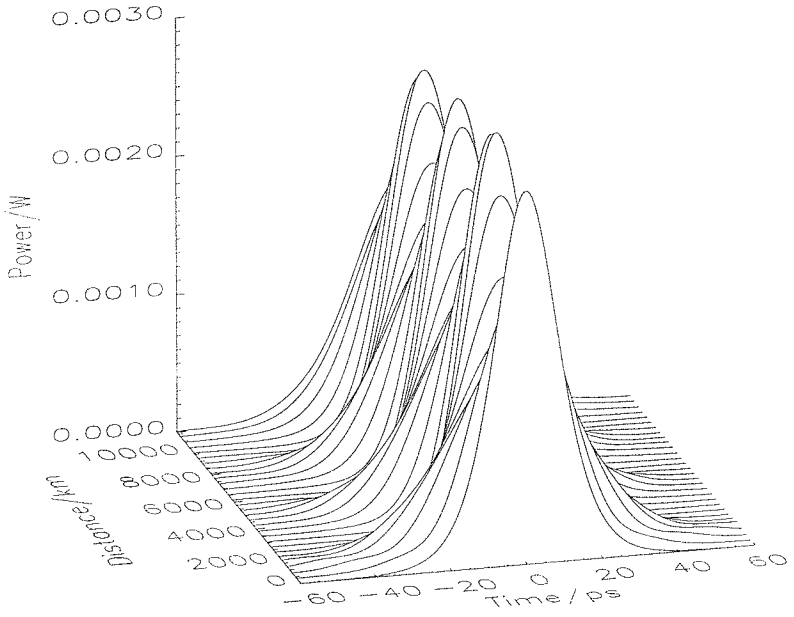

Figure 6.12: A pulse propagating in system B demonstrates that although there are still large oscillations in the pulse width they are far more regular in this system

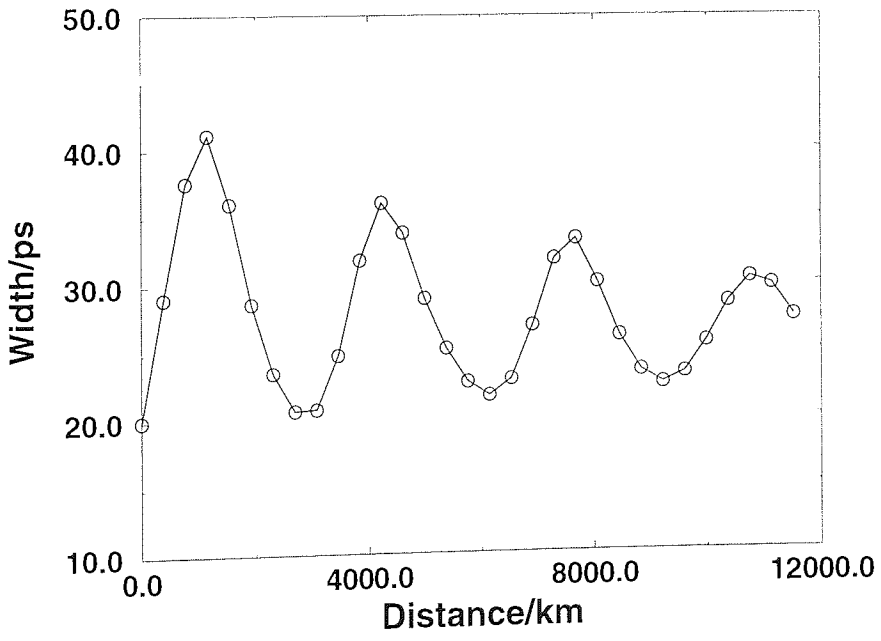

Figure 6.13: The pulse width against distance for map B.

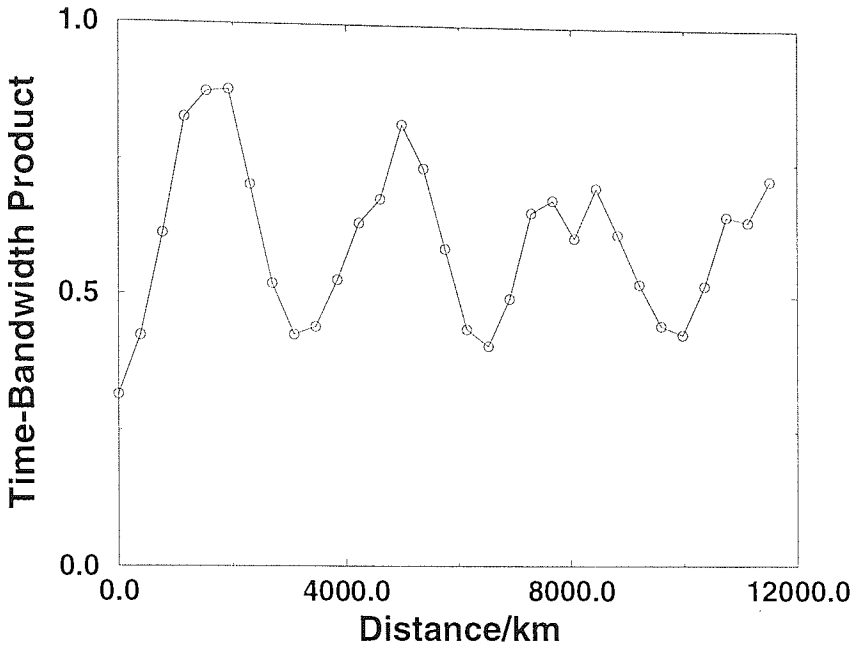

Figure 6.14: The time-bandwidth product against distance for map B.

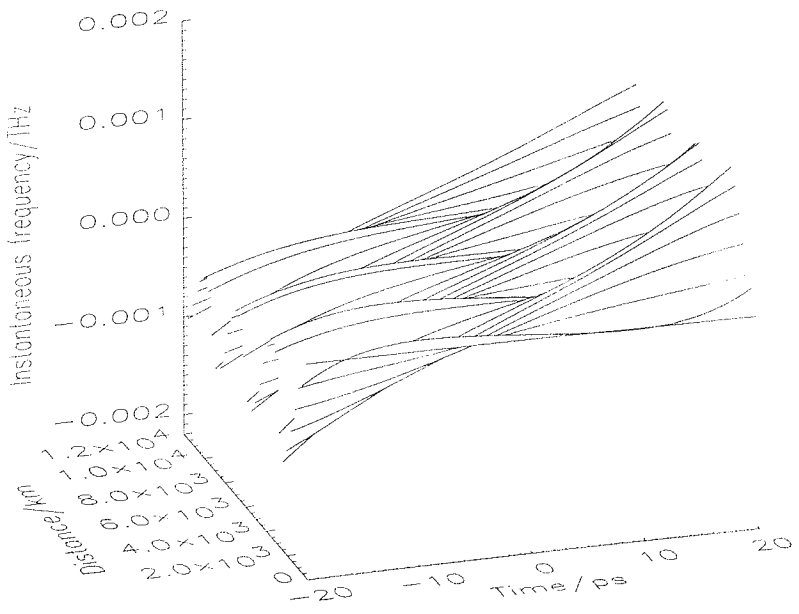

Figure 6.15: Instantaneous frequency for map B this shows how the chirp evolves during propagation. The points where the instantaneous frequency is flat relate to the points where the pulses are unchirped.

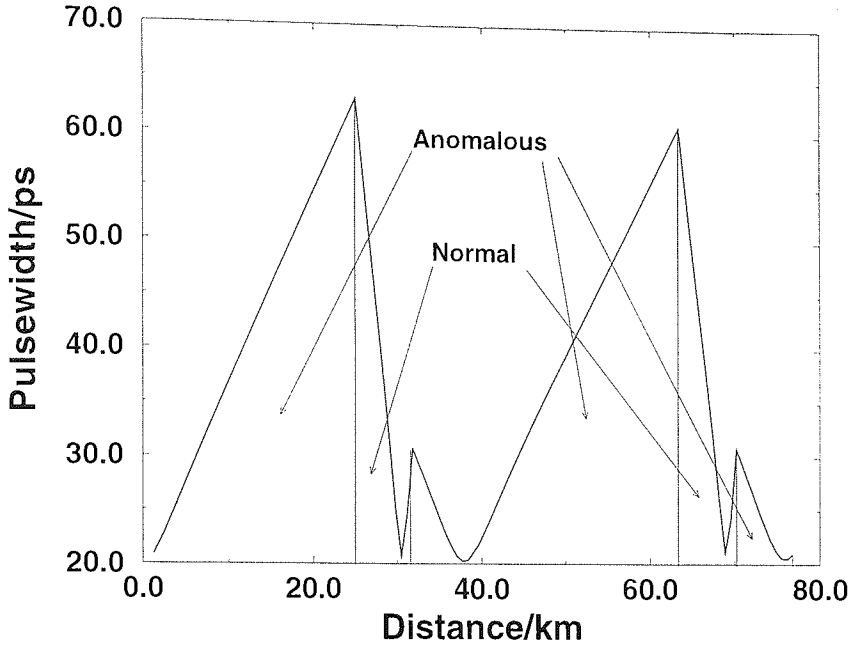

Figure 6.16: Pulsewidth evolution through two periods of the dispersion map, the amplifiers are at the border going from the anomalous dispersion fibre into the normal dispersion fibre.

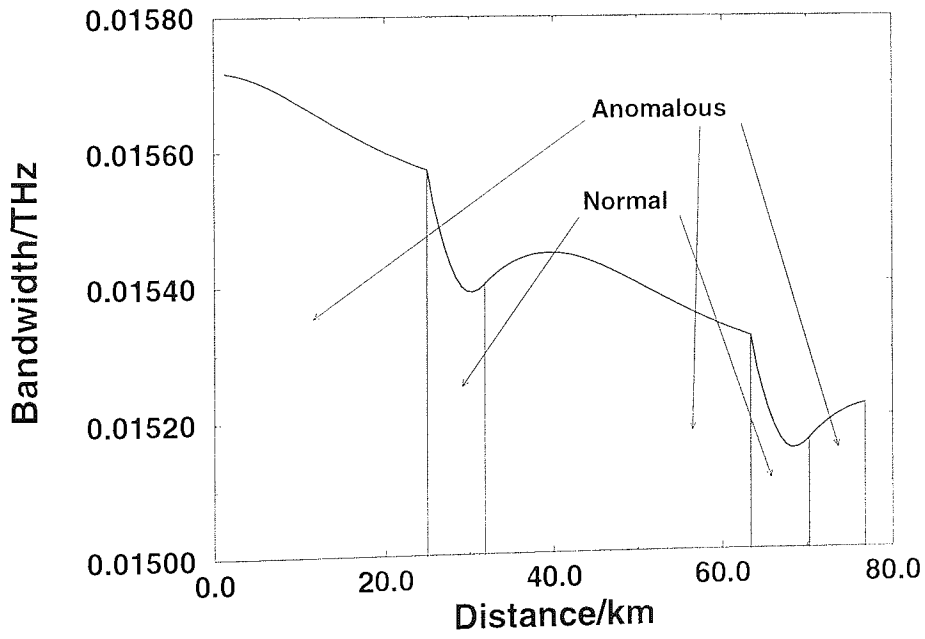

Figure 6.17: The bandwidth evolution through two dispersion maps. The bandwidth increases in the normal dispersion fibre which is situated immediately after the amplifier.

in the Q-value. In order to further suppress the oscillations the compensating fibre was moved to immediately precede the amplifier, map C in figure 6.3. The input soliton order was again changed to give the same average power over one amplifier span. The input order was set to N=3.3 which gave an input pulse energy of 0.16pJ. The Q-values for this case are shown in figure 6.18.

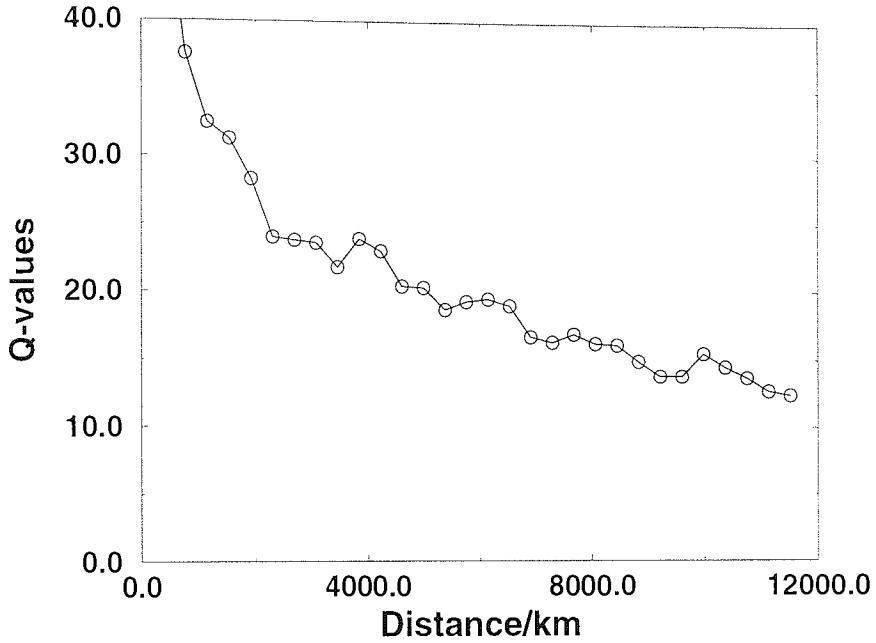

Figure 6.18: Q-value against distance for system C. There are still slight fluctuations in the Q-values.

There are still some oscillations in the Q-value, the period of the oscillations is now less than 2000km. These oscillations can still been seen in the pulse shape shown in figure 6.19 although they seem to be further reduced and there is little sign of the pulse shedding dispersive radiation. The shorter period of the oscillations is also apparent in the graphs of pulse width (figure 6.20) and time-bandwidth product (figure 6.21). The oscillations in these values are reduced when compared to the graphs from both map A and map B.

The chirp for this system again shows that the variations in pulse width can be related to the output being chirped. The variations in the chirp are greater in this system than they were in the previous ones. Although this appears to be mainly at the edges of the pulse rather than the centre so does not lead to larger variations in pulse width.

The graphs of pulse width and bandwidth for this system are given in figures 6.23 and 6.24 respectively, in this system the amplifier is positioned after the normal dispersion fibre. Once again the pulse width changes a lot during each amplifier span but does not

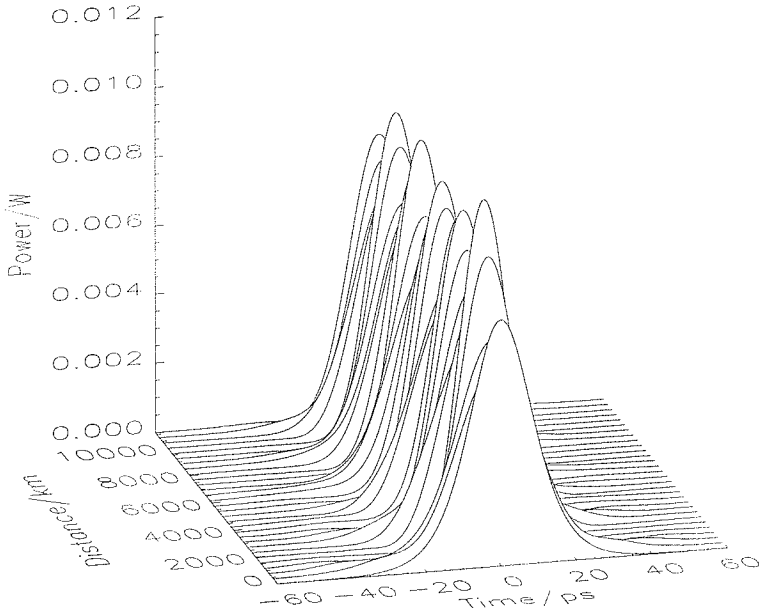

Figure 6.19: The pulse propagating in system C the oscillations and shedding of radiation are both further reduced compared to maps A and B.

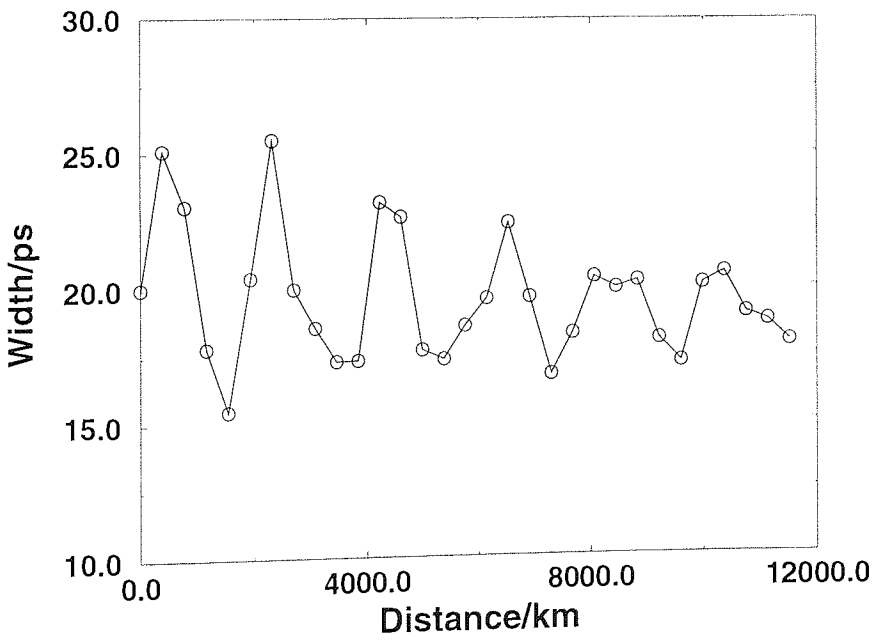

Figure 6.20: Pulse width evolution for map C. The variation in pulse width decreases slightly during propagation.

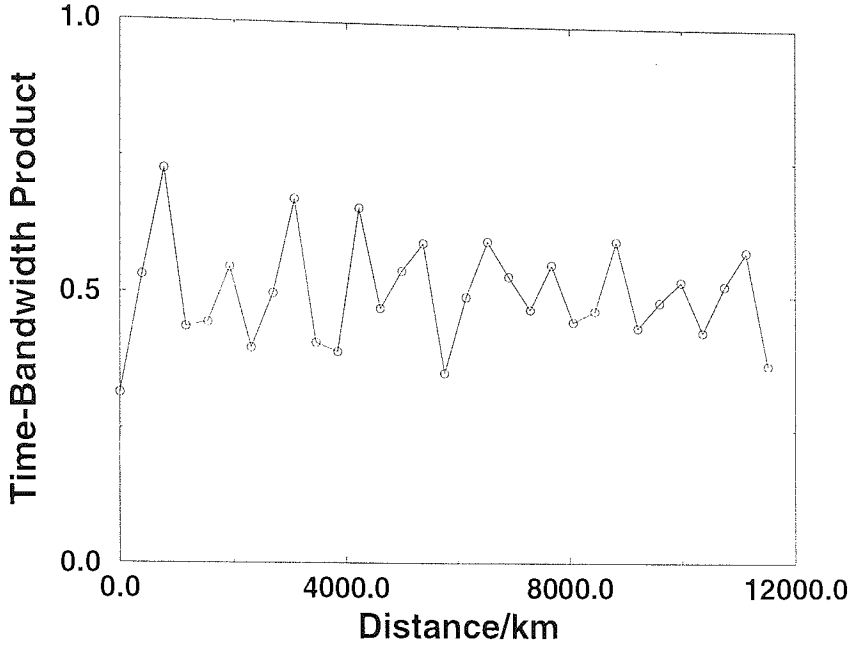

Figure 6.21: The time-bandwidth product against distance for map C.

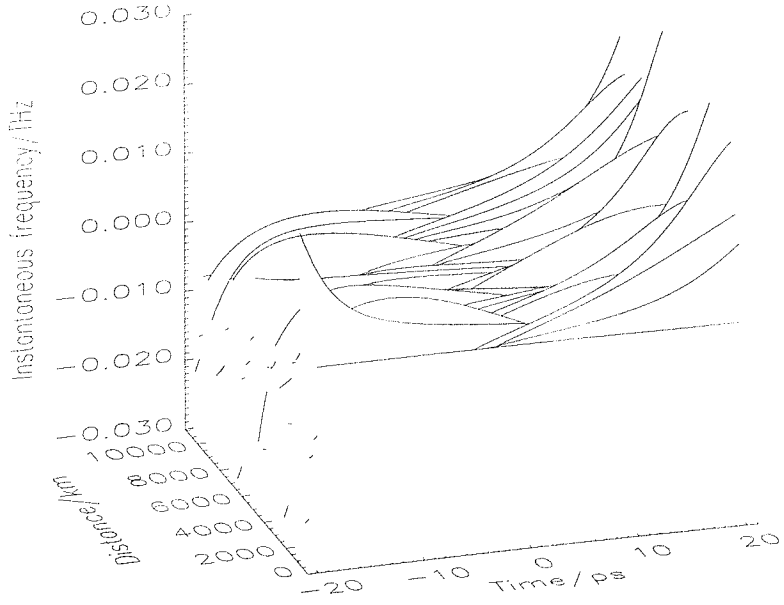

Figure 6.22: Instantaneous frequency for map C this shows how the chirp evolves during propagation. The fluctuations in the previous three graphs are visible in this plot

change much after one or two dispersion map periods. The bandwidth is not reduced by as much over one amplifier span compared to the two previous amplifier positions. It is clear that by making the two lengths of standard fibre more equal in length the bandwidth could be further stabilised, however the systems modelled here were constrained by the lengths of fibre available in the experiments on which these simulations were based.

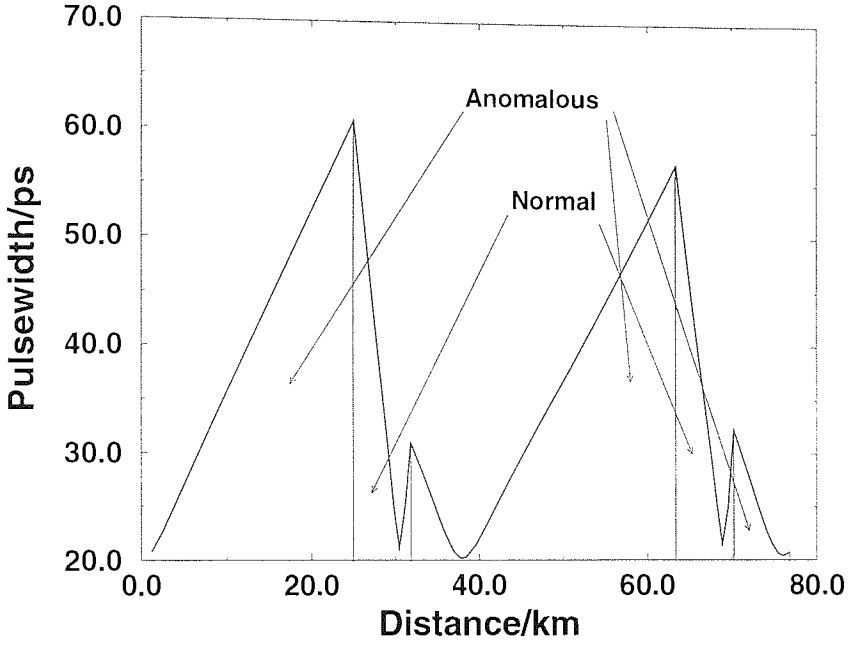

Figure 6.23: Pulsewidth evolution through two periods of the dispersion map, the amplifiers are at the border going from the anomalous dispersion fibre into the normal dispersion fibre.

The three systems that have been considered in this chapter have also been examined experimentally. The experimentally measured Q-values are given in figure 6.25. For systems A and C the experimental and numerical results show the same features with the same oscillations clearly visible in both. The reduction in the oscillations between the two setups is also clearly visible. The Q-values in the experimental results are limited by the input Q-values which are much lower than those used in the simulations where perfect input sech pulses are used. The results from map B in the simulations show reduced oscillations compared to set A, however in the experiment system B does not allow propagation for more than 1000km. The reason for the difference between the experimental results and the numerical simulation in this case is not clear. It is clear that the problem in the experimental results is related to the stability of the pulses rather than timing jitter or SNR since these problems would not have been able to accumulate in the 1000km propagation distance.

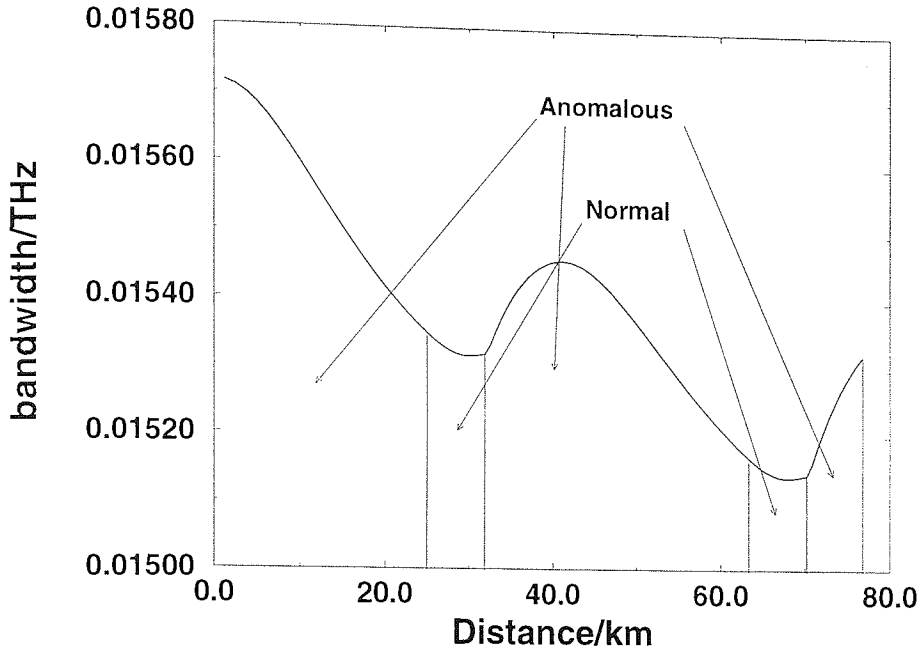

Figure 6.24: The bandwidth evolution through two dispersion maps. The bandwidth increases in the normal dispersion fibre which is situated immediately after the amplifier.

6.4 Conclusions

The transmission of dispersion managed solitons in standard fibre was studied. In particular the effect of rearranging the relative positions of the fibres and the amplifier was examined. This also included varying the length of the initial prechirping length of the fibre.

When the dispersion map was used without any prechirping fibre there were large oscillations in the Q-value over the transmission distance. These oscillations were similar to variations observed in the pulse width due to the pulses being chirped at the output. It could also be seen that the bandwidth of the pulses had a tendency to be reduced during propagation as the pulses were always chirped in the same direction and so the bandwidth did not have an opportunity to increase.

When the dispersion map was changed to give an initial step of fibre, the oscillations were reduced and made more regular. The source of the oscillation could still be seen in the fluctuations in the pulse width. The bandwidth still had a net reduction over the first two amplifier spans, however the pulse was now chirped in both directions so over some parts of the dispersion map the bandwidth increased. Moving the amplifier from just before the compensating fibre to just after the compensating fibre resulted in a further

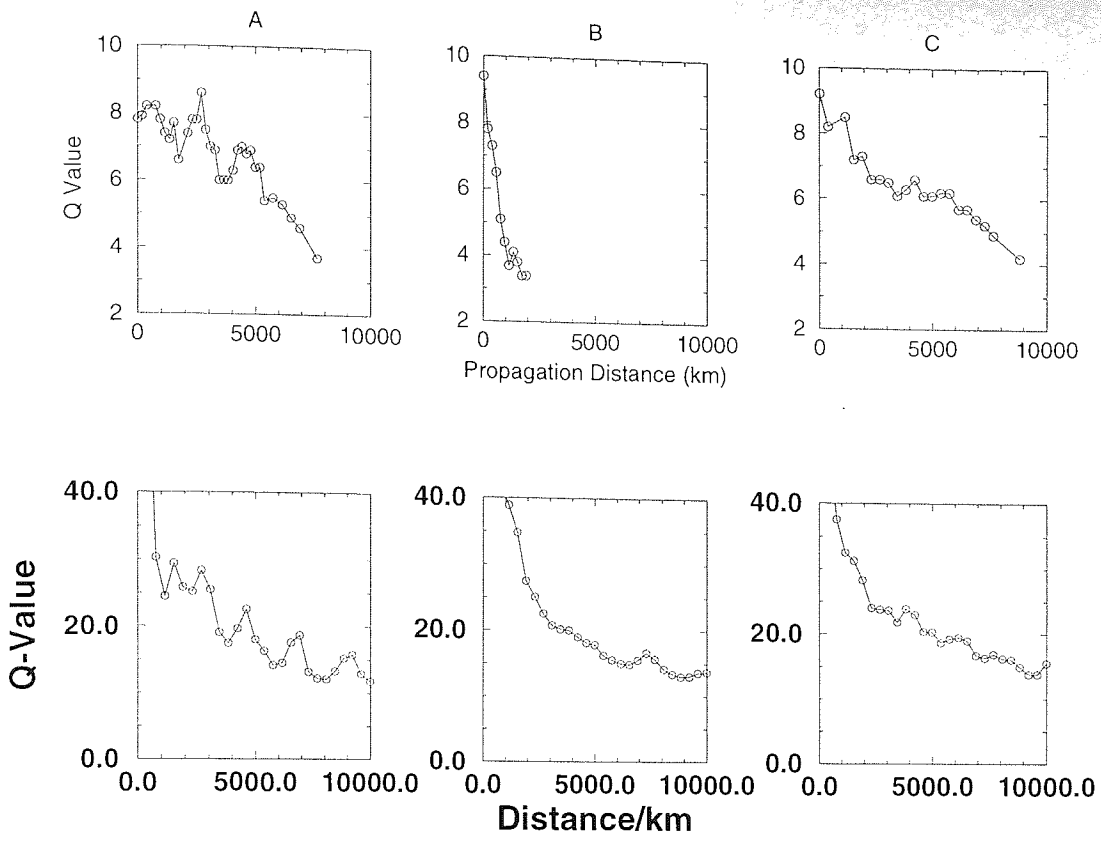

Figure 6.25: Experimental results of Q-value versus distance for the three systems, the lower graph has the simulation results for comparison.

improvement in the system. In particular this stabilised the bandwidth as the pulse peak power was now highest in the standard fibre.

The results presented in this chapter demonstrate that proper choice of the position of the amplifier and using an appropriate length of pre-chirping fibre can improve the stability of a dispersion managed soliton system. The proper choice of these parameters can reduce the oscillation is Q-value, however the Q-value at the end of the simulations was ~ 12 in all of the cases. If no pre-chirping fibre is used the pulse only gets chirped in one sense and so the pulse bandwidth suffers a reduction throughout the dispersion map period.

The simulation results were compared to experimental results and showed good agreement on two of the systems. The experimental Q-values, although smaller than the numerical ones, showed the same oscillations which were improved from system A to C. The experimental results for system B were limited to less than 1000km. These simulation showed that it is possible to propagate dispersion managed solitons at 10Gbit/s over distances long enough to cover any realistic needs. They also showed that although the system is improved by optimising the fibre and amplifier positions it does not cause a significant improvement in distance.

Chapter 7

Upgrade of standard fibre network to 40Gbit/s using RZ transmission

7.1 Introduction

In the previous chapter it was shown that the transmission of single channel data rates of 10Gbit/s is possible over transoceanic distances in standard fibre. The next challenge is to investigate the propagation of soliton-like RZ pulses at 40Gbit/s. Since one of the main purposes of this work is to study the upgrade of the current standard fibre network, the initial aim is to propagate the pulses over the more modest distances required for land based communications. This chapter identifies the prospect for the propagation of quasi-linear soliton-like pulses over more than 2000km with a single channel data rate of 40Gbit/s. This distance was attained using dispersion management utilising a symmetric dispersion map.

To date there has only been a limited experimental investigation of 40Gbit/s transmission on standard fibre as most work has centred on maximising the performance at 10Gbit/s. The two most successful techniques for 40Gbit/s transmission in standard fibre are optical phase conjugation (OPC) and dispersion management. Using OPC at the mid-point of a transmission line it has been possible to propagate over 434km of standard fibre [133]. Using dispersion management it has been possible to propagate non-soliton pulses over 80km of standard fibre [211]. Recent experiments using the soliton like quasi-linear pulses similar to those discussed in this chapter have propagated data over 500km [156] and 1200km [187] of dispersion managed standard fibre. Previous simulations have shown that use of a similar "symmetric" dispersion map allows the propagation of 40Gbit/s over 480km of standard fibre with a 120km amplifier span [212].

There are many problems associated with increasing the data rate from 10Gbit/s to 40 Gbit/s. The most serious of these is the increase in the strength of the dispersion map which is caused by the necessary reduction in the pulse width. The map strengths that this leads to are far outside the range where stable soliton propagation is expected. As stated in chapter 3 map strengths (given by $S = \frac{L_n\beta_n'' - L_a\beta_a''}{\tau^2}$) of up to $S \sim 12$ have been used for stable propagation. The maps used in this chapter range in strength from 43 to 188. The high map strengths that are used here result in many problems. It is not found to be possible to get the long term stable pulses that are found for weaker maps. Any such stable pulses would have extremely high powers due to the power enhancement which means that the pulse energy of a dispersion managed soliton scales as S^2. It will be shown later in this chapter that using these enhanced energies no stable pulses have been found.

The short pulse width (5ps) and high fibre dispersion (16.75ps/(nm km)) mean that the dispersion length (as discussed in section 2.3.2) is $\sim 0.45km$ which is short compared to the lengths of fibre used. The effect of the short dispersion length of these pulses is that the pulses broaden substantially in the standard fibre. This leads to distinct pulses only existing near to the point in the fibre where the pulses are unchirped. The final problem is that this chirp-free point moves through the standard fibre due to the relatively high average anomalous dispersion which leads to an incorrect balance between the average dispersion and the nonlinearity. The pulses used in this system are described as quasi-linear as they do not demonstrate the enhanced power that has been described in relation to dispersion managed solitons previously (see section 3.3). Indeed the pulses used here have reduced power when compared to average solitons.

A significant difference between the dispersion map used here and the one in the previous chapter for 10Gbit/s propagation is that here the compensating fibre is split with the amplifier placed between two sections of compensating fibre. Symmetric maps have previously been shown to improve the performance of dispersion managed systems used for standard fibre propagation [213, 212, 210]. This dispersion map can still be considered in relation to the upgrade of the standard fibre network as the compensating fibre is all located at the amplifier.

In this chapter the problems relating to standard fibre propagation and the dispersion map used will be considered. Then the results of the various models will be given and finally conclusions will be drawn from the results.

7.2 Modelled System

Most of the difficulties associated with propagating RZ pulses over standard fibre at 40Gbit/s are related to the short pulses which must be used to allow a mark to space ratio of 1:5 or less. This means that the maximum pulse width (FWHM) is 5ps. To use solitons at this data rate in standard fibre at $1.5\mu m$ without dispersion management would require pulses with extremely high peak powers and would lead to average powers of more than 200mW. This is an unfeasibly high value and is in fact too high for the safety regulations. Also since the soliton period of a 5ps pulse in standard fibre is 0.63km it is not practical to fulfil the average soliton criteria given in section 2.6.2 which states that the amplifier span must be substantially less than the soliton period. This means that simply using solitons without control in a purely standard fibre systems is not feasible. Figure 7.1 shows a single soliton going through 2 amplifier spans of a system with a 50km standard fibre amplifier span, it is clear that the pulse is unstable and quickly breaks up.

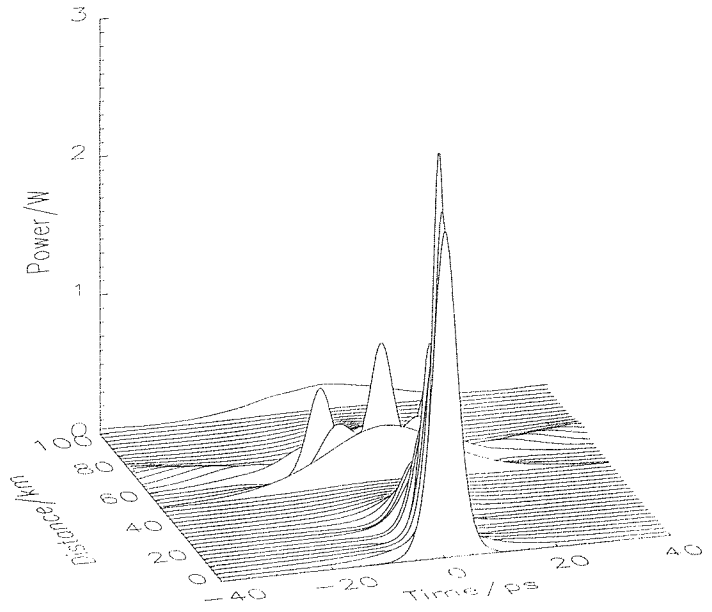

Figure 7.1: An average soliton propagating in standard fibre. This first order soliton has a pulse width of 5ps, the amplifier span is 50km.

If dispersion management is used then it is possible to reduce the average dispersion and therefore reduce the average powers required to propagate solitons and the soliton period. As noted in section 3.2 the strength of the dispersion map is given by;

$$S = \frac{L_n\beta_n - L_a\beta_a}{\tau^2} \tag{7.1}$$

Due to the pulse width squared appearing on the bottom line of this equation there is a strong dependence of dispersion map strength with pulse width. Since the energy enhancement tends to vary by S^2 there is an even stronger dependence of the power with pulse width. For weak maps the energy enhancement is given by;

$$\nu = 1 + 0.7S^2 \tag{7.2}$$

As the pulses required for 40Gbit/s are 1/4 the width of those used for 10Gbit/s the map strengths are of the order of 16 times those used in 10Gbit/s and the energy enhancement would be expected to be 256 times that used for 10Gbit/s transmission. However these problems would only arise if the energy enhancement for weak maps held for the extremely strong maps used here and long term stable dispersion managed solitons could be found. Figure 7.2 shows a pulse from one of the systems modelled here. This system has 50km of standard fibre and 6km of compensating fibre to give an average dispersion of 0.14ps/(nm km) using a 5ps pulse this should give an energy enhancement of 4481 over a first order soliton for the map strength of 50. It is clear from the figure that the pulse is not restored even after passing through this dispersion map once. The pulse at the midpoint of the standard fibre and at the end of the simulation has clearly spread out and become distorted.

One direct result of the short pulses and the high dispersion of the fibre is that the dispersion length (as defined in section 2.17) is very short compared to length of fibre being used. The dispersion length for a 5ps pulse in standard fibre is 0.45km which is far shorter than the amplifier spans that are used. This means that the pulses are in general able to be described as linear pulses where the dispersion dominates as discussed in section 2.32.

The amount of pulse spreading caused by the short dispersion length causes a significant problem when the pulses are used in a 40Gbit/s system. Figure 7.3 shows a single 5ps Gaussian pulses as it spreads due to the dispersion in 8km of standard fibre. The width of this pulse as it propagates over the same length of fibre is given in figure 7.4. It is clear that even after a very short propagation distance the pulse has broadened to

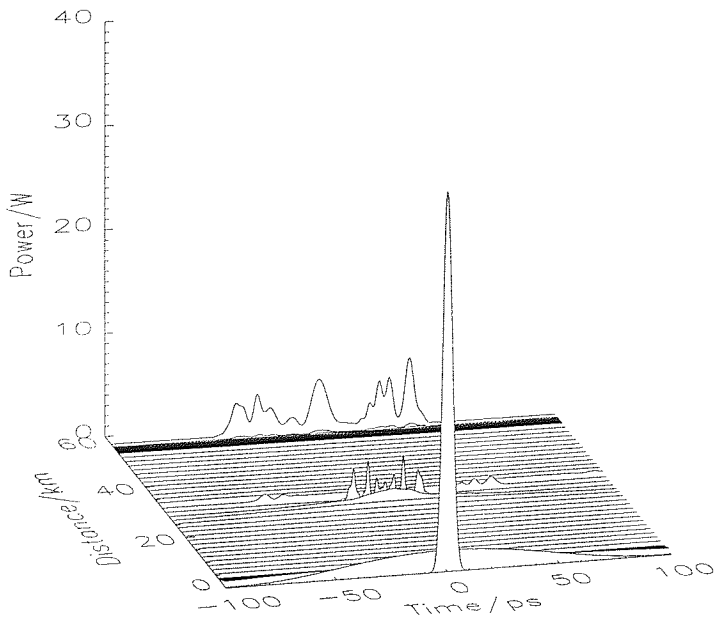

Figure 7.2: An enhanced power soliton in the dispersion map with 50km of standard fibre. The pulse has a width of 5.0ps and a pulse energy of 198.6pJ.

such an extent that it would overlap with an adjacent pulse (the pulse separation is 25ps). When the pulses overlap like this they interfere with each other which means that any information is lost. Figure 7.5 shows 2 pulses in a 40Gbit/s data stream as they overlap in the same short length of fibre. This overlapping means that it is important to take the output at the point in the dispersion map where the pulses are chirp free and so their width is at a minimum. This is clearly demonstrated in figure 7.6 which shows 4 pulses from one of the simulations as they emerge from interference caused by the pulse spreading.

In order to minimise the pulse interactions these simulations use a symmetric dispersion map. This means that the compensating fibre is split so that one section of it is placed before the amplifier with the rest following it [213]. The advantage of the symmetric dispersion map is that it effectively reduces the strength of the dispersion map. This is because there are now effectively two dispersion maps. One immediately following the amplifier where nonlinear effects are more important and another in the second half of the dispersion map where the power is lower and linear compensation takes place [214].

The dispersion map used in these simulations is given in figure 7.7. The length of standard fibre is either 27km, 50km or 100km and is taken to have dispersion of $16.75ps/(nmkm)$, third order dispersion of $0.07ps^2/(nmkm)$ and loss of 0.22dB/km. The

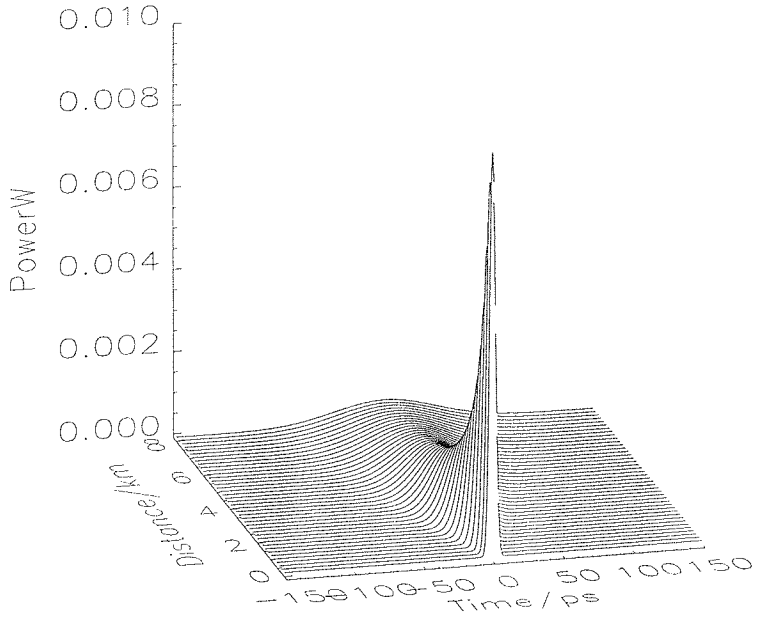

Figure 7.3: A 5ps input Gaussian pulse travelling through 8km of standard fibre. By the end of this short length of fibre the pulse width has increased to 88ps which is far greater than the pulse separation of 25ps for a 40Gbit/s data rate.

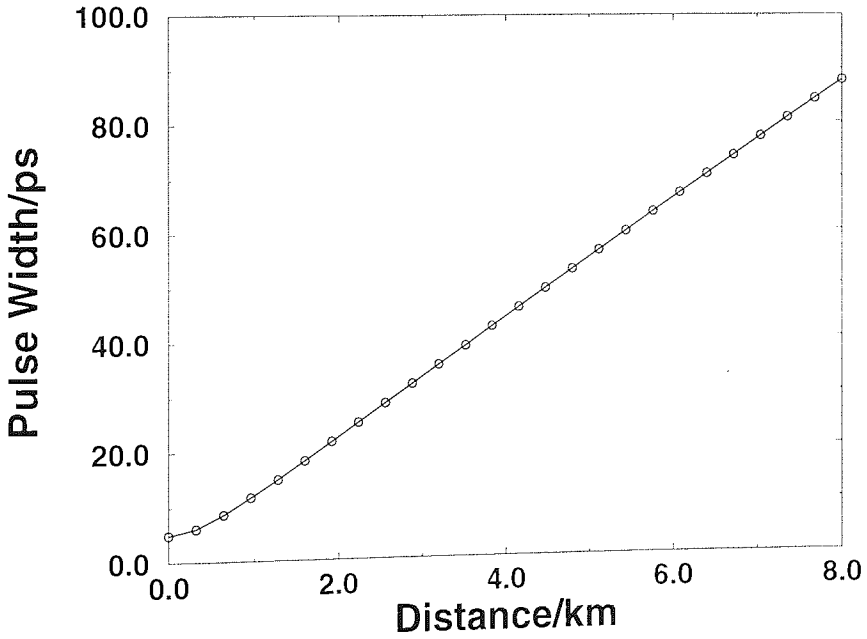

Figure 7.4: The pulse width of the 5ps Gaussian pulse as it broadens through 8km of standard fibre.

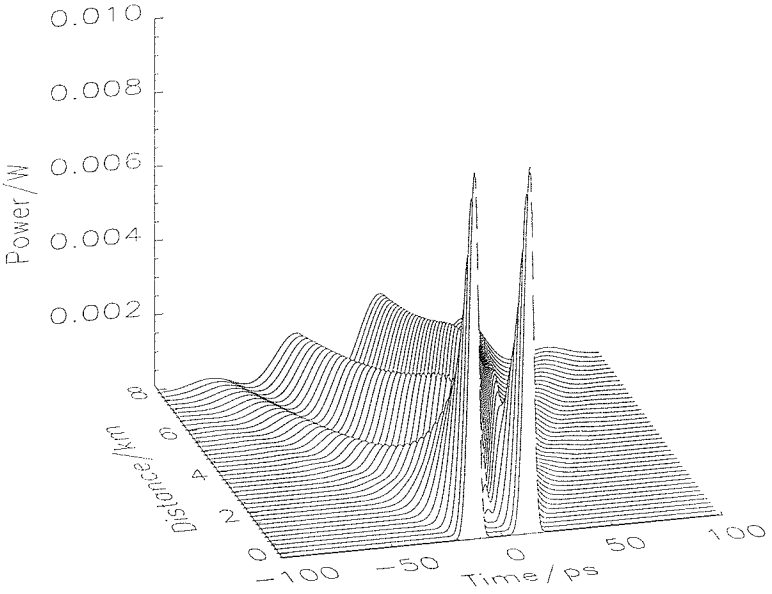

Figure 7.5: Two 5ps pulses as they broaden and interfere, note the short scale over which the interference takes place.

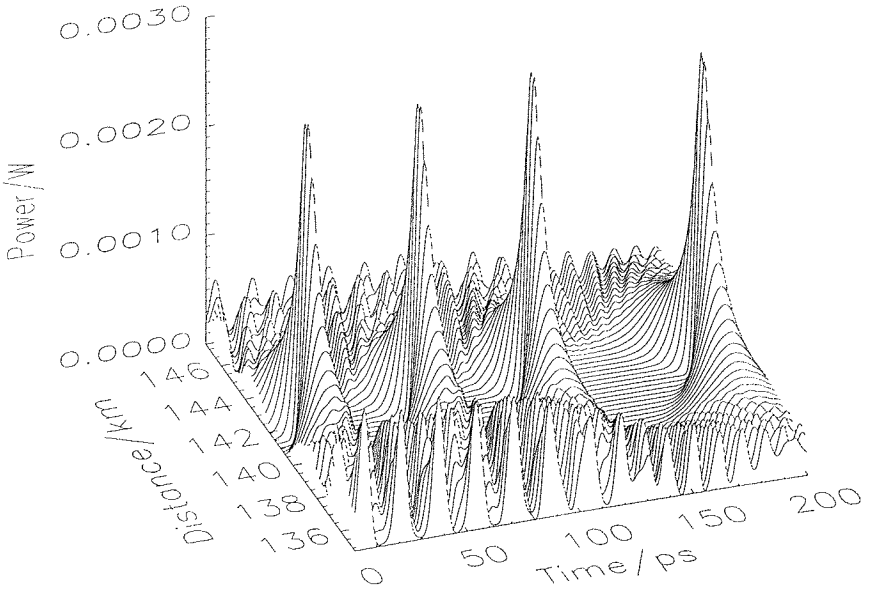

Figure 7.6: Four pulses as they reach the point in the fibre where they are unchirped. The system used here had 50km of standard fibre and an average dispersion of 0.19ps/nm/km. The input Gaussian pulses had peak power of 0.14W and a FWHM of 5.0ps.

compensating fibre is 6km long with 2.7km before the amplifier and 3.3km after it, the dispersion of the compensating fibre is varied depending on the length of standard fibre and the required average dispersion, the third order dispersion is taken to be $0.07ps^2/(nmkm)$ and loss of 0.22dB/km is used. The initial step of prechirping fibre is 3.3km, unchirped pulses are launched into this fibre before going into the first stage of standard fibre. The filter has a Gaussian profile and a pass-band of 5.25nm, this bandwidth is 8 times that of the pulses and so this filter can be considered to not have a significant effect on the pulse evolution. The amplifier has a noise figure of 4.5dB.

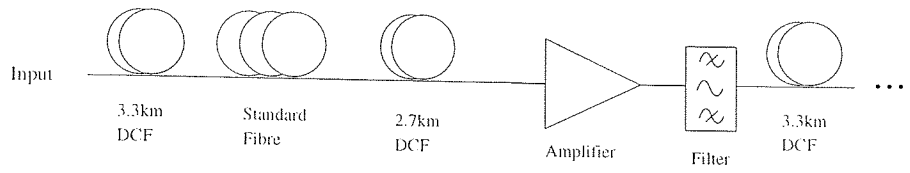

Figure 7.7: The general system used in these simulations. The length of the standard fibre was either 27, 50 or 100km and was taken to have dispersion of 16.75ps/(nm km). The 6km of compensating fibre has been split into two sections with 2.7km before and 3.3km after the amplifier respectively.

The correct splitting of the compensating fibre is found by changing the position of the amplifier in the compensating fibre and then comparing the Q-values after 500km transmission. This is done using the system with 27km of standard fibre with an average dispersion of 0.1ps/(nm.km). Gaussian pulses with a pulse width of 5ps and peak powers of 0.01W are used. As can be seen in figure 7.8 the dispersion map with 2.7km of fibre before the amplifier and 3.3km after gives the best results. The graph shows Q-values plotted against the length of fibre after the amplifier, the total length of fibre is always kept at 6km. The Q-value increased from ~ 7 to ~ 16 when the amplifier is moved from following the compensating fibre to the midpoint of the fibre.

Both sech and Gaussian pulses can be used in this dispersion map. Although there is not a large difference between the maximum possible propagation distances with the different pulses, Gaussian pulses are found to give better results (see figure 7.13) and so will be used for the majority of the simulations [141]. The input pulses have a width of around 5ps.

There are obviously a large number of parameters that can be varied in order to maximise performance in this model. As well as the parameters of the pulse (shape, width and peak power) there are the parameters relating to the dispersion map and finally there are the other components such as the filter and the receiver. In order to limit the number of parameters being varied the filter and receiver will not be changed,

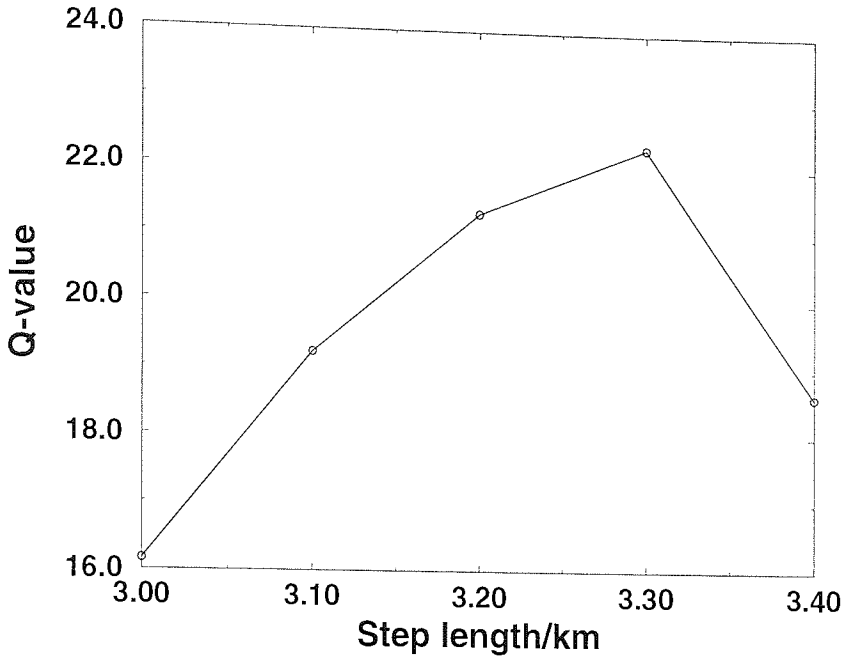

Figure 7.8: Q-values after 500km transmission plotted against the length of compensating fibre following the amplifier. The best results are found with 2.7km of fibre before the amplifier and 3.3km after it.

the lengths of the fibres being used (other than the length of standard fibre) will not be altered either. The average dispersion is varied by making small changes in the dispersion of the compensating fibre, the width and peak power of the pulses will also be varied. The optimum performance is found by varying the pulse power, width and the average dispersion of the map. The optimum performance refers to the maximum distance for which a $Q > 6.0$ is found. A random pattern of 96 bits will be used in these simulation. As given earlier in this thesis the Q-values in these simulations are found using;

$$Q = \frac{\mu_1 - \mu_0}{\sigma_1 + \sigma_0} \tag{7.3}$$

where μ_1 and μ_0 are the mean level of the 1 and 0 and σ_1 and σ_0 are the standard deviations of the 1 and 0. These values are indicated on the eye diagram given in figure 7.9.

This is the simplest method used to calculate Q-values and does not take into account the effects of patterning caused by intersymbol interference. Although including the effects of patterning is likely to give higher Q-values it is a far more complicated and is unlikely to significantly affect the conclusions drawn from these simulations [215]

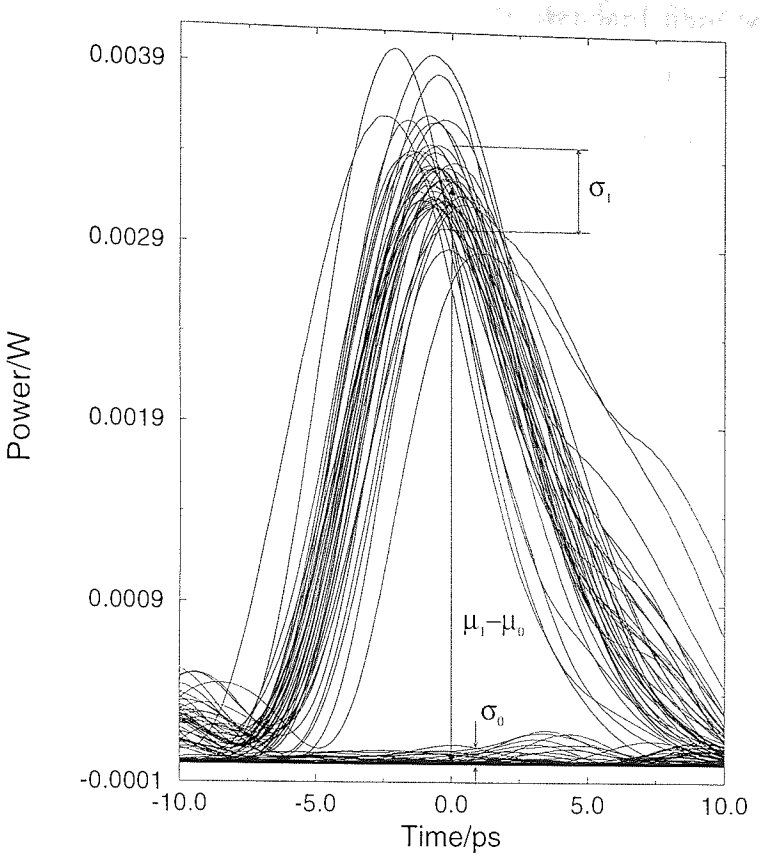

Figure 7.9: A sample eye diagram taken from 1100km in a system with 50km of standard fibre.

7.2.1 Results

The three different models that are used (27km, 50km and 100km of standard fibre) have some shared properties which will be discussed before the specific details of the parameters used in each of the systems and the maximum propagation distances attained are given.

The first shared property is related to the position of the chirp free point. It is found that in the dispersion maps that give the maximum propagation distance the chirp free point moves in the standard fibre depending on the number of times the pulses have passed through the map. Figure 7.10 shows the fractional distance through the fibre of the position of the unchirped pulses against number of amplifier spans. This shows that in all of the cases the unchirped point, where the clear pulses can be found, is intially beyond the midpoint of the standard fibre. The unchirped point occurs progressively earlier in the standard fibre in the subsequent amplifier spans. The information in the 27km and 50km maps is eventually lost when the chirp free point reaches the start of the fibre. In the 100km map the pulses are lost through pulse interactions and pulse instability before this point is reached. Given that the pulse reaching the end of the fibre is the ultimate limit on the total propagation distance it would seem reasonable that a launch point that

meant the pulses were initially chirp free later in the standard fibre would extend the total propagation distance. The results given in figure 7.8 show that this is not the case and that moving the launch position in such a manner leads to greater degradation of the signal due to interactions leading to intersymbol interference. The optimum launch point is a balance between limiting the distance due to the walk through and limiting the distance due to ISI. It is interesting to note that when fractional distance through the standard fibre is plotted against number of amplifier spans the three lines follow similar paths.

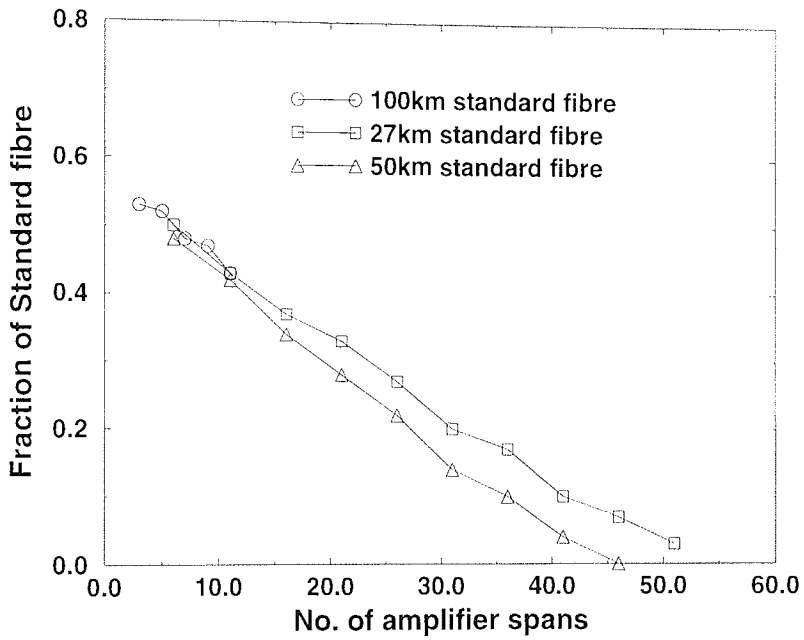

Figure 7.10: This demonstrates the movement of the unchirped point through the standard fibre for the three dispersion maps. the fractional distance through the standard fibre is plotted against the number of amplifier spans.

The movement of the unchirped point is caused by the high average dispersion and the nonlinearity. High average dispersion is used as it suppresses the interactions of the pulses which lead to intersymbol interference, however it also means that the accumulated dispersion is greater than can be compensated for through nonlinearity. In a purely linear system the pulses are unchirped at the point where the accumulated dispersion is zero. In dispersion maps like this where the dispersion is clearly the dominant factor the nonlinearity can be treated as a perturbation and so the pulses would be expected to be unchirped close to the point where the accumulated dispersion is zero but the nonlinearity does have a small effect. The effect of the nonlinearity in this case is to add an effective

anomalous dispersion. This is because, as can be seen in figure 7.11, the bandwidth of a pulse is greater in the anomalous dispersion fibre and so this fibre has a greater effect on the pulse than the normal dispersion fibre. It is interesting to note that due to the large amount of pulse spreading which occurs in this dispersion map, the bandwidth of the pulse undergoes most of its changes at the points on the fibre where the pulses are unchirped and so the peak powers are quite high. However this effect is very small compared to the average dispersion and so that is the major factor in defining the position where the unchirped pulses are found. The variation of the pulse width in the dispersion map is given in figure 7.12. There is a very large change in the pulse width with the value increasing from 5 to 300ps. By comparing the pulse width and bandwidth graphs it is clear that the changes in bandwidth occur when the pulsewidth is at a minimum and so the peak power is at a maximum. It should be noted that the bandwidth (see figure 7.11) is not periodic and is increasing on average during propagation.

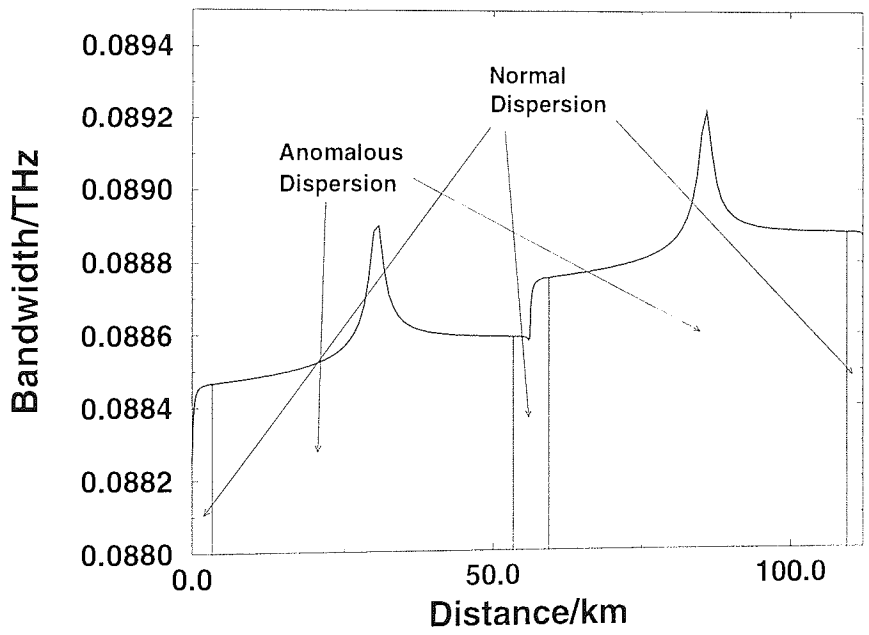

Figure 7.11: The bandwidth varying through the dispersion map. There is very little variation in the bandwidth during propagation and the change that does take place occurs around the point in the fibre where the pulses are unchirped. It should be noted that the bandwidth does not periodically return to its original value but is increasing.

It would seem reasonable that in order to counteract this problem it would be best to propagate these pulses nearer to zero dispersion or even in the average normal dispersion region, however it is found that for very low average dispersion of either sign that pulse interactions are a greatly increased problem. Figure 7.13 shows the maximum propagation

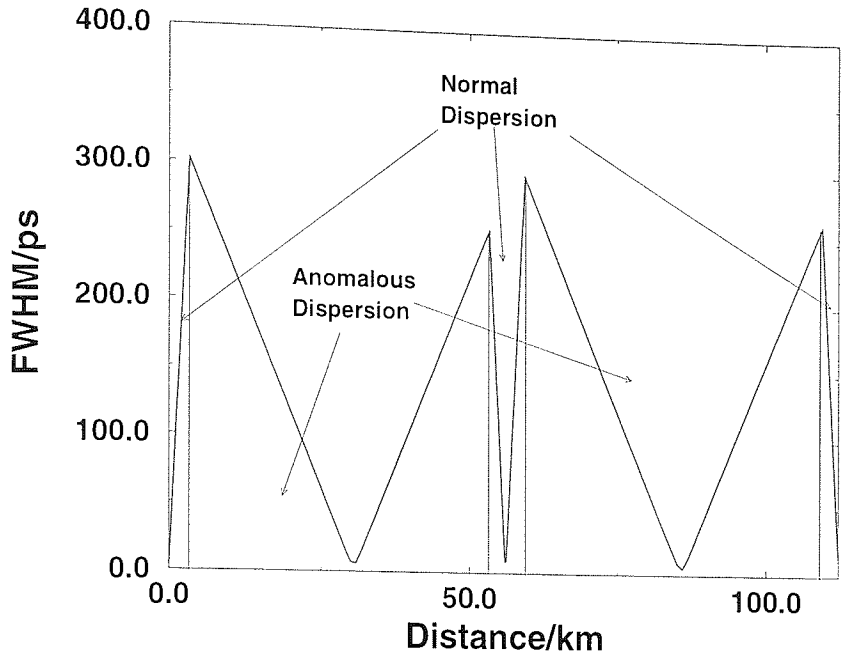

Figure 7.12: The pulsewidth varying through the dispersion map. There is a large change in pulsewidth due to the high local dispersion.

distance for different values of the average dispersion around the dispersion zero. For this set of results the pulses had a pulse width of 5.0ps and a peak power of 0.05W. Both Gaussian pulses and sech pulses were used and the output position was fixed at the output of the amplifier. This system used 50km of standard fibre and the average dispersion which gave no movement in the position of the unchirped pulses was found to be $-0.00286ps/(nmkm)$.

The propagation distance can be improved to almost 800km at the average dispersion where the unchirped point is at a fixed point in the dispersion map. This is done by varying the pulse width which reduces the pulse interactions. However decreasing the pulsewidth further increases the strength of the dispersion map and eventually reduces the distance over which the pulse is stable. A graph of pulse width against total propagation distance is given is figure 7.14.

Intersymbol interference is one of the main limitations on the propagation distances possible in these systems. Intersymbol interference is caused by a pulse interacting with the neighbouring pulses and so the effects are dependent on the bit pattern [215] in that three 1's in a row for example might be more likely to cause an error with the centre 1 growing at the expense of the outer two whereas four 1's or two 1's might be less affected. This effect, known as patterning, is demonstrated in figure 7.15 which shows a section of

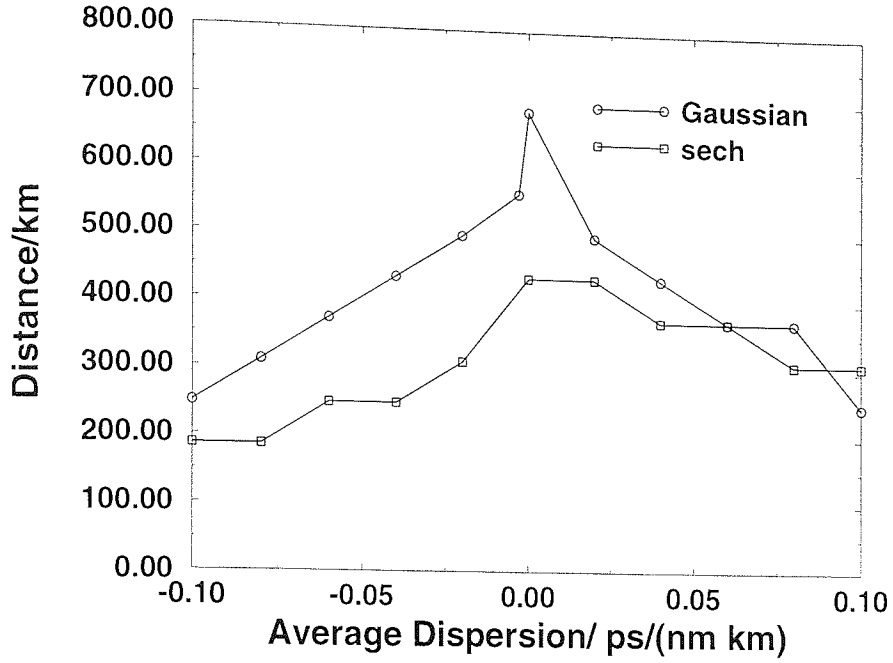

Figure 7.13: The maximum propagation distance against average dispersion around the dispersion zero. The output position was kept fixed during these simulations.

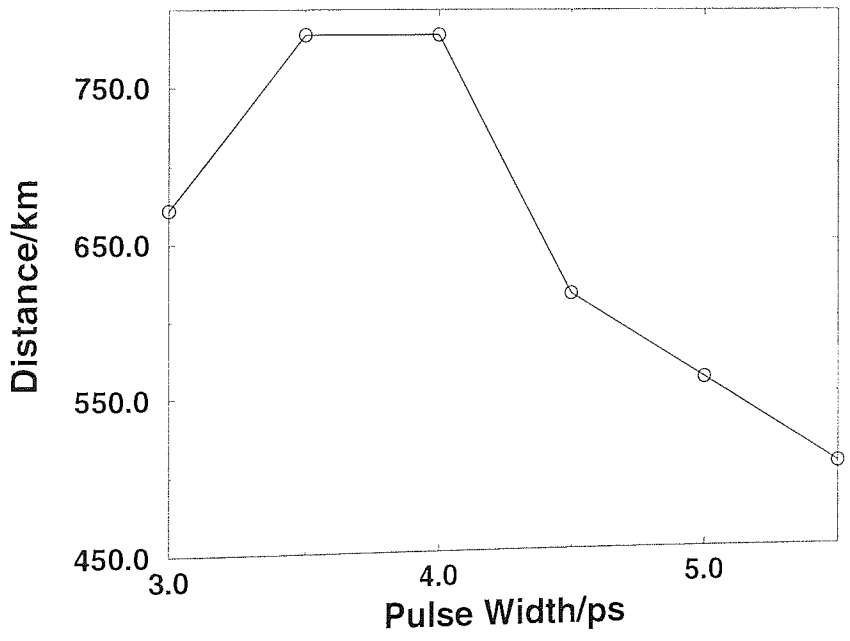

Figure 7.14: A graph of pulse width against total propagation distance. The average dispersion was set so that the unchirped point does not move.

the bit pattern with two 1's and three 1's in a row. The top picture shows the pulses at the start of the transmission whereas the lower picture is taken after 1000km. The two 1's still have similar amplitudes after 1000km but the middle of the three 1's has increased its amplitude at the expense of the outer two.

The other shared property of the pulses in these three systems is that they have suppressed energy compared to an average soliton for the same average dispersion. In general dispersion managed solitons are expected to have enhanced power when compared to average solitons. As has already been pointed out the strength of the dispersion map used here is far greater than those generally investigated. The use of a symmetric dispersion map reduces the size of the expected power enhancement but does not account for the suppressed energies found here. The relatively large average dispersions that are used to suppress the intersymbol interference could also account for the reduced energy. It is clear that these pulses are not what have become known as dispersion managed solitons they are quasi-linear pulses but require finite dispersion for optimum performance.

A graph of Q-value against distance for the greatest propagation distances attained for the three dispersion maps is given in figure 7.16. The initial Q-values are extremely high as there is no noise on the input, this leads to a large fall in Q at the start of each simulation.

The first set of simulations use the dispersion map with 27km of standard fibre and 6km of compensating fibre. In order to find the optimum performance the peak power is varied between 0.1W and 0.2W, the pulse width is varied between 4.5ps and 6ps and the average dispersion is varied between 0.1ps/(nm km) and 0.2ps/(nm km). Over most of the range of these parameters it is possible to propagate the data over more than 1000km. Varying the pulse width is not found to affect the results strongly and varying the peak power is limited due to the problems associated with the signal to noise ratio, therefore the most effective parameter to vary is found to be the average dispersion. A graph of Q-value against average dispersion is given in figure 7.17 this shows that the highest Q-value at a distance of 1500km is at 0.15ps/(nm km) but the fall off for small changes in average dispersion is not sharp The maximum propagation attained also uses 5ps pulses with a peak power of 0.01W and an average dispersion of 0.15ps/(nm km). This gives an overall map strength of S=43. An average soliton with the same pulse width and in a constant dispersion fibre would have a peak power of 0.017W which is significantly higher than the peak power of the pulses used here.

The next set of simulations use a dispersion map consisting of 50km of standard fibre

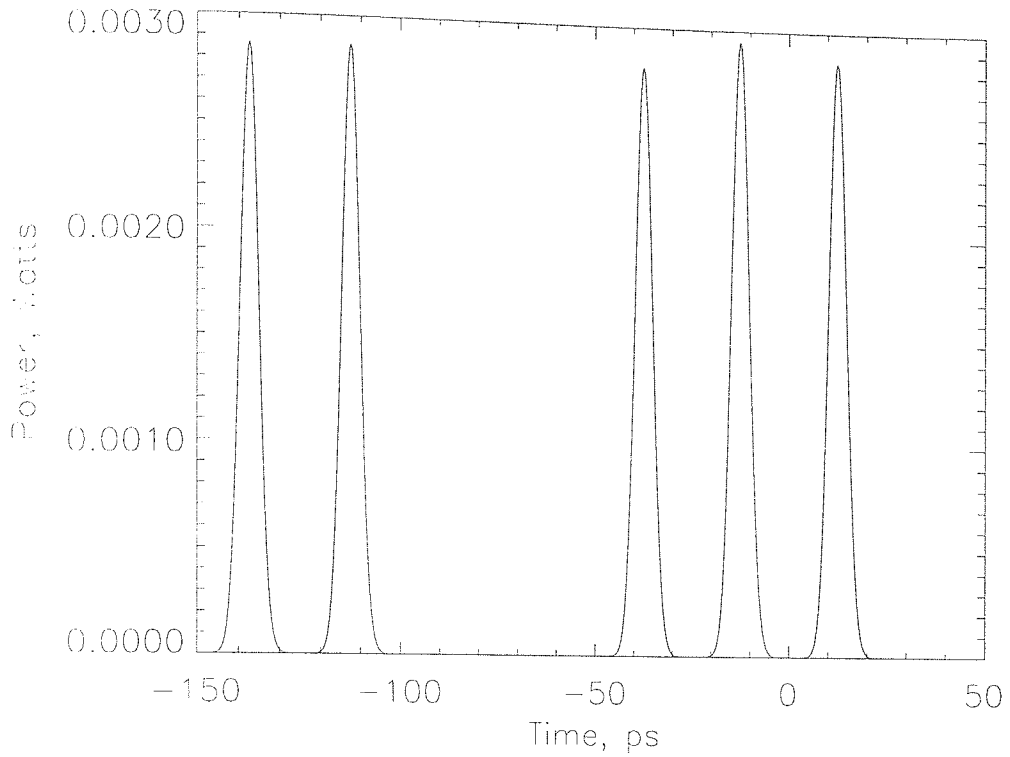

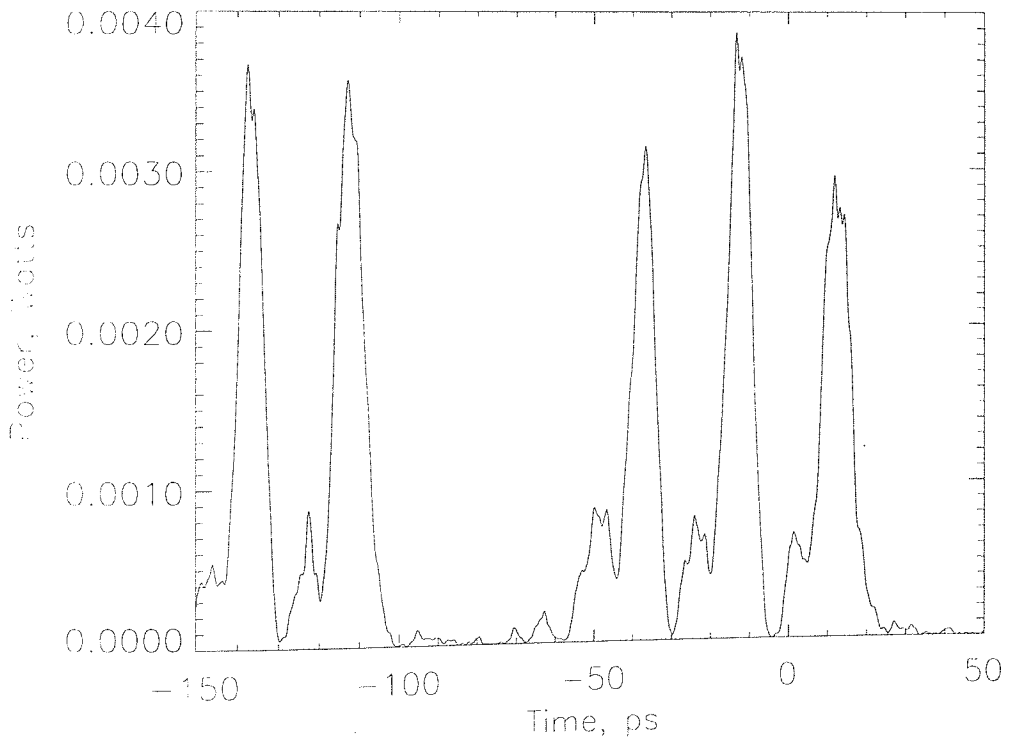

Figure 7.15: This demonstrates the effect of intersymbol interference on the bit pattern. The section of the pattern with three 1's has suffered more degradation than the section with two 1's. These simulations are taken after 1500km in the system with 50km of standard fibre with an average dispersion of 0.19ps/(nm km). The input, Gaussian pulses have a peak power of 0.01W and FWHM of 5ps

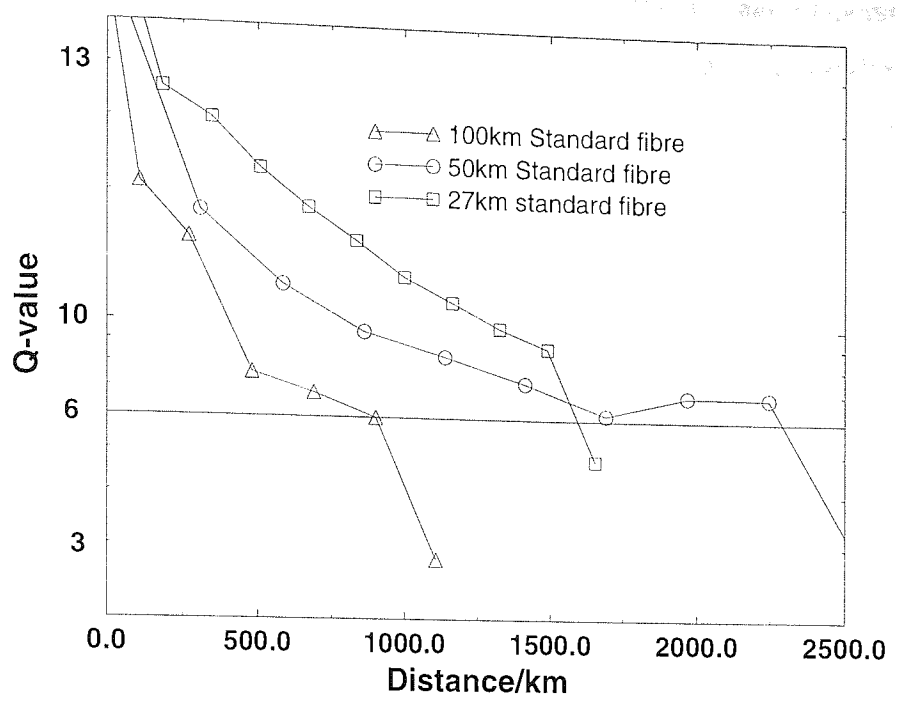

Figure 7.16: Q-figure against distance for the three systems. The horizontal line represents a Q of 6.0 which is equivalent to a bit error rate of 10^{-9}

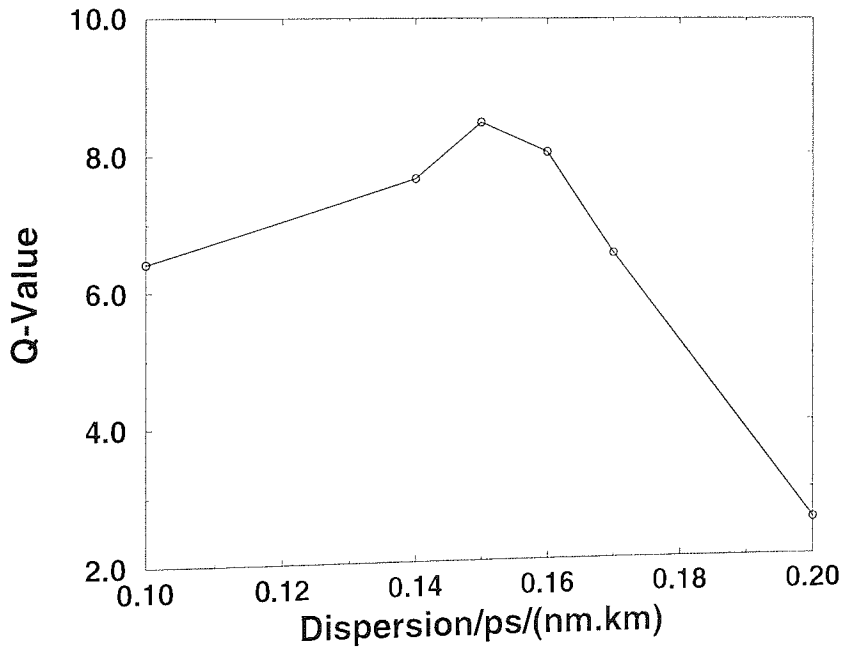

Figure 7.17: Q-value against average dispersion after 1500km in the system with 27km of standard fibre. These simulations were all run with peak powers of 0.01W and 5ps Gaussian pulses.

with 6km of compensating fibre. In this case peak powers of between 0.012W and 0.018W are used with pulse widths of between 4.5ps and 5.5ps, the average dispersion is varied between 0.15ps/(nm km) and 0.2ps/(nm km). With this length of standard fibre it is again found that it is possible to propagate the data over more than 1000km with a range of parameters. The maximum propagation distance for a range of average dispersions is given in figure 7.18, these systems all use Gaussian pulses with a peak power of 0.014 and pulse widths of 5.0ps. The maximum propagation distance of more than 2000km is found for pulses with a peak power of 0.014W and a width of 5.0ps in a dispersion map with an average dispersion of 0.19ps/(nm km). This gives a map strength of S=80 and again the peak power of these RZ pulses is substantially less than the peak power of an equivalent average soliton which would be 0.032W.

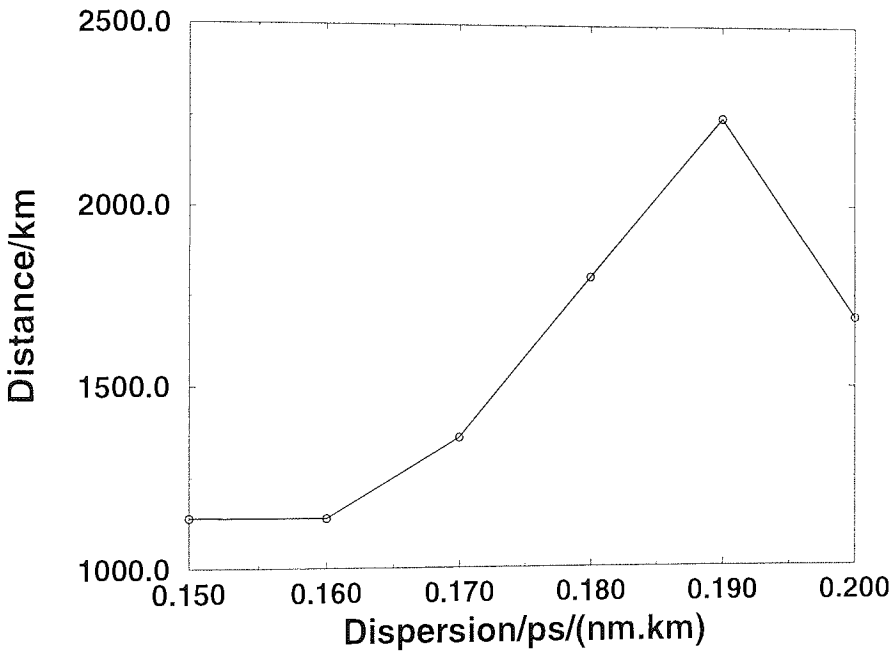

Figure 7.18: Maximum propagation distance against average dispersion for a Q-value greater than 6 in the system with 50km of standard fibre. These simulations were all run with peak powers of 0.014W and 5ps Gaussian pulses.

It is surprising that the dispersion map with more standard fibre and a higher S number gives better results than the weaker map. It can be seen in figure 7.16 that until the sudden reduction in Q at the end of the simulation the weaker map gives better Q-values. The reason for the better results from the stronger map can be seen from figure 7.10 which shows the position of the unchirped pulses. The limit of the propagation distance in both cases is that the chirp free point eventually reaches the start of the

standard fibre and after that point the pulses are no longer recovered. Since the position of the chirp free point has a linear relationship with the number of amplifier spans the total distance possible with the stronger map is greater although they both travel through the dispersion map a similar number of times.

For the final set of results the length of standard fibre is again increased, this time to 100km. Here pulses with peak powers of between 0.03W and 0.05W are used with pulse widths of between 4.4ps and 5.5ps, the average dispersion of the fibre is varied between 0.1ps/(nm km) and 0.25ps/(nm km). The propagation distances possible with this map are substantially less than those previously found. The maximum propagation distance was not strongly affected even by changing the average dispersion. As shown in figure 7.19 it is possible to get propagation over 900km for a range of average dispersions, however none of these systems still have a Q-value of more than 6 after propagating over the dispersion map again. Unlike the previous systems the reason for the degradation in the Q-value is due to interactions and pulse stability rather than problems relating to the movement of the position where the unchirped pulses occur. The greatest Q-value at 900km is attained for pulses with a peak power of 0.03W and a width of 4.5ps in a map with an average dispersion of 0.16ps/(nm km). This means that the map used here had a strength of S=188 and for this average dispersion an equivalent average soliton would have an initial peak power of 0.057W. The reason for the sudden drop in the maximum propagation distance when the length of standard fibre is increased to 100km is that the limiting factor on the distance is no longer the position of the unchirped pulses. Figure 7.10 shows that the simulation ends long before the unchirped pulses reach the start of the standard fibre. In this case pulse interactions resulting in amplitude jitter and pulse shape distortions are the limiting factor.

7.2.2 Conclusions

Simulations were carried out to investigate the propagation of data over standard fibre using dispersion management at a single channel data rate of 40Gbit/s. It was found that the greatest propagation distances of more than 2000km were possible using quasi-linear pulses.

Three dispersion maps were used, they contained; 27km, 50km or 100km of standard fibre. The maps also contained 6km compensating fibre which was split round the amplifier to give a "symmetric" dispersion map. This map greatly reduced the pulse interactions compared to a map with all the DCF preceding the amplifier. Both the map with 27km of

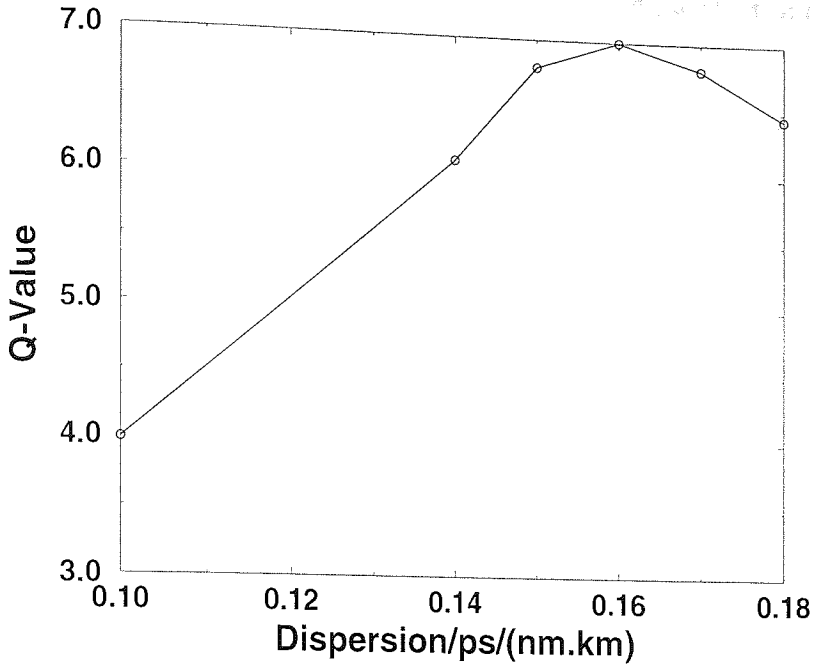

Figure 7.19: Q-value against average dispersion after 900km in the system with 100km of standard fibre. These simulations were all run with peak powers of 0.03W and 4.5ps Gaussian pulses.

standard fibre and the one with 50km were able to transmit data for more than 1500km with the longest distances of over 2000km possible with a map containing 50km of standard fibre. The map with 100km of standard fibre was able to propagate pulses for more than 800km but was then limited by interactions.

The main difficulty found in propagating at a single channel data rate of 40Gbit/s over standard fibre were due to the very strong dispersion map that had to be used. The short pulsewidth and high dispersion of the standard fibre meant that the length of the standard fibre could be more than 100 times the dispersion length of the pulses. One direct result of this was that the pulses broadened to such an extent that they overlapped and interfered with each other and so it was only possible to get a clear output at the point in the standard fibre where the pulses were unchirped. It was found that there was an added complication to taking the output at the point where the pulse were unchirped in that this point moved through the standard fibre. This was because at the low normal dispersions required to make this point stationary the system length was limited by interactions to less than 1000km. The effect of varying the output position to detect the pulses at their unchirped point could also be attained by using post-transmission dispersion compensation to unchirp the pulses. The higher anomalous dispersions required to give longer propagation distances meant that there was an excess of anomalous dispersion

which resulted in the unchirped point moving. The limit on the total propagation distance in these systems was that after the unchirped point reached the start of the standard fibre, the pulses were no longer recovered.

The relatively high average dispersion used also leads to these pulse having reduced power when compared to average soliton. This is in contrast to what is expected from dispersion managed solitons where enhanced powers are normally found. This leads to these pulse being considered to be quasi-linear rather than true dispersion managed solitons. Unlike dispersion managed solitons, no long term stable pulses were found for the strong dispersion maps used here. By better use of filtering or some other form of control it should be possible to improve the performance of this system.

Chapter 8

Conclusions

This thesis presented the results of numerical simulations relating to the use of dispersion managed solitons for high bit rate, single channel optical communications. After introducing the theory behind the propagation of optical pulse in single mode fibre (chapter 2) and the background to dispersion managed soliton propagation (in chapter 3) the results presented were in two main areas. Firstly the use a periodic saturable absorption to control dispersion managed solitons was investigated in chapters 3 and 4. The second area, considered in chapters 6 and 7 was the upgrade of the installed standard fibre network to operate at higher data rates. Most of the work in this thesis relates to laboratory experiments and where possible comparisons between the numerical results and the experimental results have been drawn.

In chapter 4 a saturable absorber was inserted periodically into a dispersion managed transmission line. Single pulses with the same input pulse width and a variety of pulse energies were able to propagate over long distances. As the energy of these pulses increased the saturable absorber was able to suppress the dispersive radiation more efficiently. The saturable absorber was also found to have a filtering effect on the pulses due to the pulses being chirped at the point in the dispersion map where the saturable absorber was placed. High peak powers were required to restore the spectrum after the saturable absorber and thus these pulses had significantly higher powers than pulses that propagate in the dispersion map alone. All these simulations were run without loss, higher order dispersion or noise and only single pulses were used in order to understand the formation of the high energy, stable pulses. This result identified a new regime of stable, high power pulses that only exists when a combination of dispersion management and saturable absorption is used.

A more realistic system was used in chapter 5. This system still used dispersion man-

agement with a periodic saturable absorber, however fibre loss and third order dispersion were now included and noise was added to the signal at the amplifier. The effects of loss and higher order dispersion were examined for a single pulse before this system was used to transmit a 10Gbit/s data pattern over 208Mm. There was very little accumulation of noise over this distance and timing jitter was not a significant problem. The suppression of the noise was clearly due to the effects of the saturable absorber. The Gordon-Haus jitter was kept to a minimum for several reason. Low average dispersion was possible due to the enhanced power of these pulses and strong filtering was used both from a filter and the saturable absorber. Strong filtering was possible because the saturable absorber suppressed the build up of linear dispersive waves at the peak of the filter passband. This demonstrated that saturable absorbers can be highly beneficial in the propagation of dispersion managed solitons at high data rates.

The final two chapters of results examined the upgrade of the installed standard fibre network to higher data rates. Standard fibre has high dispersion in the low loss region where Erbium doped fibre amplifiers operate, dispersion management can be used to lower the average dispersion allowing greater data rates to be used. In chapter 6 a simple two step dispersion map was used to propagate pulses at 10Gbit/s. The suppression of oscillations in pulse width when the launch position and the position of the amplifier were varied was examined. Although the the oscillations could be greatly reduced the final Q-values were not significantly affected.

Chapter 7 examined the use of dispersion management to further increase the data rate to 40Gbit/s. A novel dispersion map where the compensating fibre was placed both before and after the amplifier was found to give the best results. In contrast to the previous chapters, here the pulses which gave the greatest propagation distance had reduced power compared to an average soliton. As a results of this dispersive effects dominated the system although nonlinearity was still found to have a significant effect. Due to the large amount of dispersive broadening it was found that using the correct output position was critical, furthermore this position was found to move through the dispersion map in the systems that gave the greatest propagation distance. A maximum propagation distance of more than 2000km was found in this investigation.

The main new results presented in this thesis were:

- A new regime of high energy, stable soliton propagation was identified. This regime is only possible when dispersion management is used in conjunction with periodic saturable absorption.

- The individual effects of the dispersion map and the saturable absorber were identified
- The system with dispersion management and saturable absorber was used to propagate a 10Gbit/s data pattern over more than 200Mm
- A 10Gbit/s standard fibre experiment was successfully modelled and the results demonstrated the oscillations in Q-values observed experimentally
- Numerical simulations were used to demonstrate that it is possible to propagate data at 40Gbit/s over more than 2000km of standard fibre. This is the greatest distanced attained in numerical simulations to date.

8.1 Future work

There are many aspects of dispersion managed solitons that have still to be investigated. It has been shown that the position of the amplifier in the dispersion map can have a large effect on the total propagation distance. Further investigation into the reasons for this might allow greater propagation distances to be attained. The position of the filter could also have an effect on the propagation distance especially as the bandwidth of a dispersion managed soliton varies during propagation. At present the amplifier and filter are generally placed at the same point in the dispersion map, however this may not necessarily be best.

It would also be interesting to look at using dispersion maps made from more than two types of fibre. For example in the case of the symmetric map used in chapter 7 it might be advantageous to use compensating fibre with lower dispersion before the amplifier with higher dispersion fibre after the amplifier. In this way the nonlinear effects in the compensating fibre before the amplifier could be made to be of a similar size to the effect of nonlinearity in the section of fibre following the amplifier. This is because a longer section of fibre would have to be used and the rate of pulse breathing would be reduced. In this way the increase in the pulse's bandwidth that was observed could be reduced or even eliminated.

Further work into the use of saturable absorbers would also be interesting. Systems such as the one described on chapter 7 where stable pulse propagation was not possible could benefit from the stabilising effect of the saturable absorber. The position of the saturable absorber would be crucial due to the large amount of pulse breathing that occurs

in this dispersion map. If saturable absorbers are to prove useful it will be in stabilising propagation in situations like this rather than in extending propagation distances to several hundred Mm.

Short period dispersion maps where a single amplifier span is made up of several sections of fibre. These maps are likely to be used in systems with high single channel data rates where the short pulses mean that the dispersion map become very strong. There are also other fibre types such as True wave and LEAF fibre which can be used for dispersion managed systems.

8.2 The future of dispersion managed solitons

The use of dispersion management has increased the possibility of solitons being used in commercial communication networks. There have been several successful field trials which have demonstrated that dispersion managed solitons can operate successfully on installed systems that were not designed for their use [191, 192, 193, 194, 216]. Dispersion managed solitons are compatible with TDM, WDM and all optical processing which are all likely to be used in the networks of the future.

As higher data rates are required the strengths of the dispersion maps used are likely to increase. This will probably lead to the necessary use of further control to get stable pulse propagation. Saturable absorbers can be used in this respect and have the advantage over other control methods such as phase and amplitude modulation in that they are entirely passive. Although saturable absorbers are not immediately compatible with wavelength division multiplexing they can be used to enhance the performance of WDM systems [197].Dispersion managed solitons are currently the most successful method of transmitting data over standard fibre at both 10 and 40Gbit/s if the data rates are to be increased further to 160Gbit/s or through WDM to $N \times 40Gbit/s$ it seems likely that dispersion managed solitons will make this possible. As PMD is becoming of increasing concern it is possible that saturable absorbers could be used to increase the peak powers of the pulses used in dispersion managed standard fibres. This would lead to greater cross phase modulation between the polarisations of the pulses and therefore further resistance to PMD

Although not discussed in this thesis, dispersion management has also been found to offer benefits when used in WDM systems. The use of a dispersion map in a WDM systems can suppress the collision induced timing jitter between the wavelength channels.

Experiments that used WDM to propagate several hundred Gbit/s over several thousand km have been carried out [9, 217, 218] and more than a 1Tbit/s has been propagated over more modest distances [219]. Future optical networks will have to operate at data rates of this order or higher. Single channel data rates of 160Gbit/s should be possible using dispersion shifted fibre with dispersion management although the effects of Raman scattering will have to be considered. Higher data rates of more than 200Gbit/s may be possible with short period dispersion maps. The effects of nonlinearity must be considered when operating at these data rates and this can be done by using dispersion managed solitons.

Bibliography

[1] J. Wilson and J.F.B. Hawkes. *Lasers: Principles and applications*, chapter 7, page 239. Prentice Hall, 1987.

[2] G. P. Agrawal. *Nonlinear Fibre Optics*, chapter 1, page 3. Academic Press, San Diego, 1995.

[3] F. Matera and M. Settembre. Comparison of the performance of optically amplified transmission systems. *IEEE J. Lightwave Technol.*, 14(1):1–12, 1996.

[4] M. Nakazawa, E. Yamada, H. Kubota, Y. Yamamota, and A. Sahara. Numerical and experimental comparison of soliton, rz pulse and nrz pulses under two-step dispersion allocation. *Electron. Lett.*, 33(17):1480–1482, 1997.

[5] G. Aubin, T. Montalant, J. Moulu, F. Pirio, J.B. Thomine, and F. Devaux. 40Gbit/s OTDM soliton transmission over transoceanic distances. *Electron. Lett.*, 32(24):2188–2189, 1996.

[6] L.F. Mollenauer, P.V. Mamyshev, and M.J. Neubelt. Demonstration of soliton WDM transmission at 6 and 7x10Gbit/s, error free over transoceanic distances. *Electron. Lett.*, 32:471–473, 1996.

[7] D. Le. Guen, A. O'Hare, S. Del. Burgo, D. Grot, F. Favre, and T. Georges. Narrow-band 640Gbit/s soliton DWDM transmission over 1200km of standard fibre with 100km -12dB amplifier spans. *Electron. Lett.*, 34(24):2345–2346, 1998.

[8] H. Taga, M. Suzuki, N. Edagawa, N. Takeda, K. Imai, S. Yamamoto, and S. Akiba. 20WDM, 10.66Gbit/s transmission experiment over 9000km using periodic dispersion slope compensation. *Electron. Lett.*, 34(5):476–478, 1998.

[9] M. Suzuki, I. Morita, K. Tanaka, N. Edagawa, S. Yamamoto, and S. Akiba. 160Gbit/s (8x20 Git/s) soliton WDM transmission experiments using dispersion flattened fibre and periodic dispersion compensation. *Electron. Lett.*, 34(5):475–476, 1998.

[10] G. P. Agrawal. *Nonlinear Fibre Optics*, chapter 2, pages 28–46. Academic Press, San Diego, 1995.

[11] G. P. Agrawal. *Nonlinear Fibre Optics*, chapter Appendix B, pages 582–583. Academic Press, San Diego, 1995.

[12] C.R. Menyuk. Stability of solitons in birefringent optical fibers. i: Equal propagation amplitudes. *Opt. Lett.*, 12(8):614–616, 1987.

[13] G. P. Agrawal. *Nonlinear Fibre Optics*, chapter 2, page 37. Academic Press, San Diego, 1995.

[14] G. P. Agrawal. *Nonlinear Fibre Optics*, chapter 2, page 38. Academic Press, San Diego, 1995.

[15] G. P. Agrawal. *Nonlinear Fibre Optics*, chapter 2, page 41. Academic Press, San Diego, 1995.

[16] G. P. Agrawal. *Nonlinear Fibre Optics*, chapter 2, page 43. Academic Press, San Diego, 1995.

[17] G. P. Agrawal. *Nonlinear Fibre Optics*, chapter 3, page 61. Academic Press, San Diego, 1995.

[18] G. P. Agrawal. *Nonlinear Fibre Optics*, chapter 3, pages 63–70. Academic Press, San Diego, 1995.

[19] G. P. Agrawal. *Nonlinear Fibre Optics*, chapter 3, page 63. Academic Press, San Diego, 1995.

[20] G. P. Agrawal. *Nonlinear Fibre Optics*, chapter 3, pages 76–77. Academic Press, San Diego, 1995.

[21] G. P. Agrawal. *Nonlinear Fibre Optics*, chapter 1, page 10. Academic Press, San Diego, 1995.

[22] G. P. Agrawal. *Nonlinear Fibre Optics*, chapter 4, pages 89–98. Academic Press, San Diego, 1995.

[23] G. P. Agrawal. *Nonlinear Fibre Optics*, chapter 1, pages 5–7. Academic Press, San Diego, 1995.

[24] A. Hasegawa and Y. Kodama. *Solitons in Optical Communications*, chapter 1, pages 8–9. OUP, 1995.

[25] R.J. Mears, L. Meekie, I.M. Jauncey, and D.N. Payne. Low-noise erbium-doped fibre amplifier operating at 1.54μm. *Electron. Lett.*, 23(19):1026–1028, 1987.

[26] E. Desurvire, J.R. Simpson, and P.C. Becker. High-gain erbium-doped travelling-wave fiber amplifier. *Opt. Lett.*, 12(11):888–890, 1987.

[27] C.D. Poole. Statistical treatment of polarization dispersion in single-mode fiber. *Opt. Lett.*, 13:687–689, 1988.

[28] G. P. Agrawal. *Nonlinear Fibre Optics*, chapter 1, pages 13–15. Academic Press, San Diego, 1995.

[29] P.K.A. Wai and C.R. Menyuk. Polarization mode dispersion, decorrelation, and diffusion in optical fibers with randomly varying birefringence. *IEEE J. Lightwave Technol.*, 14:148–157, 1996.

[30] G. P. Agrawal. *Nonlinear Fibre Optics*, chapter 7, page 247. Academic Press, San Diego, 1995.

[31] G. P. Agrawal. *Nonlinear Fibre Optics*, chapter 1, pages 13–15. Academic Press, San Diego, 1995.

[32] H.G. Winful. Self-induced polarization changes in birefringent optical fibers. *Appl. Phys. Lett.*, 47(3):213–215, 1985.

[33] M.N. Islam, C.E. Soccolich, J.P. Gordon, and U.C. Paek. Soliton intensity-dependent polarization rotation. *Opt. Lett.*, 15(1):21–23, 1990.

[34] R.H. Stolen, J. Botineau, and A. Ashkin. Intensity discrimination of optical pulses with birefringent fibers. *Opt. Lett.*, 7(10):512–514, 1982.

[35] B. Nikolaus, D. Grischkowsky, and A.C. Balant. Optical pulse reshaping based on the nonlinear birefringence of single-mode optical fibers. *Opt. Lett.*, 8(3):189–191, 1983.

[36] M. Horowitz and Y. Silberberg. Nonlinear filtering by use of intensity-dependent polarization rotation in birefringent fibers. *Opt. Lett.*, 22(23):1760–1762, 1997.

[37] V.E. Zakharov and A.B. Shabat. Exact theory of two dimensional self focussing and one-dimensional self modulation of waves in nonlinear media. *Soviet Phys. JETP*, 34:62–69. 1972.

[38] A. Hasegawa and F. Tappert. Transmission of stationary nonlinear optical pulses in dispersive dielectric fibres 1. anomalous dispersion. *Appl. Phys. Lett.*, 23(3):142–144, 1973.

[39] L.F. Mollenauer, R.H. Stolen, and J.P. Gordon. Experimental observation of picosecond pulse narrowing and solitons in optical fibres. *Physical Review Letters*, 45:1095–1098, 1980.

[40] G. P. Agrawal. *Nonlinear Fibre Optics*, chapter 5, pages 134–141. Academic Press, San Diego, 1995.

[41] H.A. Haus. Optical fibre solitons, their properties and uses. *Proc. IEEE*, 81(7):969–983, 1993.

[42] G. P. Agrawal. *Nonlinear Fibre Optics*, chapter 5, pages 142–144. Academic Press, San Diego, 1995.

[43] C.S. Gardener, J.M. Green, M.D. Kruskal, and R.M. Miura. Method for solving the Korteweg-de Vries equation. *Phys. Rev. Lett*, 19(19):1095, 1967.

[44] G. P. Agrawal. *Nonlinear Fibre Optics*, chapter 5, pages 145–148. Academic Press, San Diego, 1995.

[45] L.F. Mollenauer, S.G. Evangelides, and H.H. Haus. Long-distance soliton propagation using lumped amplifiers and dispersion shifted fiber. *IEEE J. Lightwave Technol.*, 9(2):194–197, 1991.

[46] L.F. Mollenauer S.G., Evangelides, and J.P. Gordon. Wavelength division multiplexing with solitons in ultra-long distance transmission using lumped amplifiers. *IEEE J. Lightwave Technol.*, 9(3):362–367, 1991.

[47] G. P. Agrawal. *Nonlinear Fibre Optics*, chapter 2, pages 50–55. Academic Press, San Diego, 1995.

[48] G.M. Blair. A review of the descrete Fourier transform Part 1: Manipulating the powers of two. *Electron. & Commun. Eng. J.*, 7(7):169–177, 1995.

[49] P. Duhamel. Implementation of "split-radix" fft algorithms for complex, real, and real-symmetric data. *IEEE Trans. Acoust. Speech. Signal Processing*, 34(2):285–295, 1986.

[50] H.V. Sorensen, M.T. Heideman, and C.S. Burrus. On computing the split-radix fft. *IEEE. Trans. Acoust. Speech, Signal Processing*, 34(1):152–156, 1986.

[51] A.N. Skodras and A.G. Constantinides. Efficient computation of the split-radix fft. *IEE Prodeedings-F*, 139:56–60, 1992.

[52] P. Duhamel, B. Piron, and M. Etcheto. On computing the inverse dft. *IEEE Trans. Acoust. Speech. Signal Processing*, 36(2):285–286, 1988.

[53] K.J. Blow and D. Wood. Theoretical description of transient stimulated Raman scattering in optical fibres. *IEEE J. Quantum Electron.*, 25:2665–2673, 1989.

[54] L.F. Mollenauer, J.P. Gordon, and M.N. Islam. Soliton propagation in long fibers with periodically compensated loss. *IEEE J. Quantum Electron.*, 22:157–173, 1986.

[55] D.J. Richardson, R.P. Chamberlain, L. Dong, and D.N. Payne. High quality soliton loss-compensation in 38km dispersion-decreasing fibre. *Electron. Lett.*, 31:1681–1682, 1995.

[56] D.J. Richardson, L. Dong, R.P. Chamberlain, A.D. Ellis, T. Widdowson, and W.A. Pender. Periodically amplified system based on loss compensating dispersion decreasing fibre. *Electron. Lett.*, 32(4):373–374, 1996.

[57] R.J. Essiambre and G.P. Agrawal. Ultrahigh-bit-rate soliton communication systems using dispersion-decreasing fibers and parametric amplifiers. *Opt. Lett.*, 21:116–118, 1996.

[58] C. Lester, K. Bertilsson, K. Rottiwitt, P.A. Andrekson, M.A. Newhouse, and A.J. Antos. Soliton transmission over more ths 90km using distributed erbium-doped fibres. *Electron. Lett.*, 31:219–220, 1995.

[59] K.J. Blow and N.J. Doran. Average soliton dynamics and the operation of soliton systems with lumped amplifiers. *IEEE Photon. Technol. Lett.*, 3(4):369–371, 1991.

[60] A. Hasegawa and Y. Kodama. Guiding-centre soliton in optical fibres. *Opt. Lett.*, 15(24):1443–1445, 1990.

[61] A. Hasegawa and Y. Kodama. Guiding-centre soliton. *Phys. Rev. Lett.*, 66(2):161–164, 1991.

[62] S.M.J. Kelly. Characteristic sideband instability of periodically amplified average soliton. *Electron. Lett.*, 28(8):806–807, 1992.

[63] N. Pandit, D.U. Noske, S.M.J. Kelly, and J.R. Taylor. Characteristic instability of fibre loop soliton lasers. *Electron. Lett.*, 28(5):455–457, 1992.

[64] J.P. Gordon. Dispersive perturbations of solitons of the nonlinear schrodinger equation. *J. Opt. Soc. Am. B*, 9(1):91–97, 1992.

[65] N.J. Smith, K.J. Blow, and I. Andonovic. Sideband generation through perturbations to the average soliton model. *IEEE J. Lightwave Technol.*, 10(10):1329–1333, 1992.

[66] B. Charbonnier and T. Georges. Numerical investigations of the path-averaged soliton validity domain without soliton control. *Electron. Lett.*, 32(2):126–128, 1996.

[67] F. Bruyere and O. Audouin. Assessment of system penalties induced by polarization mode dispersion in a 5Gbit/s optically amplified transoceanic link. *IEEE Photon. Technol. Lett.*, 3(1994):443–445, 6.

[68] H. Bulow. Operation of digital optical transmission system with minimal degradation due to polarisation mode dispersion. *Electron. Lett.*, 31:214–215, 1995.

[69] F. Matera and M. Settembre. Compensation of polarization mode dispersion by means of the Kerr effect for nonreturn-to-zero signals. *Opt. Lett.*, 20(28-30), 1995.

[70] L.F. Mollenauer, K. Smith, J.P. Gordon, and C.R. Menyuk. Resistance of solitons to the effects of polarization dispersion in optical fibres. *Opt. Lett.*, 14(21):1219–1221, 1989.

[71] S.G. Evangelides, L.F. Mollenauer, J.P. Gordon, and N.S. Bergano. Polarization multiplexing with solitons. *IEEE J. Lightwave Technol.*, 10(1):28–35, 1992.

[72] A. De Angelis and S. Wabnitz. Interactions of orthogonally polarized solitons in optical fibres. *Opt. Commun.*, 125:186–196, 1996.

[73] M. Nakazawa, K. Suzuki, E. Yoshida, E. Yamada, T. Kitoh, and M. Kawachi. 160Gbit/s soliton data transmission over 200km. *Electron. Lett.*, 31(7):565–566, 1995.

[74] F. Favre, D. Le Guen, M.L. Moulinard, M. Henry, T. Georges, and F. Devaux. 40Gbit/s, 5x100km span straight line soliton transmission experiment without in-line control. *Electron. Lett.*, 32(12):1115–1116, 1996.

[75] F. Favre, D. Le.Guen, and T. Georges. 20Gbit/s soliton transmission over 5200km of non-zero-dispersion shifted fibre with 106km dispersion-compensated span. *Electron. Lett.*, 34(2):201–202, 1998.

[76] A. Yariv. Signal-to-noise considerations in fiber links with periodic or distributed optical amplification. *Opt. Lett.*, 15(19):1064–1066, 1990.

[77] J.P. Gordon and H.A. Haus. Random walk of coherently amplified solitons in optical fiber transmission. *Opt. Lett.*, 11(10):665–667, 1986.

[78] D. Marcuse. An alternative derivation of the gordon-haus effect. *IEEE J. Lightwave Technol.*, 10(2):273–278, 1992.

[79] K.J. Blow and N.J. Doran. Bandwidth limits of nonlinear (soliton) optical cimmunication systems. *Electron. Lett.*, 19(11):429–430, 1983.

[80] J.P. Gordon. Interaction forces among solitons in optical fibres. *Opt. Lett.*, 8(11):596–598, 1983.

[81] Y. Kodama and K. Nozaki. Soliton interaction in optical fibre. *Opt. Lett.*, 12(12):1038–1040, 1987.

[82] F.M. Mitschke and L.F. Mollenauer. Experimental observation of interaction forces between solitons in optical fibres. *Opt. Lett.*, 12(5):355–357, 1987.

[83] C. Desum and P.L. Chu. Soliton interaction in the presence of loss and periodic amplification in optical fibers. *Opt. Lett.*, 12(5):349–251, 1987.

[84] T. Georges and F. Favre. Modulation,filtering and initial phase control of interacting solitons. *J. Opt. Soc. Am. B*, 10(10):1880–1889, 1993.

[85] K. Bertilsson and P.A. Andrekson. Numerical study of moderate distance high bit-rate alternating-amplitude soliton systems. *IEEE J. Lightwave Technol.*, 14(3):237–241, 1996.

[86] M. Nakazawa, E. Yoshida, E. Yamada, K. Suzuki, T. Kitoh, and M. Kawachi. 80Gbit/s soliton data transmission over 500km with unequal amplitude solitons for timing clock extraction. *Electron. Lett.*, 30(21):1777–1778, 1994.

[87] K. Smith and L.F. Mollenauer. Experimental observation of soliton interaction over long fiber paths: discovery of a long-range interaction. *Opt. Lett.*, 14(22):1284–1286, 1989.

[88] J.P. Gordon. Theory of soliton self-frequency shift. *Opt. Lett.*, 11(10):662–664, 1986.

[89] F.M. Mitschke and L.F. Mollenauer. Discovery of the soliton self-frequency shift. *Opt. Lett.*, 11(10):659–661, 1986.

[90] K. Qiu. Soliton position jitter caused by periodic amplification and self-frequency shift. *Electron. Lett.*, 30(5):439–440, 1994.

[91] G. P. Agrawal. *Nonlinear Fibre Optics*, chapter 9, pages 370–375. Academic Press, San Diego, 1995.

[92] G. P. Agrawal. *Nonlinear Fibre Optics*, chapter 10, pages 404–407. Academic Press, San Diego, 1995.

[93] P.V. Mamyshev and L.F. Mollenauer. Pseudo-phase-matched four-wave mixing in soliton wavelength-division multiplexing transmission. *Opt. Lett.*, 21:396–398, 1996.

[94] A. Mecozzi, J.D. Moores, H.A. Haus, and Y. Lai. Soliton transmission control. *Opt. Lett.*, 16(23):1841–1843, 1991.

[95] Y. kodama and A. Hasegawa. Generation of asymptotically stable optical solitons and suppression of the Gordon-Haus effect. *Opt. Lett.*, 17(1):31–33, 1992.

[96] D. Marcuse. Simulations to demonstrate reduction of Gordon-Haus effect. *Opt. Lett.*, 17(1):34–36, 1992.

[97] E. Kolltveit, B. Biotteau, I Riant, F. Pitel, O. Audouin, P. Brindel, E. Brun, P. Sansonetti, and J.-P. Hamaide. Soliton frequency-guiding by UV-written fiber Fabry-Perot filter in a 2x5 Gbit/s wavelength-division multiplexing transmission over transoceanic distances. *IEEE Photon. Technol. Lett.*, 7:1498–1500, 1995.

[98] Y. Kodama and S. Wabnitz. Reduction of soliton interaction forces by bandwidth limited amplification. *Electron. Lett.*, 27(21):1931–1933, 1991.

[99] T. Georges. Study of the non-Gaussian timing jitter statistics induced by soliton interaction and filtering. *Opt. Commun.*, 123:617–623, 1996.

[100] L.F. Mollenauer, J.P. Gordon, and S.G. Evangelides. The sliding-frequency guiding filter: An improved form of soliton jitter control. *Opt. Lett.*, 17(22):1575–1577, 1992.

[101] E.A. Golovchenko, A.N. Pilipetskii, C.R. Menyuk, J.P. Gordon, and L.F. Mollenauer. Soliton propagation with up- and down-sliding-frequency guiding filters. *Opt. Lett.*, 20(6):539–541, 1995.

[102] P.V. Mamyshev and L.F. Mollenauer. Stability of soliton propagation with sliding-frequency guiding filters. *Opt. Lett.*, 19(24):2083–2085, 1994.

[103] F. Favre and V. Chandrakumar. Comparison between analytical and numerical simulations for sliding filter damped soliton jitter. *Opt. Commun.*, 126:34–37, 1996.

[104] A. Mecozzi, M. Midrio, and M. Romagnoli. Timing jitter in soliton transmission with sliding filters. *Opt. Lett.*, 21:402–404, 1996.

[105] Y. Kodama and S. Wabnitz. Analysis of soliton stablility and interactions with sliding filters. *Opt. Lett.*, 19(3):162–164, 1994.

[106] S. Kawai, K. Iwatsuki, and S. Nishi. Demonstration of error free optical soliton transmission over 30000km at 10Gbit/s with signal frequency sliding technique. *Electron. Lett.*, 31(17):1463–1464, 1995.

[107] S. Wabnitz. Role of the filter spectral profile in the control of soliton transmission. *Opt. Commun.*, 130:89–96, 1996.

[108] S. Wabnitz and E. Westin. Optical fibre soliton bound states and interaction suppression with high-order filtering. *Opt. Lett.*, 21:1235–1237, 1996.

[109] J.-C. Dung, S. Chi, and S. Wen. Reduction of soliton interactions by sliding-frequency second-order Butterworth filters. *Opt. Lett.*, 21:339–341, 1996.

[110] E. Peral, J. Capmany, and J. Marti. Soliton transmission control by super-Gaussian filters. *Opt. Lett.*, 21(23):1894–1896, 1996.

[111] G. Aubin, T. Montalant, J. Moulu, B. Nortier, F. Pirio, and J.B. Thomine. Soliton transmission at 10Gbit/s with a 70km amplifier span over one million kilometres. *Electron. Lett.*, 30(14):1163–1165, 1994.

[112] G. Aubin, T. Montalant, J. Moulu, B. Nortier, F. Pirio, and J.-B. Thomine. Record amplifier span of 105km in a soliton transmission experiment at 10Gbit/s over 1Mm. *Electron. Lett.*, 31(217-219), 1995.

[113] H. Kubota and M. Nakazawa. Soliton transmission control in time and frequency domains. *IEEE J. Quantum Electron.*, 29(7):2189–2197, 1993.

[114] O. Leclerc, P. Brindel, S. Bigo, and E. Brun-Maunand E. Desurvire. 2x20Gbit/s 3500km regenerated WDM soliton transmission with all-optical Kerr fibre modulation. *Electron. Lett.*, 34(2):199–201, 1998.

[115] T. Widdowson, D.J. Malyon, A.D. Ellis, K. Smith, and K.J. Blow. Soliton shepherding: All-optical active soliton control over global distances. *Electron. Lett.*, 30:990–991, 1994.

[116] D. Atkinson, W.H. Loh, V.V. Afanasjev, A.B. Grudinin, A.J. Seeds, and D.N. Payne. Increased amplifier spacing in a soliton system with quantum-well saturable absorbers and spectral filtering. *Opt. Lett.*, 19(19):1514–1516, 1994.

[117] M. Matsumoto, H. Ikeda, and A. Hasegawa. Suppression of noise accumulation in bandwidth-limited soliton transmission by means of nonlinear loop mirrors. *Opt. Lett.*, 19:183–185, 1994.

[118] F.X. Kartner and U. Keller. Stabilization of solitonlike pulses with a slow saturable absorber. *Opt. Lett.*, 20(1):16–18, 1995.

[119] V.V. Afanasjev. Soliton polarization rotation in fiber lasers. *Opt. Lett.*, 20(3):270–272, 1995.

[120] M.E. Fermann, F. Haberl, M. Hofer, and H. Hochreiter. Nonlinear amplifying loop mirror. *Opt. Lett.*, 15:752–754, 1990.

[121] B.E Olsson and P.A. Andrekson. Noise filtering with the nonlinear optical loop mirror. *IEEE J. Lightwave Technol.*, 13(2):213–215, 1995.

[122] J.S. Weiner, D.B. Pearson, D.A.B. Miller, D.S. Chemla, D. Sivco, and A.Y. Cho. Nonlinear spectroscopy of InGaAs/InAlAs multiple quantum well structures. *Appl. Phys. Lett.*, 49(9):531–533, 1986.

[123] A. Hirano, H. Kobayashi, H. Tsuda, T. Takahashi, M. Asobe, K. Sato, and K. Haginoto. 10Gbit/s RZ all-optical discrimination using refined saturable absorber optical gate. *Electron. Lett.*, 34(2):198–199, 1998.

[124] H. Tsuda, A. Hirano, R. Takahashi, K. Sato, and K Hagimoto. 2.4Gbit/s all-optical pulse discrimination experiment using a high-speed saturable absorber optical gate. *Electron. Lett.*, 32(4):365–366, 1996.

[125] I. Gabitov, D.D. Holm, B.P. Luce, and A. Matheus. Recovery of solitons with nonlinear amplifying loop mirrors. *Opt. Lett.*, 20(24):2490–2492, 1995.

[126] M. Matsumoto and A. Hasegawa. Numerical study of the reduction of instability in bandwidth-limited amplified soliton transmission. *Opt. Lett.*, 18:897–899, 1993.

[127] M. Matsumoto, H. Ikeda, T. Uda, and A. Hasegawa. Stable soliton transmission in the system with nonlinear gain. *IEEE J. Lightwave Technol.*, 13(4):658–665, 1995.

[128] N.J. Smith and N.J. Doran. Picosecond soliton propagation using nonlinear optical loop mirrors as intensity filters. *Opt. Lett.*, 30:1084–1085, 1994.

[129] Y. Kodama, M. Romagnoli, and S. Wabnitz. Soliton stability and interactions in fibre lasers. *Opt. Lett.*, 28:1981–1983, 1992.

[130] I.M. Uzunov, R. Muschall, M. Golles, F. Lederer, and S. Wabnitz. Effect of nonlinear gain and filtering on soliton interaction. *Opt. Commun.*, 118:577–580, 1995.

[131] S. Watanabe, T. Naito, and T. Chikama. Compensation of chromatic dispersion in a single-mode fiber by optical phase conjugation. *IEEE Photon. Technol. Lett.*, 5(1):92–95, 1993.

[132] S Watanbe, T. Chikama, G. Ishikawa, T. Terahara, and H. Kuwahara. Compensation of pulse shape distortion dueto chromatic dispersion and Kerr effect by optical phase conjugation. *IEEE Photon. Technol. Lett.*, 5(10):1241–1243, 1993.

[133] A.D. Ellis, M.C. Tathman, D.A.O. Davies, D. Nessett, D.G. Moore, and G. Sherlock. 40Gbit/s transmission over 202km of standard fibre using midspan spectral inversion. *Electron. Lett.*, 31(4):299–301, 1995.

[134] R.I. Laming, D.J. Richardson, D. Tavernor, and D.N. Payne. Transmission of 6ps linear pulses over 50km of standard fiber using midpoint spectral inversion to eliminate dispersion. *IEEE J. Quantum Electron.*, 3(9):2114–2119, 1994.

[135] C.G. Goedde, W.L. Kath, and P. Kumar. Periodic amplification and conjugation of optical solitons. *Opt. Lett.*, 20(12):1365–1367, 1995.

[136] S. Wen and S. Chi. Undoing of soliton interaction by optical phase conjugation. *Electron. Lett.*, 30(8):663–664, 1994.

[137] W. Forysiak and N.J. Doran. Conjugate solitons in amplified optical fibre transmission systems. *Electron. Lett.*, 30(2):154–155, 1994.

[138] S. Chi and S. Wen. Recovery of the soliton self-frequency shift by optical phase conjugation. *Opt. Lett.*, 19(21):1705–1707, 1994.

[139] R.A. Fisher, B.R. Suydam, and D. Yevick. Optical phase conjugation for time-domain undoing of dispersive self-phase-modulation effects. *Opt. Lett.*, 8(12):611–613, 1983.

[140] C Kurtzke. Supresion of fiber nonlinearities by appropriate dispersion management. *IEEE Photon. Technol. Lett.*, 5(10):1250–1253, 1993.

[141] N.J. Smith, F.M. Knox, N.J. Doran, K.J. Blow, and I. Bennion. Enhanced power solitons in optical fibres with periodic dispersion management. *Electron. Lett.*, 32(1):54–55, 1996.

[142] M. Nakazawa. H. Kubota, A. Sahara, and K. Tamura. Marked increase in the power margin through the use of a dispersion allocated soliton. *IEEE Photon. Technol. Lett.*, 8(8):1088–1090, 1996.

[143] J.H.B. Nijhof, N.J.Doran, W. Forysiak, and D. Berntson. Energy enhancement of dispersion-managed solitons WDM. *Electron. Lett.*, 34(5):481–482, 1998.

[144] T. Georges. Extended path-average soliton regime in highly dispersive fibers. *Opt. Lett.*, 22(10):679–681, 1997.

[145] A. Berntson, D. Anderson, N.J. Doran, W. Forysiak, and J.H.B. Nijhof. Power dependence and accessible bandwidth for dispersion-managed solitons in asymetric dispersion maps. *Electron. Lett.*, 34(21):2054–2056, 1998.

[146] M. Suzuki, I. Morita, N Edagawa, S. Yamamoto, H. Taga, and S. Akiba. Reduction of Gordon-Haus timing jitter by periodic dispersion compensation in soliton transmission. *Electron. Lett.*, 31(23):2027–2029, 1995.

[147] G.M. Carter, J.M. Jacob, C.R. Menyuk, E.A. Golovchenko, and A.N. Pilipetskii. Timing-jitter reduction for a dispersion-managed soliton syste,: experimental evidence. *Opt. Lett.*, 22(8):513–515, 1997.

[148] S. Kumar and F. Lederer. Gordon-haus effect in dispersion-managed soliton systems. *Opt. Lett.*, 22(24):1870–1872, 1997.

[149] J.N. Kutz and P.K.A. Wai. Ideal amplifier spacing for reduction of gordon-haus jitter in dispersion-managed soliton communications. *Electron. Lett.*, 34(6):522–523, 1998.

[150] R.M. Mu, V.S. Grigoryan, C.R. Menyuk, E.A. Golovchenko, and A.N. Pilipetskii. Timing-jitter reduction in a dispersion-managed soliton system. *Opt. Lett.*, 23(12):930–932, 1998.

[151] J.H.B. Nijhof, N.J. Doran, W. Forysiak, and F.M. Knox. Stable soliton-like propagation in dispersion managed systems with net anomalous, zero and normal dispersion. *Electron. Lett.*, 33(20):1726–1727, 1997.

[152] J.H.B. Nijhof, W. Forysiak, and N.J. Doran. Dispersion-managed solitons in the normal dispersion regime: a physical interpretation. *Opt. Lett.*, 23(21):1674–1676, 1998.

[153] J.N. Kutz and S. G. Evangelides. Dispersion managed breathers with average normal dispersion. *Opt. Lett.*, 23(9):635–637, 1998.

[154] S.K. Turitsyn and E.G. Shapiro. Dispersion-managed solitons in optical amplifier tranmission systems with zero average dispersion. *Opt. Lett.*, 23(9):682–684, 1998.

[155] S. Alleston, I. Penketh, P. Harper, A. Niculae, I. Bennion, and N.J. Doran. 16000km 10Gbit/s soliton transmission over standard fibre by reduction of interactions through optimum amplifier positioning. *OFC 1999*, WC4:41–43, 1999.

[156] S.B. Alleston, P. Harper, I.S. Penketh, I. Bennion, and N.J. Doran. 40Gbit/s single channel dispersion managed pulse propagation in standard fibre over 509km. *Electron. Lett.*, 35(1):57–59, 1999.

[157] J.M. Jacob, E.A. Golovchenko, A.N. Pilipetskii, G.M. Carter, and C.R. Menyuk. Experimental demonstration of soliton transmission over 28Mm using mostly normal dispersion fiber. *IEEE Photon. Technol. Lett.*, 9(1):130–132, 1997.

[158] W. Forysiak, F.M. Knox, and N.J. Doran. Stepwise dispersion profiling of periodically amplified soliton systems. *IEEE J. Lightwave Technol.*, 12:1330–1337, 1994.

[159] W. Forysiak, K.J. Blow, and N.J. Doran. Reduction of Gordon-Haus jitter by post-transmission dispersion compensation. *Electron. Lett.*, 29:1225–1226, 1993.

[160] J.P. Gordon and L.F. Mollenauer. Scheme for the chracterization of disperison-managed solitons. *Opt. Lett.*, 24(4):223–225, 1999.

[161] G.M. Carter and J.M. Jacob. Dynamics of solitons in filtered dispersion managed systems. *IEEE Photon. Technol. Lett.*, 10(4):546–548, 1998.

[162] V.S. Grigoryan, T. Yu, A. Golovchenko, C.R. Menyuk, and A. N. Pilipetskii. Dispersion-managed soliton dynamics. *Opt. Lett.*, 22(21):1609–1611, 1997.

[163] I Gabitov and S K Turitsyn. Breathing solitons in optical fiber links. *JETP Letters*, 63(10):861–866, 1996.

[164] S.K. Turitsyn, T Schafer, and V.K. Mezentsev. Self-similar core and oscillatory tails of a path-averaged chirped dispersion-managed optical pulse. *Opt. Lett.*, 23(17):1351–1353, 1998.

[165] A. Berntson, N.J. Doran, W. Forysiak, and J.H.B. Nijhof. Power dependence of dipsersion-managed solitons for anomalous, zero and normal path-average dispersion. *Opt. Lett.*, 23(12):900–902, 1998.

[166] F. Favre, D. Le. Guen, and T. Georges. Experimental evidence of pseudo-periodical soliton propagation in dispersion-managed link. *Electron. Lett.*, 34(19):1868–1869, 1998.

[167] M.K. Chin and X.Y. Tang. Quasi-stable soliton transmission in dispersion managed fiber links with lumped amplifiers. *IEEE Photon. Technol. Lett.*, 9(4):538–540, 1997.

[168] M. Hitzener, I.M. Uzunov, and F. Lederer. Optimization of soliton transmissions in dispersion-managed fiber links. *Opt. Commun.*, 145(1-6):48–52, 1996.

[169] X. Zhang, M. Karlsson, P. Andrekson, and K. Bertilsson. Impact of polarisation-mode dispersion in dispersion-managed soliton systems. *Electron. Lett.*, 34(11):1122–1124, 1998.

[170] S. Wabnitz, I. Uzunov, and F. Lederer. Soliton transmission with periodic dispersion compensation: Effects of radiation. *IEEE Photon. Technol. Lett.*, 8(8):1091–1093, 1996.

[171] S. Kumar, M. Wald. F. Lederer, and A. Hasegawa. Soliton interaction in strongly dispersion-managed optical fibers. *Opt. Lett.*, 23(13):1019–1021, 1998.

[172] T. Okamawari, Y. Ueda, A. Maruta, Y. Kodama, and A. Hasegawa. Interaction between guiding centre solitons in a periodically dispersion compensated optical transmission line. *Electron. Lett.*, 23(12):1063–1065, 1997.

[173] A.N. Pinto, G.P. Agrawal, and J.F. da Rocha. Effect of soliton interaction on timing jitter in communication systems. *IEEE J. Lightwave Technol.*, 16(4):515–519, 1998.

[174] M. Romagnoli, L. Socci, M. Midrio, P. Franco, and T. Georges. Long-range soliton interactions in dispersion-managed links. *Opt. Lett.*, 23(15):1182–1184, 1998.

[175] T. Yu, E.A. Golovchenko, A.N. Pilipetski, and C.R. Menyuk. Dispersion managed soliton interactions in optical fibers. *Opt. Lett.*, 22(11):793–795, 1997.

[176] A.M. Niculae, W. Forysiak, and N.J.Doran. Optimal amplifier location in strong dispersion-managed soliton systems. *submitted to cleo 1999*, 1999.

[177] S. Wabnitz. Stabilization of sliding-filtered soliton wavelength division multiplexing transmissions by dispersion-compensating fibers. *Opt. Lett.*, 21:638–640, 1996.

[178] K.I. Suzuki, S. Kawai, and K. Iwatsuki. 40Gbit/s adiabatic and phase-stationary soliton transmission with sliding-frequency filter over 4000km reciprocating dispersion-managed fibre. *Electron. Lett.*, 32(23):2173–2174, 1996.

[179] A.M. Niculai, W. Forysiak, A.J. Gloag, J.H.B. Nijhof, and N.J. Doran. Soliton collisions with wavelength-division multiplexed systems with strong dispersion management. *Opt. Lett.*, 23(17):1354–1356, 1998.

[180] Kaup D.J, B.A. Malomed, and J. Yang. Interchannel pulse collision in a wavelength-division-multiplexed system with strong dispersion management. *Opt. Lett.*, 23(20):1600–1602, 1998.

[181] A. Hasegawa, S.Kumar, and Y. Kodama. Reduction in collison-induced time jitters in dispersion-managed soliton transmission systems. *Opt. Lett.*, 21:39–41, 1996.

[182] E. Yamada, H Kubota, T. Yamamoto, A. Sahara, and M. Nakazawa. 10Gbit/s, 10600 km, dispersion-allocated soliton transmission using conventional 1.3μm singlemode fibres. *Electron. Lett.*, 33(7):602–603, 1997.

[183] I.S. Penketh, P.Harper, S.B. Alleston, I. Bennion, and N.J. Doran. 10Gbit/s dispersion managed soliton transmission over 16500km in standard fibre by reduction of soliton interactions. *submitted to optics letters*, 1999.

[184] B. Dany, J.P. Hamaide, and F. Neddam. Numerical study of long-haul 16x10Gbit/s soliton transmission using dispersion management and narrowband-filtering. *Electron. Lett.*, 34(21):2053–2054, 1998.

[185] H. Murai, M. Shikata, and Y. Ozeka. 20Gbit/s soliton transmission using alternating dispersion arangment in standard fibre systems. *Electron. Lett.*, 34(11):1056–1047, 1998.

[186] D. Breuer, H.J. Ehrke, F. Kuppers, R. Ludwig, K. Peterman, H.G. Webber, and K. Weich. Unrepeated 40Gb/s RZ single-channel transmission at 1.55μm using various fiber types. *IEEE Photon. Technol. Lett.*, 10(6):822–824, 1998.

[187] S.B. Alleston, P. Harper, I.S. Penketh, I. Bennion, and N.J. Doran. 1220km propagation of 40Gbit/s single channel RZ data over dispersion managed standard (non-dispersion shifted) fibre. *OFC 1999*, PD3, 1999.

[188] M. Schurch, W. Hodel, and H.P.Weber. Transmission quality improvement of 1550nm standard soliton WDM system by proper dispersion power management. *Electron. Lett.*, 34(4):391–392, 1998.

[189] A. Sahara, H. Kubota, and M. Nakazawa. Optimum fiber dispersion for two-step dispersion-allocated optical soliton, RZ at zero GVD and NRZ systems. *IEEE Photon. Technol. Lett.*, 9(8):1179–1181, 1997.

[190] A.B. Grudinin and I.A. Goncharenko. Increased amplifier spacing in soliton system with partial dispersion compensation. *Electron. Lett.*, 32(17):1602–1604, 1996.

[191] M. Nakazawa, Y. Kimura, K. Suzuki, H. Kubota, T. Komuki, E. Yamada, T. Sugawa, E. Yoshida, T. Yamamoto, T. Imai, A. Sahara, H. Nakazawa, O. Yamauchi, and M. Umezawa. Field demonstration of soliton transmision at 10Gbit/s over 2000km in Tokyo metropoliton optical loop network. *Electron. Lett.*, 31(12):992–994, 1995.

[192] A. Sahara, K. Suzuki, H. Kubota, T. Komukai, E. Yamada, T. Imai, K. Tamura, and M. Nakazawa. Single channel 40Gbit/s soliton transmission field experiment over 1000km in Tokyo metropolitan optical loop network using dispersion compensation. *Electron. Lett.*, 34(22):2154–2155, 1998.

[193] K. Suzuki, H. Kubota, T. Komukai, E. Yamada, T. Imai, K. Tamura, A. Sahara, and M. Nakzawa. 40Gbit/s soliton transmission field experiment over 1360km using in-line soliton control. *Electron. Lett.*, 34(22):2143–2145, 1998.

[194] A. Kolltveit, P.A. Andrekson, J. Brentel, B.E. Olsson, B. Bakhshi, J. Hansryd, P.O. Hedekvist, M. Karlsson, H. Sunnerud, and J. Li. Single-wavelength 40Gbit/s soliton field transmission experiment over 400km of installed fibre. *Electron. Lett.*, 35(1):75–76, 1999.

[195] F.M. Knox, P. Harper, P.N. Kean, N.J. Doran, and I. Bennion. Low jitter long distance pulse transmission near net fibre dispersion zero wavelength. *Electron. Lett.*, 31(17):1467–1468, 1995.

[196] T. Georges and B. Charbonnier. Continuum generated by chromatic dispersion and power variations in periodically amplified soliton links. *Opt. Lett.*, 21(16):1232–1234, 1996.

[197] O. Audouin, E. Pallise, E. Desuvire, and E. Maunand. Use of fast in-line saturable absorbers in wavelength-division-multiplexed soliton systems. *IEEE Photon. Technol. Lett.*, 10(6):828–829, 1998.

[198] M. Hofer, M.H. Hober, F. Haberl, and M.E. Ferman. Characterization of ultrashort pulse formation in passively mode-locked fiber lasers. *IEEE J. Quantum Electron.*, 28(3):720–728, 1992.

[199] V.J. Matsas, D.J. Richardson, T.P. Newson, and D.N. Payne. Characterization of a self-starting, passively mode-locked fiber ring laser that exploits nonlinear polarization evolution. *Opt. Lett.*, 18(5):358–360, 1993.

[200] R.P. Davey, N. Langford, and A.I. Ferguson. Role of polarisation rotation in the modelocking of an Er fibre laser. *Electron. Lett.*, 29(9):758–760, 1993.

[201] P. Harper, I.S. Penketh, S.B. Alleston, I. Bennion, and N.J. Doran. 10Gbit/s dispersion managed soliton propagation over 200Mm without active control. *Electron. Lett.*, 34(21):1997–1999, 1998.

[202] P. Harper, F.M. Knox, D.S. Govan, P.N. Kean, I. Bennion, and N.J. Doran. Long distance 10Gbit/s soliton transmission over standard fibre with periodic dispersion compensation. *NOC '97*, Core and ATM Networks:18–24, 1997.

[203] L. Reekie, I.M. Jauncey, S.B. Poole, and D.N. Payne. Diode-laser-pumped operation of an Er^{3+}-doped single-mode fibre laser. *Electron. Lett.*, 23(20):1076–1078, 1987.

[204] M.E. Fermann, D.C. Hanna, D.P. Shepherd, P.J. Suni, and J.E. Townsend. Efficient operation of an Yb-sensitised Er laser fiber at 1.56μ m. *Electron. Lett.*, 24(18):1135–1136, 1988.

[205] C. Das, U. Gaubatz, E. Gottwald, K. Kotten, L.Rapp, C.-J. Weiske, B. Hein, F. Kuppers, and A. Mattheus. Straightforward upgrading of transmission system to 4*10Gbit/s through 617km and 8*10Gbit/s through 412km of SMF. *Electron. Lett.*, 31:1374–1375, 1995.

[206] F.M. Knox, W. Forysiak, and N.J. Doran. 10Gbit/s soliton communication systems over standard fiber at 1.55 μ m and the use of dispersion compensation. *IEEE J. Lightwave Technol.*, 13:1955–1962, 1995.

[207] T. Georges and B. Charbonnier. Pre-chirping and dispersion compensation for long-haul 20Gbit/s soliton transmission at 1.55μm on nondispersion-shifted fibers. *OFC 1997*, WH2:144–145, 1997.

[208] F. Matera and M. Settembre. 10Gbit/s optically amplified single-channel systems operating in links encompassing conventional step-index fibres. *Optical and Quantum Electronics*, 29:21–34, 1997.

[209] D.M. Rothnie and J.E. Midwinter. Improved standard fibre performance by positioning the dispersion compensating fibre. *Electron. Lett.*, 32(20):1907–1908, 1996.

[210] X.Y. Tang. Performance improvement of 10Gbit/s soliton transmission over dispersion managed standard fiber by using the nonlinearity of dispersion compensating fiber. *NOC '97*, Core and ATM Networks:25–28, 1997.

[211] A.D. Ellis and D.M. Spirit. Unrepeatered transmission over 89km standard fibre at 40Gbit/s. *Electron. Lett.*, 30(1):72–74, 1994.

[212] D. Breuer, K. Petermann, A. Mattheus, and S.K. Turitsyn. Combatting fibre nonlinearity in symetrical compensation schemes using RZ-modulation format at 120km amplifier spacing over standard fibre. *ECOC 1997*, 2:261–264, 1997.

[213] D. Breuer, F. Kuppers, A. Mattheus, E.G. Shapiro, I. Gabitov, and S.K. Turitsyn. Symmetrical dispersion compensation for standard monomode-fiber-based communication systems with large amplifier spacing. *Opt. Lett.*, 22(13):982–984, 1997.

[214] L.F. Mollenauer, P.V. Mamyshev, and J.P. Gordon. Effect of guiding filters on the behaviour of dispersion managed solitons. *Opt. Lett.*, 24(4):220–222, 1999.

[215] C.J. Anderson and J.A. Lyle. Technique for evaluating system performance using Q in numerical simulations exhibiting intersymbol interference. *Electron. Lett.*, 30(1):71–72, 1994.

[216] J. Hansyrd, B. Bakhshi, B.E. Olsson, P.A. Andrekson, J. Brentel, and E. Kolltveit. 80Gbit/s single wavelength OTDMsoliton transmission over 172km installed fiber. *OFC 1999*, PD 6, 1999.

[217] T. Terahara, T. Naito, N. Shimojoh, T. Tanaka, T. Chikama, and M. Suyama. 0.7Tbit/s (66x10.66Gbit/s) WDM transmission over 2212km using broadband high-power EDFAs with pump reflector. *Electron. Lett.*, 34(10):1001–1002, 1998.

[218] H. Taga, T. Miyakawa, K. Murashige, N. Edegawa, M. Suzuki, H. Tanaka, K. Goto, and S. Yamamoto. 50 WDM, 10.66Gbit/s transmission experiment over 1600km employing gain-flattened EDFA chain. *Electron. Lett.*, 34(4):382–383, 1998.

[219] D. Le. Guen, S. Del.Burgo, M.L. Moulinard, D. Grot, M. Henry, F. Favre, and T. Georges. Narrow band 1.02Tbit/s (51x20Gbit/s) soliton DWDM transmission over 1000km of standard fibre with 100km amplifier span. *OFC 1999*, PD 4, 1999.

Appendix A

Publications

- D.S. Govan, N.J. Smith, F.M. Knox and N.J. Doran. Stable soliton transmission with increased energy using dispersion management and periodic saturable absorptio In *Proceedings NLGW 1996, 141-143*

- D.S. Govan, N.J. Smith, F.M. Knox and N.J. Doran. Stable Propagation of Solitons with Increased Energy through the Combined Action of Dispersion Management and Periodic Saturable Absorption. In *JOSAB, vol. 14, No. 11, Nov 1997, 2960-2966.*

- P. Harper, F.M. Knox, D.S. Govan, P.N. Kean, I. Bennion, and N.J. Doran. Long distance 10Gbit/s soliton transmission over standard fibre with periodic dispersion compensation. In *Eur. Conf. on Netw. and Opt. Comm. Vol.2 18-24*, Antwerp, Belgium, 1997. IOS Press.

- D.S. Govan, W Forysiak and N.J. Doran 40Gbit/s soliton transmission over standard fibre with dispersion management. In *Proceedings NLGW 1998, 89-91*

- D.S. Govan, W Forysiak and N.J. Doran. Long-distance 40Gbit/s soliton transmission over standard fiber by use of dispersion management In *Optics Letters, vol. 23, No. 19, 1523-1525, 1998*

- P Harper, I S Penketh, S B Alleston, D S Govan, I Bennion, and N J Doran. Propagation of 4ps, 10Gbit/s dispersion manage solitons over 200Mm using saturable absorption. In *Colloquium on Optical Solitons, IEE, London (Feb 1999)*